Balancing distributor and customer benefits of battery storage co-located with solar PV

Elizabeth L. Ratnam

Bachelor of Electrical Engineering

A thesis submitted in fulfilment
of the requirements for the degree of
Doctor of Philosophy

October, 2015

THE UNIVERSITY OF
NEWCASTLE
AUSTRALIA

Declaration

I hereby certify that to the best of my knowledge and belief this thesis is my own work and contains no material previously published or written by another person except where due references and acknowledgements are made. It contains no material which has been previously submitted by me for the award of any other degree or diploma in any university or other tertiary institution.

I hereby certify that this thesis is in the form of a series of published papers. I have included as part of the thesis a written statement from each co-author, endorsed in writing by the Faculty Assistant Dean (Research Training), attesting to my contribution to the jointly authored papers.

I warrant that I have obtained, where necessary, permission from the copyright owners to use any third party copyright material reproduced in the thesis, or to use any of my own published work in which the copyright is held by another party.

Elizabeth L. Ratnam
October, 2015

To Marcel, Mum and Dad.

Acknowledgements

First and foremost, I would like to thank my husband, Marcel, and our respective families. Thank you for all your love, guidance, encouragement and all-round support in all of my career choices including this PhD.

Secondly, I would like to thank A/Prof. Steven Weller for his guidance, encouragement, patience and dedicated involvement throughout my academic career. The experience of being under your supervision has been invaluable. I would also like to thank co-supervisor A/Prof. Christopher Kellett for his dedicated involvement throughout my PhD studies. The support and continual helpful feedback you both provided throughout all these years indeed made this thesis possible.

I am grateful to CSIRO and the Australian Energy Market Commission (AEMC) for the opportunity to be involved in the Integration of Storage Study; it was wonderful, and the discussions and feedback invaluable. More specifically, I would like to thank AEMC employees Stuart Slack, Claire Richards, and Chantelle Bramley for all their assistance, helpful review comments and invaluable feedback. Thank you also to CSIRO employees Dr. Sam Behrens, Dr. Luke Reedman, Mrs. Kate Cavanagh, Dr. John Ward, Dr. Jenny Hayward, Dr. Thomas Brinsmead, and Mr. Paul Graham for the helpful discussions, advice, and wonderful opportunity to collaborate with each of you. In my contribution to the study, I would like to thank Mr. Stuart Woodman and Dr. Sam Behrens for their assistance in identifying cities close to transmission and subtransmission assets. Thanks also to Steven O'Donnell from Ausgrid for assistance with providing information on ratings for distribution equipment.

My research was funded through an Australian Postgraduate Award and by a CSIRO Energy Technology Postgraduate Research Scholarship. I am very grateful for this support. Thanks also to CSIRO employees Dr. Glenn Platt, Dr. Julio Braslavsky, Dr. Adam Berry, Dr. John Ward and Dr. Cristian Perfumo for their helpful advice throughout the course of my PhD. Thanks also to the many CSIRO Energy Flagship employees that I had the pleasure to interact with throughout my PhD, I have felt very welcomed and you have always been incredibly helpful.

I am also very grateful of Dr. Anthony Laskovski, and Ausgrid employees Dr. Alan Murray, Dr. Robert Simpson, Neil Stephens, Shannon Frohlich-Terpstra, and Daniel Burke for your time,

encouragement and help. Thank you both Neil Stephens and Dr. Alan Murray for all your help and guidance on my many GridLAB-D and Smart Grid Smart City related questions.

I would also like to thank the members of the SPM research centre in Electrical Engineering at the University of Newcastle, Australia. I am very grateful for your encouragement and advice throughout the years. I would also like to thank the many friends who have encouraged and supported both Marcel and I throughout my PhD studies.

Contribution to Joint Publications

Chapter 1 consists of Sections 5.1 and 5.2.2 of a technical report published by the Australian Energy Market Commission (AEMC) titled *Future Energy Storage Trends: An Assessment of the Economic Viability, Potential Uptake and Impacts of Electrical Energy Storage on the NEM 2015-2035*. This published report is outside the the scope of Rule 39.2 i that governs research higher degrees, therefore we have sought the approval of the Dean of Graduate Studies to include this work in accordance with Rule 39.2 v. A Statement of Contribution from each co-author of this technical report is included in the thesis.

Chapters 2–6 consist of five co-authored papers that are published, in press or have been submitted for publication in scholarly journals. Specifically, three papers have been published (or accepted for publication) in refereed journals, and two papers have been submitted to journals for publication at the time of submission. For each of these five co-authored papers a written statement of contribution from each co-author follows.

Statement of Contribution 1

Technical report in Chapter 2

Brinsmead, T., Graham, P., Hayward, J., Ratnam, E., and Reedman, L. (2015). Future Energy Storage Trends: An Assessment of the Economic Viability, Potential Uptake and Impacts of Electrical Energy Storage on the NEM 2015-2035. CSIRO, Australia. Report No. EP155039.

Authors

By signing below I confirm that Elizabeth Louise Ratnam contributed to report writing and techno-economic modelling for the Australian Energy Market Commission (AEMC) Integration of Storage Study. For the purpose of this thesis, permission to reproduce Sections 5.1 and 5.2.2 of the report titled *Future Energy Storage Trends: An Assessment of the Economic Viability, Potential Uptake and Impacts of Electrical Energy Storage on the NEM 2015-2035* prepared for the AEMC is granted. The contribution of Elizabeth L. Ratnam specific to this report was to prepare, draft and edit Sections 5.1 and 5.2.2. Both the AEMC and CSIRO have reviewed these sections in the report prior to publication.

I hereby certify that this statement of contribution is accurate

Dr. Thomas Brinsmead Signed: .. ...Date: 21/9/15

Mr. Paul Graham Signed: .. ...Date: 21/9/15

Dr. Jenny Hayward Signed: .. ...Date: 6/10/15

Dr. Luke Reedman Signed: .. ...Date: 21/9/2015

Faculty Assistant Dean Research Training

Signed: .....Date: 22.10.2015

Statement of Contribution 2

Technical paper in Chapter 3

E. L. Ratnam, S. R. Weller, C. M. Kellett, A. Murray, Residential load and rooftop PV generation: An Australian distribution network dataset, International Journal of Sustainable Energy — Accepted for publication September 2015.

Authors

By signing below I confirm that Elizabeth Louise Ratnam contributed to developing the high-level framework, prepared the data, and took primary responsibility for preparing, drafting and editing the journal publication listed above.

I hereby certify that this statement of contribution is accurate

Associate Professor Steven Weller	Signed:	Date: 16/10/2015
Associate Professor Christopher Kellett	Signed:	Date: 16/10/2015
Dr Alan Murray	Signed:	Date: 11/10/2015

Faculty Assistant Dean Research Training

Signed: ..... Date: 22.10.2015

Statement of Contribution 3

Technical papers in Chapters 4-6

E. L. Ratnam, S. R. Weller, C. M. Kellett, An optimization-based approach to scheduling residential battery storage with solar PV: Assessing customer benefit, Renewable Energy 75 (2015) 123 134.

E. L. Ratnam, S. R. Weller, C. M. Kellett, Scheduling residential battery storage with solar PV: Assessing the benefits of net metering, Applied Energy 155 (2015) 881891.

E. L. Ratnam, S. R. Weller, C. M. Kellett, An optimization-based approach to power management in distribution networks with residential battery storage, Submitted to journal for publication January 2015.

Authors

By signing below I confirm that Elizabeth Louise Ratnam contributed to developing the high-level framework, algorithms, simulations and took primary responsibility for preparing, drafting and editing the journal publications listed above.

I hereby certify that this statement of contribution is ~~accurate~~

Associate Professor Steven Weller Signed: . Date: 16/10/2015

Associate Professor Christopher Kellett Signed: . Date: 16/10/2015

Faculty Assistant Dean Research Training

Signed: ..... Date: 22.10.2015

Statement of Contribution 4

Technical paper in Chapter 7

E. L. Ratnam, S. R. Weller, Receding horizon optimization-based approaches to manage supply voltages and power flows in a distribution grid with battery storage, Submitted to journal for publication 2015.

Authors

By signing below I confirm that Elizabeth Louise Ratnam contributed to developing the high-level framework, algorithms, simulations and took primary responsibility for preparing, drafting and editing the journal publication listed above.

I hereby certify that this statement of contribution is accurate

Associate Professor Steven Weller Signed: ..Date: 16/10/2015

Faculty Assistant Dean Research Training

Signed: ..Date: 22.10.2015

Contents

Contents xi

Abstract xii

Introduction 1

Part 1 Overview and context 10

1 Assessment of the economic viability of energy storage 11

2 An Australian distribution network dataset 34

Part 2 Battery scheduling: A single residential system 55

3 Assessing customer benefit of battery scheduling 56

4 Assessing the benefits of net metering 69

Part 3 Battery scheduling: Coordinated residential systems 81

5 Power management in a distribution network 82

6 A case study incorporating a Gridlab-d distribution model 105

Conclusions and future work 126

A Appendix 131

Bibliography 132

Abstract

In recent years, a rapid and dramatic increase in electrical power generation from renewable energy sources has been observed in many countries. Rapid increases in grid-connected small-scale solar photovoltaics (PV) have been driven by government incentives and renewable energy rebates, including residential feed-in tariffs and the financial policy of net metering. However, new challenges arise in balancing the generation of electricity with variable demand at all times as traditional fossil fuel-fired generators are retired and replaced with intermittent renewable electricity sources.

This thesis looks at ways to balance distributor and customer benefits of battery storage co-located with solar PV, with a view to facilitating continual increases in grid-connected solar PV. Two issues that arise when accommodating significant residential-scale PV generation are addressed: the first is reverse power flow that leads to considerable voltage rise; the second corresponds to peak loads that occur infrequently, but potentially lead to the need for costly network augmentation when PV generation is unavailable. The benefits associated with addressing these two distributor issues are balanced with the benefit of scheduling battery storage to improve operational savings that accrue to customers.

Conventional approaches to managing peak loads and reverse power flows in distribution networks vary from country-to-country, since they are often driven by government policies and regulation. In the Australian context, the first part of the thesis introduces typical costs associated with the design and operation of electrical networks to assess the economic viability of large-scale energy storage. We also introduce a publicly available dataset consisting of load and rooftop PV generation for 300 de-identified Australian residential customers in a distribution network. All simulation-based results in the thesis incorporate data from this publicly available dataset.

The second part of the thesis considers potential savings that accrue to residential customers that co-locate battery storage with solar PV. We address reverse power flow and peak-loads coincident with peak pricing periods where the residential customer designs battery charge and discharge schedules. This leads us to a constrained optimization-based problem that we formulate as a quadratic program.

The third part of the thesis focuses on coordinated approaches to charge and discharge residential battery storage. Emphasis is given to the management of bi-directional power flows in a distribution grid, and the maintenance of supply voltages within prescribed limits. This has motivated a novel approach to Adaptive-Receding Horizon Optimization (A-RHO). We implement our A-RHO approach in a GridLAB-D model of an Australian distribution network to assess the distributor benefits.

Introduction

Climate change, national energy security, and the declining economic availability of fossil fuel resources are key drivers for the integration of renewable energy sources such as solar into the modern power grid [1–4]. These drivers, in conjunction with renewable energy incentives such as feed-in tariffs [4–7] and the financial policy of net metering [8–11], have lead to a rapid and dramatic uptake of residential-scale solar photovoltaics (PV) in some countries [12,13]. As the capital cost of small-scale PV continues to drop [14], and electricity prices continue to increase [12], it is expected that this trend in significant PV uptake will continue into the next decade [13, 15].

However, there are significant challenges in converting the abundant solar resource into reliable, high-quality electricity [16–19]. Challenges include the variability of solar irradiance on both daily and seasonal timescales in addition to intermittency arising from moving cloud cover on much shorter timescales [17, 18]. Further, new challenges in balancing the generation of electricity with variable demand at all times arise as traditional fossil fuel-fired generators are retired and replaced with these intermittent renewable sources [19–21]. Despite the challenges, there was a 480% increase in Australian solar PV installations in a single year from 2009 to 2010, of which 99% was grid-connected [22, 23]. Further, there is more than 3.8 GW of installed rooftop PV in Australia [24], up from 1 GW in 2012 [23]. In the United States, there is more than 16 GW of installed solar PV [25], up from 0.8 GW in 2010 [26]. PV plant installations in Germany exceed 1.2 million, and as of September 2012, peak PV capacity reached 31 GW with about 70% of this capacity being connected to the low voltage grid [27].

Literature Overview

As residential PV penetration continues to increase, the management of supply voltages within operational limits becomes increasingly challenging for distribution operators [27–44]. For example, if PV generation exceeds the demand of a residential customer in addition to demand in the downstream distribution feeder, the excess PV generation is pushed upstream creating voltage rise [29–32]. Voltage rise that exceeds an upper tolerance with respect to the nominal supply voltage, potentially occurs when a large number of rooftop PV generators are connected in close proximity to each other [33–39]. Voltage dips are another concern when grid-connecting a large

number of rooftop PV generators in close proximity to each other [28]. For example, a voltage dip potentially occurs when passing cloud cover results in a significant drop in rooftop PV generation that would otherwise be servicing residential load [35–37,40]. If these voltage deviations fall outside power quality standards, either the utility covers the direct cost of mitigation or the burden of voltage regulation falls to the PV producer [18,27,29,33,38].

There are two common approaches to managing voltage rise in the low voltage grid. The first is to augment the distribution grid by increasing conductor size and/or upgrading transformers to lower network impedances [27,34,41,45]. The second is to constrain PV generation at times of low electricity consumption in order to preserve compliance of allowable voltage deviations [29,42,46]. Neither approach is optimal for significant PV penetration, as network augmentation adds to the overall PV grid integration costs [34,45] whereas spilling PV generation leads to lost revenue for the producer [31,32].

There are a number of emerging approaches to overcome non-compliant voltage deviations arising from the intermittency and variability of solar PV, with applicable incentives, mandates and regulation driving the solutions. Some of these approaches include energy storage [47–50], direct load control [51,52], price-responsive load control [53–56], active PV generation curtailment [57], and enhanced PV inverter control to manage real and reactive power output [58,59]. Different incentives driving these approaches include dynamic day-ahead electricity tariffs [53,60], reductions in appliance-specific electricity billing [51,61], standards curbing PV production [42], and energy storage mandates such as those in California [62]. Depending on the incentives and regulatory environment, one or more of these approaches may serve as a demand management option for a distribution operator faced with significant PV penetration [63,64]. More specifically, enhanced PV inverter control alone does not always maintain distribution voltages within set tolerances [64]. Consequently, coordinated control of PVs and battery energy storage has been proposed in [65–68].

Without careful coordination, however, the potential benefits of demand-side approaches to managing bi-directional power flows in a distribution network might not be realized [14,51,69,70]. For example, a second load peak in the distribution grid may occur when autonomous, time-based battery charging schedules are implemented [14,51], potentially leading to a need for costly distribution reinforcement [14]. Furthermore, increases in reverse power flows (or peak loads) potentially occur when battery storage units connected to a distribution grid are discharged (or charged) in response to time-varying electricity prices [71], which may also necessitate network investment. In recent work [11] we illustrate a second 'rebound' load peak in addition to an increase in reverse power flow occurs across a day, when customers schedule battery storage co-located with solar PV

with the aim of minimizing their electricity bill (or maximizing their operational savings).

Several authors have considered approaches that co-locate battery storage with solar PV with a focus on reducing network peak demand [72–78], potentially leading to battery schedules that either mitigate or exacerbate voltage rise associated with reverse power flow when inverters operate at unity power factor [58,77]. The reduction of network peak demand is incorporated into a linear program in [72], where the energy flowing from the point of common coupling (PCC) to the customer is minimized when residential load exceeds residential PV production. Otherwise the battery is scheduled in [72] to charge during the off-peak pricing period, and discharge during the peak pricing period, with no limit on reverse power flow (i.e., the power delivered to the grid). Consequently, battery scheduling in [72] potentially induces voltage rise at the PCC. The reduction of network peak demand is also incorporated into an optimization problem in [73], where the objective function includes financial incentives for residents to deliver energy to the grid when the purchase cost of electricity is high. Hence, when interconnected customers in close proximity minimize the objective function in [73], large voltage swings associated with reverse power flow potentially arise due to the battery scheduling.

In contrast, peak demand and reverse power flow is reduced by solving the optimization problems in [74,79], where the objective functions eliminate residential subsidies for electricity delivered to the grid and include payments for electricity received from the grid. Thus, the optimization problems in [74, 79] potentially reduce voltage rise associated with reverse power flow. The optimization problem in [75] also removes incentives for reverse power flow associated with battery scheduling, while permitting incentives encouraging solar PV uptake. In addition, the optimization problem in [75] includes residential payments for electricity received from the grid. Consequently, the optimization problem in [75] leads to reductions in both peak demand and reverse power flow, potentially mitigating voltage rise. Another method for reducing both peak demand and reverse power flow is incorporated into the optimization problem in [76], where a sophisticated dynamic pricing environment provides additional incentives for customers to smooth their day-ahead energy consumption. Hence, the optimization problem in [76] potentially abates voltage rise associated with reverse power flow.

Alternatively, coordinated approaches to managing bi-directional power flows in a distribution network have been proposed in the recent literature [71,80,81]. For example, a linear program (LP) is employed in [71] to reduce peak power flows (potentially in the reverse direction) through a distribution substation. Furthermore, [71] proposes direct control of a customer's battery schedule by the distributor when the LP-based power flow reductions are required. The optimization problem

in [80] includes penalties for large power fluctuations to and from an interconnection point that connects a smart grid to an upstream electricity network. To reduce power fluctuations within a distribution grid, [80] proposes direct control of demand-side battery schedules by a distributor. In contrast, a central energy management system (EMS) in [81] coordinates supply and demand within a microgrid in a number of ways. For example, a central EMS in [81] either dispatches power flow references to customers connected to a microgrid, or directly controls battery charge and discharge schedules of each microgrid customer. That is, each microgrid customer in [81] has a local EMS that manages residential battery schedules subject to central EMS references or directives.

Other coordinated approaches to improving supply voltages in a distribution network are considered in [65, 82–85], and include charging a residential battery co-located with solar PV when a predetermined threshold for PV generation is exceeded [82]. In [83–85] a main control center coordinates battery charge/discharge rates, where the main control center in [83] collects supply voltages, supply frequencies, and the state of charge of each battery. With the exception of our recent work [84, 85], none of these approaches incorporate and balance increases in operational energy savings that accrue to customers with battery storage as defined in Chapter 3.

In this thesis we consider a balance in benefits to a utility and customer, in the context of grid-connected residential-scale battery storage co-located with solar PV. We propose optimization-based approaches to schedule residential battery storage, with a direct focus on balancing financial benefits for a customer with utility benefits in managing bi-directional distribution power flows, and an indirect focus on incorporating low requirements for sensing and communications infrastructure. In our assessment of the financial benefits that accrue to a customer with battery storage, we consider operational savings or reductions in energy bills for a cross-sectional sample of customers located in Sydney and regional New South Wales (NSW), Australia. In our assessment of the utility benefits we present aggregate power flows to or from residential customers, and consider supply voltages within an Australian distribution network with significant residential PV penetration. Our overarching objective is to balance distributor and customer benefits of battery storage co-located with solar PV, with a view to facilitate continued increases in distributed, small-scale PV generation.

Key Contributions of this Thesis

The key contributions of this thesis are:

- a report extract that informed Australian policy makers on the economic viability and impacts of electrical energy storage on the National Electricity Market (NEM) 2015–2035,
- a detailed description of a publicly available dataset comprised of interval readings of load and PV generation for each of 300 residential customer, that forms the basis of each case study presented in the thesis,
- a linear program (LP)-based scheduling algorithm that maximizes operational savings that accrue to customers with grid-connected battery storage,
- a case study demonstrating the LP-based approach potentially leads to undesirable consequences for a distributor, that is, when all customers discharge battery storage during the peak pricing period, reverse power flow creating significant voltage rise potentially occurs,
- a quadratic program (QP)-based scheduling algorithm that minimizes of the energy supplied by, or to, the grid in a residential PV system with co-located battery storage,
- a greedy-search heuristic that selects the key design parameters in the QP-based scheduling algorithm to improve operational savings that accrue to customers,
- a case study demonstrating a balance in the customer and utility benefits of the QP-based scheduling algorithm,
- two coordinated QP-based approaches to adjust and improve the balance in managing bi-directional distribution power flows with increases in operational savings that accrue to customers,
- a case study confirming a centralized approach to coordinating residential battery storage is preferable in that no customer is disproportionately penalized for reducing peak load and/or reverse power flow in a distribution network,
- a case study confirming the customer payback period for a 10 kWh battery is in the vicinity of 6 years when a centralized approach to coordinating residential battery storage is implemented,
- two receding horizon optimization (RHO)-based algorithms for coordinating residential battery storage to further improve the balance in managing (1) bi-directional distribution power

flows and associated supply voltages, with (2) increases in operational savings that accrue to customers,

- a case study confirming an adaptive (A)-RHO algorithm more directly improves supply voltages in a low voltage network,
- a case study with a realistic distribution-level electricity network model, showing a peak load reduction of 32% along a medium voltage feeder when approximately 50% of residential customers implemented a distributed (D)-RHO algorithm.

List of Publications

A complete list of publications related to this thesis is provided below.

Refereed Journal Articles

E. L. Ratnam, S. R. Weller, C. M. Kellett, and A. T. Murray, "Residential load and rooftop PV generation: An Australian distribution network dataset," *International Journal of Sustainable Energy*, accepted for publication 11 September 2015.

E. L. Ratnam, S. R. Weller, and C. M. Kellett, "An optimization-based approach to scheduling residential battery storage with solar PV: Assessing customer benefit," *Renewable Energy*, vol. 75, pp. 123–134, 2015.

E. L. Ratnam, S. R. Weller, and C. M. Kellett, "Scheduling residential battery storage with solar PV: Assessing the benefits of net metering," *Applied Energy* vol. 155 pp. 881–891, 2015.

E. L. Ratnam, S. R. Weller, and C. M. Kellett, "Central versus localized optimization-based approaches to power management in distribution networks with residential battery storage," *International Journal of Electrical Power and Energy Systems,* accepted for publication 27 January 2016.[1]

E. L. Ratnam, and S. R. Weller, "Receding horizon optimization-based approaches to manage supply voltages and power flows in a distribution grid with battery storage," submitted for publication 15 October 2015, under review.

Technical Reports

T. Brinsmead, P. Graham, J. Hayward, E. L. Ratnam, and L. Reedman, *Future Energy Storage Trends: An Assessment of the Economic Viability, Potential Uptake and Impacts of Electrical*

[1] This paper was titled "An optimization-based approach to power management in distribution networks with residential battery storage," prior to publication.

Energy Storage on the NEM 2015-2035, 2015, CSIRO, Australia. Report No. EP155039.

Others (related to the research, but not included in this thesis)

K. Cavanagh, J. K. Ward, S. Behrens, A. I. Bhatt, E. L. Ratnam, E. Oliver, and J. Hayward, *Electrical Energy Storage: Technology Overview and Applications*, 2015, CSIRO, Australia. Report No. EP154168.

E. L. Ratnam, S. R. Weller, and C. M. Kellett, "An optimization-based approach for assessing the benefits of residential battery storage in conjunction with solar PV," *IREP Symposium-Bulk Power System Dynamics and Control -IX (IREP)*, Rethymnon, Greece, 25–30 Aug. 2013, pp. 1–8.

E. L. Ratnam, S. R. Weller, and C. M. Kellett, "Assessing the benefits of net metering with residential battery storage," in Proc. 3rd ASEAN Australian Engineering Congress on Innovative Technologies for Sustainable Development and Renewable Energy (AAEC 2015), Singapore, 11–13 Mar. 2015, pp. 78–83.

Overview of Thesis Content

The remainder of this thesis is organized into three thematic parts, and we include an additional chapter for conclusions. The first part includes background material, provides context, includes a detailed description of the dataset used throughout the thesis, and serves as a high-level overview. Part 2 introduces a single residential system, and Part 3 incorporates the residential system into a larger distribution network. The introduction of each chapter in Part 2 and Part 3 incorporates a focused literature review, that places the work in an established body of knowledge and links papers (from prior chapters) included in the thesis. At the beginning of each chapter of the thesis, an explanatory overview is provided to link the separate papers included in the thesis.

References at the end of the thesis refer to the introductory and concluding chapters of the thesis, and main body chapters contain a literature review and a list of references. An outline of the remaining chapters of the thesis follows.

Part 1 Overview and context

- **Chapter 1** investigates the economic viability of large-scale battery storage. We propose two case studies to investigate factors influencing the economic viability of energy storage for (1) power system operators and (2) large industrial-sized customers, respectively. Background material is included to provide context for the underlying

assumptions considered in this chapter and the remainder of the thesis.

- **Chapter 2** reports a publicly available dataset considered in the remaining chapters of the thesis. The dataset consists of load and rooftop PV generation for 300 de-identified residential customers in an Australian distribution network. Following a detailed description of the dataset, we identify several means by which anomalous records (e.g. due to inverter failure) are identified and excised. All papers in this thesis incorporate data from this publicly available dataset.

Part 2 Battery scheduling: A single residential system

- **Chapter 3** proposes an optimization-based algorithm for the scheduling of residential battery storage co-located with solar PV, in the context of PV incentives such as feed-in tariffs. We present a quadratic program (QP)-based algorithm that is applied to measured load and generation data from 145 residential customers located in an Australian distribution network. The results of the case study confirm the QP-based scheduling algorithm significantly penalizes reverse power flow and peak loads corresponding to peak time-of-use billing.
- **Chapter 4** presents a linear programming (LP)-based approach to designing day-ahead battery charge and discharge schedules when any generation in excess of residential load is compensated by the electricity retailer via net metering. We further show that when net metering is used, that it is possible to balance the objective of the utility in limiting reverse power flow, with the customer objective of increasing operational savings, with the QP-based approach first presented in Chapter 3.

Part 3 Battery scheduling: Coordinated residential systems

- **Chapter 5** addresses the problem of managing reverse power flow and peak loads within a distribution network. We propose a two optimization-based algorithms for coordinating residential battery storage when solar photovoltaic (PV) generation in excess of load is compensated via net metering, extending the framework presented in Chapter 4. A case study confirms a centralized approach to coordinating residential battery storage is preferable to a more localized approach, in that no customer is disproportionately penalized for reducing peak load and/or reverse power flow in a distribution network.
- **Chapter 6** considers three key problems that may occur infrequently in Australian distribution networks, but could potentially lead to costly remediation for distributors:

  1. significant reverse power flows along a medium voltage feeder that may render existing voltage control and/or protection schemes (designed for uni-directional power

flow) inadequate,

2. peak electricity demand non-coincident with PV generation approaching a medium voltage network capacity, and
3. supply voltages in a low voltage network that are above or below allowable thresholds.

To address these three key problems we propose two receding horizon optimization-based algorithms that incorporate updates in forecast information at each time step. Both algorithms include one or more of the objective functions presented in Chapter 5, and are applied to a GridLAB-D model of an Australian distribution region located in the suburb of Elermore Vale, NSW to assess the distributor benefits.

- The final chapter draws conclusions and describes possible future research directions.

Part 1

Overview and context

1

Assessment of the economic viability of energy storage

Part 1 of this thesis is comprised of Chapter 1 and Chapter 2. These chapters provide a high-level overview, introduce an Australian historical load and PV generation dataset, and set the scene for the contributions in the remainder of the thesis.

Chapter 1 is comprised of Sections 5.1 and 5.2.2 of a technical report published by the AEMC titled *Future Energy Storage Trends: An Assessment of the Economic Viability, Potential Uptake and Impacts of Electrical Energy Storage on the NEM 2015-2035* [14]. To improve clarity, we have reformatted the referencing in this report extract.

The full AEMC report [14] informs Australian policy makers on the economic viability and impacts of electrical energy storage on the National Electricity Market (NEM) in the context of the present day and into the foreseeable future. Material from Section 5 of the AEMC report is included in Chapter 1 to clearly establish that the findings of the thesis are indeed relevant and applicable to present-day electrical networks. For example, in Chapter 1 a preview for some of the results presented later in Chapter 5 of this thesis is provided to highlight the relevance of coordinated residential battery scheduling for peak demand reduction and reverse power flow management in an electrical power network. The costs computed at the end of the report extract (page 22) are considered reasonable in the context of the full AEMC report, where Li-ion battery technology costs are reported to be in the vicinity of \$500/kWh today, with prices expected to drop below \$300/kWh in the foreseeable future (see Fig. 4 and Table 1 in the full AEMC report.)

Chapter 2 reports a publicly available dataset of historical load and PV generation for 300 Australian residential customers. This dataset is considered in the remaining chapters of the thesis, and provides context for the case studies in the following two parts in the thesis.

5. Economic viability of storage

5.1 Distribution and transmission networks

Various factors affect the economic viability of Energy Storage (ES) for power system operators responsible for the design, operation and maintenance of electrical networks that supply the essential service of electricity to homes, businesses and industry. These factors include:

- annual consumption and electricity demand profiles in the distribution or transmission networks
- generation profiles of grid-connected renewables (e.g. solar PV)
- capacity limits and reliability indices as prescribed in the licence conditions for electrical operators
- the upfront and ongoing costs of Energy Storage Systems (ESS)
- expected life and operational performance of ESS.

This section considers costs associated with the design and operation of electrical networks to assess the economic viability of ES for distribution or transmission operators.

5.1.1 Background

In the transmission of electricity, the role of the network is to deliver electrical energy from large-scale generators to a bulk supply point. The subtransmission network then delivers this electricity to zone substations and large industrial customers. The distribution network subsequently delivers this electricity directly to the end user via a point of common coupling. In more detail, distribution 'feeders' operate at medium voltages (MV), for example, at a nominal 11 kV. From these feeders, MV loads are supplied, or small distribution transformers step the voltage down to a more practical low nominal voltage from which a number of low voltage (LV) loads are supplied, as shown in Figure 1.

Australia has thousands of kilometres of MV distribution network. Most of the distribution feeders consist of overhead lines, since overhead construction costs are significantly less then underground ones [1]. Moreover, in the Australian context, it is typical for rural distribution networks to incorporate single wire earth return (SWER) feeders. SWER systems use the earth as a return path for the current drawn by loads, and are typically cheaper than more traditional feeder topologies of similar capacity.

Distribution networks typically incorporate active network components such as on-load tap changing transformers, voltage-regulating transformers and shunt capacitors. Transformers that supply distribution feeders (e.g. 33 kV/11 kV transformers) are often fitted with voltage regulation capabilities, such as control schemes that operate on-load tap changers (OLTC). Transformers that step down MV to LV typically have fixed tap setting that can be changed by a distribution network service provider (DNSP) if required. Rural MV distribution feeders often incorporate one or more voltage-regulating transformers along a feeder to ensure that the nominal LV delivered to

customers is within the +10% to –6% tolerance required [2, 3]. Moreover, shunt capacitors on MV feeders or within zone substations are often fitted with controls to provide voltage regulation or power factor correction (or both), in order to improve the quality of the electricity supplied to customers.

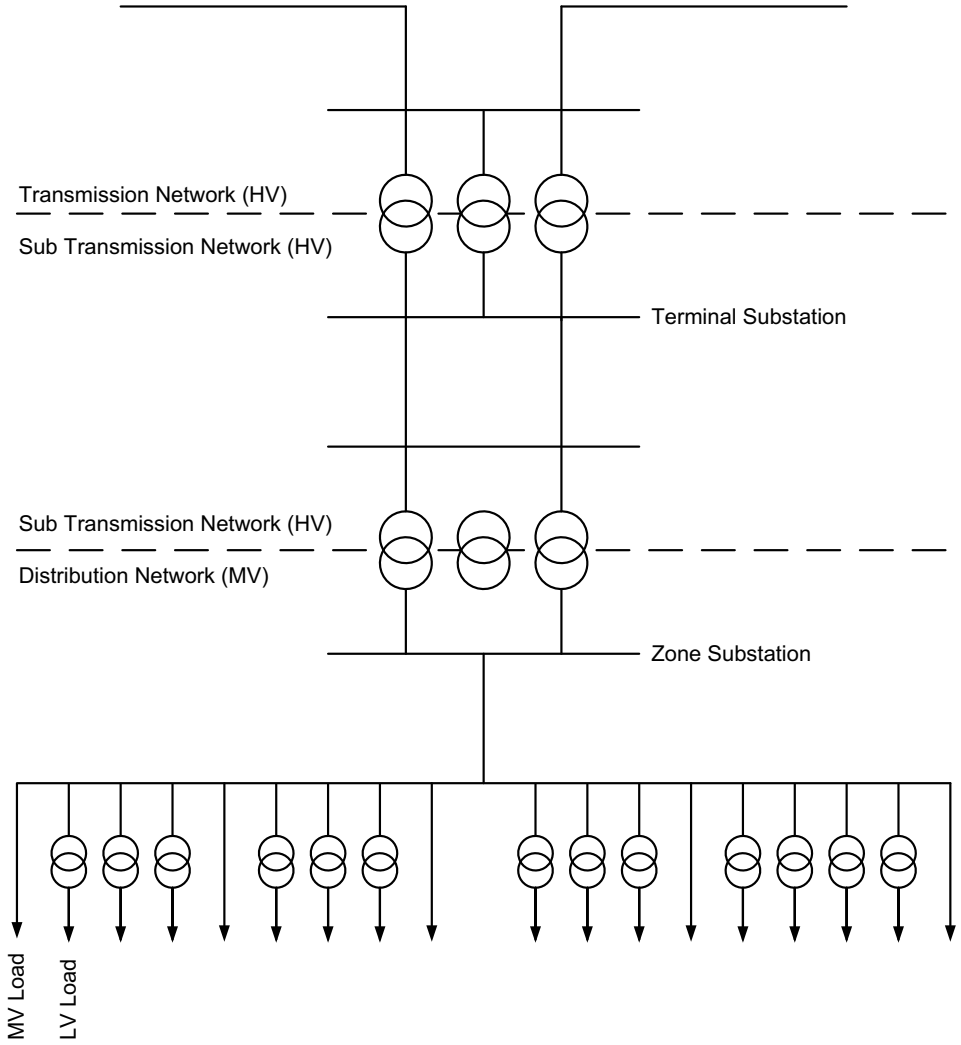

Figure 1: Indicative single-line diagram of the electrical network as a whole, showing where MV and LV distribution networks are placed

HV, high voltage; LV, low voltage; MV medium voltage

Note that the distribution networks effectively begin at the secondary side of zone substation transformers and end at MV and LV loads.

DNSPs are responsible for design, operation and maintenance of distribution networks that supply the essential service of electricity to homes, businesses and industry. The reliability of a distribution network is measured by a number of indices [4,5]. These indices are prescribed in the licence conditions for electricity distributors [6, 7] and they comprise:

- the average minutes off supply per customer due to planned and unplanned outages (the system average interruption duration index, SAIDI)
- the average number of unplanned interruptions per customer, excluding momentary interruptions (the system average interruption frequency index, SAIFI).

These indices are used to calculate penalty payments owing to customers when DNSPs fail to meet guaranteed service levels set by the Australian Energy Regulator [6].

In what follows we define LV phase-to-neutral by a nominal 230 V, with a tolerance of +10% to –6%, as defined in the Australian Standard AS 60038 [2]. MV are defined by a range of phase-to-phase values, from a nominal 1 kV to a nominal 22 kV. Any phase-to-phase voltage from a nominal 33 kV up to 132 kV is recognised as a subtransmission voltage. Voltages above and including 220 kV phase-to-phase are recognised as a nominal transmission voltage.

5.1.2 What are grid infrastructure costs?

To meet guaranteed services levels set by the Australian Energy Regulator [6], a DNSP might seek to use battery storage. For example, if peak demand in a distribution grid is expected to exceed network capacity, then battery storage may provide a cost-effective solution if the alternative is to increase the capacity of the distribution grid. Before considering the potential of battery storage to reduce capital costs that would otherwise be incurred by electric power system operators, we first define some generic costs associated with transmission and distribution infrastructure. A number of sources have been identified that provide estimates of the costs associated with installing and connecting distribution or transmission infrastructure to the electricity grid in Australia [8–22]. In what follows we have collated and adjusted these estimates in order to estimate present-day costs for installing and connecting such infrastructure. The generic estimates presented in what follows have an uncertainty of approximately ±50%. Table 1 shows the assumed overhead and underground construction costs to a feeder or substation.

Table 1: Assumed overhead and underground construction and connection costs (to a feeder or substation) for the period 2015–2020, by voltage

Voltage	UG construction costs	OH construction cost	Connection costs
415 V	$0.6 m/km	$0.010 m/km	$450–$40,000
11 kV	$0.7 m/km	$0.014 m/km	$0.1 m–$1 m (connection in a substation or an OH/UG teed[a] connection, including protection and control infrastructure)
66 kV	$5 m/km	$0.55 m/km	$6 m (connection in a substation or an OH teed connection, including protection and control infrastructure)
132 kV	$6 m/km	$0.75 m/km	$10 m (connection in a substation or an OH teed connection, including protection and control infrastructure)
220 kV	$10 m/km	$1 m/km	$20 m (connection in a substation or an OH teed connection, including protection and control infrastructure)
330 kV	$15 m/km	$1.8 m/km	$30 m (connection in a substation or an OH teed connection, including protection and control infrastructure)

OH, overhead; UG, underground

Costs are in AUD, where 'm' denotes a factor of $1 000 000

[a] A teed connection is one that is parallel to an existing UG or OH line.

5.1.3 What are grid capacity limits?

When infrastructure in the electricity grid reaches a capacity limit, distributors or transmission operators typically incur costs associated with re-enforcing the electricity grid. Capacity limits are often described in terms of thermal limits (with current or power ratings) or voltage limits, for particular network configurations [7].

Because overhead conductors are exposed to the elements, differences in ambient air temperature and wind speed affect the current carrying capacity of a conductor. To reflect temperature extremes, two ambient air temperatures are often assumed: summer noon, 35 °C, and winter night, 10 °C. These operating conditions, together with an assumed wind speed, are used to derive maximum and minimum thermal capabilities for overhead lines on a summer day and a winter night, respectively [23]. To determine the maximum steady-state current carrying capacity of overhead conductors at specific ambient temperature conditions, the installation characteristics such as height and span between supports are also required, to ensure that a conductor has adequate safety and structural clearances [24,25].

The design and construction of underground cables varies significantly. For example, single-core and three-core cables are available with aluminium or copper conducting materials, which are constructed for various fault levels [26]. Underground cables are often directly buried (with or without thermal backfill); they may also be placed in conduits. The method in which specific types of underground cables are buried, together with preceding load variations, informs calculations

that determine the maximum current carrying capacity of specific underground cables, which is described in more detail in IEC standards 60853-1 and 60287-1-1 [27, 28].

The current carrying capacity of transformers connected to the electrical grid depends on preceding load variations as well as the cooling systems implemented [29]. In determining the current carrying capacity of distribution transformers connected to MV feeders, daily load profiles (Figure 2) are often considered by distribution operators. Figure 2 illustrates eight normalised daily load cycles commonly seen at distribution transformers. The load cycle or cycles illustrate:

- an industrial or commercial load cycle (top left, a)
- mixed industrial or residential load cycles (bottom left to middle, e-g)
- domestic load cycles with or without water heating (top middle to right, b-d)
- a continuous load cycle (bottom right, h).

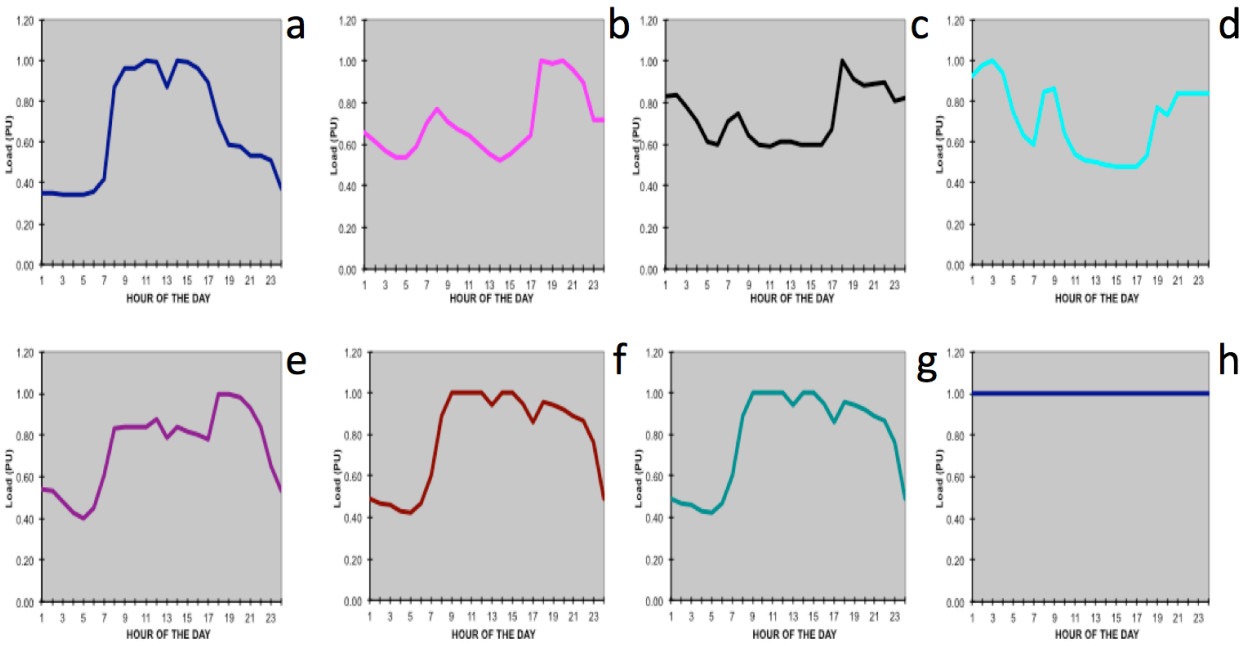

Figure 2: Typical daily load profiles as seen by a distribution transformer

The x-axis of each graph denotes the hours in a day, and the y-axis denotes the normalised load
Source: Personal communication with Ausgrid

In Figure 2(h), the continuous load cycle has a continuous rating; however, the remaining load cycles in the figure permit a higher cyclic rating to be applied to a transformer. That is, a daily load cycle that leads to a transformer cooling for a period of time results in a higher short-term (cyclic) rating.

In Table 2, continuous ratings are represented by a factor of 1; the table also presents higher cyclic rating factors that are often applied to distribution transformers. For example, if a distribution transformer has a continuous rating of 400 kVA, then a cyclic rating of 588 kVA may be applied to the transformer in cases where the daily load cycle is defined by the domestic case presented in Figure 2(b-d).

Table 2: Indicative cyclic rating factors for a single distribution transformer substation

Load cycle	Cyclic rating factor for a single transformer	Description
Industrial	1.14	Industrial Mixed predominantly industrial Commercial
Mixed	1.38	Mixed predominantly domestic
Domestic	1.47	Domestic little hot water load Domestic much hot water load
Continuous	1	Mixed predominantly domestic

Source: Personal communication with Ausgrid

Residential load cycles as seen by distribution transformers may also vary from summer to winter. Figure 3(a), which was generated from residential data provided in [30], shows that in summer the residential load profile increases throughout the day, peaking in the early evening. Figure 3(b) shows that in winter there is a morning and an evening peak. Consequently, residential cyclic rating factors applied in the electrical grid potentially vary from summer to winter.

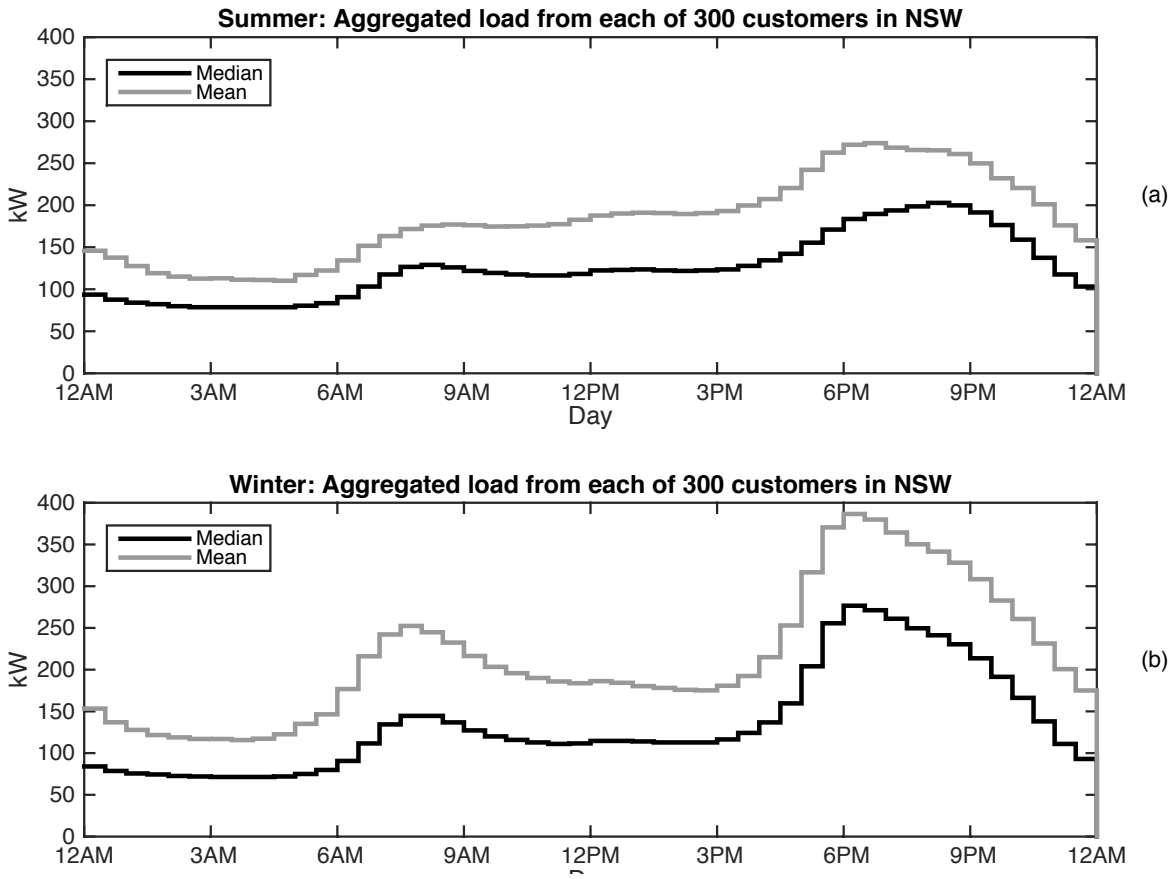

Figure 3: Aggregate residential load from 300 customers in New South Wales

NSW, New South Wales

Sources: [30,31]

5.1.4 How often do peak loads occur?

Peak loads on MV/LV distribution transformers may or may not align with peak loads in the upstream feeder, zone substation, and the transmission or subtransmission network. A domestic load cycle at an MV/LV transformer potentially leads to a peak load driven by high ambient temperatures on weekdays or weekends. In the upstream feeder, a mixed commercial–domestic load cycle potentially leads to a peak load driven by high ambient temperatures on weekdays rather than weekends. An example is given in Figure 4, wherein residential loads from 300 customers in New South Wales, Australia, are aggregated over the 3-year period from July 2010 to June 2013 [30,31]. Figure 4(a) shows a single day where the aggregate residential load exceeds 800 kW. This peak load occurred on Sunday 6 February 2011, during a heatwave in Sydney [32]. In contrast, during 2011, the peak demand across New South Wales occurred on Tuesday 1 February 2011 [33]. Peak loads that lead to capacity constraints within the distribution network are investigated by utilities on a case-by-case basis.

The frequency of peak load events varies at different locations in the distribution network. However, ambient temperature is typically a good indication of the potential for a peak load event. In particular, a very low ambient temperature or a very high ambient temperature on a weekday outside of a school holiday or a public holiday commonly coincides with peak load events in parts of the distribution or transmission network. Thus, Figure 4(b) shows that the aggregate residential load exceeds 400 kW approximately 2% of the time, and Figure 4(a) shows that the aggregate residential load exceeds 400 kW in both summer and winter. Cases where the load is zero in Figure 4 correspond to changes in daylight saving time, rather than events where no load is consumed [31].

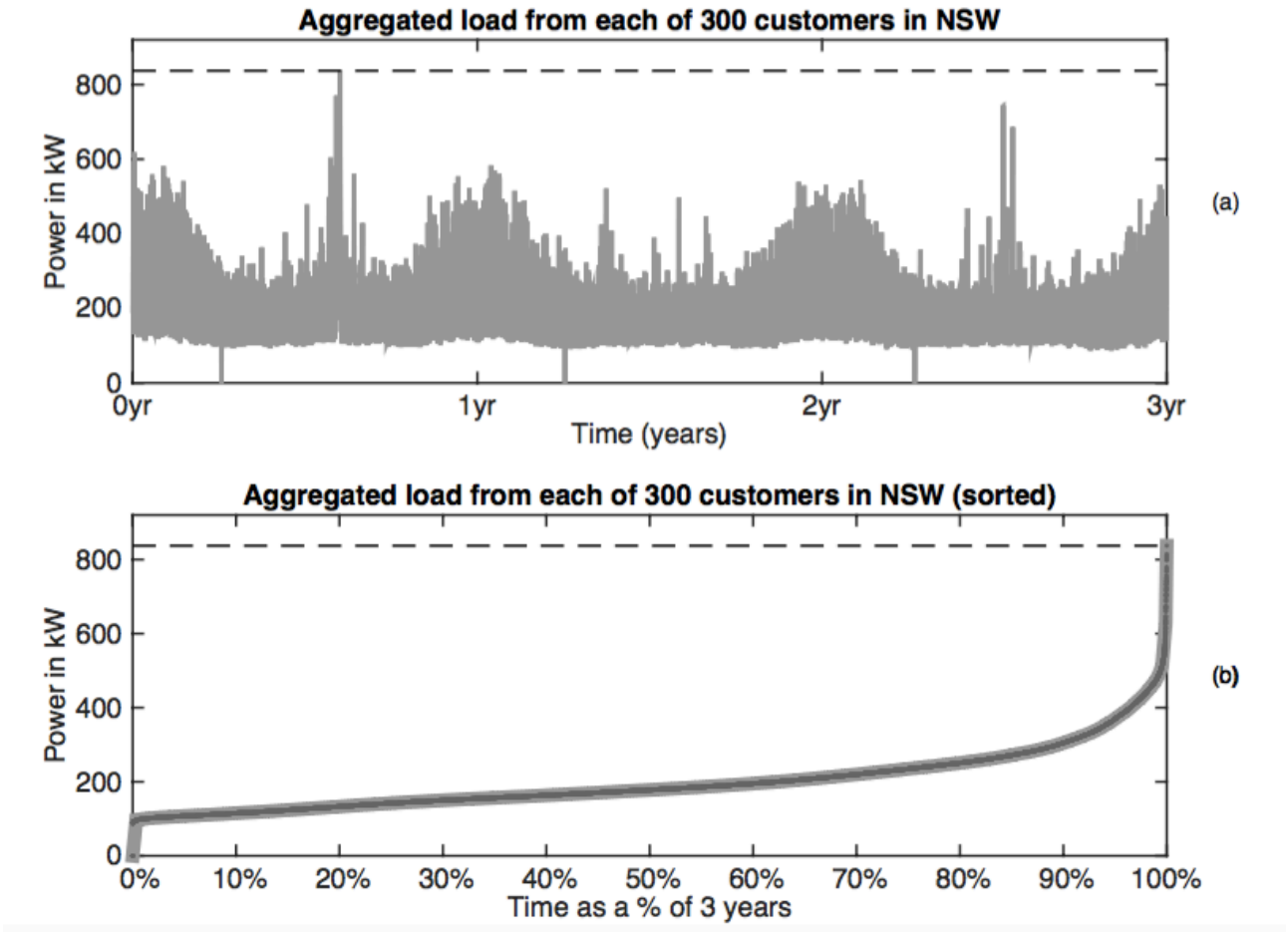

Figure 4: Aggregate residential load from 300 customers in New South Wales from 1 July 2010 to 30 June 2013

NSW, New South Wales

Sources: [30,31]

The duration of a peak load event – together with ambient or conductor or transformer winding temperatures – assists in calculations of the throughput capacity of infrastructure in the electricity grid. Peak loads that occur in summer rather than winter, over a number of hours, are more likely to lead to capacity constraints requiring remediation in the electricity grid.

5.1.5 What is the effect of significant reverse power flow from residential PV?

Traditionally, distribution networks and their voltage control and protection systems have been designed and constructed in a radial fashion, to facilitate unidirectional power flow. The primary purpose of network protection equipment is to disconnect faulty network components in order to prevent damage to plant and ensure safety to the public and network personnel. In cases with light feeder loading or high distributed generation (DG) penetration, the distribution network may need to be able to accommodate reversed (negative) power flow, which could interfere with traditional voltage and protection system designs [34]. This is particularly important in cases where MV protection systems have been designed with directional relays that may now see power flow in the opposite direction [35, 36].

Figure 5 presents aggregate residential demand from 300 customers located in New South Wales, generated from data proved by the distributor Ausgrid [30]. If these 300 customers were located

in close proximity to each other, we would see significant reverse power flow in the distribution grid, as in Figure 5 (a). Figure 5 (b) shows that this reverse power flow would occur about 20% of the time. The reverse power flow would lead to investigation of the effectiveness of existing voltage control protection schemes, with replacement schemes potentially leading to significant costs for an electrical distributor [37].

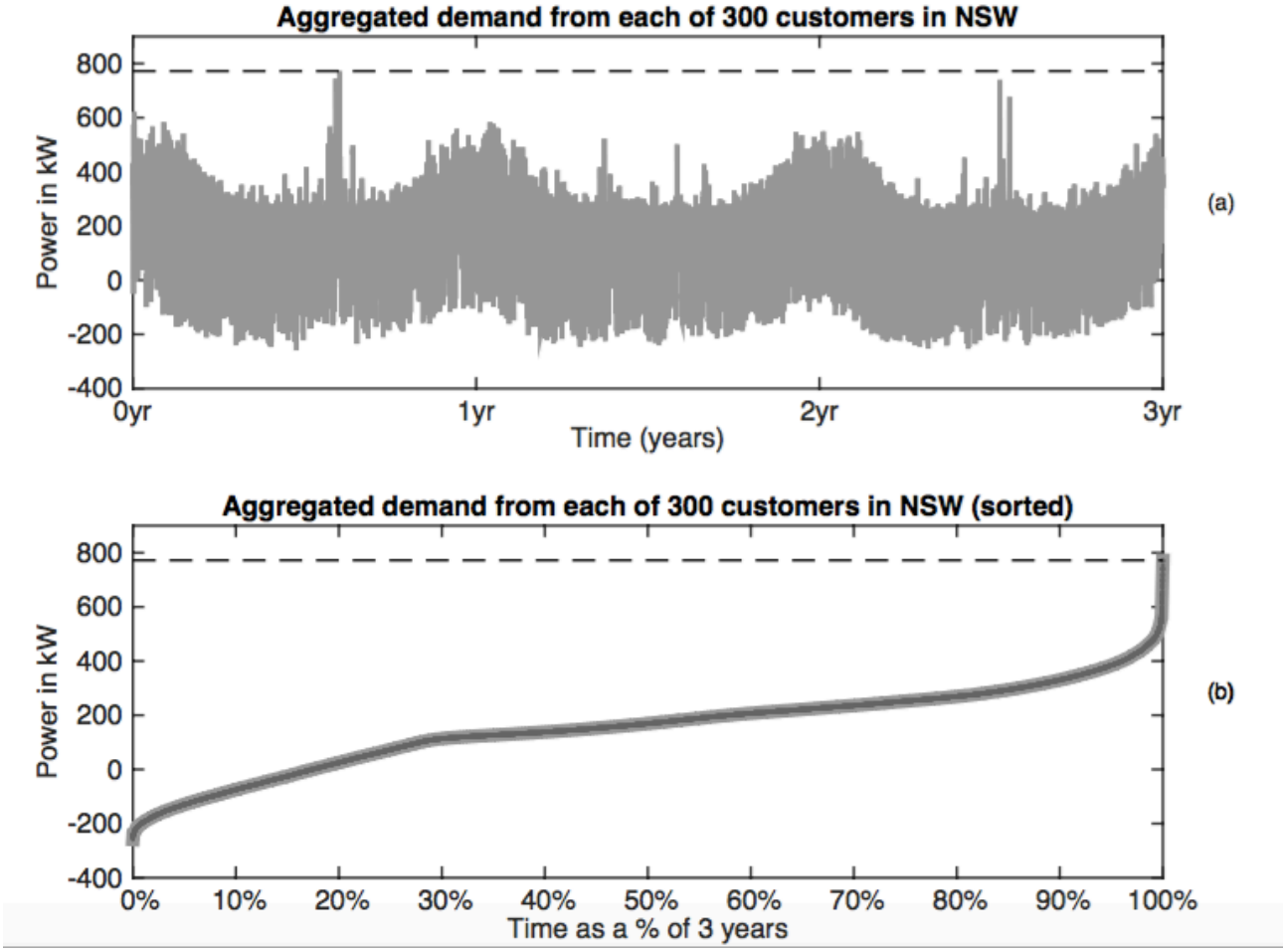

Figure 5: Aggregate residential demand (load minus PV generation) from 1 July 2010 to 30 June 2013 for 300 customers in New South Wales

NSW, New South Wales; PV, photovoltaic

Sources: [30,31]

5.1.6 Case study: batteries and network cost reduction

The introduction of high Distributed Generation (DG) penetrations together with battery storage brings opportunities to implement more adaptive design techniques (e.g. islanding) to potentially further improve the reliability performance of distribution networks (cf. Section 5.1.1). Moreover, battery storage co-located with DG potentially provides opportunities to improve the quality of the voltage supplied to customers [31, 34, 38–40], together with reducing demand that leads to capacity constraints within the electricity grid (see Sections 5.1.3, 5.1.4) [41].

Charging battery storage co-located with DG when significant reverse power flow presents in the electrical grid may also lead to cost savings for power system operators. For example, existing voltage control or protection schemes may continue to operate as traditionally designed when

excess generation from rooftop solar PV is stored in a battery (see Section 5.1.5). In contrast, end-of-line voltage measurements and associated communication infrastructure may be required by distributors when significant reverse power flow is present in the distribution grid in order to detect and mitigate either of the following:

- voltages rise outside Australian Standard AS 60038 [2]
- faults at the end of distribution feeders [37].

DNSPs will typically incur costs associated with these additional measurements, communication infrastructure, and associated control and protection schemes.

Discharging battery storage to reduce peaks in electrical demand across the grid may defer capital expenditure in the distribution or transmission grid. In cases where residential-scale battery storage is charged and discharged in order to smooth load cycle peaks and valleys across the state, steady-state ratings applied in the distribution grid may be reduced from a cyclic to a continuous rating (see Section 5.1.3). Case-by-case assessments of a distribution grid would therefore be required to determine the impact of potential rating reductions. Moreover, it is currently not possible to proscribe the optimal load profile for a distribution grid, because factors such as temperature, wind speed, overhead line construction (including high and span between conductors), cable arrangements (including thermal backfill properties), and transformer top oil temperatures are required to determine the existing capacity of a distribution grid at a point in time (as discussed in Section 5.1.3) [42].

In [41], two approaches to charging and discharging residential battery storage co-located with solar PV are proposed. Each approach seeks to limit peak demand and significant reverse power flow across a point (e.g. a zone substation) in the electricity power grid, in addition to enabling residential customers to accrue savings from battery charge or discharge schedules. Some of the results presented in [41] are considered below.

Figure 6 shows daily peaks and minimums in aggregate residential demand from 112 customers with a gross feed-in meter recording solar PV generation. Each customer is located in New South Wales, and was identified with the data obtained during the Smart Grid Smart City (SGSC) trial [43]. The figure shows 7 days in a year when residential peak demand exceeds 210 kW, a representative continuous rating for the purpose of this case study. It also shows 9 days in a year when reverse power flow exceeds 100 kW in magnitude, which potentially leads to voltage excursions outside power quality standards.

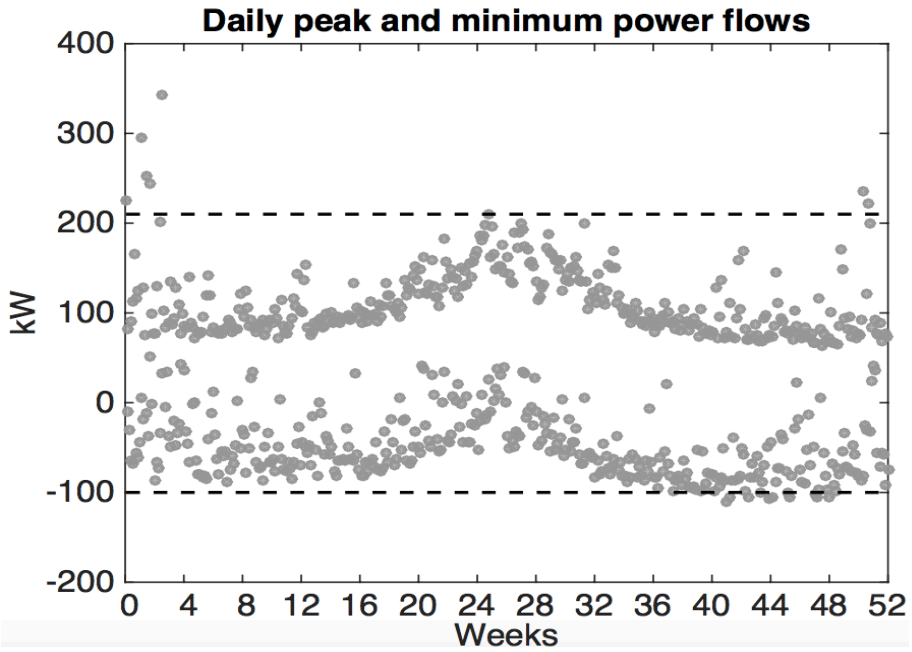

Figure 6: Aggregate residential demand for 112 customers in New South Wales, each with solar PV

PV, photovoltaic; SGSC, Smart Grid Smart City

Source: Residential load and solar PV generation data that was collected from 1 January 2012 to 31 December 2012 as part of the federally funded SGSC [41].

Two approaches to charging and discharging battery storage at each household are proposed [41] (and are included in Chapter 5 of this thesis). The objective is to reduce the aggregate peak load to 210 kW together with limiting reverse power flow to 100 kW in magnitude (e.g. a reverse power flow constraint of –100 kW is considered), in addition to permitting customers to accrue operational savings as defined in [40, 41]. The results are shown in Figure 7, wherein Figure 7(a) presents the results of the localised approach and Figure 7(b) presents the results of the centralised approach.

In the localised approach, the energy management system of each household incorporates simple directives from the utility (in the form of three weights) together with time-of-use (TOU) pricing signals when determining day-ahead battery charge and discharge schedules. The three weights balance three objectives included in the residential energy management system: increase profits, reduce reverse power flow, and reduce peak load. Using the localised approach, Figure 7(a) shows just 2 days in the year where peak demand exceeds 210 kW, and on all days reverse power flow is less than 100 kW in magnitude. In the centralised approach, the utility directly specifies the charge and discharge schedule of each residential battery, which provides improved performance in peak load reduction across the entire year, as shown in Figure 7(b). Further, in the centralised approach, TOU pricing is included in the objective function, which leads to each customer accruing operational savings from the utility-prescribed battery schedule.

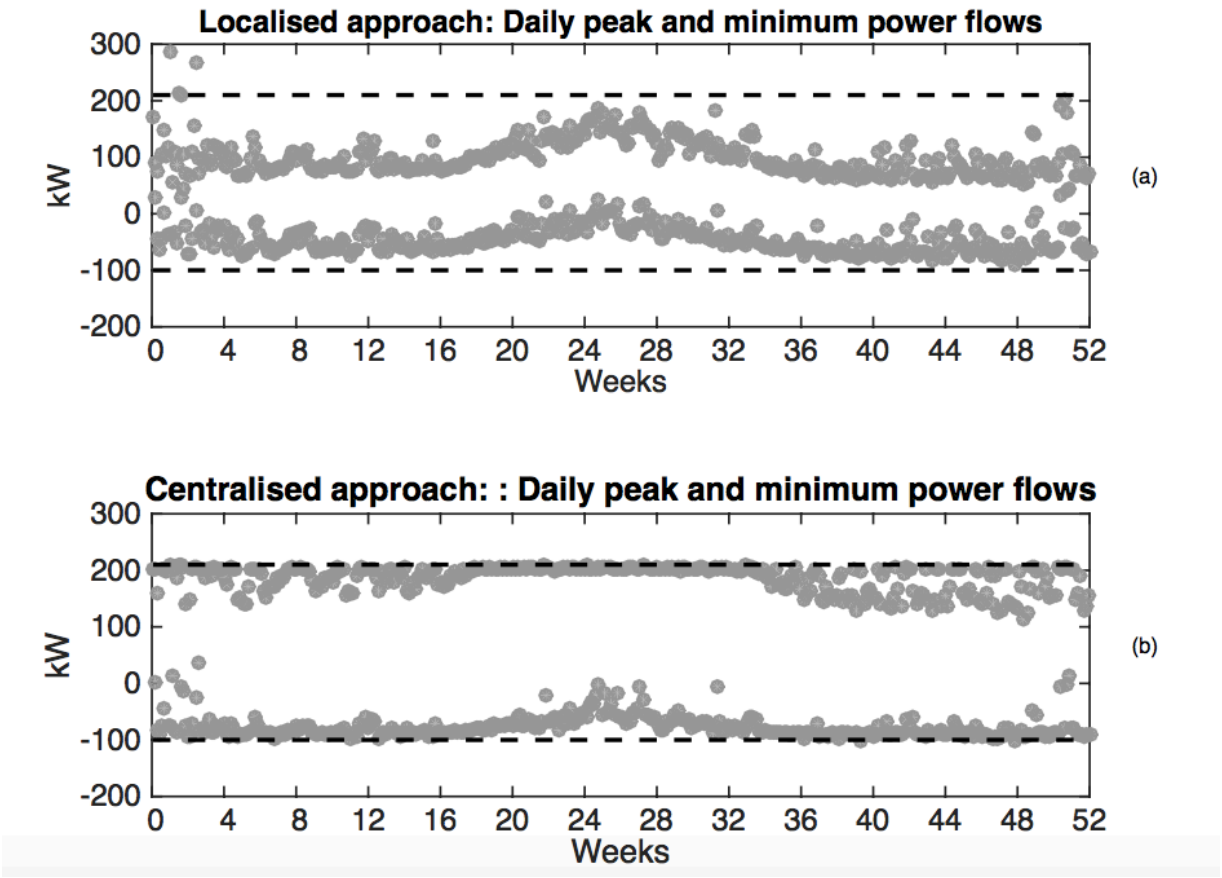

Figure 7: Aggregate residential demand for 112 customers in New South Wales when each customer installs a 10 kWh battery co-located with solar PV

PV, photovoltaic; SGSC, Smart Grid Smart City

Source: Residential load and solar PV generation data for each of the 112 customers was collected from 1 January 2012 to 31 December 2012 as part of the federally funded SGSC, and was used to generate this figure. The centralised and localised approach to scheduling the battery of each customer is described in more detail in [41].

A centralised approach to charging and discharging residential battery storage co-located with solar PV, similar to that proposed in [41], may potentially be used by distribution and transmission operators when there are capacity constraints in the electrical power grid. Such an approach demonstrates potential in deferring (indefinitely) costly investment in grid re-enforcements driven by peak demand or power quality excursions outside prescribed network limits (see Section 5.1.2). However, we cannot say whether the benefits of centrally controlling battery storage are always economically viable, given that the costs associated with increasing the electrical network capacity are case specific, as are the costs associated with alternative (demand management) approaches to peak demand reduction or power quality improvements, as outlined in [8–22].

5.1.7 Case study: batteries and demand management

This case study examines the viability of battery storage as a demand management strategy for transmission network operators. To better understand the cost-effectiveness of large-scale, grid-connected battery banks we consider three sites in close proximity to both transmission and subtransmission assets. We additionally consider a scenario where a peak demand reduction of

25 MW is required in 2020 on the transmission network that passes through Eastern Creek, New South Wales.

For the purpose of this case study, we initially identified cities that are very close to large load centres, in addition to both transmission and subtransmission assets within the NEM [44–47]. We further restrict our search to cities that are not located in central business district (CBD) locations, where the cost of land associated with installing a very large battery bank together with underground construction costs (see Table 1) are presumed to be prohibitive. Figure 8 presents an overview of all cities considered, wherein three cities in close proximity to each other are further considered based on our selection criteria. Based on observations in Google Maps, the case study substation was located in one of the selected cities, namely Eastern Creek in New South Wales.

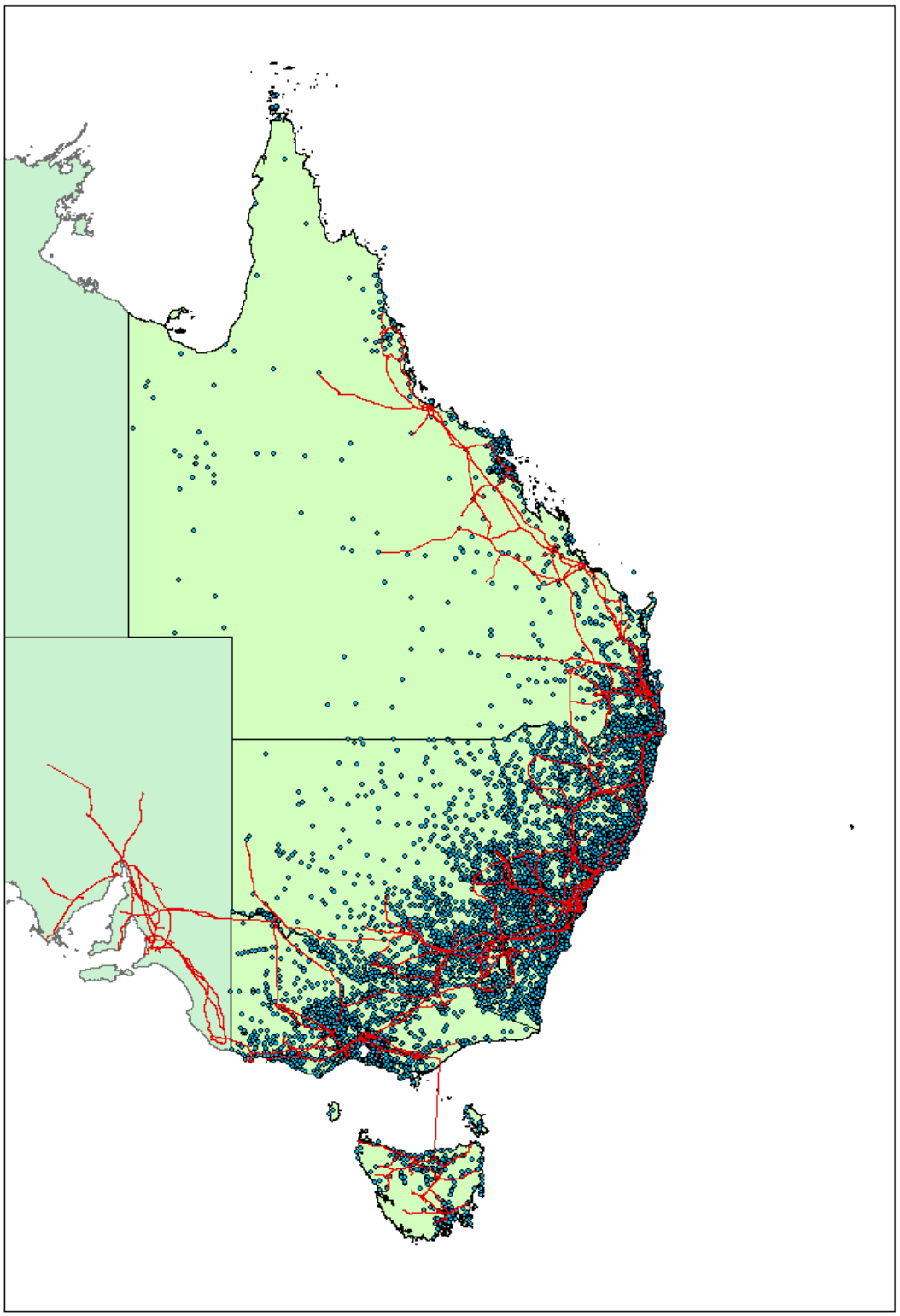

Figure 8: Each blue dot represents a city, town or place considered in this case study. The red lines represent transmission and subtransmission assets within the National Electricity Market

Sources: [44–47]

With the demand management study in [48] considered as background, we propose the following hypothetical demand management case study, where we assume the following:

- a 25 MW reduction in peak demand is required in 2020 on the transmission network in Eastern Creek, New South Wales
- Eastern Creek has a 330 kV/132 kV substation and a 132 kV/66 kV substation, each with a spare bay for connecting 330 kV, 132 kV or 66 kV, respectively
- the peak demand on the Eastern Creek transmission network typically occurs on hot summer weekdays between about 3 pm and 6 pm, on a few days in the year, and has a typical duration of 3 hours
- the expected cost to increase the capacity of the 330 kV network (by 25 MW) in Eastern Creek exceeds $200 million
- three suitable sites for a 50 MW/75 MWh battery bank have been identified close to the Eastern Creek 66 kV, 132 kV and 330 kV networks; each site covers 0.6 ha of land
- the distance from each of the three sites to a respective substation in Eastern Creek is as presented in Table 3; these distances were calculated using data provided in [44–46].

Table 3: Assumed distances (km) from each site to a 330 kW/132 kV or a 132 kV/66 kV substation in Eastern Creek

Site location	66 kV	132 kV	330 kV
Eastern Creek, NSW	1.96	1.83	1.94
Erskine Park, NSW	2.58	0.29	0.19
Horsley Park, NSW	2.82	0.02	2.86

NSW, New South Wales

Table 4 combines the distances in Table 3 with the generic construction and connection costs in Table 1 to show the cost of connecting the 50 MW/75 MWh battery bank to different voltage levels. It shows that a connection to the 66 kV in Eastern Creek costs significantly less than a connection to the 132 kV and 330 kV networks in Eastern Creek.

Table 4: Assumed cost to connect a battery bank from each site to a respective subtransmission or transmission substation in Eastern Creek

Site location	66 kV	132 kV	330 kV
Eastern Creek, NSW	$7.08 m	$11.37 m	$33.49 m
Erskine Park, NSW	$7.42 m	$10.21 m	$30.34 m
Horsley Park, NSW	$7.55 m	$10.02 m	$35.15 m

NSW, New South Wales

Table 5 shows projected minimum and maximum costs of a 50 MW/75 MWh battery bank (including inverter and land costs). Specifically, it shows the costs of an Li-ion–based battery bank and a flow battery bank in the years 2020 and 2035. The table shows a significant reduction in the cost of both battery technologies over the 15-year period, and that the cost of Li-ion technology is significantly less than the cost of flow-based technology in both 2020 and 2035.

Table 5: Assumed cost of a 50 MW/75 MWh battery bank, including inverter and land costs of 0.6 hectares (please refer to the full report for more details)

Year	Li-ion minimum	Li-ion maximum	Flow battery minimum	Flow battery maximum
2020	$35.5 m	$91 m	$100.5 m	$206.5 m
2035	$14.5 m	$46 m	$30.5 m	$74.5 m

Li, lithium

Table 6 shows the projected total cost of a 50 MW/75 MWh battery bank connected to a spare 66 kV feeder bay in an Eastern Creek subtransmission substation for the year 2020. The projected costs include a step-down transformer from 66 kV to 11 kV at each of the three sites. The table shows that a Li-ion 50 MW/75 MWh battery bank would potentially provide cost savings to a transmission operator in cases where a battery bank connection in close proximity to a 66 kV feeder bay was available. However, in 2020, a flow-based battery bank of 50 MW/75 MWh could potentially cost the transmission operator more than $200 m at each of the three site locations, as shown by the maximum costs in Table 6.

Table 6: Assumed total cost of installing and grid-connecting a 50 MW/75 MWh battery bank, including land costs of 0.6 ha, a DC/AC converter and an associated step-up transformer

Site location	Year	Li-ion minimum	Li-ion maximum	Flow battery minimum	Flow battery maximum
Eastern Creek, NSW **66 kV**	2020	$53 m	$108 m	$118 m	$224 m
Erskine Park, NSW **66 kV**	2020	$54 m	$109 m	$119 m	$224 m
Horsley Park, NSW **66 kV**	2020	$53 m	$109 m	$118 m	$224 m

DC/AC, direct current/alternating current; Li, lithium; NSW, New South Wales

The results of this case study confirm that battery storage may become a viable demand management strategy for operators of transmission or subtransmission networks. Also, the costs associated with Li-ion battery technology are rapidly decreasing; hence, managing peak demand in both transmission and distribution networks in the near future will become increasingly cost-effective with battery storage. However, costs associated with land in CBD locations, together with connection costs at transmission or subtransmission voltages, are significant. Therefore, a case-by-case demand management assessment is required to determine the cost-effectiveness of large-scale, grid-connected battery banks at different network locations. This finding is not consistent with the demand management study in [48], since battery costs in 2009 were more than $2000/kVA.

5.2 Commercial or industrial customers

5.2.2 Industrial Customers: Reducing the cost of connection

Connection costs for large industrial-sized customers depend on a number of factors, including the distance to nearby transmission or subtransmission assets, the proposed use of those assets, and any capacity constraints requiring remediation to facilitate the proposed connection. Therefore, a large industrial customer may seek to use battery storage to alleviate any capacity constraints restricting or to decrease the cost of the proposed new connection.

This section explores whether it is economically viable to install battery storage to reduce the new connection costs of a large industrial-sized customer. The economic proposition is much the same whether that customer is a load or a small generation source. Given the availability of locational data in [50], we have chosen to assume a small generation source.

We identified cities that are close to both transmission and subtransmission assets within the NEM, with data obtained from [44–47]. We further restricted our search to cities with (or proposals for) a bagasse-fired plant,[1] wind farms or solars farms, as outlined in [50, 51]. See Figure 8 for an overview of all cities considered, with further consideration of three cities in either Queensland or Victoria, based on our selection criteria.

The three cities considered with respect to reducing the cost of connecting a 30 MW wind farm or solar farm to the NEM were Beaconsfield, Queensland; Invermay Park, Victoria; and St Helens Plains, Victoria. We assumed that power quality or capacity constraints in the subtransmission network would restrict the connection of each wind or solar farm, so we further assumed that:

- the maximum output of the wind or solar farm in Queensland would be limited to 20 MW in order to connect to the 132 kV network (we therefore assumed a 30 MW connection to the 330 kV network)
- the maximum output of the wind or solar farm at each site in Victoria would be limited to 20 MW in order to connect to the 66 kV network (we therefore assumed a 30 MW connection to the 220 kV network for each site).

With the above as background, we investigated the differences in connection costs from the subtransmission to the transmission network. From these cost differences, we considered the break-even cost associated with installing battery storage at each site to limit the maximum output of the wind or solar farm to 20 MW. Table 7 presents assumed costs to connect a solar or wind farm to the electrical grid at a particular voltage. These costs assume a direct (otherwise known as a teed) connection to a nearby overhead conductor, and include protection and control cost. They do not consider customer-specific step-down transformers that would be located on the generator's site. The costs in Table 7 are estimated from the generic overhead construction costs and connection costs assumed in Table 1.

Table 7: Assumed costs to connect a wind or solar farm to a subtransmission or transmission substation

City	66 kV	132 kV	220 kV	330 kV
Beaconsfield, Qld	–	$10.5 m	–	$32 m
Invermay Park, Vic	$6.2 m	–	$23 m	–
St Helens Plains, Vic	$6.2 m	–	$27 m	–

Qld, Queensland; Vic, Victoria

Table 7 shows that a battery storage system that limits the maximum output of the wind or solar farm to 20 MW would need to cost less than:

- $21.5 m to facilitate a connection to the 132 kV network in Beaconsfield, Queensland
- $16.8 m to facilitate a connection to the 66 kV network in Invermay Park, Victoria

[1] Bagasse is the fibrous material that is left after sugarcane or sorghum stalks are crushed to extract their juice

- $20.8 m to facilitate a connection to the 66 kV network in St Helens Plains, Victoria.

Therefore, battery storage co-located with large-scale solar PV or wind farms potentially facilitates a reduction in the cost to connect to the electrical power grid. However, realising these potential savings will probably always require a detailed case-by-case assessment given the diversity of loads and generation profiles of each large industrial-sized customer.

References

[1] Australian Energy Regulator, “Electricity distribution network service providers: annual benchmarking report”, 2014.

[2] Ausgrid, “Network Standard NS238 SUPPLY QUALITY”, 2015.

[3] Energex, “Power quality strategic plan 2015–20: Asset Management Division”, 2014.

[4] Ausgrid, “Electricity network performance report 2012/2013”, 2013.

[5] Ausgrid, “Electricity network performance report 2013/2014”, 2014.

[6] The Hon Anthony Roberts MP, Minister for Resources and Energy, “Reliability and performance license conditions for electricity distributors”, 2014.

[7] Ausgrid, “Attachment 5.05: Design, reliability and performance license conditions for DNSP, Minister for Energy, Dec 2007”, AER, 2014.

[8] Independent Pricing and Regulatory Tribunal of New South Wales, “Review of capital and operating expenditure of the NSW electricity distribution network service providers – Final report”, September 2003.

[9] SKM, “Accommodating DG in the CitiPower Network”, 2009.

[10] Ausgrid, “Demand Management Screening Test: Hunters Hill 11kV capacity constraint”, 2010. [Online]. Available: http://www.ausgrid.com.au/~/media/Files/Network/Demand%20Management/Demand%20Management%202/Progress%20tracking/Screening%20tests/DMST_Hunter_Hill_11kV_Load_Transfer.pdf. [Accessed 2015].

[11] PB Associates, “Energy Australia's forward (transmission) capital expenditure requirements”, Australian Competition & Consumer Commission, 2004.

[12] Parsons Brinckerhoff Australia, “Indicative costs for replacing SWER lines”, Department of Primary Industries, 2009.

[13] Powerlink Queensland, “Final recommendation to address forecast reliability of supply requirements in 2007–2010: North and Far North Queensland,” 2005.

[14] United Energy Distribution, “Distribution system planning report 2008”, 2008.

[15] United Energy Distribution, “Distribution system planning report 2010”, 2010.

[16] Meritec, “Review of capital and operating expenditure of the NSW Electricity Distribution Network Service Providers – Final report”, Independent Pricing and Regulatory Tribunal of New South Wales, 2003.

[17] Schneider Electric, “Power and distribution transformers: Australian catalogue 2014”, 2014.

[18] SP AusNet, “Distribution system planning report 2011–2015”, 2015.

[19] Ausgrid, “Demand Management Screening Test: Establishment of SOPA 132/11kV zone substation”, 2010.

[20] CitiPower, “Consultation Paper: Brunswick Terminal Station”, 2008.

[21] TransGrid, “Demand Management Investigation Report”, 2009.

[22] Western Power, “New connections”, 2015. [Online]. Available: http://www.westernpower.com.au/residential-customers-new-connections.html. [Accessed 24 June 2015].

[23] Nexans Olex, “Aerial”, 2015. [Online]. Available: http://www.olex.com.au/Australasia/2012/OLC12641_AerialCat.pdf [Accessed 24 September 2015].

[24] "IEC 1597 Technical report: overhead electrical conductors — calculation methods for stranded bare conductors", 1995.

[25] Ausgrid, "Ausgrid NS220: Overhead design manual", 2011. [Online]. Available: http://www.ausgrid.com.au/~/media/Files/Network/Documents/NS%20and%20NUS/NS220.pdf. [Accessed 21 September 2015].

[26] Nexans Olex, "High voltage", 2015. http://www.olex.com.au/eservice/Australia-en_AU/navigate_289409/High_Voltage.html.

[27] IEC, "IEC 60853–1 International Standard: calculation of the cyclic and emergency current rating of cables. Part 1: Cyclic rating factor for cables up to and including 18/30 (36) kV", IEC, 1985.

[28] IEC, "IEC 60287–1-1: Electric cables — calculation of the current rating. Part 1–1: Current rating equations (100% load factor) and calculation of losses — General", 2014.

[29] Dynamic Ratings, "Systems technical overview", 2013. [Online]. Available: http://www.dynamicratings.com/Asia/Products/Transformers/DRPL%20TechOverview%20Rev2.pdf. [Accessed 21 September 2015].

[30] Ausgrid, "Solar home electricity data", 2014. [Online]. Available: http://www.ausgrid.com.au/Common/About-us/Corporate-information/Data-to-share/Data-to-share/Solar-household-data.aspx#.Vas6kBNCqu4. [Accessed 19 July 2015].

[31] E. L. Ratnam, S. R. Weller and C. M. Kellett, "Residential load and rooftop PV generation: an Australian distribution network dataset", International Journal of Sustainable Energy, pp. 1-20, 11 Sep., 2015.

[32] Australian Government Bureau of Meteorology, "Sydney in February 2011: 2nd warmest on record", 1 March 2011. [Online]. Available: http://www.bom.gov.au/climate/current/month/nsw/archive/201102.sydney.shtml. [Accessed 21 September 2015].

[33] Australian Energy Regulator, "State of the Energy Market 2011, Chapter 1: National electricity market". [Online]. Available: http://www.aer.gov.au/publications/state-of-the-energy-market-reports. [Accessed 24 September 2015].

[34] Energex Asset Management Division, "Power quality strategic plan 2015–20", 2014.

[35] R. A. Walling, R. Saint, R. C. Dugan, J. Burke and L. A. Kojovic, "Summary of distributed resources impact on power delivery systems", IEEE Transactions on Power Delivery, vol. 23, no. 3, pp. 1636–1644, 2008.

[36] E. Coster, J. Myrzik, B. Kruimer and W. Kling, "Integration issues of distributed generation in distribution grids", Proceedings of the IEEE, vol. 99, no. 1, pp. 28–39, Jan 2011.

[37] DGDS216 - ARUP - Microgrid Protection Research. [Online]. https://ich.smartgridsmartcity.com.au/Home/Final-Report/Technical-Compendia/Distributed-Generation-and-Distributed-Storage/Distributed-Generation-and-Distributed-Storage-Dow/DGDS216_ARUP_Microgrid_Protection_Research.aspx.

[38] E. L. Ratnam, S. R. Weller, and C. M. Kellett, "Scheduling residential battery storage with solar PV: assessing the benefits of net metering", Applied Energy, vol. 155, p. 881–891, 2015.

[39] E. L. Ratnam, S. R. Weller and C. M. Kellett, "Assessing the benefits of net metering with residential battery storage", in ASEAN – Australian Engineering Congress on Innovative Technologies for Sustainable Development and Renewable Energy, Singapore, 2015.

[40] E. L. Ratnam, S. R. Weller and C. M. Kellett, "An optimization-based approach to scheduling residential battery storage with solar PV: assessing customer benefit", Renewable Energy, vol. 75, pp. 123–134, 2015.

[41] E. L. Ratnam, S. R. Weller and C. M. Kellett, “Central versus localized optimization-based approaches to power management in distribution networks with residential battery storage”, International Journal of Electrical Power and Energy Systems, accepted for publication 2016.

[42] M. Z. Degefa, M. Humayun, A. Safdarian, M. Koivisto, R. J. Millar and M. Lehtonen, “Unlocking distribution network capacity through real-time thermal rating for high penetration of DGs”, Electric Power Systems Research, vol. 117, pp. 36–46, December 2014.

[43] Ausgrid, “Smart Grid, Smart City Information Clearing House”, [Online]. Available: https://data.gov.au/dataset/smart-grid-smart-city. [Accessed 24 September 2015].

[44] K. Orr and B. Allan, “National electricity transmission lines database”, Geoscience Australia, Canberra, 2015.

[45] OpenStreetMap© contributors, July 2015. [Online]. Available: OpenStreetMap.org. [Accessed 21 September 2015]

[46] MapCruzin.com (Copyright © 1996–2015 Michael Meuser). [Online]. http://www.mapcruzin.com/download-free-arcgis-shapefiles.htm. [Accessed 21 September 2015].

[47] Australian Bureau of Statistics, “1259.0.30.001 — Australian Standard Geographical Classification (ASGC) Digital Boundaries, Australia, July 2011”, July 2015. [Online]. Available: http://www.abs.gov.au/AUSSTATS/abs@.nsf/Lookup/1259.0.30.001Main+Features1July%202011?OpenDocument. [Accessed 21 September 2015]

[48] TransGrid and EnergyAustralia, “Demand management investigation report: Sydney inner metropolitan area”, November 2009.

[49] Frontier Economics, “Electricity market forecasts: 2015. A report prepared for the Australian Energy Market Operator (AEMO)”, 2015.

[50] Energy Supply Association of Australia (ESAA), “Electricity gas Australia 2015”, 2015.

[51] Rural Industries Research and Development Corporation, “Biomass producer: bioenergy information for Australia's primary industries”, July 2013. [Online]. Available: http://biomassproducer.com.au/case_study/maximising-sugar-mill-revenue-in-mackay/#.VaIr1BOUets. [Accessed 21 September 2015]

2

An Australian distribution network dataset

Chapter 1 investigated the economic viability of grid-connected battery storage for Australian policy makers. Chapter 1 also introduced two optimization-based approaches to scheduling residential battery storage for the purpose of peak load reduction in a distribution grid (cf. Chapter 1, Figure 7). In Part 3 of this thesis we formalize these two battery scheduling approaches.

Chapter 2 consists of the paper titled *Residential load and rooftop PV generation: an Australian distribution network dataset*, that reports a publicly available dataset of historical load and PV generation for 300 de-identified residential customers in an Australian distribution network. One of the key contributions of this paper is a detailed description of the dataset highlighting diversity in individual residential load and generation profiles, followed by an approach to identify and excise anomalous records (e.g. due to inverter failure). This dataset is used to evaluate our proposed battery scheduling algorithms in the remaining chapters of the thesis. Chapter 2 also introduces the financial policy of net metering that is defined later in Part 2.

INTERNATIONAL JOURNAL OF SUSTAINABLE ENERGY, 2015
http://dx.doi.org/10.1080/14786451.2015.1100196

Taylor & Francis
Taylor & Francis Group

Residential load and rooftop PV generation: an Australian distribution network dataset

Elizabeth L. Ratnam[a], Steven R. Weller[a], Christopher M. Kellett[a] and Alan T. Murray[b]

[a]School of Electrical Engineering and Computer Science, University of Newcastle, University Drive, Callaghan NSW 2308 Australia; [b]Independent, Newcastle, Australia

ABSTRACT

Despite the rapid uptake of small-scale solar photovoltaic (PV) systems in recent years, public availability of generation and load data at the household level remains very limited. Moreover, such data are typically measured using bi-directional meters recording only PV generation in excess of residential load rather than recording generation and load separately. In this paper, we report a publicly available dataset consisting of load and rooftop PV generation for 300 de-identified residential customers in an Australian distribution network, with load centres covering metropolitan Sydney and surrounding regional areas. The dataset spans a 3-year period, with separately reported measurements of load and PV generation at 30-min intervals. Following a detailed description of the dataset, we identify several means by which anomalous records (e.g. due to inverter failure) are identified and excised. With the resulting 'clean' dataset, we identify key customer-specific and aggregated characteristics of rooftop PV generation and residential load.

ARTICLE HISTORY
Received 2 July 2015
Accepted 11 September 2015

KEYWORDS
Solar photovoltaics; residential load; dataset; time-of-use metering; feed-in tariffs

1. Introduction

In many countries, electricity distribution operators have installed metering equipment to separately record small-scale ('rooftop') photovoltaic (PV) generation and residential load. To incentivise the installation of rooftop PV the New South Wales (NSW) state government in Australia introduced the Solar Bonus Scheme (NSW Government 2010) on 1 January 2010, wherein customers were offered generous feed-in tariffs for grid-connected PV generation. As a consequence, the NSW-based utility Ausgrid installed additional metering infrastructure at premises of each eligible customer to enable the recording of power flows from PV inverters for the purpose of calculating feed-in tariff payments.

The financial policy of 'net metering' widely adopted in the USA also incentivises grid-connected rooftop PV generation (Black 2004; Campoccia et al. 2009; Darghouth, Barbose, and Wiser 2014; Ratnam, Weller, and Kellett 2015a,b). To offer the financial policy of net metering, an electricity distributor typically installs a bi-directional meter at the premises of each eligible customer. The bi-directional meter records any PV generation in excess of residential load for the purpose of calculating net metering credits. The bi-directional meter also records any load drawn from the electricity grid (i.e. load not met by the rooftop PV generator) for the purpose of calculating net metering bills (Black 2004; Campoccia et al. 2009; Ratnam, Weller, and Kellett 2015b). In contrast, implementing the feed-in tariff proposed under the NSW Solar Bonus Scheme requires two meters to be

CONTACT Elizabeth L. Ratnam elizabeth.ratnam@ieee.org

installed at residential premises. A dedicated meter recording solar generation direct from the PV inverter and a separate meter recording residential load are installed at premises for the purpose of subsidising and billing customers, respectively. A consequence of the NSW Solar Bonus Scheme is, therefore, more complete PV generation data available for collection.

Datasets with separate (more complete) records of load and PV generation are useful in the area of forecasting supply and demand in the electricity grid. To ensure generation supply meets electricity demand and that the power supplied to customers is of a high quality, network planners, and operators rely on forecasts of both system load and generation – including distributed PV generation (Holttinen et al. 2013). However, accurate predictions of fluctuations in day-ahead PV generation at a system level is an active research topic (Hart, Stoutenburg, and Jacobson 2012; Holttinen et al. 2013; Chow, Belongie, and Kleissl 2015). For example, fluctuations in aggregate residential PV generation as observed in an upstream feeder typically arise from moving cloud cover on timescales ranging from minutes to hours (Hart, Stoutenburg, and Jacobson 2012; Chow, Belongie, and Kleissl 2015). In contrast, fluctuations in aggregate load as observed in an upstream feeder are fairly slow and predictable for the day-ahead (Hart, Stoutenburg, and Jacobson 2012). Historical datasets with separately reported measurements of PV generation potentially assist in the development of forecasting algorithms that predict PV generation from prior PV measurements.

The recent dramatic increase in grid-connected solar PV has been driven by the decreasing cost of PV panels (Bazilian et al. 2013; Lang, Gloerfeld, and Girod 2015) together with generous feed-in tariffs and/or net metering polices (Ogimoto et al. 2013; Moosavian et al. 2013; von Appen et al. 2013). In Australia, Germany, and the USA, net metering policies and/or feed-in tariffs have been available to residents in recent years. As a consequence, in Australia, there was a 480% increase in solar PV installations in a single year from 2009 to 2010, of which 99% was grid-connected (Moosavian et al. 2013). In the USA, there is more than 16 GW of installed solar PV (Kroposki and Mather 2015), up from 0.8 GW in 2010 (Kroposki, Margolis, and Lynn 2011). PV plant installations in Germany exceed 1.2 million, and as of September 2012, peak PV capacity reached 31 GW with about 70% of this capacity being connected to the low voltage grid (von Appen et al. 2013).

The uptake of residential solar PV in NSW Australia was greater than expected under the generous Solar Bonus Scheme (Independent Pricing and Regulatory Tribunal 2012). In response, the NSW state government initiated a review of feed-in tariff prices to manage the cost of the Scheme together with encouraging further adoption of renewable energy in NSW (Ausgrid 2014e; Independent Pricing and Regulatory Tribunal 2012). As a consequence of this review, Ausgrid publicly released a small sample of PV data collected for feed-in tariff payments (Ausgrid 2014e). More specifically, in 2014 Ausgrid publicly released residential PV generation and load data for a subset of 300 (de-identified) customers spanning a 3-year period from 1 July 2010. Other utilities offering feed-in tariffs potentially store data similar to that released by Ausgrid (Nykamp et al. 2013; Independent Pricing and Regulatory Tribunal 2012). Furthermore, smart grid deployments in some countries have also provided opportunities for data collection relating to solar PV generation and/or residential load (Rhodes et al. 2014; Yang et al. 2014; Quilumba et al. 2015; Pereira et al. 2015). However, the public availability and analyses of these load and generation datasets in the open literature is very limited. The Ausgrid dataset, therefore, is a valuable resource for researchers and policy-makers alike.

In this paper, we present a detailed description of the Ausgrid dataset in Section 2 with a view to facilitating use of the dataset by interested researchers.[1] The Ausgrid dataset has already been used in several research publications investigating co-locating battery storage with solar PV (Ratnam, Weller, and Kellett 2013; Keerthisinghe, Verbic, and Chapman 2014a,b; Khalilpour and Vassallo 2015; Braun et al. 2015; Worthmann et al. 2015; Ratnam, Weller, and Kellett 2015a,b), and this paper aims to serve as an archival reference for future research. In Section 3, we describe various anomalies that arise in the dataset. We remove customers with *any* anomalous data, leaving a 'clean dataset' consisting of reliable data for 54 customers for the entire 3 years covered by the dataset. It is worth noting that, for any given day, significantly more than the 54 customers in the clean dataset will have reliable data.[2] An analysis of the clean dataset is presented in Section 4.

2. Ausgrid dataset

The Ausgrid distribution network covers 22,275 km^2 and includes load centres in Sydney and regional NSW as depicted in Figure 1. The Ausgrid distribution network supplies in excess of 25,523 GWh of electricity annually to more than 1.64 million customers (2013/2014 financial year), comprised of over 1.4 million residential customers together with major industries including mining, manufacturing, and agriculture (Ausgrid 2014a). From the Ausgrid customer base, a subset of 300 residential customers were chosen as follows:

(1) Ausgrid identified residential customers with a separate meter that recorded PV generation directly from the PV inverter (i.e. customers receiving a feed-in tariff) over the period 1 July 2010–30 June 2013. Approximately 15,000 customers were included in this group (Ausgrid 2014b).
(2) From this group of around 15,000 customers, Ausgrid removed customers in the top or bottom 10% of annual household energy consumption (in kWh) or PV production (in kWh).

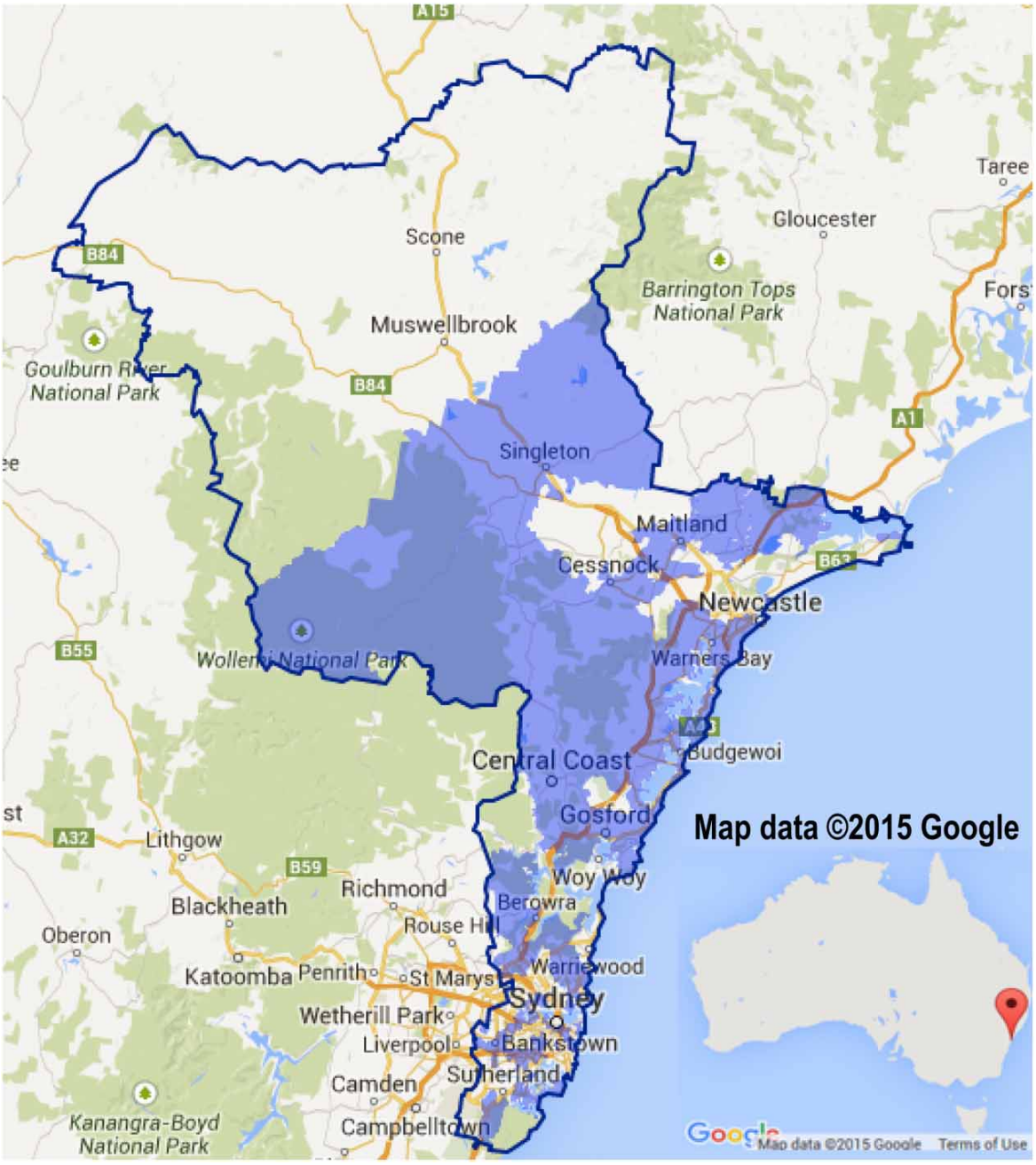

Figure 1. Outline of the Ausgrid distribution network that covers 22,275 km^2 and includes load centres in Sydney and regional NSW. Shaded regions within the Ausgrid network correspond to postcode areas included in the dataset of 300 customers (ABS 2006). Map data: ©2015 Google

(3) From the remaining residential customers, 300 were selected at random by Ausgrid.

To protect the privacy of these 300 residential customers, all personally identifiable information was removed from the Ausgrid dataset (Ausgrid 2014d). Consequently, the postcode of each customer provides the only context of geographical spread included in the Ausgrid dataset. In total, there are 100 unique postcodes in the Ausgrid dataset. The shaded regions in Figure 1 depict these 100 postcode areas within the Ausgrid boundary. Information regarding the relationship between socio-economic or demographic characteristics in the context of solar PV uptake in different areas of Australia is provided in ACIL Allen Consulting (2013).

By default, the time format in the Ausgrid dataset is Australian Eastern Standard Time (AEST), though for the summer period (approximately October–April) Australian Eastern Daylight Savings Time (AEDT) is used. For each of the 1096 days in the Ausgrid dataset (3 years from 1 July 2010), load and generation data were recorded at intervals of $\Delta = 0.5$ h duration. In what follows, we introduce terminology provided by Ausgrid in Ausgrid (2014e) that describes the daily load and generation data recorded against each of the 48 intervals of 0.5 h duration. We also introduce additional terminology, where appropriate, with a view of facilitating use of the Ausgrid dataset by interested researchers.

2.1. *Residential load and generation data*

The Ausgrid dataset includes information on the installed capacity for each of the 300 residential-scale rooftop solar PV units (in kilowatt-peak kWp). The solar PV generation data for each customer in the Ausgrid dataset is obtained with a meter installed to measure solar generation for feed-in tariff payments.

The meter recording solar generation operates in gross metering mode, in which power flow measurements are recorded in a single direction (e.g. from the PV inverter) (Ratnam, Weller, and Kellett 2015a). In the Ausgrid dataset, residential PV generation (in kWh) is referred to as *Gross Generation* (GG), recorded at the conclusion of each half hour interval. More specifically, each customer in the Ausgrid dataset has 48 GG entries on each day, where each entry represents the energy produced by the PV panel over the preceding half hour, as seen by the meter. We denote by $\mathrm{gg}(j)$ the conversion of the daily half hour interval GG entries, to an average power (i.e. PV generation in kW) over the half hour period $((j-1)\Delta, j\Delta)$, where j denotes a time index.

A separate meter operating in gross metering mode is located at each residential premises to measure and record energy consumption. Residential energy consumption is billed according to a time-of-use or an inclining block rate, where each customer selects their respective preference (Ausgrid 2014c). In the Ausgrid dataset, residential energy consumption (in kWh) is referred to as *General Consumption* (GC), recorded at the conclusion of each half hour interval. More specifically, each customer has 48 GC entries on each day, where each entry represents the energy consumed by the customer over the preceding half hour. We denote by $\mathrm{gc}(j)$ the conversion of the daily half hour interval GC data to an average power (i.e. load in kW) over the half hour period $((j-1)\Delta, j\Delta)$, where j denotes a time index.

A third meter that measures and records *Controllable Load* (CL) associated with water heating is located in 137 of the 300 residential premises. That is, 137 of the 300 residents in the Ausgrid dataset allow the utility to control their all-electric-heated water systems for periods in the day (in a manner that ensures minimal impact to the network) given a financial incentive. The two financial incentives offered to customers are referred to as an off-peak 1, or an off-peak 2 tariff. The off-peak 1 tariff is offered to customers that allow the utility to switch 'off' their all-electric-heated water systems for 18 h per day. The more expensive off-peak 2 tariff is offered to customers that allow the utility to switch 'off' their all-electric-heated water systems for 8 h per day. While the precise tariff is not shown in the dataset, customer-specific switching times associated with off-peak 1 and off-peak 2 tariffs may be inferred in the CL dataset, where residential CL data (in kWh) is recorded after each half hour interval on each day. We denote by $\mathrm{cl}(j)$ the conversion of daily half hour interval CL data, to an average power (i.e. load in kW) over the period $((j-1)\Delta, j\Delta)$, where j denotes a time index.

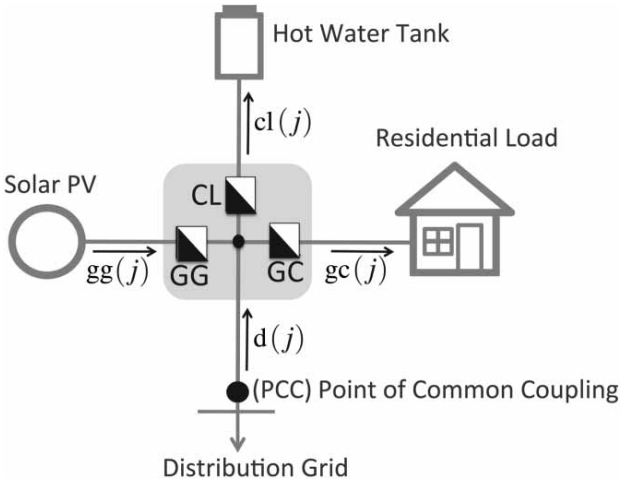

Figure 2. Residential system illustrating the direction of positive power flows and meters recording gross generation (GG), general consumption (GC), and controllable load (CL) consumption. Arrows associated with gg(j), gc(j), cl(j) , and d(j) illustrate the direction of positive power flow, and j denotes a time index. Power flows against the direction of the arrow associated with d(j) are, therefore, negative. The meters in the shaded region are co-located at residential premises.

The meter recording CL is co-located with the meters recording GG and GC, depicted by the shaded region in Figure 2. The demand or average power flow (in kW) from (to) the grid to (from) the residential system over the period $((j-1)\Delta, j\Delta)$ is denoted by $\mathrm{d(j)} > 0$ ($\mathrm{d(j)} < 0$), where j is a time index. The power balance equation for the residential energy system depicted in Figure 2 is

$$\mathrm{d(j)} = \mathrm{gc(j)} - \mathrm{gg(j)} + \mathrm{cl(j)}, \tag{1}$$

which must hold for all time indices j.

Note that customers that do not have a controllable load do not have a meter recording CL data. In this case, the power balance equation in Equation (1) reduces to $\mathrm{d(j)} = \mathrm{gc(j)} - \mathrm{gg(j)}$ for all j.

A summary of the key Ausgrid dataset parameters is included in Table 1. The consumption category in Table 1 is consistent with terminology provided by Ausgrid (2014e).

2.2. *Daylight saving time*

We present observations when moving from AEST to AEDT (or vice versa). This time change is commonly referred to as the start (or end) of 'daylight saving time'. On 3 October 2010 (the start of daylight saving time), we observe 0 entries from 2 am to 3 am in the respective GC and CL fields. Further, PV generation (in the GG field) is time-shifted back an hour. On 3 April 2011 (the end of

Table 1. Key Ausgrid dataset parameters.

Area of the Ausgrid network	22,275 km^2
Number of customers	300
Number of unique postcodes	100
Date: 1 July 2010 to the 30 June 2013	1096 days
Time format	AEST or AEDT
A single day: T	24 h from midnight
Number of daily intervals: s	48
Interval period: Δ	$\Delta = T/s = 0.5$ h
Generator capacity (in kWp)	Tested capacity of each PV unit
Consumption category: CL (in kWh)	Controllable load consumption
Consumption category: GC (in kWh)	General consumption
Consumption category: GG (in kWh)	Gross generation
Number of customers with CL data	137
Number of customers with GC data	300
Number of customers with GG data	300

daylight saving time), we do not observe an extra hour of data in any of the data-fields, GG, GC, CL, respectively. We therefore assume that turning back the clock over-writes the previous hour of data.

During October of each year, CL data entries vary due to the commencement of daylight saving time. On 4 October 2010, the hot water systems of some customers are switched on an hour later, others are not. On the last week of October, some of the CLs are switched on an hour earlier, consistent with the commencement in daylight saving time prior to 2007.[3] We recommend CL switching times be inferred from the CL data on each day, for each customer. When approximating these switching times, note that each CL is switched 'on' minutes or hours apart in a manner that ensures minimal impact to the network.

3. Clean dataset: methodology

In principle, the dataset in the previous section consists of load and generation data for each of 300 customers at 30-min resolution for a 3-year period. In practice, however, several factors exist which lead to anomalous measurements in the dataset (e.g. when a PV inverter fails). In this section, we describe how these anomalous measurements are identified and subsequently excised, producing a 'clean dataset'. Moreover, our approach is very conservative as we place a higher value on the quality of the clean dataset rather than the quantity of data records. Further work to qualify anomalous data records removed in this section is certainly possible.

3.1. *Residential load: GC*

We remove customers with anomalous load recordings on any day in a 3-year period that potentially arise when customers go on holidays and disconnect (i.e. switch off) most appliances. More specifically, we remove customers with a maximum load less than 6 W on any day of the year (i.e. any day where $\mathrm{gc}(j) < 0.006$ for all $j = 1, \ldots, s$). Customers removed often have data suitable for analysis on many days of each year, but not all. The customers removed based on this criterion are presented in Table 2.

In Figure 3, we present a small sample of days that contributed to four of the seven customers being removed from the Ausgrid dataset. That is, each subplot in Figure 3 corresponds to one of the four customers, where the daily load of each customer is presented on three separate occasions.

In Figure 3(a) and 3(c), we observe that Customer 9 and Customer 221, respectively, have days where no load is recorded. In contrast, Customer 191 and Customer 229 in Figure 3(b) and 3(d), respectively, have days with very low load recordings (i.e. 2 W). These daily low load (or no load) recordings potentially indicate that a customer is on holidays on the respective day.

The residential load of the remaining 293 customers is presented in Figure 4 in an aggregated form. We sum the load $\mathrm{gc}(j)$ of each customer with reference to time index j, and we repeat this process for each time index j on each of the 1096 days, with the results presented in Figure 4(a). Each year in Figure 4(a) (on the x-axis) denotes 365 days (or 366 days during a leap year) from 1 July of the previous year. To present a load duration curve, we sort the aggregated data presented in Figure 4(a) across the complete set of 1096 days, which is depicted in Figure 4(b).

In Figure 4(a), we observe a peak load of 828 kW, which occurs during the 2010–2011 summer. This peak occurred during the first week in February 2011, one of the warmest days (i.e. high ambient temperatures) on record in Sydney (Australian Government Bureau of Meteorology 2011). During the 2012–2013 summer, the peak load in Figure 4(a) is 730 kW, which is again significantly greater than the winter peaks of each year. We also observe three occasions where the aggregated load is zero, consistent with the change from AEST to AEDT. In Figure 4(b), we observe that the aggregate load is below 400 kW at least 98% of the time.

Table 2. Anomalous load data: Customer ID.

Customer ID	9	121	150	191	221	229	260

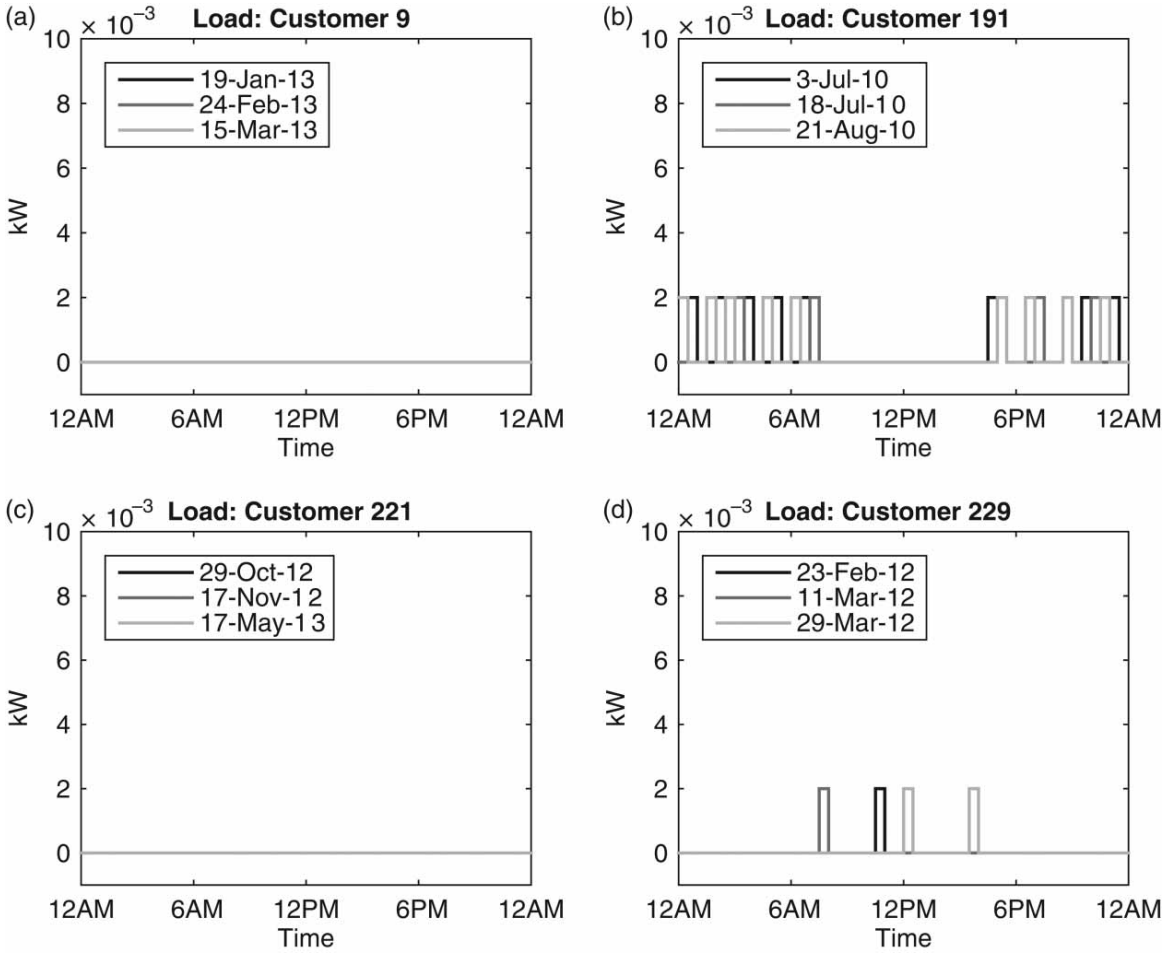

Figure 3. Example days and associated load consumption contributing to the removal of four customers from the Ausgrid dataset.

3.2. *Residential generation: GG*

In this section, we remove customers with anomalous generation recordings on any day in the 3-year period. Each customer removed often has data suitable for analysis on many days of each year, but not all. Customers removed have PV generation data that falls into one of the following three categories:

- Category 1 includes customers with a maximum generation less than 0.06 kW on any day of each year (i.e. any day where $\mathrm{gg}(j) < 0.06$ for all $j = 1, \ldots, s$). Data removed by this category potentially arise when PV inverters fail, or generation production is very low. A consequence of this category is the removal of 209 customers from the Ausgrid dataset.
- Category 2 includes customers with a daily generation less than 0.325 kWh and a maximum generation less than 0.101 kW on any of the 1096 days (i.e. any day where $\mathrm{gg}(j) < 0.101$ for all $j = 1, \ldots, s$, and $\mathrm{gg}(1) + \cdots + \mathrm{gg}(s) \leq 0.65$ kW). Data removed by this category potentially arise when daily PV generation profiles fall below a threshold whereby there is significant uncertainty regarding the quality of the data. Further work to confirm the quality of data removed by this category is certainly possible. A consequence of this category is the removal of 191 customers from the Ausgrid dataset, of which 36 customers are in addition to those customers identified in Category 1.
- Category 3 includes customers that generate more than 0.02 kWh during the early morning before 5 am on any day of each year (i.e. any day where $\mathrm{gg}(1) + \cdots + \mathrm{gg}(10) > 0.04$ kW). Data removed by this category potentially arise when measurement errors exist.[4] A consequence of this category is the removal of six customers from the Ausgrid dataset, of which one customer (ID 248) is in addition to those customers identified with Categories 1 and 2.

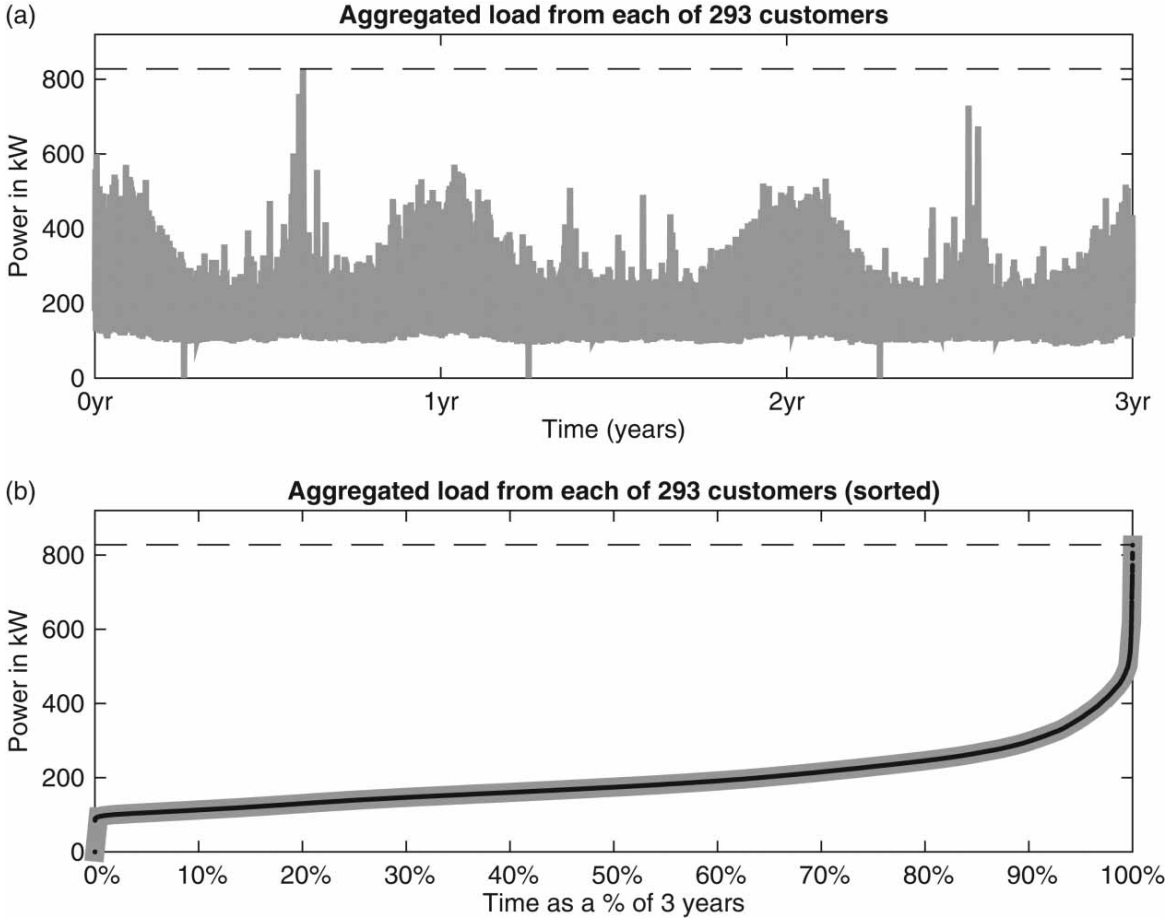

Figure 4. Aggregated load of 293 customers over 1096 days: (a) the aggregated load is presented chronologically from 1 July 2010 and (b) the aggregated load is sorted to obtain the load duration curve.

We present a small sample of days that contributed to 4 of the 246 customers being removed from the Ausgrid dataset. Each subplot in Figure 3 corresponds to one of the four customers, where the daily generation of each customer is presented on three separate occasions.

In Figure 5(a), we observe that Customer 1 has days where no generation is recorded, and these days were identified via a Category 1 removal. In Figure 5(c), we observe that Customer 215 has days where very little generation is recorded, and these days were identified via a Category 2 removal. In contrast, both Customer 145 and Customer 248 have days with a very small amount of generation recorded in the early morning before 5 am, and these days were identified via a Category 3 removal. A careful examination of Figure 5(b) and 5(d), respectively, is required to observe the very small amount of PV generation recorded in the early morning before 5 am for both Customer 145 and Customer 248.

The *clean dataset* (defined later in Section 3.4) includes the PV generation and GC of the remaining 54 customers. That is, 54 customers did not present load or generation abnormalities as outlined above. The aggregate PV generation of these 54 customers is presented in Figure 6(a), where each year on the x-axis denotes 365 days (or 366 days during a leap year) from 1 July of the previous year. More specifically, in Figure 6(a), we sum the generation $\mathrm{gg}(j)$ of each customer with reference to time index j, and we repeat this process for each time index j on each of the 1096 days. In Figure 6(b), we sort the aggregated generation in Figure 6(a) across the complete set of 1096 days.

We observe PV generation peaks at approximately 110 kW during each summer period in Figure 6(a). We observe in Figure 6(b), the PV units generate electricity 45% of the time (or do not generate power 55% of the time), consistent with the daily variability of solar irradiance.

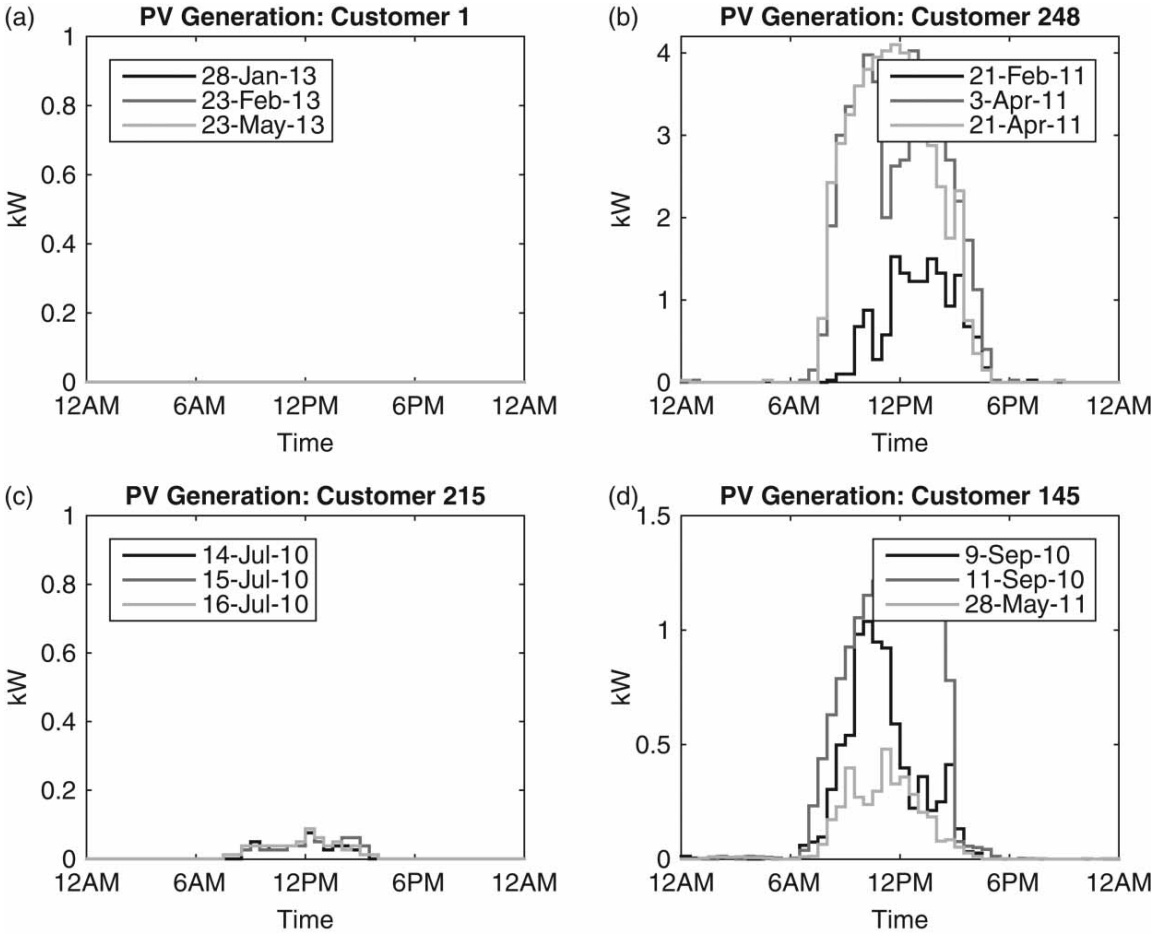

Figure 5. Example days and associated PV generation contributing to the elimination of four customers from the Ausgrid dataset.

3.3. *Controllable load*

In identifying the clean dataset, we ignored anomalous CL data. In this subsection, we look to assist the interested researcher seeking to identify anomalous CL data in the Ausgrid dataset.

The removal of utility controlled all-electric heated water systems often occurs when a customer upgrades to a gas-heated, solar-heated, or a heat pump water system. Customers that potentially remove utility controlled all-electric heated water systems are identified in the Ausgrid dataset via the CL field. That is, days where a customer allows a utility to control their all-electric heated water systems are identified via the presence of a daily CL field, and days where a customer removes permission for a utility to control their all-electric heated water systems are identified via the absence of a daily CL field. In the Ausgrid dataset, 11 customers with a daily CL field on a fraction of the 1096 days listed are included in Table 3.

Two additional customers not listed in Table 3 have potentially removed a utility controlled all-electric heated water system. That is, on each day no data are recorded against the CL field of Customer 37 and Customer 281 (with the slight exception of a single half hour interval entry for customer 37 on a single day). Hence, at least 13 customers have anomalous CL data in the Ausgrid dataset.

Further analysis to clean the CL dataset is certainly possible. For example, residential customers potentially reduce or increase the period of time a utility switches 'off' their all-electric heated water systems. This change in preference is reflected in the off-peak tariffs offered to residential customers.

Table 3. CL change: Customer ID.

ID	27	68	95	161	187	248	272	284	289	293	294

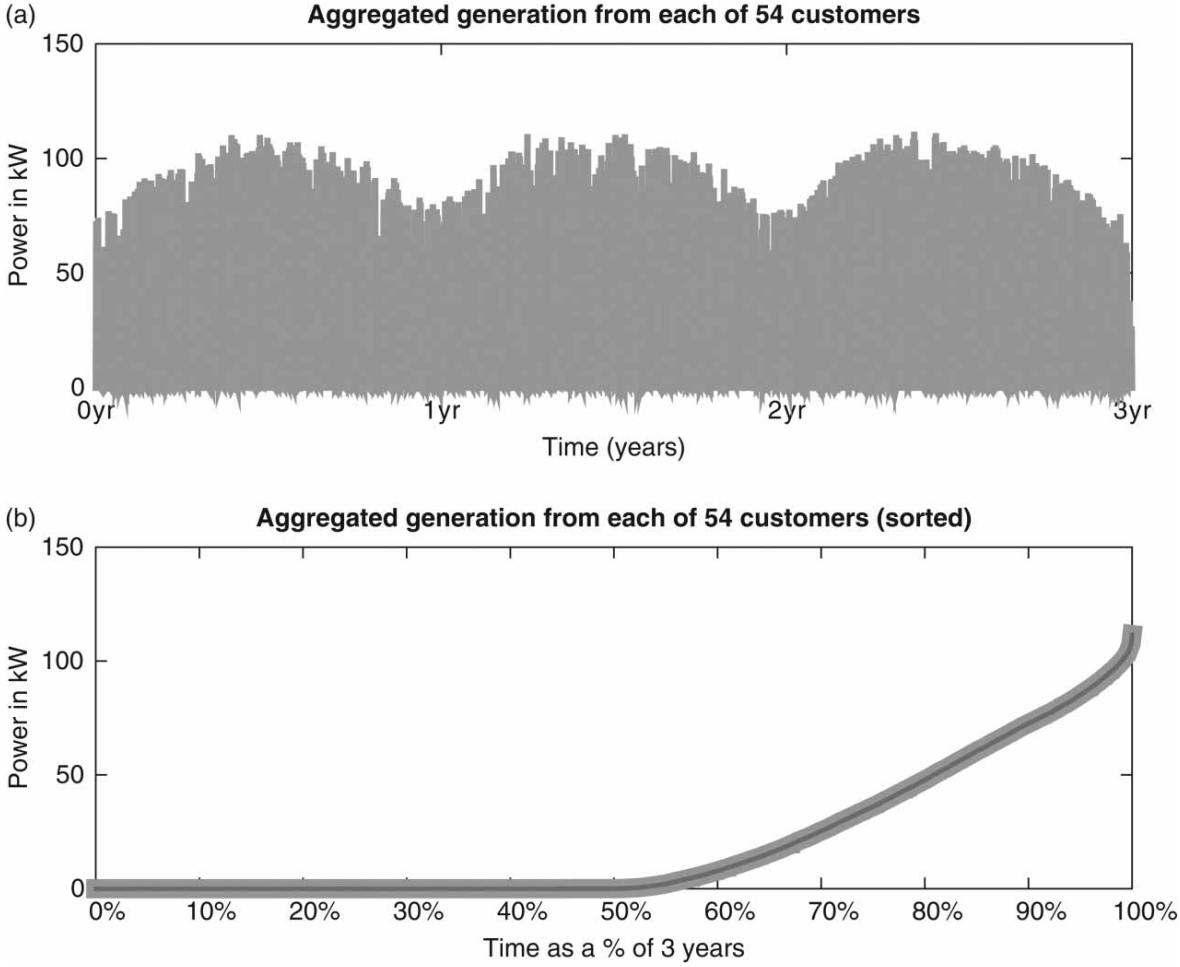

Figure 6. Aggregated generation of 54 customers over 1096 days: (a) the aggregate generation is presented chronologically from 1 July 2010 and (b) the aggregated generation is sorted to obtain the generation duration curve.

A change from an off-peak 1 to an off-peak 2 tariff (or vice versa) potentially leads to anomalous CL data within the Ausgrid dataset.

3.4. *Customer ID and location*

We define the *clean dataset* as the subset of 54 customers (from the total of 300), which are free of both load anomalies and PV generation anomalies. Note that 7 of the 300 customers had both load anomalies and PV generation anomalies. Customer 161 (cf. Table 3) is included in the clean dataset since we do not remove customers with anomalous CL. Customer 2 is included in the clean dataset since no anomalous load or generation recordings were identified; however, we note that from 12 October 2012 to 31 December 2012, data recordings were missing for this particular customer. We present the 28 postcode regions containing these 54 customers in Figure 7. The ID of each customer included in the clean dataset is presented in Table 4. In Figure 7, we observe that the majority of customers in the clean dataset are located in urban regions. Further, postcodes with smaller areas denote regions with higher population densities.

4. Clean dataset: analysis

In this section, we identify key characteristics of the clean dataset. We investigate aggregated demand, daily residential load and daily residential PV generation, and the orientation of 'rooftop' PV panels.

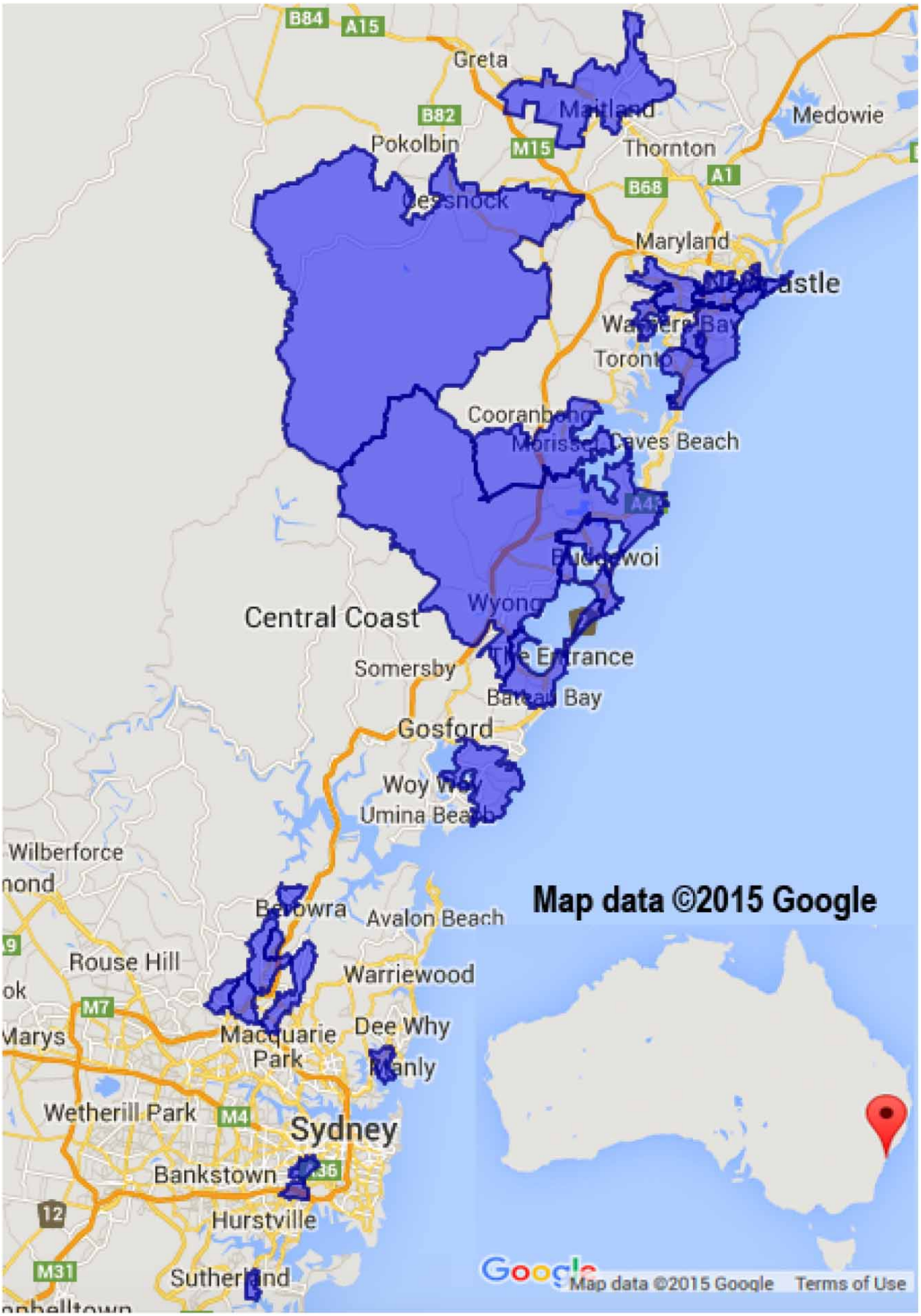

Figure 7. Each customer in the clean dataset belongs to a postcode region highlighted (ABS 2006). Map data: ©2015 Google

Table 4. Customer IDs in the clean dataset.

2	13	14	20	33	35	38	39	56
69	73	74	75	82	87	88	101	104
106	109	110	119	124	130	137	141	144
152	153	157	161	169	176	184	188	189
193	201	202	204	206	207	210	211	212
214	218	244	246	253	256	273	276	297

4.1. *Aggregated analysis*

The residential demand of 54 customers included in the clean dataset is presented in Figure 8 in an aggregated form. In Figure 8(a), we sum the demand d(j) of each customer with reference to time index *j*, and we repeat this process for each time index *j* on each of the 1096 days. Each year on the *x*-axis commences on 1 July. In Figure 8(b), we sort the aggregated demand across the complete set of 1096 days.

In Figure 8(a), we observe the peak aggregated demand is 185 kW during the 2010–2011 summer. During the 2012–2013 summer, the peak aggregated demand is greater than the winter aggregated peak of each year. Aggregated negative demand that arises from surplus PV generation peaks at 85 kW. In Figure 8(b), we observe that the duration of the summer aggregated peak is less than 2% of the time, and aggregated negative demand (from surplus PV generation) occurs 23.4% of the time.

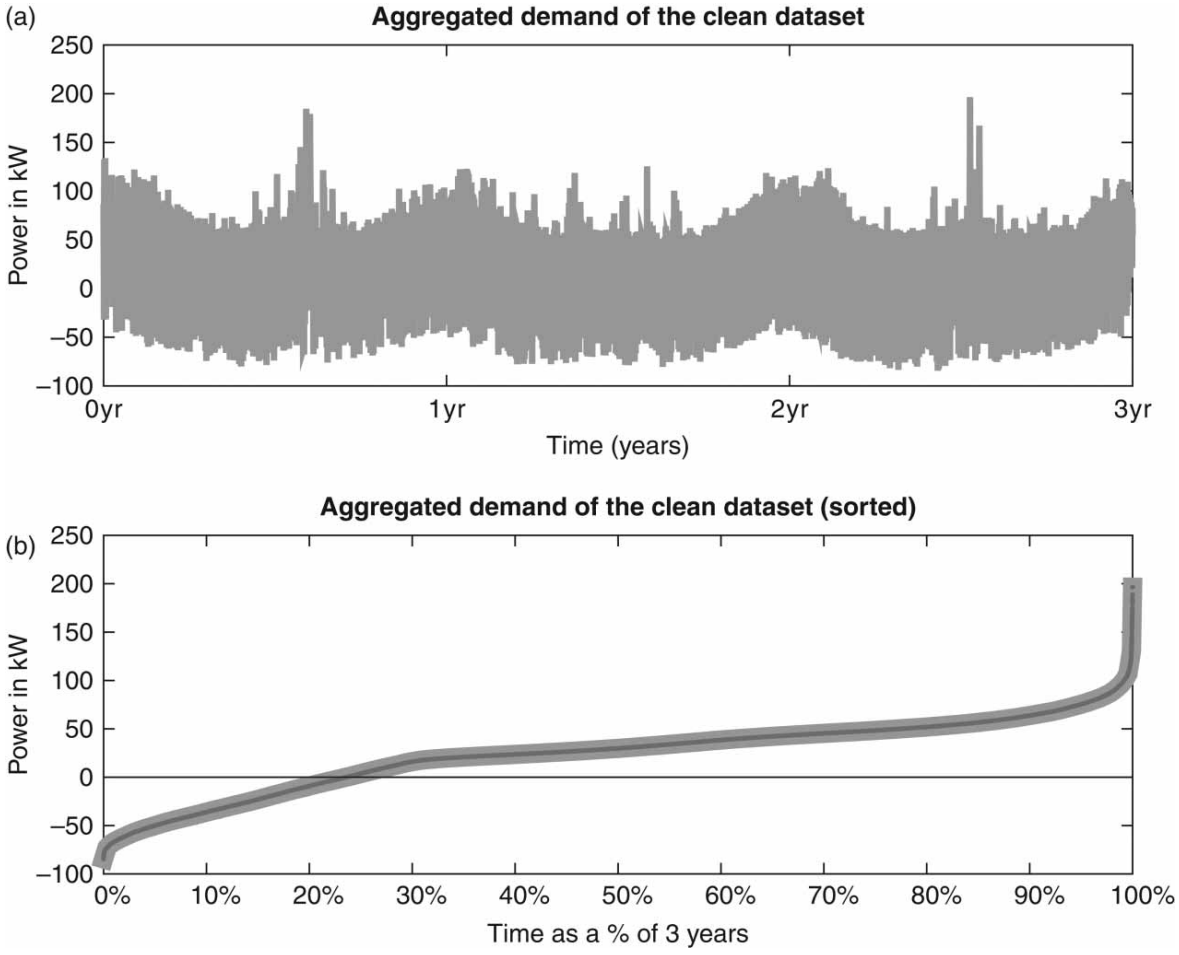

Figure 8. Aggregated demand of 54 customers over 1096 days: (a) the aggregate demand is presented chronologically from 1 of July 2010 and (b) the aggregated demand is sorted to obtain the demand duration curve.

To present the aggregated data in another form, we consider daily aggregate load and generation profiles, respectively, for each of the 54 customers in the clean dataset. In Figure 9, we present the daily mean and median aggregated generation profiles for summer and winter, respectively, with error bars that indicate one standard deviation about the mean. All references to standard deviation refer to one standard deviation ($\pm 1\sigma$) about a mean aggregate generation profile, or a mean aggregate load profile, where the context will make clear the intended meaning.

In Figure 9(a), we observe that the summer median aggregated generation is slightly greater than the summer mean aggregated generation during peak PV production (i.e. 85.3 kW compared to 76.7 kW). The summer PV generation occurs between 6.30 am and 7.30 pm. Also, the standard deviation in Figure 9(a) increases as PV production increases, highlighting that many days are impacted by cloud cover.

In Figure 9(b), we observe that the winter median aggregated generation profile is slightly greater than the winter mean aggregated generation profile during peak PV production (i.e. 72.7 kW compared to 62.3 kW). The winter PV generation occurs between 7 am and 5 pm. The standard deviation in Figure 9(b) increases as PV production increases. Thus, the results in Figure 9 are consistent with the availability of solar irradiance, which is greater in summer than winter and variable on each day.

In Figure 10, we present the daily mean and median aggregated load profile for summer and winter, respectively, with error bars that indicate one standard deviation about the mean. In Figure 10(a), we observe that the summer mean aggregated load is slightly greater than the summer median aggregated load during evening peak (i.e. 61.6 kW compared to 53.7 kW). Also, the summer residential load often peaks between 6 pm and 6.30 pm. The standard deviation in Figure 10(a) increases

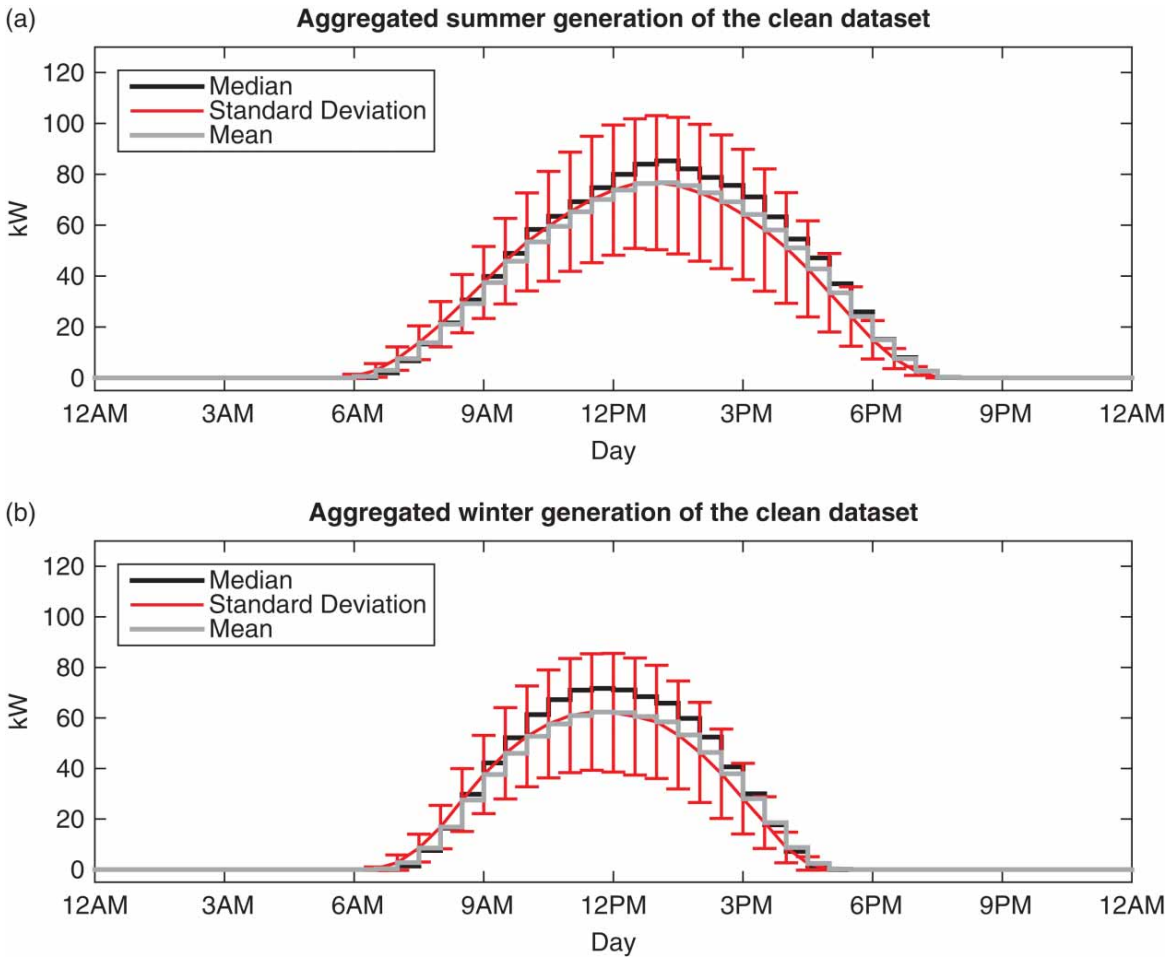

Figure 9. Aggregated generation: mean and median with error bars that indicate one standard deviation about the mean in (a) summer and (b) winter.

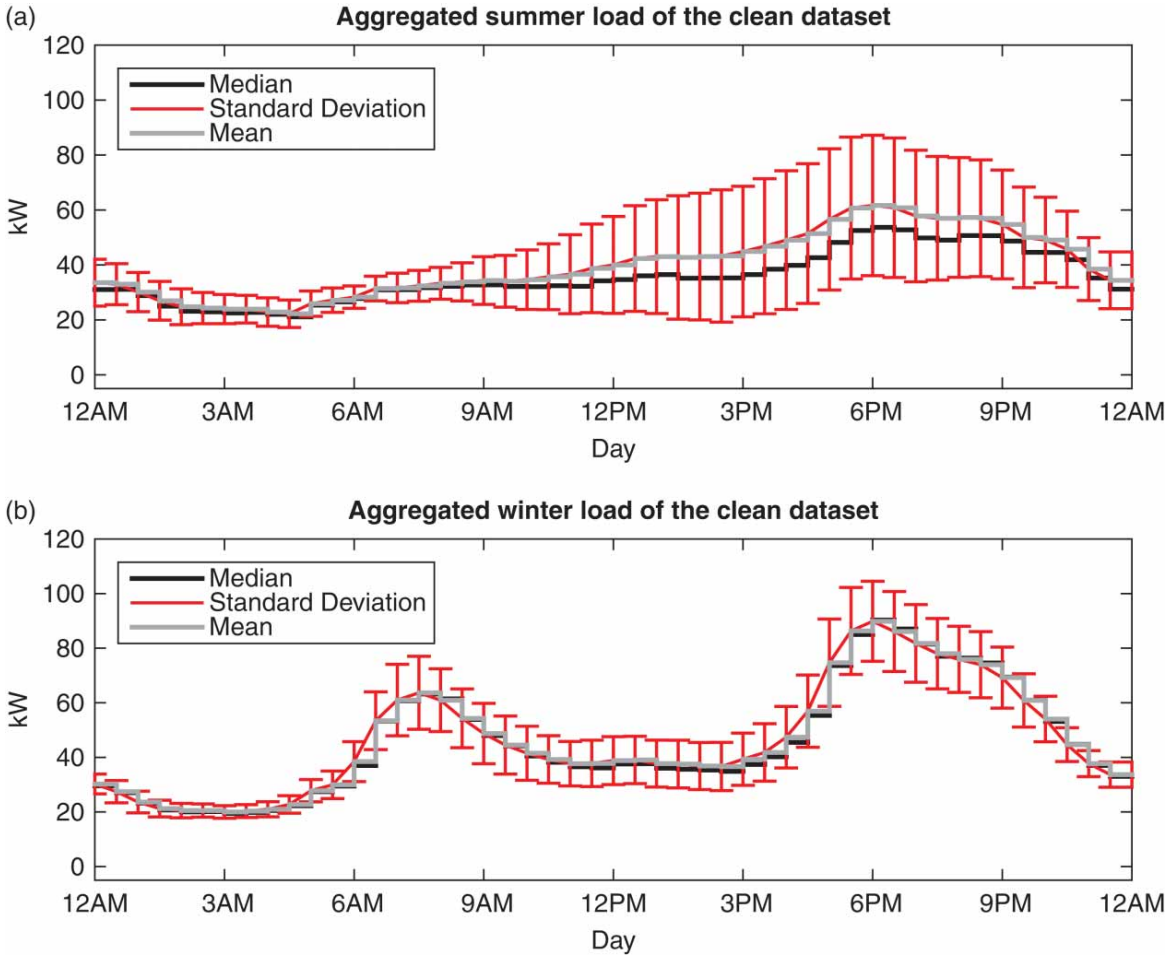

Figure 10. Aggregated load: mean and median with error bars that indicate one standard deviation about the mean in (a) summer and (b) winter.

from 9 am until the early evening when mean aggregate load peaks. In Figure 10(a), we observe that residential load from midnight till 9 am more closely corresponds to the time-of-day, since the standard deviation during this period is small.

In Figure 10(b), the winter mean aggregated load is slightly greater than the winter median aggregated load during the evening peak (i.e. 90.3 kW compared to 89.9 kW). We observe that residential loads often peak between 6 pm and 6.30 pm in winter. From midnight till 5 am, and from 10 am until midnight, the standard deviation in winter is clearly less than the standard deviation in summer, highlighting residential loads in winter are more closely tied to the time-of-day during periods outside the morning peak. Also, peak winter loads on most days are typically (but not always) larger than peak summer loads. Recall, in Figure 8(a) the peak aggregated demand often occurred in summer.

4.2. *Residential analysis*

In Section 4.1, we analysed aggregate load and generation profiles for the clean dataset. In this section, we investigate daily residential load and PV generation variability for a small number of customers in the clean dataset. With an intention to highlight the daily variability in customer-specific load and PV generation profiles, we select three arbitrary dates for the purpose of comparison. More specifically, residential load and generation profiles for the first four customers in the clean dataset are presented on three consecutive Mondays from 1 July 2010, respectively. These four customers are located in the Central Coast region of NSW towards the northern coastline, and are in close proximity to one another. Due to this close geographical proximity, it is to be expected that the PV generation profiles of each respective customer would be similarly affected by cloud cover.

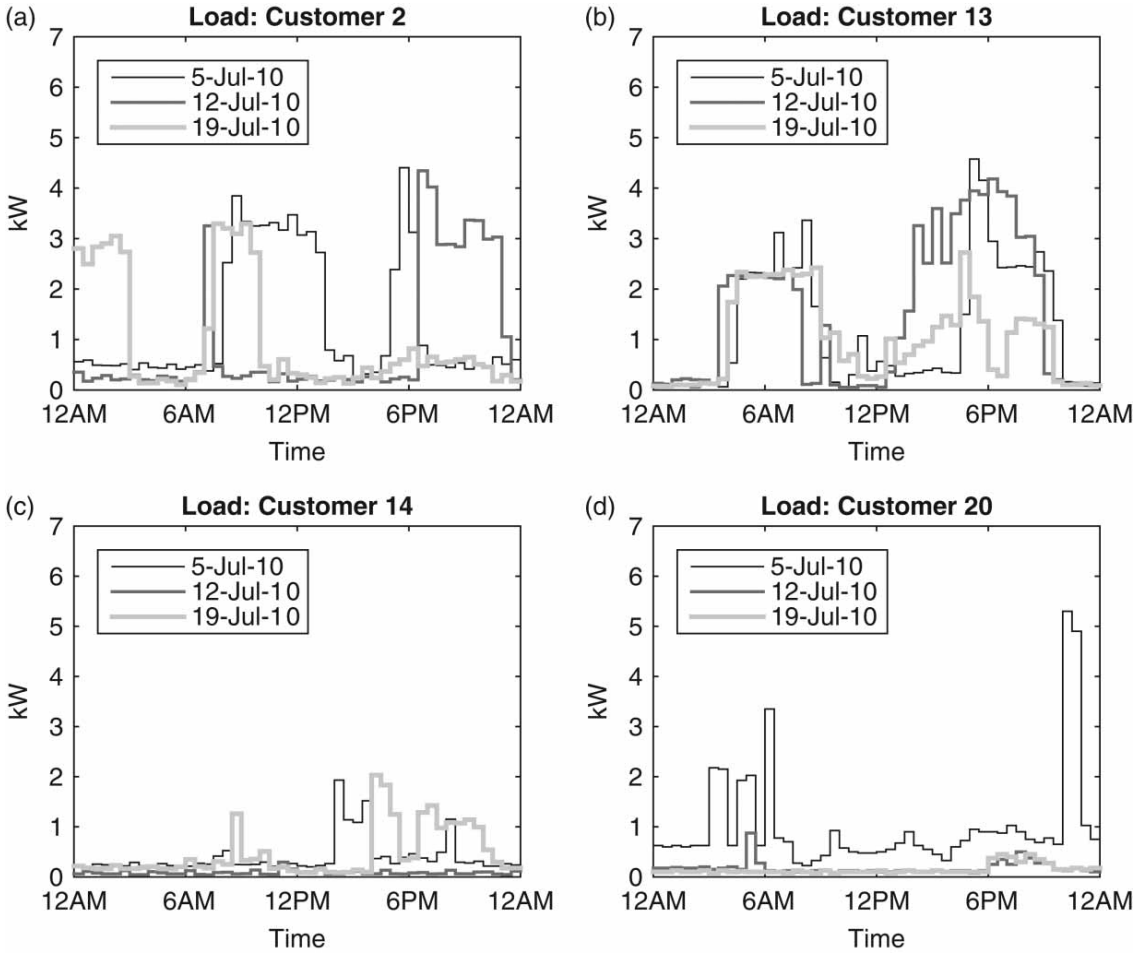

Figure 11. Load profiles for customers 2, 13, 14, and 20, on consecutive Mondays, respectively.

In Figure 11, we present load profiles on three consecutive Mondays for the first four customers in the clean dataset. We observe that the shape of the load profiles in Figure 11(a)–(c) is significantly different on each day, for each customer. In contrast, we observe that the shape of the load profile in Figure 11(d) on 12 July 2010 and 19 July 2010 is flatter and lower for Customer 20. As such, no visual confirmation regarding a strong relationship in energy consumption on consecutive weekdays is evident in Figure 11. Information regarding customer behaviour that affects energy use that leads to these variations in residential load profiles is provided in Slini, Giama, and Papadopoulos (2015) and Pothitou et al. (2014).

In Figure 12, we present generation profiles on three consecutive Mondays for the first four customers in the clean dataset. In Figure 12(a)–(d), we observe that daily peaks in PV generation vary across the customers, with peak generation on 19 July 2010 reaching 0.9 kW for Customer 2, 1.01 kW for Customer 13, 0.64 kW for Customer 14, and 0.89 kW for Customer 20. Likewise, the installed capacity of each rooftop PV unit varies, with the installed PV capacity in the Ausgrid dataset recorded as 1.62 kWp for Customer 2, 2.22 kWp for Customer 13, 1.48 kWp for Customer 14, and 1.57 kWp for Customer 20.

In Figure 12(b), we observe that the shape of the generation profiles is significantly different on each day. In contrast, we observe the shape of the generation profiles for Customer 2, Customer 14, and Customer 20 in Figure 12(a), 12(c), and 12(d) on 19 July 2010 are similar, yet vastly different to the generation profile of Customer 13 on 19 July 2010 (wherein PV production in the afternoon is much greater than PV production in the morning). We observe that fluctuations in PV production for some customers in close proximity to one another are potentially related. To assist the interested researcher looking to further describe these observations for each customer, information regarding solar irradiance, a key factor in PV production is provided in Elliston et al. (2015), Dehghan et al. (2014), and Šúri, Huld, and Dunlop (2005).

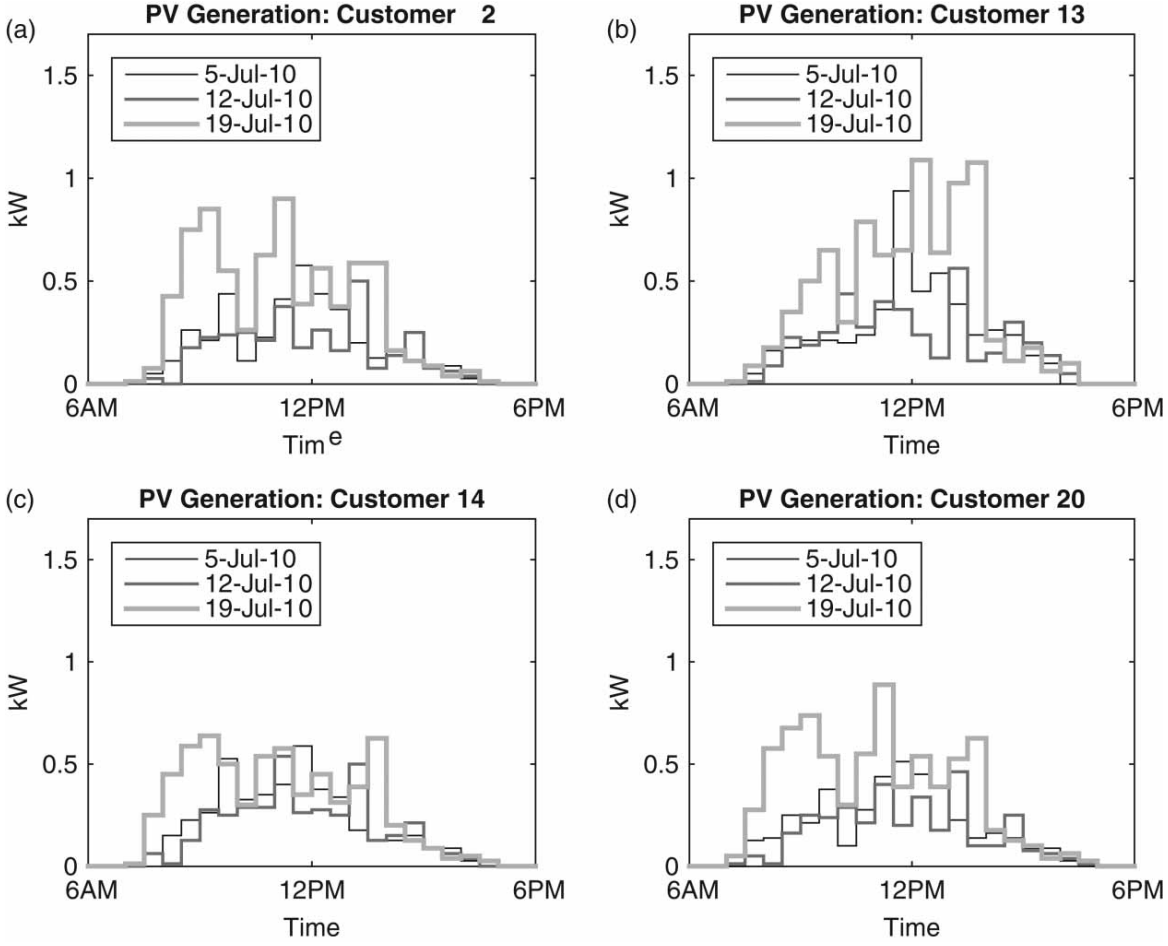

Figure 12. Generation profiles for customers 2, 13, 14, and 20, on three consecutive Mondays, respectively.

4.3. *Orientation of the PV panels*

To increase the amount of solar energy received on PV panels, residential customers generally orientate their PV panels due north in the southern hemisphere (Kacira et al. 2004; Šúri et al. 2007; Chatters 2015). However, PV incentives designed to reduce the evening peak demand (i.e. time-of-use net metering) potentially encourage customers to orientate their PV panels towards the west (Mondol, Yohanis, and Norton 2007). Another motivation to orientate PV panels to the west or east is the prevalence of shade from multistory dwellings (or large trees) that cover north-facing PV panels. Therefore, the optimum PV panel orientation potentially shifts from due north (in the southern hemisphere) to another orientation that is more specific to an individual residential dwelling.

The PV panel orientation of each customer in the Ausgrid dataset is unknown. Each customer in the clean dataset potentially orientates their rooftop PV panels close to due north. To assist with future research that verifies the PV panel orientation of each customer in the Ausgrid dataset, we examine generation profiles ($gg(j)$ for all $j = 1, \ldots, s$) for four of the customers in the clean dataset. We present PV generation profiles on 5 February 2011 (a day in summer), and on 9 July 2012 (a day in winter) for Customer 2 in Figure 13(a), for Customer 69 in Figure 13(b), for Customer 106 in Figure 13(c), and for Customer 214 in Figure 13(d).

In Figure 13, we observe the generation profiles of Customer 2, Customer 69, and Customer 214 peak around midday on 5 February 2011 and on 9 July 2012. These customers potentially orientated their respective PV panels due north (Ward, Moore, and Lindsay 2012). In contrast, the generation profile of Customer 106 peaked around 3 pm on 5 February 2011, consistent with a west-facing PV panel orientation (Ward, Moore, and Lindsay 2012). Further work to verify and infer the PV panel orientation of each customer in the clean dataset is certainly possible.

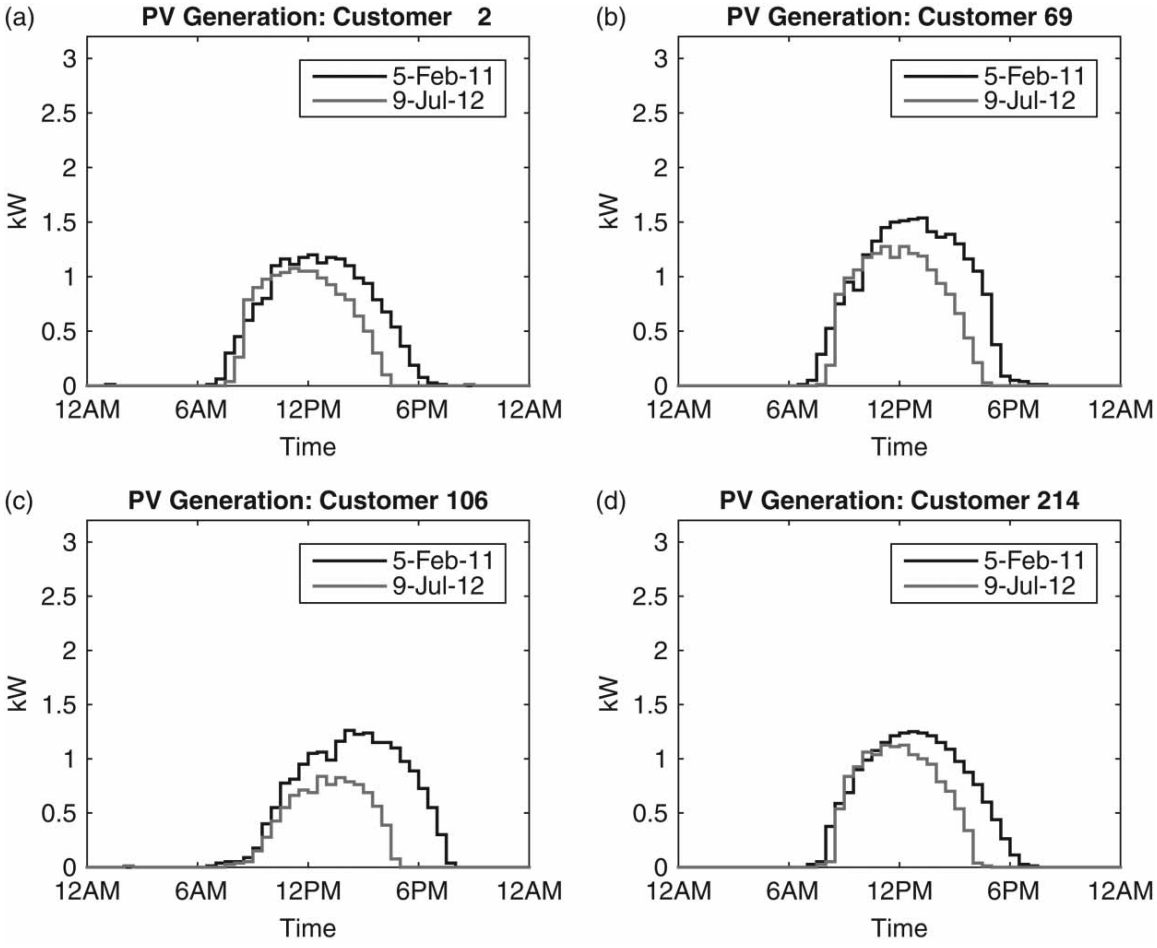

Figure 13. PV generation for (a) Customers 2, (b) Customers 69, (c) Customers 106, and (d) Customers 214, on 5 February 2011 and 9 July 2012, respectively.

5. Conclusions

In this paper, we have reported a publicly available dataset of measured load and PV generation from 300 residential customers located in an Australian distribution network. This dataset is a valuable resource to researchers and policy-makers alike since (1) residential load is measured separately to residential PV generation, (2) time-of-use meters record residential load and PV generation energy measurements after each half hour interval on each day, and (3) the dataset spans a 3-year period. To facilitate use of the dataset, we have presented an approach to remove customer-specific anomalous load and anomalous generation profiles (e.g. when a PV inverter fails), leaving a so-called clean dataset. Analysis of the clean dataset is presented on daily, seasonal, and annual timescales. We envision that the clean dataset will assist future research in the area of categorisation and forecasting of PV generation variability and intermittency.

Notes

1. Ausgrid information published in this paper is publicly available and no permission for publication was required.
2. For the time period 1 July 2012–30 June 2013, 187 customers make it into the 'clean dataset'.
3. In 2007 the AEDT commencement date was moved from the last Sunday of October to the first Sunday of October.
4. Anomalous data relating to clock recording were rectified by Ausgrid in March 2015. These anomalous data were identified via a category 3 elimination.

Acknowledgments

The assistance of Dr Robert Simpson in facilitating access to the Ausgrid dataset is gratefully acknowledged.

Disclosure Statement

No potential conflict of interest was reported by the authors.

References

ACIL Allen Consulting. 2013. *Drivers of Domestic PV Uptake Characteristics of Households with Solar Photovoltaic Systems*. The Australian Renewable Energy Agency. Tech. Rep. Accessed February 16, 2015. http://arena.gov.au/resources/.

von Appen, J., M. Braun, T. Stetz, K. Diwold, and D. Geibel. 2013. "Time in the Sun: the Challenge of High PV Penetration in the German Electric Grid." *IEEE Power and Energy Magazine* 11 (2): 55–64.

Ausgrid. 2014a. *Ausgrid Annual Report 2013/14*. Accessed May 1, 2015. http://www.ausgrid.com.au.

Ausgrid. 2014b. *Data to Share*. Accessed February 16, 2015. http://www.ausgrid.com.au/Common/About-us/Corporate-information/Data-to-share/Data-to-share.aspx.

Ausgrid. 2014c. *Network Price List 2013–2014*. Accessed February 3, 2015. http://www.ausgrid.com.au/Com-mon/Industry/Regulation/Network-prices/Price-lists-and-policy/Historical-network-prices.aspx.

Ausgrid. 2014d. *Privacy Policy*. Accessed February 16, 2015. http://www.ausgrid.com.au/Common/About-us/Privacy-Policy.aspx.

Ausgrid. 2014e. *Solar Home Electricity Data*. Accessed January 28, 2015. http://www.ausgrid.com.au/Common/About-us/Corporate-information/Data-to-share/Data-to-share/Solar-household-data.aspx.

ABS (Australian Bureau of Statistics). 2006. "Census of Population and Housing: Census Geographic Areas Digital Boundaries, Australia, 2006." Data cube: Postal Areas (POA) 2006 Digital Boundaries in MapInfo Interchange Format, cat. no. 2923.0.30.001. Accessed February 1, 2015. http://www.abs.gov.au/ausstats/abs@.nsf/detailspage/2923.0.30.0012006?opendocument.

Australian Government Bureau of Meteorology. 2011. *Sydney in February 2011: 2nd Warmest on Record*. Accessed February 11, 2015. http://www.bom.gov.au/clim-ate/current/month/nsw/archive/201102.sydney.shtml.

Bazilian, M., I. Onyeji, M. Liebreich, I. MacGill, J. Chase, J. Shah, D. Gielen, D. Arent, D. Landfear, and S. Zhengrong. 2013. "Re-Considering the Economics of Photovoltaic Power." *Renewable Energy* 53, 329–338.

Black, A. J. 2004. "Financial Payback on California Residential Solar Electric Systems." *Solar Energy* 77 (4): 381–388.

Braun, P., L. Grüne, C. M. Kellett, S. R. Weller, and K. Worthmann. 2015. "A Distributed Optimization Algorithm with Centralized Performance Properties." *Proceedings of the 54th IEEE Conference on Decision and Control (CDC 2015)*, Osaka, Japan.

Campoccia, A., L. Dusonchet, E. Telaretti, and G. Zizzo. 2009. "Comparative Analysis of Different Supporting Measures for the Production of Electrical Energy by Solar PV and Wind Systems: Four Representative European Cases." *Solar Energy* 83 (3): 287–297.

Chatters, M. "DGDS215 – Optimising Photovoltaic Panel Orientation for Customer Benefits – A Grid PS+EDGE Modelling Platform Case Study." Smart Grid Smart City. Tech. Rep. Accessed February 16, 2015. https://ich.smartgridsmartcity.com.au/Home/SGSC-Report/Technical-Compendia/Distributed-Generation-and-Distributed-Storage.

Chow, C. W., S. Belongie, and J. Kleissl. 2015. "Cloud Motion and Stability Estimation for Intra-Hour Solar Forecasting." *Solar Energy* 115, 645–655.

Darghouth, N. R., G. Barbose, and R. H. Wiser. 2014. "Customer-Economics of Residential Photovoltaic Systems (Part 1): The Impact of High Renewable Energy Penetrations on Electricity Bill Savings with Net Metering." *Energy Policy* 67, 290–300.

Dehghan, A., A. A. Prasad, S. C. Sherwood, and M. Kay. 2014. "Evaluation and Improvement of TAPM in Estimating Solar Irradiance in Eastern Australia." *Solar Energy* 107, 668–680.

Elliston, B., I. MacGill, A. Prasad, and M. Kay. 2015. "Spatio-Temporal Characterisation of Extended Low Direct Normal Irradiance Events Over Australia Using Satellite Derived Solar Radiation Data." *Renewable Energy* 74, 633–639.

Hart, E. K., E. D. Stoutenburg, and M. Z. Jacobson. 2012. "The Potential of Intermittent Renewables to Meet Electric Power Demand: Current Methods and Emerging Analytical Techniques." *Proceedings of the IEEE* 100 (2): 322–334.

Holttinen, H., A. Tuohy, M. Milligan, E. Lannoye, V. Silva, S. Muller, and L. Soder. 2013. "The Flexibility Workout: Managing Variable Resources and Assessing the Need for Power System Modification." *IEEE Power and Energy Magazine* 11 (6): 53–62.

Independent Pricing and Regulatory Tribunal. 2012. *Final Report– Solar feed-in tariffs– March 2012*. Accessed February 16, 2015. http://www.ipart.nsw.gov.au/.

Kacira, M., M. Simsek, Y. Babur, and S. Demirkol. 2004. "Determining Optimum Tilt Angles and Orientations of Photovoltaic Panels in Sanliurfa, Turkey." *Renewable Energy* 29 (8): 1265–1275.

Kroposki, B., R. Margolis, and K. Lynn. 2011. "Power to the People." *IEEE Power and Energy Magazine* 9 (3): 16–22.
Kroposki, B., and B. Mather. 2015. "Rise of Distributed Power: Integrating Solar Energy into the Grid." *IEEE Power and Energy Magazine* 13 (2): 14–18.
Keerthisinghe, C., G. Verbic, and A. C. Chapman. 2014a. "Addressing the Stochastic Nature of Energy Management in Smart Homes." *Power Systems Computation Conference 2014 (PSCC)*, Wroclaw, Poland, 1–7.
Keerthisinghe, C., G. Verbic, and A. C. Chapman. 2014b. "Evaluation of a Multi-Stage Stochastic Optimisation Framework for Energy Management of Residential PV-Storage Systems." *Australasian Universities 2014 Power Engineering Conference (AUPEC)*, Perth, Australia, 1–6.
Khalilpour, R., and A. Vassallo. 2015. "Leaving the Grid: An Ambition or a Real Choice?" *Energy Policy* 82, 207–221.
Lang, T., E. Gloerfeld, and B. Girod. 2015. "Don't Just Follow the Sun – A Global Assessment of Economic Performance for Residential Building Photovoltaics." *Renewable & Sustainable Energy Reviews* 42, 932–951.
Mondol, J. D., Y. G. Yohanis, and B. Norton. 2007. "The Impact of Array Inclination and Orientation on the Performance of a Grid-Connected Photovoltaic System." *Renewable Energy* 32 (1): 118–140.
Moosavian, S. M., N. A. Rahim, J. Selvaraj, and K. H. Solangi. 2013. "Energy Policy to Promote Photovoltaic Generation." *Renewable & Sustainable Energy Reviews* 25, 44–58.
NSW Government. 2010. *Solar Bonus Scheme*. Accessed February 16, 2015. http://www.resourcesandenergy.nsw.gov.au/energy-consumers/solar/solar-bonus-scheme.
Nykamp, S., M. G. C. Bosman, A. Molderink, J. L. Hurink, and G. J. M. Smit. 2013. "Value of Storage in Distribution Grids–Competition or Cooperation of Stakeholders?" *IEEE Transactions on Smart Grid* 4 (3): 1361–1370.
Ogimoto, K., I. Kaizuka, Y. Ueda, and T. Oozeki. 2013. "A Good Fit: Japan's Solar Power Program and Prospects for the New Power System." *IEEE Power and Energy Magazine* 11 (2): 65–74.
Pereira, R., J. Figueiredo, R. Melicio, V. M. F. Mendes, J. Martins, and J. C. Quadrado. 2015. "Consumer Energy Management System with Integration of Smart Meters." *Energy Reports* 1, 22–29.
Pothitou, M., A. J. Kolios, L. Varga, and S. Gu. 2014. "A Framework for Targeting Household Energy Savings through Habitual Behavioural Change." *International Journal of Sustainable Energy* 1–15. July 16, 2014.
Quilumba, F. L., W.-J. Lee, H. Huang, D. Y. Wang, and R. L. Szabados. 2015. "Using Smart Meter Data to Improve the Accuracy of Intraday Load Forecasting Considering Customer Behavior Similarities." *IEEE Transactions on Smart Grid* 6 (2): 911–918.
Ratnam, E., S. Weller, and C. Kellett. 2013. "An Optimization-Based Approach for Assessing the Benefits of Residential Battery Storage in Conjunction with Solar PV." *Proceedings of the IX IEEE International Symposium on Bulk Power System Dynamics and Control (IREP'13)*, Rethymnon, Greece, August 25–30, 1–8.
Ratnam, E. L., S. R. Weller, and C. M. Kellett. 2015a. "An Optimization-Based Approach to Scheduling Residential Battery Storage with Solar PV: Assessing Customer Benefit." *Renewable Energy* 75, 123–134.
Ratnam, E. L., S. R. Weller, and C. M. Kellett. 2015b. "Scheduling Residential Battery Storage with Solar PV: Assessing the Benefits of Net Metering." *Applied Energy* 155, 881–891.
Rhodes, J. D., C. R. Upshaw, C. B. Harris, C. M. Meehan, D. A. Walling, P. A. Navrátil, A. L. Beck, et al. 2014. "Experimental and Data Collection Methods for a Large-Scale Smart Grid Deployment: Methods and First Results." *Energy* 65, 462–471.
Slini, T., E. Giama, and A. M. Papadopoulos. 2015. "The Impact of Economic Recession on Domestic Energy Consumption." *International Journal of Sustainable Energy* 34 (3–4): 259–270.
Šúri, M., T. A. Huld, and E. D. Dunlop. 2005. "PV-GIS: A Web-Based Solar Radiation Database for the Calculation of PV Potential in Europe." *International Journal of Sustainable Energy* 24 (2): 55–67.
Šúri, M., T. A. Huld, E. D. Dunlop, and H. A. Ossenbrink. 2007. "Potential of Solar Electricity Generation in the European Union Member States and Candidate Countries." *Solar Energy* 81 (10): 1295–1305.
Ward, J. K., T. Moore, and S. Lindsay. 2012. "The Virtual Power Station – Achieving Dispatchable Generation from Small Scale Solar." *Proceedings of the 50th Annual Australian Solar Council Conference on Solar 2012 (AuSES)*, Melbourne, Australia, December 6–7, 1–10.
Worthmann, K., C. M. Kellett, P. Braun, L. Grüne, and S. R. Weller. 2015. "Distributed and Decentralized Control of Residential Energy Systems Incorporating Battery Storage." *IEEE Transactions on Smart Grid* 6 (4): 1914–1923.
Yang, Y., H. Li, A. Aichhorn, J. Zheng, and M. Greenleaf. 2014. "Sizing Strategy of Distributed Battery Storage System with High Penetration of Photovoltaic for Voltage Regulation and Peak Load Shaving." *IEEE Transactions on Smart Grid* 5 (2): 982–991.

Appendix. Selected customer ID data

The Customer ID's and corresponding dates presented in Figures 3, 5, 11–13 of this paper are included in Table A1.

Table A1. Index of each Customer ID and corresponding dates presented in Figures 3, 5, 11–13.

Section	Figure	Customer ID	Date		
3.1	3	9	19 January 13	24 February 13	15 March 13
		191	3 July 10	18 July 10	21 August 10
		221	29 October 12	17 November 12	17 May 13
		229	23 February 12	11 March 12	29 March 12
3.2	5	1	28 January 13	23 February 13	23 May 13
		145	9 September 10	11 September 10	28 May 11
		215	14 July 10	15 July 10	16 July 10
		248	21 February 11	3 April 11	21 April 11
4.2	11	2	5 July 10	12 July 10	19 July 10
		13	5 July 10	12 July 10	19 July 10
		14	5 July 10	12 July 10	19 July 10
		20	5 July 10	12 July 10	19 July 10
4.2	12	2	5 July 10	12 July 10	19 July 10
		13	5 July 10	12 July 10	19 July 10
		14	5 July 10	12 July 10	19 July 10
		20	5 July 10	12 July 10	19 July 10
4.3	13	2	5 February 11	9 July 12	
		69	5 February 11	9 July 12	
		106	5 February 11	9 July 12	
		214	5 February 11	9 July 12	

Part 2

Battery scheduling: A single residential system

3

Assessing customer benefit of battery scheduling

Part 2 of this thesis is comprised of Chapter 3 and Chapter 4, in which is defined a single residential energy system with solar PV co-located with battery storage. Renewable energy incentives such as feed-in tariffs and the financial policy of net metering, when offered in conjunction with time-of-use pricing, are also defined. The results in all case studies are based on the dataset reported in Chapter 2.

Chapter 3 consists of the paper titled *An optimization-based approach to scheduling residential battery storage with solar PV: Assessing customer benefit*. One of the key contributions of this paper is a quadratic program (QP)-based scheduling algorithm for residential battery storage that is co-located with solar PV. The QP-based scheduling algorithm is designed to increase the operational savings that accrue to a residential customer, while penalizing large voltage swings stemming from reverse power flow and peak load in the distribution grid. We define incentives for PV generation, and their required metering topologies, to assess the financial benefits of the QP-based algorithm. Our framework for defining a residential energy system is consistent with all thesis chapters, with the exception of some notational changes made to improve the clarity and presentation of subsequent chapters.

In Chapter 4 we benchmark the QP-based algorithm introduced in Chapter 3, when customers are offered the financial policy of net metering. In the context of scheduling battery storage, we benchmark the maximum day-ahead operational savings that accrue to customers with the operational savings that accrue when implementing the QP-based algorithm. Further, by means of a case study, we benchmark reductions in reverse power flow in the context of average grid profiles.

Renewable Energy 75 (2015) 123–134

Contents lists available at ScienceDirect

Renewable Energy

journal homepage: www.elsevier.com/locate/renene

An optimization-based approach to scheduling residential battery storage with solar PV: Assessing customer benefit

Elizabeth L. Ratnam*, Steven R. Weller [1], Christopher M. Kellett [1]

The University of Newcastle, School of Electrical Engineering and Computer Science, University Drive, Callaghan, NSW 2308, Australia

ARTICLE INFO

Article history:
Received 31 January 2014
Accepted 5 September 2014
Available online 11 October 2014

Keywords:
Photovoltaics
Battery scheduling
Feed-in tariffs
Time-of-use pricing
Peak-load reduction

ABSTRACT

Several studies have suggested that battery storage co-located with solar photovoltaics (PV) benefits electricity distributors in maintaining system voltages within acceptable limits. However, without careful coordination, these potential benefits might not be realized. In this paper we propose an optimization-based algorithm for the scheduling of residential battery storage co-located with solar PV, in the context of PV incentives such as feed-in tariffs. Our objective is to maximize the daily operational savings that accrue to customers, while penalizing large voltage swings stemming from reverse power flow and peak load. To achieve this objective we present a quadratic program (QP)-based algorithm. To complete our assessment of the customer benefit, the QP-based scheduling algorithm is applied to measured load and generation data from 145 residential customers located in an Australian distribution network. The results of this case study confirm the QP-based scheduling algorithm significantly penalizes reverse power flow and peak loads corresponding to peak time-of-use billing. In the context of feed-in tariffs, the majority of customers exhibited operational savings when QP energy-shifting.

1. Introduction

Climate change, energy security, and limited fossil fuel resources are drivers for the integration of renewable energy sources such as solar into the modern power grid. Significant challenges in converting the abundant solar resource into reliable, high-quality electricity include variability of solar irradiance on both daily and seasonal timescales in addition to intermittency arising from moving cloud cover on timescales of much shorter duration [1,2].

Despite these challenges, governments around the world have in recent years encouraged grid-integrated residential-scale (rooftop) solar photovoltaic (PV) generation through financial incentives such as feed-in-tariffs (FiTs) paid directly to customers [3–5]. These financial incentives in conjunction with a sharp drop in the capital cost of small-scale PV, and increasing electricity prices, have led to the dramatic uptake of residential PV in some countries [6,7]. For example, in Germany PV plant installations exceed 1.2 million, and as of September 2012, peak PV capacity reached 31 GW with about 70% of this 31 GW being connected to the low voltage grid [6].

An adverse consequence of such significant PV penetration in the low voltage electricity distribution network is voltage rise leading to reverse power flow. Voltage rise is particularly pronounced when large numbers of rooftop PV generators are connected in close proximity to each other [8–14]. A further adverse consequence of significant PV penetration is voltage dip. This occurs, for example, when passing cloud cover results in a significant drop in rooftop PV generation [10–12,15]. If these voltage deviations fall outside power quality standards, either the utility covers the direct cost of mitigation or the burden of voltage regulation falls to the PV producer [2,6,8,13,14].

There are two common approaches to managing voltage rise in the low voltage grid. The first is to augment the distribution grid by increasing conductor size and/or upgrading transformers to lower network impedances [6,9,16]. The second is to constrain PV generation at times of low electricity consumption in order to preserve compliance of allowable voltage deviations [13,17,18]. Neither approach is optimal for increased PV penetration as network augmentation adds to the overall PV grid integration costs [9] whereas spilling PV generation leads to lost revenue for the producer.

* Corresponding author. Tel.: +61 2 492 16026; fax: +61 2 492 16993.
E-mail addresses: elizabeth.ratnam@ieee.org (E.L. Ratnam), Steven.Weller@newcastle.edu.au (S.R. Weller), Chris.Kellett@newcastle.edu.au (C.M. Kellett).
[1] Tel.: +61 2 492 16026; fax: +61 2 492 16993.

http://dx.doi.org/10.1016/j.renene.2014.09.008
0960-1481/

Alternative approaches to managing PV generation in the low voltage grid are facilitated through Advanced Metering Infrastructure (AMI) [19–23]. When two way communication is enabled between the utility and customer via AMI, opportunities exist for more advanced demand-side management initiatives that include direct [20,24–28], and price-responsive [21–23,29,30] load control. For example, the utility can enact price-responsive load control by broadcasting a day-ahead time-varying electricity tariff to the AMI. To maintain an existing energy usage level, the customer may choose to schedule battery storage in response to the time-varying electricity tariff or pay a higher energy bill. However without careful coordination of the residential battery schedules, network load curve smoothing via demand-side management initiatives may not be realized [26,31,32].

Several authors have investigated energy-time shifting through battery storage with a focus on minimizing residential energy bills and reducing network peak demand [33–37], leading to battery schedules that either assist or exacerbate non-compliant voltage deviations associated with solar PV. The reduction of network peak demand is incorporated into an optimization problem in Ref. [34], where the objective function includes financial incentives for residents to deliver energy to the grid when the purchase cost of electricity is high. Hence, when interconnected customers in close proximity implement the objective function in Ref. [34], large voltage swings associated with reverse power flow potentially arise due to the battery scheduling. The reduction of network peak demand is also incorporated into a linear program in Ref. [33], where the energy flowing from the point of common coupling (PCC) to the customer is minimized when residential load exceeds residential PV production. Otherwise the battery is scheduled in Ref. [33] to charge during the off-peak pricing period, and discharge during the peak pricing period, with no penalty on increased reverse power flow, potentially exacerbating voltage rise. In contrast, the reduction of network peak demand and the mitigation of undesirable reverse power flow, i.e., load curve smoothing, is incorporated into the optimization problems in Refs. [35–37]. The optimization problem in Ref. [35] achieves load curve smoothing by omitting financial incentives encouraging solar PV uptake (e.g., feed in tariffs or net metering) in the objective function. The optimization problem in Ref. [36] also achieves load curve smoothing by removing incentives for reverse power flow associated with battery scheduling, while permitting incentives encouraging solar PV uptake. Another method for reducing network peak demand while potentially abating reverse power flow is incorporated into the optimization problem in Ref. [37], where a sophisticated dynamic pricing environment provides additional incentives for customers to smooth their day-ahead energy consumption.

Our objective in this paper is similar to [36] in one respect, we seek to maximize residential PV generation co-located with battery storage so that there is a financial benefit to the resident whilst simultaneously alleviating the utility burden associated with peak demand and reverse power flow. Our approach achieves this objective for a range of financial incentives offered for solar PV uptake, such as feed-in tariffs [3–5,36] and net metering [34,38,39], in addition to other more sophisticated dynamic day-ahead pricing rates [23,29,37]. We assume peak billing rates coincide with generation shortages or peak grid demand and look to minimize energy flow from the grid to the customer during these events, while additionally reducing reverse power flow.

Implicit in our approach is the expectation that residential customers have installed Home Energy Management (HEM) systems that: (1) forecast the day-ahead residential load and solar PV generation, (2) coordinate with the AMI to receive day-ahead prices for energy delivered to and from the grid, including any additional PV incentives, (3) run optimization-based algorithms daily, and (4) schedule battery storage in the day-ahead. In this paper we assume the day-ahead forecast of load and generation from the HEM system are known and perfect, and we focus on the formulation of an optimization-based algorithm that provides the day-ahead battery schedule. We also assume the customers' HEM system is fully automated and employs a wireless communication architecture, similar to the description in Ref. [27]. Furthermore, we expect global investment and government mandates will drive both technology improvements and economies of scale for battery storage as has happened with solar PV [40–43]. Therefore our focus is on the operational savings that accrue to a resident when the HEM schedules a battery, and we exclude the capital costs of purchasing a battery from our consideration.

In this paper we consider the quadratic program (QP)-based minimization of the energy supplied by, or to, the grid in a residential PV system with co-located battery storage, first presented in Ref. [44]. Our objective is to smooth network load curves while providing incentives to customers to energy time-shift. In the present paper we remove a bias in the QP-based algorithm in Ref. [44] by including an additional battery constraint related to the state of charge, and with a modification to the greedy-search heuristic that selects the key design parameters in this QP we reduce computational time. Furthermore, we apply the improved QP-based scheduling algorithm to measured load and generation data from 145 Australian residential customers, and investigate the financial savings that accrue to customers. In the present paper, the financial benefit associated with the daily battery charge/discharge schedule is our primary focus in the context of financial incentives offered for solar PV generation such as feed-in tariffs, rather than the utility benefit of load curve smoothing.

This paper is organized as follows. In Section 2 we introduce the optimization-based approach for scheduling battery storage in a residential PV system, and include a motivating example. To assess the customer benefit, we introduce a framework in Section 3 that incorporates different demand-side management approaches for price-response load control, which integrates applicable incentives for PV generation. With this framework we define the daily energy bill for a single customer with and without battery storage. In Section 4 we describe the operations savings associated with battery scheduling, and in Section 5 we present an algorithm for selecting a key design parameter in the QP described in Section 2. In Section 6 we implement the QP-based algorithm given real-world data from 145 residential customers located in an Australian distribution network in the context of feed-in tariffs, and investigate the customer benefit to changes in different elements within the QP (e.g., battery size).

1.1. Notation

Let $\mathbb{R}^s$ denote s-dimensional vectors of real numbers and $\mathbb{R}^s_{\geq 0}$ s-dimensional vectors with all non-negative components where, as usual, $\mathbb{R}^1 = \mathbb{R}$. $\mathbf{I}$ denotes the s-by-s identity matrix and $\mathbb{1} \in \mathbb{R}^s_{\geq 0}$ denotes the all-1 s column vector of length s. $\mathbf{0}$ denotes an all-zero matrix, or an all-zero column vector, where the context will make clear the dimension intended, and $\mathbf{T}=[t_{ij}]$ denotes the s-by-s matrix satisfying $t_{ij}=1$ for $i \geq j$ and $t_{ij}=0$ elsewhere.

2. Problem formulation

2.1. Definitions and constraints

Fig. 1 illustrates the topology of the system under consideration, including a set of meters $\mathscr{M} = \{M_1, M_2, M_3\}$ installed for the purpose of billing and compensation. For each $k \in \{1, \ldots, s\}$, meter M_1 measures the average PV generation g_k (in kW), meter M_2 measures

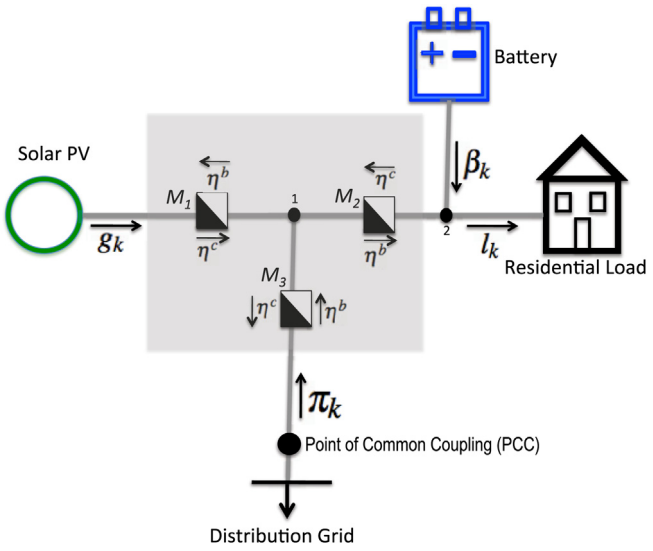

Fig. 1. Residential system illustrating the direction of positive power flows and financial incentives to energy time-shift. Arrows associated with g_k, l_k, β_k and π_k illustrate the assumed direction of positive power flow. Financial incentives for each meter M_1, M_2 and M_3 are represented by vectors η^b and η^c (in \$/kWh), in which arrows illustrate the direction of power flow relevant for η^b and η^c.

the average power from node 1 to node 2 ($l_k-\beta_k$ in kW), and meter M_3 measures the average power π_k (in kW) supplied by (or to) the grid. Meters M_2 and M_3 may be bi-directional, whereas meter M_1 needs only be unidirectional since PV generation satisfies $g_k\geq 0$ for all k. Also shown in Fig. 1 are vectors η^b and η^c, which represent financial incentives for billing and compensation respectively, defined in Section 3.2.

The power flows indicated in Fig. 1 are represented by vectors of length s, where s is the number of time intervals of length Δ, and $T=s\Delta$ (in hours) is the time window of interest. In this paper we generally consider T=24 h, $\Delta = 1/2$ hour (30 min), which implies s=48. Other choices are certainly possible, subject only to commensurability of T, Δ and s.

We represent the average power delivered to the residential load (in kW) over the period $((k-1)\Delta, k\Delta)$ by l_k for all $k\in\{1,\ldots,s\}$, and define the *load profile* over $[0,T]$ as $l := [l_1,\ldots,l_s]^T\in\mathbb{R}^s_{\geq 0}$. Likewise we represent the average PV generation (kW) over the period $((k-1)\Delta,k\Delta)$ by g_k for all $k\in\{1,\ldots,s\}$, and define the *generation profile* over $[0,T]$ as $g := [g_1,\ldots,g_s]^T\in\mathbb{R}^s_{\geq 0}$. In what follows, we assume the day-ahead forecasts of load and generation profiles are known and perfect.

We represent the average power (in kW) supplied by (or to) the grid over the period $((k-1)\Delta,k\Delta)$ by π_k for all $k\in\{1,\ldots,s\}$ and define the *grid profile* over $[0,T]$ as $\pi := [\pi_1,\ldots,\pi_s]^T\in\mathbb{R}^s$. By convention we represent power flowing from (to) the grid to (from) the energy system by $\pi_k>0$ ($\pi_k<0$).

We represent the average power (kW) delivered from (or to) the battery over the period $((k-1)\Delta,k\Delta)$ by $\beta_k>0$ (or $\beta_k<0$), and define the *battery profile* over $[0,T]$ as $\beta := [\beta_1,\ldots,\beta_s]^T\in\mathbb{R}^s$. By convention we represent charging (discharging) of the battery by $\beta_k<0$ ($\beta_k>0$).

From the configuration of the residential energy system in Fig. 1, we observe that the following power balance equation

$$l_k = \pi_k + g_k + \beta_k \quad \text{for all } k\in\{1,\ldots,s\}, \tag{1}$$

must hold.

The inclusion of the battery in Fig. 1 leads to additional constraints, which we now detail. To capture the limited "charging/discharging capacity" of the battery, we constrain β by

$$\underline{B}\mathbb{1} \leq \beta \leq \overline{B}\mathbb{1} \tag{2}$$

where $\underline{B}\in\mathbb{R}_{\leq 0}$ and $\overline{B}\in\mathbb{R}_{\geq 0}$.

Given β, the *state of charge* of the battery (in kWh) at time $k\Delta$ is denoted by χ_k, where

$$\chi_k := \chi_0 - \sum_{j=1}^{k}\beta_j\Delta \quad \text{for all } k\in\{1,\ldots,s\}, \tag{3}$$

and χ_0 denotes the initial state of charge of the battery. We represent the *state of charge profile* by $\chi := [\chi_0,\ldots,\chi_s]^T\in\mathbb{R}^{s+1}$.

If we represent the battery capacity (in kWh) by $C\in\mathbb{R}_{\geq 0}$, it necessarily follows that the state of charge profile is constrained by

$$\mathbf{0} \leq \chi \leq C\begin{bmatrix}1\\ \mathbb{1}\end{bmatrix}. \tag{4}$$

For a fixed initial state of charge satisfying $0\leq\chi_0\leq C$, we define $\underline{\mathbf{C}} := (\chi_0/\Delta)\mathbb{1}$, and $\overline{\mathbf{C}} := (1/\Delta)(C-\chi_0)\mathbb{1}$, and rewrite the battery constraints equations (3) and (4) as

$$-\underline{\mathbf{C}} \leq -\mathbf{T}\beta \leq \overline{\mathbf{C}}. \tag{5}$$

In this paper, we optimize a battery profile over a single day. In order to avoid an energy-shifting bias in these results, we insist that the state of charge of the battery at the end of a day is the same as the state of charge of the battery at the beginning of the day, i.e.,

$$\chi_s = \chi_0, \tag{6}$$

where χ_s is the final state of charge at time $s\Delta$.

Let $A_1\in\mathbb{R}^{4s\times s}$, and $b_1\in\mathbb{R}^{4s}$ be defined by

$$A_1 := [\mathbf{I} \quad -\mathbf{I} \quad \mathbf{T} \quad -\mathbf{T}]^T, \quad b_1 := \begin{bmatrix}\overline{B}\mathbb{1}^T & \underline{B}\mathbb{1}^T & \mathbf{C}^T & \overline{\mathbf{C}}^T\end{bmatrix}^T. \tag{7}$$

We now substitute equation (7) into equations (2) and (5), and equation (6) into (3), to succinctly write the battery constraints as

$$A_1\beta \leq b_1, \tag{8}$$

$$\mathbb{1}^T\beta = 0. \tag{9}$$

2.2. Objectives

In what follows, we seek to minimize the impact of the residential energy system on the grid, given a financial incentive to energy time-shift, by minimizing

$$\sum_{k=1}^{s} h_k\pi_k^2, \tag{10}$$

where h_k is a selectable weighting such that $h_k\geq 1$ for all $k\in\{1,\ldots,s\}$.

Specifically, given load and generation profiles l and g, and given battery constraints χ_0, C, and $\overline{B}$, $\underline{B}$ we seek a battery profile β and a grid profile π which minimize the expression in (10), subject to satisfaction of the power balance in equation (1).

The minimization in (10) is subject to both inequality and equality constraints imposed by the battery (8) and (9) and the power balance equation in (1), respectively. Lemma 1 below establishes this constrained minimization as a quadratic program (QP).

Lemma 1. The minimization of expression (10), subject to battery constraints (8) and (9) and the power balance equation (1), can be written as

$$\min_{x\in\mathbb{R}^{2s}} x^T H x \tag{11}$$

such that

$$\overline{A}_1 x \le b_1, \tag{12}$$

$$A_2 x = b_2, \tag{13}$$

where

$$x := \begin{bmatrix} \pi^T & \beta^T \end{bmatrix}^T \in\mathbb{R}^{2s}, \quad H := \begin{bmatrix} \mathbf{H} & \mathbf{0} \\ \mathbf{0} & \mathbf{0} \end{bmatrix} \in\mathbb{R}^{2s\times 2s},$$

$$\mathbf{H} := \mathrm{diag}(h_1,\ldots,h_s) \in\mathbb{R}^{s\times s}, \quad \overline{A}_1 := \begin{bmatrix} \mathbf{0} & A_1 \end{bmatrix} \in\mathbb{R}^{4s\times 2s},$$

$$A_2 := \begin{bmatrix} \mathbf{0}^T & \mathbb{1}^T \\ \mathbf{I} & \mathbf{I} \end{bmatrix} \in\mathbb{R}^{(s+1)\times 2s}, \quad b_2 := \begin{bmatrix} 0 \\ l-g \end{bmatrix} \in\mathbb{R}^{s+1}.$$

Proof. The result follows directly from equations (1), (8) and (9).

The grid profile obtained by solving (11) subject to constraints (12) and (13) is said to be *QP energy-shifted* and we will refer to the process of a customer implementing the daily battery and grid profiles obtained by solving (11) subject to constraints (12) and (13) as QP energy-shifting.

2.3. Example

In this example we consider two battery capacities, C=1 kWh and 10 kWh, to illustrate QP energy-shifting at a residence. For both battery capacities, let $\chi_0 = 0.5\,C$ (initial battery state of charge), and $\overline{B} = -\underline{B} = 1$kW (charge/discharge limits).

Let the load and generation profiles l and g be specified as shown in Fig. 2(a), where the residence load includes a utility controlled heated water cylinder [45].[2] Both load and generation profiles are specified for T=24 h, Δ=30 minutes and $s=T/\Delta$=48. Additionally, we let the weights h_k=1 for all $k\in\{1,\ldots,s\}$.

In Fig. 2(a) we observe the load profile peaks around midnight, consistent with the utility switching on the all-electric-heated water cylinder at the customer premises, and the generation profile peaks around midday. Consequently the peak generation does not align with the peak load at the residence.

Fig. 2(b) illustrates the *base-line* grid profile to which we compare the grid profiles in Fig. 2(c) and (d). The base-line grid profile has no battery to time-shift the grid profile π appearing in (10) (C=0 kWh). Therefore π is calculated directly from the power balance equation in (1) with β_k=0. The grid profiles π illustrated in Fig. 2(c) and (d) arise from the solution of the QP in Lemma 1. Comparing the base-line results in Fig. 2(b) to the grid profile in Fig. 2(c), we observe the 1 kW battery charges (β_k<0) to increase the base-line grid profile (e.g., from −1.26 kW to −0.81 kW between 11.30-Midday), and discharges (β_k>0) to reduce the base-line grid profile (e.g., from 3.69 kW to 2.69 kW between 23.30-Midnight). In Fig. 2(d) we observe further reductions in the magnitude of π, except between 23.30-Midnight, due to the battery discharge constraint of 1 kW.

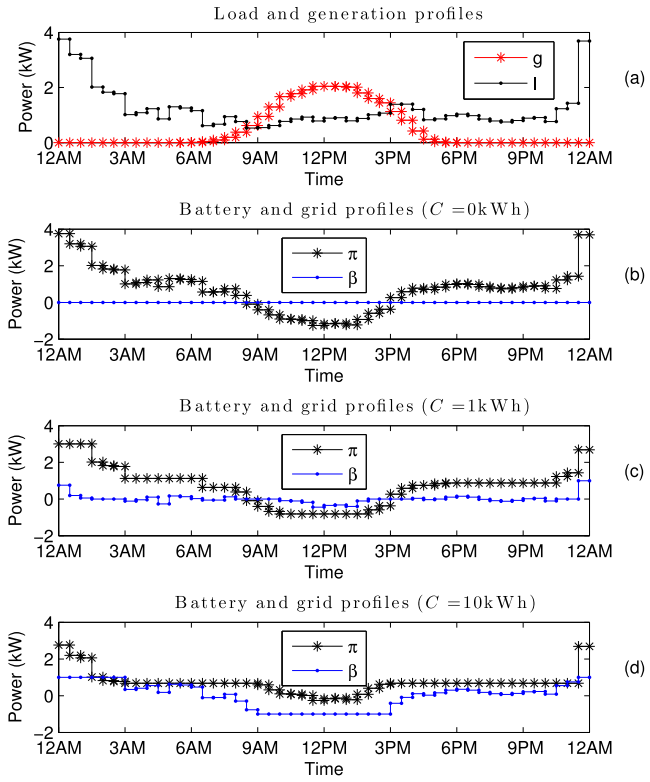

Fig. 2. (a) Load and generation profiles l and g; (b) grid and battery profiles π and β for C = 0 kWh; (c) grid and battery profiles π and β for C = 1 kWh; (d) grid and battery profiles π and β for C = 10 kWh.

This example demonstrates the reductions in magnitude of the grid profile π subject to the battery charge/discharge constraints and capacity C. Hence, QP energy-shifting smooths residential load curves when h_k=1 for all $k\in\{1,\ldots,s\}$. In what follows we design a weighting matrix $\mathbf{H}$ in the QP that reduces residential energy bills, and network peak load corresponding to peak pricing tariffs, while penalizing reverse power flow.

2.4. Extended definition of grid profile

We now extend our definition of *grid usage* over the period $((k-1)\Delta,k\Delta)$ to include explicit reference to the battery capacity C and weights h_k as follows:

$$\pi_k^C(h_k) := l_k - g_k - \beta_k \quad \text{for all } k\in\{1,\ldots,s\}, \tag{14}$$

where l_k, g_k, β_k and h_k remain as previously defined. We consequently denote the *grid profile* over [0,T] by

$$\pi^C(\mathbf{H}) := \left[\pi_1^C(h_1),\ldots,\pi_s^C(h_s)\right]^T \in\mathbb{R}^s. \tag{15}$$

When battery capacity C=0, it follows that

$$\pi_k^0 = l_k - g_k \quad \text{for all } k\in\{1,\ldots,s\}, \tag{16}$$

since the battery charging/discharging capacity β_k=0, $k\in\{1,\ldots,s\}$. The case where C=0 is defined as a *base-line* grid profile against which we compare future grid profiles and is denoted by

[2] In some countries, residents allow the utility to control their all-electric-heated water systems for periods in the day, given a financial incentive. For these customers, the utility switches their water-heating services on during periods of low load, and off during periods of peak-load, in a manner that ensures minimal impact to the network.

$$\pi^0 := \left[\pi_1^0, \ldots, \pi_s^0\right]^T. \quad (17)$$

We note π^0 is not a function of the selectable weights in **H**, as the base-line grid profile is solely a function of load and generation profiles in (16).

Remark 1. The grid profile π obtained from solving the quadratic program in Lemma 1 depends not only on the battery constraints C, $\overline{B}, \underline{B}, \chi_0$, and selected weightings h_k, but also the load and generation profiles l and g, respectively. Consequently π is a function $\pi = \pi(l, g, C, \overline{B}, \underline{B}, \chi_0, \mathbf{H})$. For notational simplicity, however, we will henceforth omit the functional dependence of π on the load/generation profiles and all the battery constraints other than the battery capacity C, preferring instead to simply write $\pi^C(\mathbf{H})$, where no ambiguity arises. This notational convention reflects our primary degrees of design flexibility, namely battery capacity C and the weighting matrix **H**.

3. Billing for a single customer

In this section we define the *energy bill* for a single residential customer for the household PV system depicted in Fig. 1. To reduce the day-ahead energy bill when the customer uses QP energy-shifting (Lemma 1), we require a *financial policy* (in $/kWh) and a battery of capacity C. Since the *financial policy* requires meters in certain locations, with particular modes of operation, we also define the *metering topology* in Section 3.1.

3.1. Metering topology

To formulate the energy bill for a single residential customer, we require the measured power flows from the residential energy system in Fig. 1. The *metering topology* defines how the power flows are to be measured. To formalize the notion of *metering topology* we define two *metering modes* in terms of the meters $M \in \mathscr{M}$, and provide an example with respect to meter M_2 shown in Fig. 1.

1. *Gross metering mode*: We say that meter M_2 operates in *gross metering mode* if it measures power flow from node 1 to the battery/load node 2, but not power delivered in the reverse direction. That is, meter M_2 measures and records only power flows for which $l_k - \beta_k \geq 0$. In the event $l_k - \beta_k < 0$, the meter records 0 kW. Consequently gross metering mode requires only uni-directional metering.
2. *Net metering mode*: We say that meter M_2 operates in *net metering mode* if it measures power flow in both directions, i.e., from node 1 to the battery/load node 2 ($l_k - \beta_k \geq 0$), as well as power delivered in the reverse direction (i.e., $l_k - \beta_k < 0$). Consequently net metering mode requires bi-directional metering [46].

The metering topology is defined by the mode of operation (gross or net) of each meter $M \in \mathscr{M}$ in Fig. 1. In order to consider gross metering mode, the direction of power flow must also be included.

The metering topologies considered in this paper are defined below, with the direction of positive power flow as per Fig. 1, defined in Section 2.1.

- *Metering topology 1*: M_1 and M_2 operate in gross metering mode. M_3 is not installed. M_1 measures and records the generation profile $g_k \geq 0$ for all k, M_2 measures and records the power flow $l_k - \beta_k \geq 0$ for all k.
- *Metering topology 2*: M_3 operates in net metering mode. M_1 and M_2 are not installed.

3.2. Financial policies

To calculate the energy bill for a single residential customer, we require the measured power flows from the residential energy system in Fig. 1, and the corresponding electricity prices. Our definition of a *financial policy* (in $/kWh) formalizes the electricity prices and includes incentives intended to influence customer energy utilization. Example incentives include *time-of-use* (TOU) pricing, *feed-in-tariffs* and *net metering* [3,46]. Our definition of a financial policy below is sufficiently general to include these incentives in addition to more sophisticated dynamic day-ahead pricing rates [23,29,37].

Our definition of a financial policy requires an *electricity billing profile* and an *electricity compensation profile* over $[0,T]$, for each installed meter in $\mathscr{M}$. The direction of power flow associated with electricity billing/compensation is defined with reference to the direction of positive power flow that is specified at each meter $M \in \mathscr{M}$. We denote *electricity billing* (in $/kWh) at meter $M \in \mathscr{M}$ over the period $((k-1)\Delta, k\Delta)$ by $\eta_k^b(M)$ for all $k \in \{1, \ldots, s\}$, and define the *electricity billing profile* over $[0,T]$ at M as $\eta^b(M) := [\eta_1^b(M), \ldots, \eta_s^b(M)]^T \in \mathbb{R}^s_{\geq 0}$. Likewise we denote the *electricity compensation* (in $/kWh) at meter $M \in \mathscr{M}$ over the period $((k-1)\Delta, k\Delta)$ by $\eta_k^c(M)$ for all $k \in \{1, \ldots, s\}$, and define the *electricity compensation profile* over $[0,T]$ at M as $\eta^c(M) := [\eta_1^c(M), \ldots, \eta_s^c(M)]^T \in \mathbb{R}^s_{\geq 0}$.

In order to implement a financial policy, certain types of meters are required in particular locations. For example a financial policy may require the meter M_1 (in Fig. 1), which records positive power flows from the solar PV to node 1. For this meter the financial policy will specify the electricity billing and compensation profiles $\eta^b(M_1)$, $\eta^c(M_1)$, respectively. If the electricity billing (or compensation) profile at meter M_1 is defined by $\eta_k^b(M_1) = 0$ (or $\eta_k^c(M_1) = 0$) for all $k \in \{1, \ldots, s\}$, then it is sufficient that meter M_1 operates in gross metering mode. In this case the power flow to be measured is in the same direction specified for electricity compensation (or billing).

We now define a *financial policy* over $[0,T]$ by using the day ahead electricity billing and compensation profiles at each installed meter in $\mathscr{M}$. An example financial policy is defined with reference to Fig. 1 for $\mathscr{M} = \{M_1, M_2, M_3\}$. The direction of positive power flow at meter M_1 is defined by g (from the solar PV to node 1) and electricity is compensated in this direction $\eta^c(M_1)$. The direction of positive power flow at meter M_2 is defined by $l - \beta \geq 0$ (from node 1 to node 2) and electricity is billed in this direction $\eta^b(M_2)$. The direction of positive power flow at meter M_3 is defined by π (from the PCC to node 1) and electricity is billed in this direction $\eta^b(M_3)$. For each electricity compensation (or billing) profile $\eta^b(M)$ (or $\eta^c(M)$), there also exists an electricity billing (or compensation) profile $\eta^c(M)$ (or $\eta^b(M)$) for power flowing against the positive direction at meter $M \in \mathscr{M}$.

The financial policies considered in this paper are defined with reference to metering topologies 1 and 2 defined in Section 3.1. The financial policy associated with metering topology 1 includes an electricity compensation profile at meter M_1 (for power flow from the solar PV to node 1), and an electricity billing profile at meter M_1 (for power flows in the reverse direction), represented by $\eta^c(M_1)$ and $\eta^b(M_1)$ respectively; and an electricity compensation profile at meter M_2 (for power flow from node 2 to node 1), and an electricity billing profile at meter M_2 (for power flows from node 1 to node 2), represented by $\eta^c(M_2)$ and $\eta^b(M_2)$ respectively. Furthermore, $\eta_k^b(M_1) = 0$ and $\eta_k^c(M_2) = 0$, for all $k \in \{1, \ldots, s\}$ and hence it is sufficient that meters M_1 and M_2 operate in gross metering mode, as per the definition of metering topology 1.

The financial policy associated with metering topology 2 has an electricity compensation profile at meter M_3 (for power flow from node 1 to PCC) and an electricity billing profile at meter M_3 (for

Table 1
Electricity billing and compensation profiles for metering topologies 1 and 2.

Meter	Metering topology 1		Metering topology 2	
	Billing	Compensation	Billing	Compensation
M_1	$\eta^b(M_1)=\mathbf{0}$	$\eta^c(M_1)$		
M_2	$\eta^b(M_2)$	$\eta^c(M_2)=\mathbf{0}$		
M_3			$\eta^b(M_3)$	$\eta^c(M_3)$

power flow from the PCC to node 1), represented by $\eta^c(M_3)$ and $\eta^b(M_3)$ respectively. Table 1 summarizes the electricity billing and compensation profiles for metering topologies 1 and 2.

To implement a gross feed-in tariff, we observe metering topology 1 is sufficient. To implement a net feed-in tariff, or net metering, we observe metering topology 2 is sufficient.

3.3. Energy bill

To define the energy bill for the residential energy system in Fig. 1, we combine the financial policy (in \$/kWh) with the measured power flows defined in Section 2.1. To reduce the energy bill when QP energy-shifting, we seek a weighting matrix $\mathbf{H}$ given a fixed battery capacity C.

In what follows we define the *energy bill* (in \$/day) in terms of the respective financial policy associated with metering topologies 1 and 2 (Section 3.2). We assume the day-ahead billing and compensation profiles in the respective financial policies are fixed by the utility or regulatory body and available to the consumer.

In equation (6) we constrained the initial and final states of charge of the battery to be equal. Consequently, we assume the cost associated with charging the battery to χ_0 can be compensated for with the remaining charge at the end of the day χ_s. Therefore, in defining of the energy bill, we ignore the cost associated with charging the battery to an initial state of charge.

To formalize the energy bill associated with metering topology 1, we select the electricity prices that correspond to measured power flows at meters M_1 and M_2. That is, for the financial policy relating to metering topology 1, we define $\sigma_k(M_1)$ and $\sigma_k(M_2)$ as follows:

$$\sigma_k(M_1)=\begin{cases}\eta^c_k(M_1), & \text{if } g_k\geq 0\\ \eta^b_k(M_1), & \text{if } g_k<0,\end{cases} \tag{18}$$

$$\sigma_k(M_2)=\begin{cases}\eta^b_k(M_2), & \text{if } l_k-\beta_k\geq 0\\ \eta^c_k(M_2), & \text{if } l_k-\beta_k<0,\end{cases} \tag{19}$$

and denote $\sigma(M_1):=[\sigma_1(M_1),\ldots,\sigma_s(M_1)]^T\in\mathbb{R}^s_{\geq 0}$ and $\sigma(M_2):=[\sigma_1(M_2),\ldots,\sigma_s(M_2)]^T\in\mathbb{R}^s_{\geq 0}$ over the period $[0,T]$. Recall $\eta^b_k(M_1)=0$ and $\eta^c_k(M_2)=0$, for all $k\in\{1,\ldots,s\}$.

In order to minimize the energy bill associated with metering topology 1, we choose the weighting matrix for a given battery capacity with constraints (8) and (9) known and fixed as

$$\mathbf{H}_1:=\mathbf{H}(\sigma(M_1),\sigma(M_2)). \tag{20}$$

Hence the choice of weighting matrix in the cost function (11) is dependent on the implemented financial policy.

Having fixed $\mathbf{H}_1$ in equation (20), we define the residential energy bill associated with metering topology 1, denoted by $\Sigma^C(\mathbf{H}_1)$ (in \$/day) by

$$\Sigma^C(\mathbf{H}_1):=\Delta\Big((l-\beta)^T\sigma(M_2)-g^T\sigma(M_1)\Big). \tag{21}$$

When the battery capacity $C=0$, the energy bill defined in (21) reduces to

$$\Sigma^0:=\Delta\Big(l^T\eta^b(M_2)-g^T\eta^c(M_1)\Big), \tag{22}$$

since the battery charging/discharging capacity $\beta_k=0$ for all $k\in\{1,\ldots,s\}$, rendering the selectable weights in $\mathbf{H}_1$ irrelevant. The case where $C=0$ also serves as a *base-line energy bill*, which we use as a comparison when assessing the financial benefits of battery storage.

Remark 2. The energy bill notation convention $\Sigma^C(\mathbf{H}_1)$ is simplified, and consistent with the suppression of functional dependence described in Remark 1. That is, our notation reflects our primary degrees of design flexibility, the battery capacity C and the weighting matrix.

To formalize the energy bill associated with metering topology 2, we select the electricity prices that correspond to measured power flows at meter M_3. That is, we define $\sigma_k(M_3)$ in terms of the financial policy as

$$\sigma_k(M_3)=\begin{cases}\eta^b_k(M_3), & \text{if } \pi^C_k(h_k)\geq 0\\ \eta^c_k(M_3), & \text{if } \pi^C_k(h_k)<0,\end{cases} \tag{23}$$

and we denote $\sigma(M_3):=[\sigma_1(M_3),\ldots,\sigma_s(M_3)]^T\in\mathbb{R}^s_{\geq 0}$ over the period $[0,T]$. In order to minimize the energy bill associated with metering topology 2, we choose the weighting matrix for a given battery capacity with constraints (2)–(4) known and fixed as

$$\mathbf{H}_2:=\mathbf{H}(\sigma(M_3)). \tag{24}$$

Having fixed $\mathbf{H}_2$ in (24), we define the energy bill associated with the financial policy relating to metering topology 2 by

$$\Sigma^C(\mathbf{H}_2):=\Delta\pi^C(\mathbf{H}_2)^T\sigma(M_3), \tag{25}$$

which reduces to the *base-line energy bill* for $C=0$ given by

$$\Sigma^0:=\Delta(l-g)^T\sigma(M_3), \tag{26}$$

where $\pi^0=l-g$ since the battery charging/discharging capacity satisfies $\beta_k=0$ for all $k\in\{1,\ldots,s\}$.

4. Savings for a single customer

In this section we define the energy savings for the household PV system depicted in Fig. 1. The results in this section allow a single customer to assess the cost-effectiveness of installing a battery of a given size. Recall, this paper focuses on the operational energy savings associated with QP energy-shifting and as such we omit the capital cost of installing a battery.

4.1. Energy savings

To examine the effectiveness of QP energy-shifting for a given size battery, we define the *energy savings* (in \$/day). The energy savings are denoted by $\Psi^C(\mathbf{H})$ and defined by

$$\Psi^C(\mathbf{H}):=\Sigma^0-\Sigma^C(\mathbf{H}). \tag{27}$$

We recall from Section 3.3, the energy bill $\Sigma^C(\mathbf{H})$ is defined for a particular financial policy and selection of weights in $\mathbf{H}$, given load and generation profiles l and g, a battery of a given size C, with constraints (2)–(4) known and specified. When $C=0$, Σ^0 denotes the base-line energy bill.

Given unique load and generation profiles for 365 consecutive days and a battery of a given size C, with constraints (2)–(4) known

and specified, their exists a unique energy saving $\Psi^C(\mathbf{H})$ for each of the 365 days. We define the summation of these unique energy savings by $\Theta^C(\mathbf{H})$ in \$/yr and label this summation the *annual savings*. Thus when the annual savings are positive, there exists an operational benefit to QP energy-shifting.

Hence $\Theta^C(\mathbf{H})>0$ implies the installation is operationally cost-effective, $\Theta^C(\mathbf{H})=0$ implies the installation is operationally cost-neutral and $\Theta^C(\mathbf{H})<0$ implies no financial benefit for battery storage for that given year.

4.2. Special case: zero energy savings

Consider the special case where there is a fixed price for electricity (in \$/kWh) at all installed meters in $\mathscr{M}$, irrespective of power flow direction and time of day. Lemma 2 below demonstrates that under these circumstances, there is no financial incentive for a resident to install battery storage. That is, since the battery acts as an energy time-shifter, the lack of differential pricing at any point in time gives no incentive to energy time-shift.

Lemma 2. Fix $\eta>0$ and let the electricity billing and compensation profiles in the financial policy satisfy the following for all $M\in\mathscr{M}$:

$$\eta_j^b = \eta_k^c = \eta \quad \text{for all } j,k\in\{1,\ldots,s\}, \tag{28}$$

$$\eta^b = \eta^c = \eta\mathbb{1}. \tag{29}$$

Assume all meters $M\in\mathscr{M}$ are installed such that all power flowing to or from the grid is quantifiable (for example metering topology 1 or 2). Then for all choices of battery capacity C and weighting matrix $\mathbf{H}$, the energy savings are $\Psi^C(\mathbf{H})=0$.

Proof. Consider metering topology 2. Rearranging equation (3) yields

$$\chi_0 - \chi_s = \sum_{k=1}^{s} \beta_k \Delta. \tag{30}$$

Recall from the definition of the time window T, we require Δ to be positive ($\Delta > 0$) and a constant. Combining the definition of Δ with the constraint in equation (6) implies

$$\sum_{k=1}^{s} \beta_k = \beta^T\mathbb{1} = 0. \tag{31}$$

Furthermore, definitions (14) and (15) imply

$$\pi^C(\mathbf{H}_2) = l - g - \beta. \tag{32}$$

Additionally, substituting equations (28) and (29) into equation (23) yields

$$\sigma(M_3) = \eta\mathbb{1}. \tag{33}$$

Therefore, from equation (25) the energy bill is

$$\begin{aligned}\Sigma^C(\mathbf{H}_2) &= \Delta\pi^C(\mathbf{H}_2)^T\sigma(M_3) = \Delta(l-g-\beta)^T\eta\mathbb{1}\\ &= \Delta(l-g)^T\eta\mathbb{1} - \Delta\eta\beta^T\mathbb{1} = \Delta(l-g)^T\sigma(M_3) = \Sigma^0,\end{aligned}$$

where the final equality is defined in equation (26).

The energy savings (27) are then

$$\Psi^C(\mathbf{H}_2) = \Sigma^0 - \Sigma^C(\mathbf{H}_2) = 0. \tag{34}$$

A similar calculation can be performed for other metering topologies, provided the meters in $\mathscr{M}$ are installed such that all power flowing to or from the grid is quantifiable.

5. Heuristic for selecting the weighting matrix

In this paper our objective is to maximize the daily operational savings that accrue to a single customers, while penalizing large voltage swings observed in the distribution network stemming from reverse power flow and peak load. We assume peak electricity billing rates coincide with generation shortages or peak grid demand and look to prioritize the minimization of energy flow from the grid during these events, while penalizing reverse power flow. To achieve our objective, we seek a weighting matrix $\mathbf{H}$ in the QP for a single customer with battery storage in the residential setting shown in Fig. 1. Given perfect day-ahead load and generation forecasts, and battery constraints (8) and (9), the HEM system computes the weighting matrix $\mathbf{H}$ via a heuristic for each day-ahead. We define the heuristic in what follows.

In Section 2.2, the minimization of expression (10) was presented as a constrained quadratic program (Lemma 1), where the weights h_k in $\mathbf{H}$ were selectable. In this section we consider the specification of the matrix $\mathbf{H}$ that maximizes the annual savings, while reducing the impact of the residential system on the grid. In practice, the matrix $\mathbf{H}$ is difficult to obtain, as it depends on a variety of factors including financial policies, metering topologies and daily variations in load and generation profiles. To address this problem we propose a greedy-search heuristic for obtaining a so-called *preferred* $\mathbf{H}$, which is in turn based upon a *base-line* weighting matrix denoted by $\mathbf{H}_0$.

When selecting the weights in the preferred $\mathbf{H}$, our rationale is to increase base-line weights when electricity billing is high and decrease base-line weights when electricity billing is low, and to continue increasing/decreasing so long as the daily residential savings increase. This rational reduces network peak loads without contributing to reverse power flow during the peak pricing period, and increases operational savings that accrue to customers.

The basic idea of the heuristic is to increase each weight h_k in $\mathbf{H}_0$, as long as this increase leads to an increased energy saving in (27). To mitigate against numerical difficulties with the solution of the quadratic program in Lemma 1, we increase weights in $\mathbf{H}_0$ until a maximum allowable value of h_k is reached. To this end, weights in $\mathbf{H}_0$ are scaled by the minimum cost and capped at a maximum value. To cap the weights h_k we introduce the following saturation operation:

$$\text{sat}_1^{\overline{h}}(h_k) := \begin{cases} 1, & \text{if } h_k < 1 \\ h_k, & \text{if } 1 \le h_k \le \overline{h} \\ \overline{h}, & \text{if } h_k > \overline{h}, \end{cases} \tag{35}$$

where the lower bound is 1 in accordance with the definition of h_k in Section 2.2 and $\overline{h}>1$ is fixed. The constant $\overline{h}$ is chosen to mitigate against numerical difficulties in solving the QP in Lemma 1. In this paper, we set $\overline{h}=1000$.

To formalize the definition of the base-line weighting matrix, let

$$\tilde{\eta}_k := \sum_{M\in\mathscr{M}} \eta_k^b(M), \quad \forall\ k\in\{1,\ldots,s\} \tag{36}$$

$$\eta^\star := \min_{k\in\{1,\ldots,s\}} \tilde{\eta}_k, \tag{37}$$

and define the base-line weighting matrix $\mathbf{H}_0$ as

$$\mathbf{H}_0 := \mathrm{diag}\left[\mathbf{H}_0^{(1)}, \ldots, \mathbf{H}_0^{(k)}, \ldots, \mathbf{H}_0^{(s)}\right], \tag{38}$$

where $\mathbf{H}_0^{(k)} := \mathrm{sat}_1^{\bar{h}}(\tilde{\eta}_k/\eta^\star)$

Given $\mathbf{H}_0$, the proposed heuristic requires the function for energy savings $\Psi(\cdot)$ defined in (27). Recall the energy savings function $\Psi(\cdot)$ requires the constraints and solution to the QP in Lemma 1 and the energy bill $\Sigma(\cdot)$ pertaining to a given metering topology and financial policy as defined in Section 3. To simplify the notation, we use $\Psi(\cdot)$ rather than $\Psi^C(\mathbf{H})$ to indicate that the battery capacity C is fixed.

The main loop in the heuristic below (lines 6–19), doubles weights in $\mathbf{H}_0$ progressively, from the largest to the smallest element in $\mathbf{H}_0$. If there exist multiple elements in $\mathbf{H}_0$ with the same magnitude, we double the multiple elements concurrently. The set of live indices $\tilde{s}$ keeps track of the indices in $\mathbf{H}_0$ that are yet to be increased, and $\mathbf{I}^{\tilde{s}}$ denotes an s-by-s matrix in which $\mathbf{I}^{\tilde{s}}_{j,j} = 1$ if $j \in \tilde{s}$ and zero otherwise.

6. Application of QP energy-shifting

We analyzed measured load and generation profiles from July 1st 2010 to the 30th of June 2011, for each of 300 randomly selected low voltage customers located in an Australian distribution network, operated by Ausgrid. The Ausgrid distribution network covers 22,275 km^2 and includes load centers in Sydney and regional New South Wales.

The load and generation profiles l and g for each of the 300 customers are defined with T=24 h, Δ=30 minutes, and s=T/Δ=48, for each day in the 365 days.

We eliminated customers with a maximum load or PV generation less than 5 W on any day of the year (l_k<0.005 or g_k<0.005 for all $k \in \{1, \ldots, s\}$), leaving 145 of the original 300 customers. We refer to this set of 145 customers as *the ensemble*.

When QP energy-shifting, the annual savings for each customer in the ensemble are dependent on a variety of factors and we investigate four of the most important factors in what follows. In Section 6.2 we investigate the influence of daily variations in the load and generation profiles on savings for particular customers in the ensemble. In Section 6.3 we compare annual savings for different metering topologies. In Section 6.4 we compare annual savings with and without the preferred $\mathbf{H}$. In Section 6.5 we investigate the influence of battery capacity on annual savings. The computational time when QP energy-shifting (including the time to find the preferred $\mathbf{H}$) on each day for each ensemble member is on average 0.422 s with an Intel i7-2630QM processor.

6.1. Simulation parameters

In the following we use the heuristic to find the $\mathbf{H}$ matrix when QP energy-shifting, except as specified in Section 6.4. To calculate the annual savings for the ensemble when QP energy-shifting, we fix the battery capacity at 10 kWh, except in Section 6.5 where we vary the battery capacity within the range 0 kWh $\leq C \leq$30 kWh. In all cases, the remaining battery constraints (2)–(4) are chosen as

Heuristic: Returns the preferred $\mathbf{H}$ given $\Psi(\cdot)$

Input: $l, g, C, \overline{B}, \underline{B}, \chi_0, \pi^0, \bar{h}, \mathbf{H}_0,$
$\mathbf{H} = \mathbf{I}, \Psi_0 = \Psi(\mathbf{H}_0), \tilde{s} = \{1, \ldots, s\}$

1 **for** $k \in \{1, \ldots, s\}$ **do**
2 **if** $\pi_k^0 = 0$ **then**
3 $q = \{p \in \{1, \ldots, s\} | \pi_p^0 = 0\}$
4 $\tilde{s} = \tilde{s} \setminus q$
5 $\mathbf{H}_0^{(q)} = 1$
6 **while** $\mathbf{H}_0^{(\tilde{s})} > 1$ **do**
7 $k^\star = \arg\max_{\tilde{s}}(\mathbf{H}_0^{(\tilde{s})})$
8 $J = \{j \in \{1, \ldots, s\} | \mathbf{H}_0^{(j)} = \mathbf{H}_0^{(k^\star)}\}$
9 $\forall j \in J \quad \overline{\mathbf{H}}_0 = \mathrm{diag}\left[\mathbf{H}_0^{(1)}, \ldots, 2\mathbf{H}_0^{(j)}, \ldots, \mathbf{H}_0^{(s)}\right]$
10 $\forall j \in J \quad \overline{\mathbf{H}}_0^{(j)} = \mathrm{sat}_1^{\bar{h}}\left(\overline{\mathbf{H}}_0^{(j)}\right)$
11 $\overline{\Psi}_0 = \Psi(\overline{\mathbf{H}}_0)$
12 **while** $\overline{\Psi}_0 > \Psi_0$ **and** $\overline{\mathbf{H}}_0^{(k^\star)} < \bar{h}$ **do**
13 $\Psi_0 = \Psi(\overline{\mathbf{H}}_0)$
14 $\mathbf{H}_0 = \overline{\mathbf{H}}_0$
15 $\forall j \in J \quad \overline{\mathbf{H}}_0 = \mathrm{diag}\left[\mathbf{H}_0^{(1)}, \ldots, 2\mathbf{H}_0^{(j)}, \ldots, \mathbf{H}_0^{(s)}\right]$
16 $\forall j \in J \quad \overline{\mathbf{H}}_0^{(j)} = \mathrm{sat}_1^{\bar{h}}\left(\overline{\mathbf{H}}_0^{(j)}\right)$
17 $\overline{\Psi}_0 = \Psi(\overline{\mathbf{H}}_0)$
18 $\forall j \in J \quad \mathbf{H} = \mathrm{diag}\left[\overline{\mathbf{H}}_0^{(1)}, \ldots, \overline{\mathbf{H}}_0^{(j)}, \ldots, \overline{\mathbf{H}}_0^{(s)}\right]$
19 $\tilde{s} = \tilde{s} \setminus J$
20 $\mathbf{H} = \mathbf{H} + \mathbf{I}^{\tilde{s}}$

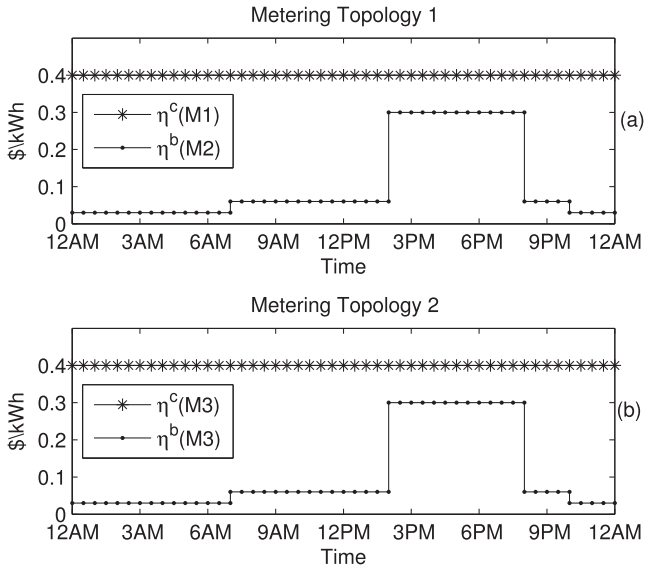

Fig. 3. Non-zero billing and compensation profiles for metering topologies 1 and 2.

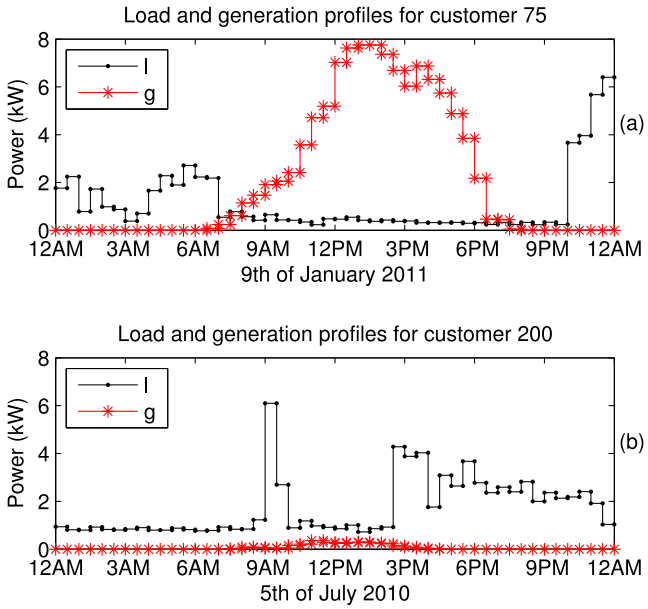

Fig. 4. Representative load and generation profiles for customers 75 and 200.

χ_0=0.5 C, and $\overline{B} = -\underline{B} = 5$kW. We also fix the length-s billing and compensation profiles (each given in \$/kWh) for metering topology 1 as follows:

$$\eta^b(M_1) = \eta^c(M_2) = [0, \ldots, 0]^T,$$

$$\eta^c(M_1) = [0.4, \ldots, 0.4]^T,$$

$$\eta^b(M_2) = \left[\ldots, \eta^b_k, \ldots\right]^T,$$

where $\eta^b_{1-14} = 0.03, \eta^b_{15-28} = 0.06, \eta^b_{29-40} = 0.3, \eta^b_{41-44} = 0.06$, and $\eta^b_{45-48} = 0.03$. The non-zero profiles are shown in Fig. 3(a).

For metering topology 2, the length-s compensation and billing profiles (in \$/kWh) are again fixed and given by

$$\eta^c(M_3) = [0.4, \ldots, 0.4]^T,$$

$$\eta^b(M_3) = \left[\ldots, \eta^b_k, \ldots\right]^T,$$

such that $\eta^b(M_3)$=$\eta^b(M_2)$. The non-zero profiles are shown in Fig. 3(b).

For both metering topologies in Fig. 3 we describe electricity billing from 10pm to 7am at the rate of \$0.03/kWh as an *off-peak pricing period*, electricity billing from 7am to 2pm and again from 8pm to 10 pm at the rate of \$0.06/kWh as a *shoulder pricing period* and electricity billing from 2pm to 8pm at the rate of \$0.30/kWh as a *peak pricing period*.

For metering topology 1 in Fig. 3 we describe electricity compensation $\eta^c(M_1)$ as a gross feed-in tariff. For metering topology 2 in Fig. 3 we describe electricity compensation $\eta^c(M_3)$ as a net feed-in tariff.

6.2. Influence of load and generation profiles

In this section we identify typical load and generation profiles that result in either a positive or negative operational saving when QP energy-shifting under metering topology 1. To do this we compare daily energy savings for two customers in the ensemble. The selected two customers are chosen with significant differences in their respective load and generation profiles (l and g). The two representative customers are denoted Customer 75 and Customer 200.

Fig. 4 illustrates the significant differences in the respective load and generation profiles for customers 75 and 200. In Fig. 4(a) we observe Customer 75 consumed most of its energy during the off-peak pricing period between 10pm and 7am. Meanwhile the solar PV unit delivered energy from 7am to 7:30pm and was in excess of the residential energy demand from 8am to 7:30pm. Consequently, Customer 75 delivered energy to the grid from 8am to 7:30pm on the 9th of January 2011.

In Fig. 4(b) we observe Customer 200 consumed a significant proportion of its energy during the peak pricing period (2pm-8pm) and very little energy during the off-peak pricing period (10pm − 7am). In Fig. 4(b) we also observe the generation profile is less than the load profile for the entire day (g_k<l_k for all $k \in \{1, \ldots, s\}$).

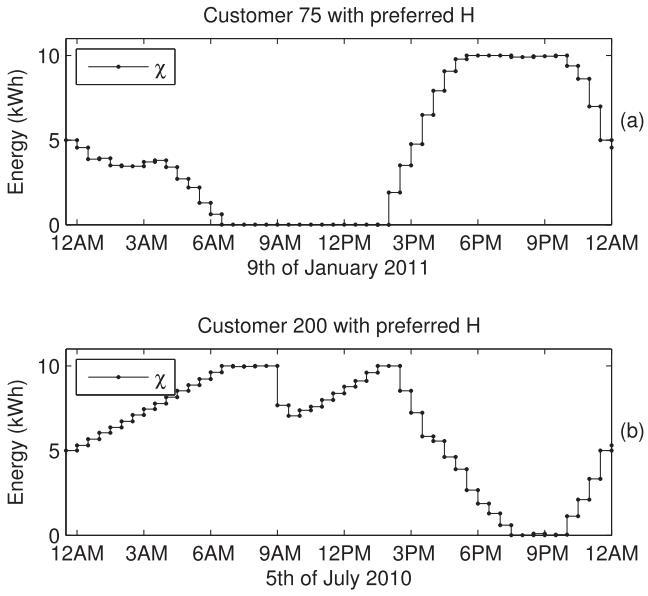

Fig. 5. The battery SOC for customers 75 and 200 when using QP energy-shifting on the 9th of January 2011 and the 5th of July 2010, respectively.

Consequently, there was no energy delivered to the grid by Customer 200 on the 5th of July 2010.

For both customers 75 and 200, given a financial policy associated with metering topology 1 and simulation parameters defined in Section 6.1, we calculate the daily energy savings given a 10 kWh battery. From these daily energy savings we find Customer 75 would have lost $2.68 on the 9th of January 2011 and Customer 200 would have saved $2.70 on the 5th of July 2010 by using QP energy-shifting.

To understand why QP energy-shifting would save Customer 200 $2.70, while costing Customer 75 $2.68, given the load and generation profiles in Fig. 4, we compare the respective battery states of charge. In Fig. 5(a) we observe the battery discharges mostly during the off-peak pricing period when Customer 75 consumed most of its energy and charges during the peak pricing period rather than the shoulder pricing period when PV generation was high and load low due to the weightings imposed via the heuristic. Consequently the cost of charging the battery is not offset by the cost of discharging the battery for Customer 75 on the 9th of January 2011.

In Fig. 5(b) we observe the battery discharges mostly during the peak pricing period when the customer consumed most of its energy and charges during the off-peak pricing period as well as when the solar PV generated energy. Therefore the cost of charging the battery is offset by the cost of discharging the battery for Customer 200 on the 5th of July 2010.

On each day from the 1st of July 2010 to the 30th of June 2011 we calculated the daily energy savings for customers 75 and 200. Fig. 6 illustrates the distribution of these daily savings. In Fig. 6(a) we observe QP energy-shifting results in Customer 75 losing money over the course of a year, even though some days provide savings. This loss of money is attributed to load and generation profiles that caused the battery to charge during peak pricing periods and discharge during off-peak pricing periods, consistent with our observations in Fig. 5(a).

In Fig. 6(b) we observe QP energy-shifting results in Customer 200 saving money over the course of a year. This saving is attributed to load and generation profiles that cause the battery to charge

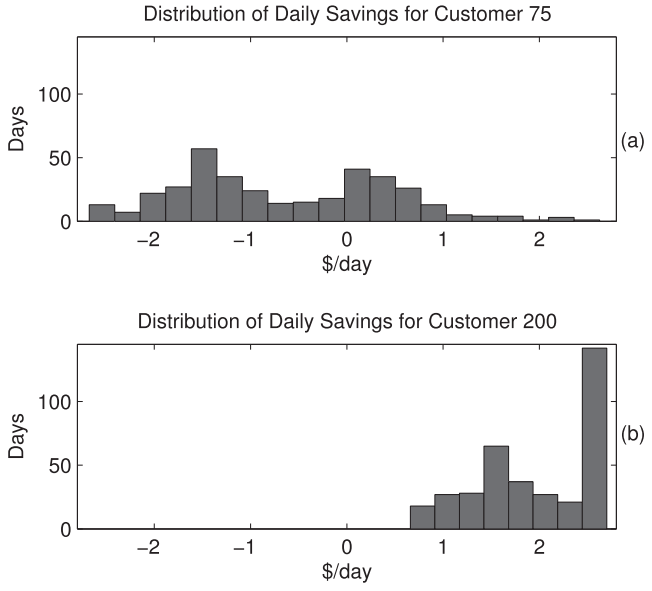

Fig. 6. Distribution of daily saving resulting form QP energy-shifting for customers 75 and 200.

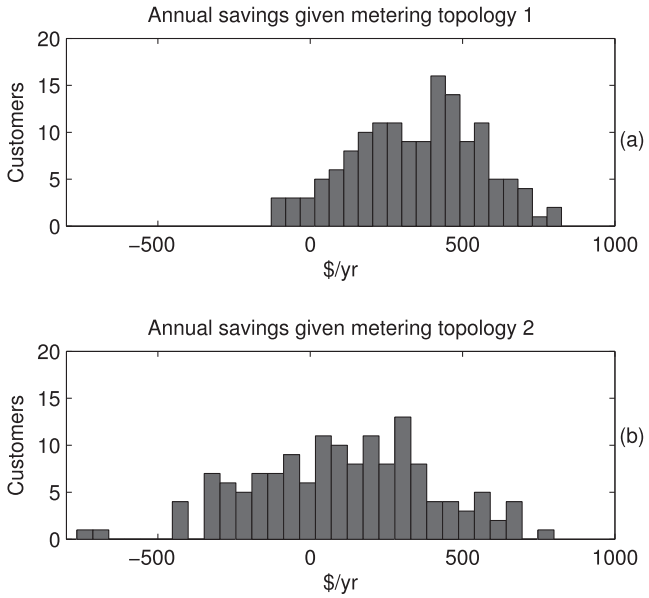

Fig. 7. Annual savings distribution for the ensemble resulting from metering topologies 1 and 2.

during the off-peak pricing periods and discharge during the peak pricing periods, consistent with our observations in Fig. 5(b).

Consequently, given metering topology 1, the daily cost of charging a given battery must be offset by the daily cost of discharging a given battery for a customer to reap the benefits of QP energy-shifting. Therefore, given the financial policy associated with metering topology 1 described in Section 6.1, customers that consume most of their energy during the off-peak pricing period and generate more energy then they consume, will not financially benefit from QP energy-shifting. On the other hand, those who consume most of their energy during the peak pricing period and generate less energy then they consume, will financially benefit from QP-energy shifting.

6.3. *Influence of metering topologies*

For each customer in the ensemble, we now calculate and compare the annual savings associated with QP energy-shifting given the financial policy associated with either metering topology 1 or 2 as presented in Section 3.1. For each customer, the annual savings are again calculated for a 10 kWh battery and in all cases, the simulation parameters are as defined in Section 6.1.

Fig. 7 illustrates the distribution of annual savings for all customers in the ensemble under two metering topologies. In Fig. 7(a) we observe metering topology 1 saves the ensemble on average $350/yr, however nine customers lose money, including Customer 75. In Fig. 7(b) we observe metering topology 2 saves the ensemble on average $100/yr, however fifty customers lose money, including Customer 75. Hence some customers do not benefit from QP energy-shifting, irrespective of the metering topology.

We again visit the representative load and generation profiles for Customer 75 in Fig. 4(a) to understand the underlying principles that result in Customer 75 not benefiting from QP energy-shifting, given metering topology 2. In Fig. 4(a) we observed Customer 75 generated energy and delivered most of this energy to the grid and was compensated for this at $0.40/kWh. However if Customer 75 employed QP energy-shifting, the generated energy would instead charge a battery when in excess of the load, leading to a loss in compensation at $0.40/kWh. Given the financial policy relating to

Table 2
Mean Annual Savings for the ensemble.

Battery	Metering topology 1		Metering topology 2	
	$\mathbf{H}_0$	**H**	$\mathbf{H}_0$	**H**
10 kWh	$266/yr	$348/yr	$9/yr	$90/yr

metering topology 2, it is not possible for this customer to recoup this compensation loss by discharging the battery, as the maximum billing rate is $0.30/kWh. Therefore, customers that would ordinarily deliver energy to the grid, may not profit from QP energy-shifting when electricity compensation is in excess of electricity billing.

6.4. Influence of the selection of **H**

In this section we verify the heuristic proposed in Section 5. The heuristic finds a matrix **H** that increases the annual savings, with comparison to the base-line **H** (denoted $\mathbf{H}_0$). The results in this section are based on the battery constraints and financial policies as per Section 6.1.

For each customer in the ensemble we calculate the annual savings when QP energy-shifting using both the preferred **H** and $\mathbf{H}_0$ given the financial policies associated with metering topologies 1 and 2. We then average the annual savings of the ensemble and label this average the *mean annual savings* (in $/yr).

We record the mean annual savings for both the preferred **H** and $\mathbf{H}_0$ in Table 2. From this table we observe the preferred **H** increases mean annual savings when QP energy-shifting, irrespective of the metering topology. Hence the heuristic given in Section 5 successfully increases the mean annual savings for the ensemble, with comparison to $\mathbf{H}_0$.

6.5. Influence of the battery capacity

To assess the influence of battery capacity (in kWh) on residential annual savings when QP energy-shifting we consider again customers 75 and 200 from the ensemble. For these customers we vary the battery capacity (C) given the set of battery capacities (in kWh) C={0,0.1,1,2,4,6,8,10,15,20,30} and plot the results in Fig. 8.

In Fig. 8 we observe that an increase in the battery capacity results in an increase in financial losses for Customer 75. In comparison, an increase in battery capacity results in an increase in annual savings for Customer 200. Furthermore, the increase in annual savings for Customer 200 rapidly approaches an asymptotic value with a 30 kWh battery providing minimal additional savings over a 15 kWh battery. Consequently, not all customers benefit from battery storage and increasing the size of the battery does not necessarily increase the annual savings for a given customer.

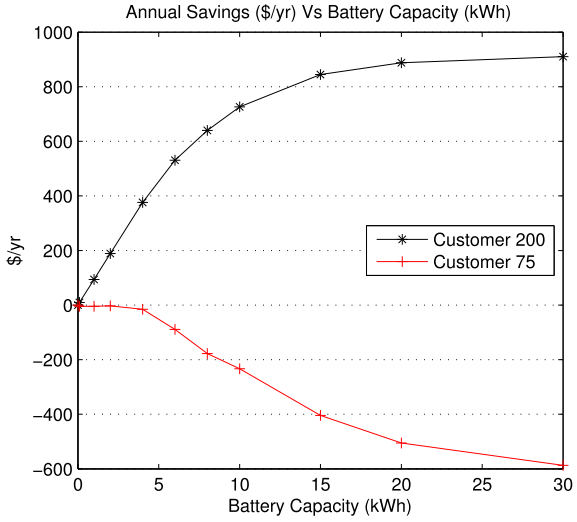

Fig. 8. Comparison of annual savings for customers 200 and 75 with variable battery capacities, under the financial policy pertaining to metering topology 1.

Considering the subset of customers who do financially benefit from QP energy-shifting, if we know the capital cost of installing a battery of a given size, with constraints known and specified, Fig. 8 may be useful in identifying the most cost-effective battery capacity. Furthermore, given the capital cost of installing a battery, we expect there also exists a critical annual saving where increases in battery capacity may no longer be cost-effective.

7. Conclusions

In this paper we have presented a QP-based algorithm for day-ahead scheduling of residential battery storage co-located with solar PV. The QP-based algorithm is formulated to balance two objectives. The first objective is to minimize the impact of the residential system on the grid, by reducing the network peak demand and non-compliant voltage deviations associated with reverse power flow. The second objective is to increase the daily operational savings that accrue to customers, by time-shifting residential load from peak pricing periods to off-peak pricing periods. In particular, we balance the reduction of load during during peak pricing periods with penalties for reverse power flow during the same period so that voltage rise associated with solar PV is not simply time-shifted to the peak pricing periods. Furthermore, our proposed framework allows for a variety of financial incentives and their required metering topologies.

Our QP-based algorithm requires a user-specified weighting matrix, **H**. We have presented a heuristic approach to the specification of **H**. Other approaches are possible, and may provide improved customer benefits.

In the context of feed-in tariffs we assessed the customer benefit of QP energy-shifting by using measured load and generation data from 145 residential customers located in an Australian distribution network. In assessing the potential benefit for each of these customers, we observed that most, but not all, customers see operational savings. Customers who are offered incentives to generate more electricity then they consume, with peak load falling outside the peak and shoulder pricing periods, are included in the category of negative operational savings. Further work is needed to more completely characterize suitable financial policies, metering topologies, and battery size with respect to financial benefits of QP energy-shifting for customers who observed negative operational savings.

Acknowledgments

Elizabeth L. Ratnam acknowledges the financial support of an Australian Postgraduate Award (APA) and a CSIRO – Energy Technology Postgraduate Research Scholarship (Ref: 2011094123).

References

[1] Radchik A, Skryabin I, Maisano J, Novikov A, Gazarian T. Ensuring long term investment for large scale solar power stations: Hedging instruments for green power. Part B Sol Energy 2013;98:167–79.
[2] CSIRO. Solar intermittency: Australia's clean energy challenge. Tech. rep. CSIRO; June 2012.
[3] Del Carpio-Huayllas TE, Ramos DS, Vasquez-Arnez RL. Feed-in and net metering tariffs: An assessment for their application on microgrid systems. In: Proc. 6th IEEE/PES Latin America Conf. and Exposition on Transmission and Distribution (T&D-LA'12), Montevideo, Uruguay; 2012. p. 1–6.

[4] Campoccia A, Dusonchet L, Telaretti E, Zizzo G. Feed-in tariffs for grid-connected PV systems: The situation in the European community. In: Proc. IEEE Conf. on Power Tech, Lausanne, Switzerland; 2007. p. 1981–6.
[5] Hirth L, Ueckerdt F. Redistribution effects of energy and climate policy: The electricity market. Energy Policy 2013;62:934–47.
[6] von Appen J, Braun M, Stetz T, Diwold K, Geibel D. Time in the sun: the challenge of high PV penetration in the German electric grid. IEEE Power Energy Mag 2013;11(2):55–64.
[7] Ogimoto K, Kaizuka I, Ueda Y, Oozeki T. A good fit: Japan's solar power program and prospects for the new power system. IEEE Power Energy Mag 2013;11(2):65–74.
[8] van Werven MJN, Scheepers MJJ. The changing role of distribution system operators in liberalised and decentralising electricity markets. In: Proc. IEEE Int. Conf. on Future Power Systems, Amsterdam, Netherlands; 2005. p. 1–6.
[9] Stetz T, Marten F, Braun M. Improved low voltage grid-integration of photovoltaic systems in Germany. IEEE Trans Sustain. Energy 2013;4(2):534–42.
[10] Tzartzev R, Grady WM, Patel J. Impact of high-penetration PV on distribution feeders. In: Proc. 3rd IEEE PES Int. Conf. and Exhibition on Innovative Smart Grid Technologies (ISGT Europe), Berlin, Germany; 2012. p. 1–6.
[11] Baran ME, Hooshyar H, Shen Zhan, Huang A. Accommodating high PV penetration on distribution feeders. IEEE Trans Smart Grid 2012;3(2):1039–46.
[12] Tonkoski R, Turcotte D, El-Fouly THM. Impact of high PV penetration on voltage profiles in residential neighborhoods. IEEE Trans Sustain. Energy 2012;3(3):518–27.
[13] Masters CL. Voltage rise the big issue when connecting embedded generation to long 11 kV overhead lines. Power Eng J 2002;16(1):5–12.
[14] Katiraei F, Agüero JR. Solar PV integration challenges. IEEE Power Energy Mag 2011;9(3):62–71.
[15] Hill CA, Such MC, Chen Dongmei, Gonzalez J, Grady WM. Battery energy storage for enabling integration of distributed solar power generation. IEEE Trans Smart Grid 2012;3(2):850–7.
[16] Nykamp S, Molderink A, Hurink JL, Smit GJM. Storage operation for peak shaving of distributed PV and wind generation. In: Proc. 2013 IEEE PES Conf. on Innovative Smart Grid Technologies (ISGT'13), Washington, DC; 2013. p. 1–6.
[17] Ueda Yuzuru, Kurokawa K, Tanabe T, Kitamura K, Sugihara H. Analysis results of output power loss due to the grid voltage rise in grid-connected photovoltaic power generation systems. IEEE Trans Ind Electron 2008;55(7):2744–51.
[18] Tonkoski R, Lopes LAC, El-Fouly THM. Coordinated active power curtailment of grid connected PV inverters for overvoltage prevention. IEEE Trans Sustain. Energy 2011;2(2):139–47.
[19] Farhangi H. The path of the smart grid. IEEE Power & Energy Mag 2010;8(1):18–28.
[20] Alam MJE, Muttaqi KM, Sutanto D. Mitigation of rooftop solar PV impacts and evening peak support by managing available capacity of distributed energy storage systems. IEEE Trans Power Syst 2013;28(4):3874–84.
[21] Erol-Kantarci M, Mouftah HT. Wireless sensor networks for cost-efficient residential energy management in the smart grid. IEEE Trans Smart Grid 2011;2(2):314–25.
[22] Corradi O, Ochsenfeld H, Madsen H, Pinson P. Controlling electricity consumption by forecasting its response to varying prices. IEEE Trans Power Syst 2013;28(1):421–9.
[23] Vrettos E, Lai KuanLin, Oldewurtel F, Andersson G. Predictive control of buildings for demand response with dynamic day-ahead and real-time prices. In: Proc. 2013 IEEE European Control Conference, Zürich, Switzerland; 2013. p. 2527–34.
[24] Shao Shengnan, Pipattanasomporn M, Rahman S. Demand response as a load shaping tool in an intelligent grid with electric vehicles. IEEE Trans Smart Grid 2011;2(4):624–31.
[25] Bashash S, Fathy HK. Modeling and control of aggregate air conditioning loads for robust renewable power management. IEEE Trans Control Syst Technol 2013;21(4):1318–27.
[26] Callaway DS, Hiskens IA. Achieving controllability of electric loads. Proc IEEE 2011;99(1):184–99.
[27] Pipattanasomporn M, Kuzlu M, Rahman S. An algorithm for intelligent home energy management and demand response analysis. IEEE Trans Smart Grid 2012;3(4):2166–73.
[28] Bitar EY, Poolla K. Selling wind power in electricity markets: the status today, the opportunities tomorrow. In: Proc. American Control Conference (ACC'12), Montreal, QC; 2012. p. 3144–7.
[29] Ibars C, Navarro M, Giupponi L. Distributed demand management in smart grid with a congestion game. In: Proc. 1st IEEE Int. Conf. on Smart Grid Communications (SmartGridComm'10), Gaithersburg, MD; 2010. p. 495–500.
[30] Mohsenian-Rad A-H, Leon-Garcia A. Optimal residential load control with price prediction in real-time electricity pricing environments. IEEE Trans Smart Grid 2010;1(2):120–33.
[31] Nykamp S, Bosman MGC, Molderink A, Hurink JL, Smit GJM. Value of storage in distribution grids – competition or cooperation of stakeholders? IEEE Trans Smart Grid 2013;4(3):1361–70.
[32] Palensky P, Dietrich D. Demand side management: demand response, intelligent energy systems, and smart loads. IEEE Trans Ind Informatics 2011;7(3):381–8.
[33] Nottrott A, Kleissl J, Washom B. Energy dispatch schedule optimization and cost benefit analysis for grid-connected, photovoltaic-battery storage systems. Renew Energy 2013;55:230–40.
[34] Ru Yu, Kleissl J, Martínez S. Storage size determination for grid-connected photovoltaic systems. IEEE Trans Sustain. Energy 2013;4(1):68–81.
[35] Ru Yu, Kleissl J, Martínez S. Exact sizing of battery capacity for photovoltaic systems. Eur J Control 2014;20(1):24–37.
[36] Riffonneau Y, Bacha S, Barruel F, Ploix S. Optimal power flow management for grid connected PV systems with batteries. IEEE Trans Sustain. Energy 2011;2(3):309–20.
[37] Hubert T, Grijalva S. Modeling for residential electricity optimization in dynamic pricing environments. IEEE Trans Smart Grid 2012;3(4):2224–31.
[38] Darghouth NR, Barbose G, Wiser RH. Customer-economics of residential photovoltaic systems (Part 1): The impact of high renewable energy penetrations on electricity bill savings with net metering. Energy Policy 2014;67:290–300.
[39] Black AJ. Financial payback on California residential solar electric systems. Sol Energy 2004;77(4):381–8.
[40] Sweet B. California's energy-storage mandate. 6th Nov. 2013. Tech. rep., IEEE Spectrum EnergyWise Newsletter.
[41] Candelise C, Winskel M, Gross RJK. The dynamics of solar PV costs and prices as a challenge for technology forecasting. Renew Sustain Energy Rev 2013;26:96–107.
[42] Nair N-KC, Garimella N. Battery energy storage systems: assessment for small-scale renewable energy integration. Energy & Build 2010;42(11):2124–30.
[43] Brown S, Pyke D, Steenhof P. Electric vehicles: the role and importance of standards in an emerging market. Energy Policy 2010;38(7):3797–806.
[44] Ratnam EL, Weller SR, Kellett CM. An optimization-based approach for assessing the benefits of residential battery storage in conjunction with solar PV. In: Proc. IX IEEE Int. Symp. Bulk Power System Dynamics and Control (IREP'13), Rethymno, Greece; 2013. p. 1–8.
[45] Nair NC, Nayagam R, Francis R. New Zealand utility experiences with demand side management. In: Proc. 2008 IEEE Power & Energy Society General Meeting, Pittsburgh, PA; 2008. p. 1–5.
[46] Sedghisigarchi K. Residential solar systems: technology, net-metering, and financial payback. In: Proc. IEEE Conf. on Electrical Power & Energy (EPEC), Montreal, Canada; 2009. p. 1–6.

4

Assessing the benefits of net metering

In Chapter 3 we presented a quadratic program (QP)-based algorithm for the day-ahead scheduling of residential battery storage co-located with solar PV, in the context of PV incentives such as feed-in tariffs. A greedy-search heuristic that selected the key design parameters in the QP-based scheduling algorithm was proposed to improve operational savings that accrue to customers.

Chapter 4 includes the paper titled *Scheduling residential battery storage with solar PV: Assessing the benefits of net metering*. One of the key contributions of this paper is a day-ahead linear program (LP)-based scheduling algorithm that maximizes the operational savings that accrue to residential PV customers with battery storage, in the context of net metering. By means of a case study, we evaluate and benchmark the LP-based approach against the QP-based approach as defined in Chapter 3. Our framework for defining a residential energy system is consistent with Chapter 3, with the exception of some notational changes made to improve the clarity and presentation of the published manuscript.

Applied Energy 155 (2015) 881–891

Contents lists available at ScienceDirect

Applied Energy

journal homepage: www.elsevier.com/locate/apenergy

Scheduling residential battery storage with solar PV: Assessing the benefits of net metering

Elizabeth L. Ratnam *, Steven R. Weller, Christopher M. Kellett

School of Electrical Engineering and Computer Science, University of Newcastle, University Drive, Callaghan, NSW 2308, Australia

HIGHLIGHTS

- Linear- and quadratic-program based scheduling of residential battery storage.
- Increase daily operational savings in the context of net metering.
- Consider large voltage swings that stem from reverse power flow and peak loads.
- Applied to a real dataset consisting of 145 Australian residential customers with PV.
- Reverse power flow is absent in the case study when all customers QP energy-shift.

ARTICLE INFO

Article history:
Received 22 October 2014
Received in revised form 4 June 2015
Accepted 22 June 2015
Available online 7 July 2015

Keywords:
Photovoltaics
Battery scheduling
Net metering
Peak-load reduction
Reverse power flow

ABSTRACT

In this paper we propose a linear program (LP)-based algorithm to schedule battery storage co-located with residential solar photovoltaics (PV), when excess generation is compensated via net metering. While the objective of this LP-based approach is to maximize the operational savings that accrue to customers, an undesirable consequence to the utility is reverse power flow during the peak pricing period. We show in this paper that it is possible to balance the objective of the utility in limiting reverse power flow, with the customer objective of increasing operational savings, in the context of net metering. To balance the specified utility and customer objectives we employ a quadratic program (QP)-based algorithm, which explicitly penalizes reverse power flow. To complete our assessment of net metering, both the LP-based and QP-based scheduling algorithms are applied to measured load and generation data from 145 residential customers located in an Australian distribution network. The results of this case study confirm the absence of reverse power flow when all customers employ a QP-based battery schedule, with the majority of customers exhibiting operational savings.

1. Introduction

Government incentives, renewable energy rebates and concerns for sustainable energy growth have led to the rapid uptake of residential solar photovoltaics (PV), a trend expected to continue over the next decade [1,2]. However, the daily and seasonal variability of the solar resource, in addition to intermittency arising from moving cloud cover, poses challenges for distributors in maintaining system voltages within operational limits [3,4]. Moreover, distribution grids are typically designed for one way power from high voltage substations to low voltage customers, therefore, a significant penetration of residential PV potentially degrades the effectiveness of existing voltage control and protection schemes [5,6].

As residential PV penetration increases, the management of system voltages within operational limits becomes increasingly challenging. For example, if PV generation exceeds both local demand at the point of common coupling (PCC), and that of the downstream feeder, the excess PV generation is pushed upstream creating voltage rise [7–9]. Furthermore, if a passing cloud results in a loss of PV generation along a feeder, the voltage across the feeder will dip [10,11]. When these voltage deviations either exceed the upper voltage limit, or fall below the lower voltage limit, solutions are needed to mitigate the system non-compliance [12,13].

There are a number of emerging approaches to overcome non-compliant voltage deviations arising from the intermittency and variability of solar PV, with applicable incentives, mandates and regulation driving the solutions [14]. Some of these approaches include energy storage [15,16], direct load control [17], price-responsive load control [18], active PV generation curtailment [19], and enhanced PV inverter control to manage real

* Corresponding author. Tel.: +61 2 492 16026; fax: +61 2 492 16993.
E-mail addresses: elizabeth.ratnam@ieee.org (E.L. Ratnam), Steven.Weller@newcastle.edu.au (S.R. Weller), Chris.Kellett@newcastle.edu.au (C.M. Kellett).

http://dx.doi.org/10.1016/j.apenergy.2015.06.061
0306-2619/

and reactive power output [20,21]. Moreover, Kabir er al. [22] shows that reactive compensation from PV inverters alone is not always sufficient to maintain acceptable voltage profiles along a distribution feeder. Different incentives driving these approaches include dynamic day-ahead electricity tariffs [23–25], reductions in appliance-specific electricity billing [17,26], standards curbing PV production [27], and energy storage mandates such as those in California [28]. Depending on the incentives and regulatory environment, a combination if not all of these approaches are suitable demand management options for distribution operators faced with significant PV penetration.

Several authors have investigated co-locating battery storage with solar PV with a focus on reducing network peak demand [29–36], leading to battery schedules that either assist or exacerbate voltage rise associated with reverse power flow when inverters operate at unity power factor [21,35]. The reduction of network peak demand is incorporated into a linear program in [29], where the energy flowing from the point of common coupling (PCC) to the customer is minimized when residential load exceeds residential PV production. Otherwise the battery is scheduled in [29] to charge during the off-peak pricing period, and discharge during the peak pricing period, with no limit on reverse power flow (i.e., the power delivered to the grid). Consequently, battery scheduling in [29] potentially induces voltage rise at the PCC. The reduction of network peak demand is also incorporated into an optimization problem in [30], where the objective function includes financial incentives for residents to deliver energy to the grid when the purchase cost of electricity is high. Hence, when interconnected customers in close proximity minimize the objective function in [30], large voltage swings associated with reverse power flow potentially arise due to the battery scheduling.

In contrast, peak demand and reverse power flow is reduced by solving the optimization problems in [31,32], where the objective functions eliminate residential subsidies for electricity delivered to the grid and include payments for electricity received from the grid. Thus, the optimization problems in [31,32] potentially reduce voltage rise associated with reverse power flow. The optimization problem in [33] also removes incentives for reverse power flow associated with battery scheduling, while permitting incentives encouraging solar PV uptake. In addition, the optimization problem in [33] includes residential payments for electricity received from the grid. Consequently, the optimization problem in [33] leads to reductions in both peak demand and reverse power flow, potentially mitigating voltage rise. Another method for reducing both peak demand and reverse power flow is incorporated into the optimization problem in [34], where a sophisticated dynamic pricing environment provides additional incentives for customers to smooth their day-ahead energy consumption. Hence, the optimization problem in [34] potentially abates voltage rise associated with reverse power flow.

Increasing the accuracy of load and generation forecasts in [30,29,31–34] will improve battery scheduling, leading to additional savings for customers [34], and further reductions in peak demand [33]. Approaches to improving PV generation forecasts are considered in [37]. Incorporating continuous updates in PV generation forecasts when charging or discharging the battery is considered in [29,38], where the authors implement Receding Horizon Optimization (RHO). Likewise, the receding horizon approach in [29] incorporates updates in load forecasts. Moreover, RHO together with real time prediction of weather forecasts are implemented in [39] to optimally operate a hybrid renewable energy system consisting of solar, wind, diesel generators, and battery storage, with the purpose of supporting the load of a single residential household.

In this paper we present a linear programming (LP)-based approach to designing day-ahead battery charge and discharge schedules when any generation in excess of residential load is compensated by the electricity retailer via net metering [30,40,41]. In the LP-based approach we consider two customer objectives: the first is to reduce the daily payments for electricity received from the grid; and the second is to increase daily profits arising from the delivery of electricity to the grid. These two customer objectives are combined in the day-ahead operational savings, which we maximize. In the context of net metering, we also show the operational savings pertaining to the LP-based battery charge and discharge schedules are independent of any power flows related to load and PV generation. Hence the LP-based approach that maximizes the day-ahead operational savings does not require day-ahead forecasts of load and PV generation. Further, the LP-based algorithm presented in this paper did not previously appear in our earlier work [42,43], or to the best of our knowledge elsewhere.

An undesirable consequence of the battery schedule maximizing operational savings in this LP-based approach is reverse power flow during peak pricing periods. More specifically, the financial policy of net metering together with time-of-use electricity prices incentivize customers to discharge battery storage during the peak pricing period. To mitigate against non-compliant voltage deviations arising from reverse power flow, we consider a quadratic program (QP)-based scheduling algorithm, first presented in [42,43]. Our earlier work in [42,43] assessed the customer benefit of the QP-based algorithm for a range of metering topologies, in the context of feed-in tariffs (FiTs). In the present paper we consider both the customer and utility benefits of the QP-based scheduling algorithm, in the context of net metering. Furthermore, the LP-based and QP-based results in this paper have not previously appeared in [42,43], or elsewhere.

In the present paper we demonstrate that the QP-based scheduling algorithm with net metering effectively balances the customer's objective of increasing the daily operational savings with the distributor's need to reduce reverse power flow that leads to non-compliant voltage rise. We anticipate load flow analysis will assist distributors in identifying non-compliant voltage rise ahead of time, so that the QP-based scheduling algorithm may be implemented before the expected voltage rise occurs. Implicit in our approach is the expectation that inverters operate at unity power factor, and electricity prices correspond to energy purchased by or from the resident.

To implement our approach each residential customer requires an energy management system that (1) coordinates with Advanced Metering Infrastructure (AMI) to receive day-ahead prices for energy delivered to and from the grid; (2) runs optimization-based algorithms daily; and (3) schedules battery storage in the day-ahead. Additionally, if implementing the QP-based algorithm, the energy management system will forecast the day-ahead power-flows of residential load and PV generation. In this paper, for the purpose of implementing the QP-based algorithm, we assume the day-ahead forecasts of residential load and PV generation are known and error-free.

Implicit in our approach is the expectation that global investment and government mandates will drive both technology improvements and economies of scale for battery storage as has happened with solar PV [28,44–46]. Therefore we do not explicitly consider the capital cost of purchasing a battery, rooftop solar panels, and the associated cost of inverters. Instead we focus on increasing the operational savings that accrue to a resident when scheduling a battery. Furthermore, we employ a deliberately simplified battery model to assess the maximum operational savings when net metering, which may be extended for more specific battery technologies. For example, battery storage combined with an ultra-capacitor is expected to assist in increasing the battery lifetime [47].

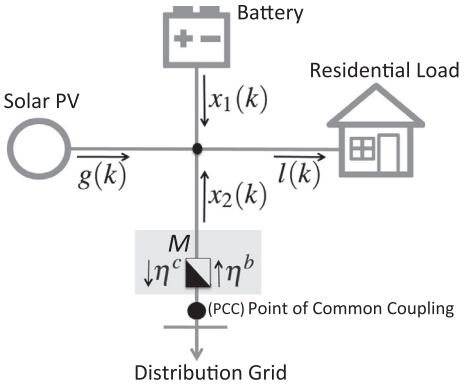

Fig. 1. Residential network illustrating the direction of positive power flows and financial incentives to energy time-shift. Arrows associated with $g(k), l(k), x_1(k)$ and $x_2(k)$ illustrate the assumed direction of positive power flow. Financial incentives for meter M are represented by vectors η^b and η^c (in \$/kWh), in which arrows illustrate the direction of power flow relevant for η^b and η^c.

This paper is organized as follows. In Section 2 we define the energy bill and operational savings associated with the measured power flows illustrated in Fig. 1. To increase the operational savings, algorithms for finding the preferred rate to charge and discharge a battery are introduced in Section 3. In Section 4 the algorithms are implemented and evaluated given real-world data from an Australian electricity distributor.

1.1. Notation

Let $\mathbb{R}^s$ denote s-dimensional vectors of real numbers and $\mathbb{R}^s_{\geqslant 0}$ s-dimensional vectors with all non-negative components where, as usual, $\mathbb{R}^1 = \mathbb{R}$. $\mathbf{I}$ denotes the s-by-s identity matrix and $\mathbb{1} \in \mathbb{R}^s_{\geqslant 0}$ denotes the all-1s column vector of length s. $\mathbf{0}$ denotes an all-zero matrix, or an all-zero column vector, where the context will make clear the dimension intended, and $\mathbf{T} = [t_{ij}]$ denotes the s-by-s matrix satisfying $t_{ij} = 1$ for $i \geqslant j$ and $t_{ij} = 0$ elsewhere.

2. Problem formulation

In this section we define a single residential customer's energy bill and associated operational savings when scheduling a battery in the day-ahead, considering the network topology depicted in Fig. 1. We include detailed definitions of electricity prices and power flows to show that the operational savings when net-metering are independent of any power flows related to load and PV generation.

2.1. Definitions

Fig. 1 illustrates the topology of the system under consideration, where bi-directional meter M measures the power flow $x_2(k)$. By combining the power flow $x_2(k)$ with prices for buying and selling electricity, we can determine if a resident will incur an energy bill or be compensated for excess generation. We represent electricity prices by the vectors η^b (the price at which a customer *buys* electricity) and η^c (the price at which a customer is *compensated* for supplying electricity to the grid) in Fig. 1.

In Fig. 1 the measured power flow (in kW) over the kth interval of length Δ is denoted by $x_2(k)$. To represent all measured power flows over a time window $[0, T]$ we define a vector of length s, where s is the number of time intervals of length Δ, and $T = s\Delta$ (in hours) is the time window of interest. We define the *grid profile* over the period $[0, T]$ by $x_2 := [x_2(1), \ldots, x_2(s)]^T \in \mathbb{R}^s$, where by convention we represent the average power flowing from (to) the grid to (from) the energy system over the period $((k-1)\Delta, k\Delta)$ by $x_2(k) > 0 (x_2(k) < 0)$ for all $k \in \{1, \ldots, s\}$. In this paper we generally consider $T = 24$ h and $\Delta = 1/2$ h (30 min), which implies $s = 48$. Other choices are certainly possible, subject only to commensurability of T, Δ and s.

The average power $x_2(k)$ (in kW) supplied by (or to) the grid, is billed (or compensated), according to the *financial policy* associated with meter M. To define the financial policy we denote *electricity billing* (in \$/kWh) at meter M over the period $((k-1)\Delta, k\Delta)$ by $\eta^b(k)$ for all $k \in \{1, \ldots, s\}$, and define the *electricity billing profile* over $[0, T]$ by $\eta^b := [\eta^b(1), \ldots, \eta^b(s)]^T \in \mathbb{R}^s_{\geqslant 0}$. Likewise, we denote *electricity compensation* (in \$/kWh) at meter M over the period $((k-1)\Delta, k\Delta)$ by $\eta^c(k)$ for all $k \in \{1, \ldots, s\}$, and define the *electricity compensation profile* over $[0, T]$ by $\eta^c := [\eta^c(1), \ldots, \eta^c(s)]^T \in \mathbb{R}^s_{\geqslant 0}$. Thus, a financial policy is defined by the day-ahead *electricity billing profile* applied when power flows in the direction $x_2(k) > 0$ (from the PCC to node 1), and the day-ahead *electricity compensation profile* applied when power flows in the reverse direction $(x_2(k) < 0)$.

In this paper our focus is on a financial policy of *net metering* defined by a resident being billed at the same rate as they are compensated for excess generation [40,41], i.e., $\eta^b(k) = \eta^c(k)$ for all $k \in \{1, \ldots, s\}$, irrespective of the direction of $x_2(k)$. We denote the financial policy of net metering by $\eta \in \mathbb{R}^s_{\geqslant 0}$ where

$$\eta = \eta^b = \eta^c. \tag{1}$$

The remaining power flows represented in Fig. 1 are defined as follows. We represent the average power delivered to the residential load (in kW) over the period $((k-1)\Delta, k\Delta)$ by $l(k)$ for all $k \in \{1, \ldots, s\}$, and define the *load profile* over $[0, T]$ as $l := [l(1), \ldots, l(s)]^T \in \mathbb{R}^s_{\geqslant 0}$. Likewise we represent the average PV generation (kW) over the period $((k-1)\Delta, k\Delta)$ by $g(k)$ for all $k \in \{1, \ldots, s\}$, and define the *generation profile* over $[0, T]$ as $g := [g(1), \ldots, g(s)]^T \in \mathbb{R}^s_{\geqslant 0}$. In this paper, we assume the day-ahead load and generation profiles are known and perfect.

We represent the average power (kW) delivered from (or to) the battery over the period $((k-1)\Delta, k\Delta)$ by $x_1(k) > 0$ (or $x_1(k) < 0$) for all $k \in \{1, \ldots, s\}$, and define the *battery profile* over $[0, T]$ as $x_1 := [x_1(1), \ldots, x_1(s)]^T \in \mathbb{R}^s$. By convention we represent charging (discharging) of the battery by $x_1(k) < 0 (x_1(k) > 0)$, where $x_1(k)$ is a linear function of a fixed and known battery voltage and the respective input (or output) battery current. The linear relationship between the battery charge/discharge power and the charge/discharge current is described in [48].

From the configuration of the residential energy system in Fig. 1, we observe that the power balance equation

$$x_2(k) = l(k) - g(k) - x_1(k) \tag{2}$$

must hold for all $k \in \{1, \ldots, s\}$.

In the absence of a battery in Fig. 1 the measured power flow at meter M is denoted by $\tilde{x}_2(k)$, and the power balance equation reduces to

$$\tilde{x}_2(k) = l(k) - g(k) \quad \text{for all } k \in \{1, \ldots, s\}, \tag{3}$$

since the battery charging/discharging power $x_1(k) = 0$ for all $k \in \{1, \ldots, s\}$. We denote the grid profile for the case in (3) by the *baseline* grid profile, defined as

$$\tilde{x}_2 := [\tilde{x}_2(1), \ldots, \tilde{x}_2(s)]^T. \tag{4}$$

2.2. Battery constraints

The inclusion of the battery in Fig. 1 leads to additional constraints, which we now detail. To capture the limited "charging/discharging power" of the battery, we constrain x_1 by

$$\underline{B}\mathbb{1} \leqslant x_1 \leqslant \overline{B}\mathbb{1}, \tag{5}$$

where $\underline{B} \in \mathbb{R}_{\leqslant 0}$ and $\overline{B} \in \mathbb{R}_{\geqslant 0}$ reflect a "charge/discharge" current limitation in the battery [48].

Given the battery profile x_1, the *state of charge* of the battery (in kWh) at time $k\Delta$ is denoted by $\chi(k)$ where

$$\chi(k) \;:=\; \chi(0) - \sum_{j=1}^{k} x_1(j)\Delta \qquad \text{for all } k \in \{1,\ldots,s\}, \tag{6}$$

and $\chi(0)$ denotes the initial state of charge of the battery. We represent the *state of charge profile* by $\chi := [\chi(0),\ldots,\chi(s)]^T \in \mathbb{R}^{s+1}$. For lead-acid batteries, more complicated state of charge models have been developed in [30,33,49].

We represent the battery capacity (in kWh) by $C \in \mathbb{R}_{\geqslant 0}$, and it necessarily follows that the state of charge profile is constrained by

$$\mathbf{0} \leqslant \chi \leqslant C\begin{bmatrix}1\\ \mathbb{1}\end{bmatrix}. \tag{7}$$

For a fixed initial state of charge satisfying $0 \leqslant \chi(0) \leqslant C$, we define $\underline{\mathbf{C}} := (\chi(0)/\Delta)\mathbb{1}$, and $\overline{\mathbf{C}} := (1/\Delta)(C-\chi(0))\mathbb{1}$, and rewrite the battery constraints (6) and (7) as

$$-\underline{\mathbf{C}} \leqslant -\mathbf{T}x_1 \leqslant \overline{\mathbf{C}}. \tag{8}$$

In this paper, we optimize a battery profile over a single day. To assess the benefits of net metering, we perform this optimization over consecutive days. To account for battery aging, we may reduce the battery capacity C on each consecutive day. To avoid an energy-shifting bias in our results, we insist that the state of charge of the battery at the end of a day is the same as the state of charge of the battery at the beginning of the day, i.e.,

$$\chi(s) = \chi(0), \tag{9}$$

where $\chi(s)$ is the final state of charge at time $s\Delta$. In particular, constraint (9) ensures the battery energy-shifts across a day, such that no additional charge is expended by the battery or stored at the completion of each day [42].

Let $A_1 \in \mathbb{R}^{4s\times s}$, and $b_1 \in \mathbb{R}^{4s}$ be defined by

$$A_1 \;:=\; \begin{bmatrix}\mathbf{I}\\ -\mathbf{I}\\ \mathbf{T}\\ -\mathbf{T}\end{bmatrix}, \quad b_1 \;:=\; \begin{bmatrix}\overline{B}\mathbb{1}^T & \underline{B}\mathbb{1}^T & \underline{\mathbf{C}}^T & \overline{\mathbf{C}}^T\end{bmatrix}^T. \tag{10}$$

With the above as background, we substitute Eq. (10) into Eqs. (5) and (8), and Eq. (9) into (6), to succinctly write the battery constraints as

$$A_1x_1 \leqslant b_1, \tag{11}$$

$$\mathbb{1}^Tx_1 = 0. \tag{12}$$

In what follows, we assess the annual operational benefits pertaining to battery storage by optimizing a battery profile x_1 subject to constraints (11) and (12), one day at a time for 365 consecutive days, where $\chi(0)$ is known and fixed. More specifically, in the simulations that follow the battery constraints in (11) and (12) include a battery capacity limit of $C = 10$ kWh, and an initial state of charge of $\chi(0) = 5$ kWh. The 10 kWh battery capacity is consistent with the Tesla Powerwall unit available to customers in the United States [50]. In the illustrative example presented in Section 3.2 we include a battery charge/discharge limit of $\overline{B} = -\underline{B} = 2$ kW, consistent with the continuous power limit of the Tesla Powerwall [50]. In Section 4 we include a charging/discharging limit of $\overline{B} = -\underline{B} = 5$ kW, which would require a specially purposed power outlet rather than a General Purpose Outlet (GPO) at the residential premises. We anticipate 5 kW power outlets will be available to residential customers with electric vehicles in the near future.

2.3. Energy bill

To define the energy bill for the residential energy system in Fig. 1, we combine the relevant electricity prices (in \$/kWh) with measured power flows (in kW). In Section 2.1 we defined day-ahead electricity prices in terms of the financial policy applied at meter M. We assume the day ahead billing and compensation profiles in the financial policy are fixed by the utility or regulatory body, and are available to the consumer.

In defining the daily residential energy bill, we ignore the cost associated with charging the battery to an initial state of charge $\chi(0)$, assuming the final state of charge $\chi(s)$ will provide adequate compensation, cf. (9).

We now define the energy bill associated with the financial policy of net metering, relating to meter M by

$$\Sigma \;:=\; \Delta\eta^Tx_2, \tag{13}$$

which, by (3), reduces to the *baseline energy bill* for $C = 0$ defined as

$$\widetilde{\Sigma} \;:=\; \Delta\eta^T\tilde{x}_2 = \Delta\eta^T(l-g). \tag{14}$$

2.4. Operational savings

The *operational savings* (in \$/day) allow us to examine the effectiveness of scheduling a battery. We define the operational savings Ψ as the difference between the energy bills obtained with and without a battery as follows:

$$\Psi \;:=\; \widetilde{\Sigma} - \Sigma. \tag{15}$$

We recall from Section 2.3 the energy bill Σ is defined for a particular financial policy of net metering, given load and generation profiles l and g, a battery of a given size C, with constraints in (11) and (12) known and specified.

For a financial policy of net metering (1) the following Lemma quantifies the operational savings in terms of battery profile x_1 and demonstrates that the operational savings are independent of load and generation forecasts.

Lemma 1. *Consider a residential energy network employing a financial policy of net metering as defined in* Eq. (1)*, where $\eta \in \mathbb{R}^s_{\geqslant 0}$ is assumed fixed and known. Let $x_1 \in \mathbb{R}^s$ represent the battery profile over $[0,T]$ where $T = s\Delta$. Then the operational savings are given by*

$$\Psi = \Delta\eta^Tx_1. \tag{16}$$

Proof. Substituting the power balance equation in (2) into the energy bill defined in (13) yields

$$\Sigma = \Delta\eta^Tx_2 = \Delta\eta^T(l-g-x_1) = \Delta\eta^T\tilde{x}_2 - \Delta\eta^Tx_1,$$

and with (15) we obtain

$$\Psi = \widetilde{\Sigma} - \Sigma = \Delta\eta^T\tilde{x}_2 - \left(\Delta\eta^T\tilde{x}_2 - \Delta\eta^Tx_1\right) = \Delta\eta^Tx_1.$$

□

Remark 1. If the price of electricity is constant then there exists $a \in \mathbb{R}_{>0}$ such that $\eta = a\mathbb{1}$, and the operational savings in Eq. (16) are reduced to \$0 [42, Lemma 2].

To investigate the longer term benefits of net metering, we sum the daily operational savings over a year [32,42]. We define the summation of each daily operational savings over 365 days in \$/yr as the *annual savings*. Thus, when the annual savings are positive, there exists an operational benefit to scheduling a battery and when the annual savings are negative there is an operational cost to scheduling a battery.

Through we do not do so in this paper, the general approach described above may be extended in two useful ways. First, the battery capacity C, in Eq. (7) can be reduced by a small amount each day to account for battery aging. Second, the electricity prices, η, can be adjusted daily to account for generation shortages or network constraints.

3. Algorithms for scheduling a battery

In this section we present two approaches for scheduling a battery in a residential energy network given a financial policy of net metering (1). The first approach maximizes the operational savings in (16). The second approach aims to reduce the impact of the residential energy system on the grid, where priority is given to the reduction of energy flowing to and from the grid during the peak pricing period.

3.1. Maximizing residential savings

To maximize the operational savings in (16) we require the day-ahead net metering financial policy (1) and the battery constraints (11) and (12). Lemma 1 indicates that the battery profile that maximizes the operational savings is independent of day-ahead load and generation profiles, and subsequently the power balance equation in (2). Lemma 2 below establishes this constrained maximization as a linear program (LP).

Lemma 2. *Consider a residential energy network employing a financial policy of net metering as defined in* Eq. (1)*, with* $\eta \in \mathbb{R}^s_{\geqslant 0}$ *assumed fixed and known. The maximum operational savings are obtained by solving the linear program*

$$\max_{x_1 \in \mathbb{R}^s} c^T x_1 \tag{17}$$

such that

$$A_1 x_1 \leqslant b_1, \tag{18}$$

$$\mathbb{1}^T x_1 = 0, \tag{19}$$

where $c := \Delta\eta \in \mathbb{R}^s$.

Proof. The result follows directly from Lemma 1 given the battery constraints (11) and (12) defined in Section 2.2, and a financial policy of net metering (1). □

We will refer to the process of a customer implementing the daily battery profile obtained by solving (17) subject to constraints (18) and (19) as *LP energy-shifting*. When LP energy-shifting, the grid profile obtained through substitution of the load, generation and battery profiles into the power balance equation in (2) is said to be *LP energy-shifted*.

3.2. Example

In this example we consider a 10 kWh battery to illustrate LP energy-shifting in the residential energy network given in Fig. 1. Let $C = 10$ kWh (battery capacity), $\chi(0) = 0.5C$ (initial state of charge of the battery), and $\overline{B} = -\underline{B} = 2$ kW (charge/discharge limits).[1] Let $T = 24$ h, $\Delta = 0.5$ h and $s = T/\Delta = 48$ be fixed throughout.

Let the financial policy of net metering (1) associated with meter M be specified as shown below in Fig. 2(a). In Fig. 2(a) we observe the electricity prices peak from 2 pm to 8 pm, and are ten times the cost of electricity from 10 pm to 7 am. From 7 am to 2 pm, and again from 8 pm to 10 pm, electricity is billed, or compensated, at the rate of \$0.06/kWh.

Let the load and generation profiles l and g be specified as shown in Fig. 2(b), where the residential load includes a utility controlled heated water cylinder [26].[2] Due to the water heater, the load profile peaks around midnight in Fig. 2(b), which does not align with the generation profile peak around midday.

Using the above setup, Fig. 2(c) illustrates the *baseline* grid profile $\tilde{x}_2$ (corresponding to the absence of a battery), as defined in Eq. (4). By contrast, maximization of operational savings using the solution of the linear program in Lemma 2 yields the battery profile x_1 illustrated in Fig. 2(d). Substituting the battery profile x_1 into the power balance equations in (2) returns the corresponding grid profile x_2, also shown in Fig. 2(d). Comparing the baseline grid profile in Fig. 2(c) to the grid profile in Fig. 2(d), we observe the 10 kW battery charges ($x_1 < 0$) between 11:30 pm–midnight, increasing the grid profile peak (from 3.5 kW to 5.5 kW), and discharges ($x_1 > 0$) between 2 pm and 8 pm, reducing the grid profile such that power is delivered to the grid for the entire peak pricing period.

This example demonstrates that the grid profile x_2 is not penalized for reverse power flow, nor for increased peaks in the grid profile when LP energy-shifting. Hence, net metering with an unrestricted grid profile will not aid distribution operators in maintaining system voltages within operational limits.

3.3. Including utility benefits

In the previous example we observed the solution to the LP-based algorithm scheduled a battery to discharge during peak pricing periods, which resulted in reverse power flow at the point of common coupling (PCC). The reverse power flow observed between 2 pm and 8 pm in Fig. 2(d) will increase the voltage at the PCC during the peak pricing period [21,35]. For voltage increases that exceed power quality standards, approaches are needed to mitigate system non-compliance. Moreover, significant reverse power flows in the distribution grid potentially degrade the effectiveness of existing voltage control and protection schemes that are typically designed for one-way power flow from the high voltage substation to the low voltage customer [5,4,6]. Problems that potentially occur when significant reverse power flows present in the existing distribution grid include:

- blinding of protection [5], or more specifically, overcurrent and earth fault relay under-reach [6, Section 3.4.1],
- false tripping of protection relays [6, Section 3.4.2], also known as sympathetic tripping [5],
- circuit breakers reclosing after a transient fault that is not extinguished when reverse power flow is present [4–6], and
- over-voltages at a customers' premises when existing on-line tap changing transformers have insufficient taps to lower the

[1] Other battery specifications are certainly possible in the battery model presented in Section 2.2.

[2] In some countries, residents often allow the utility to control their all-electric-heated water systems for periods in the day, given a financial incentive. For these customers, the utility switches their water-heating services on during periods of low load, and off during periods of peak-load, in a manner that ensures minimal impact to the network.

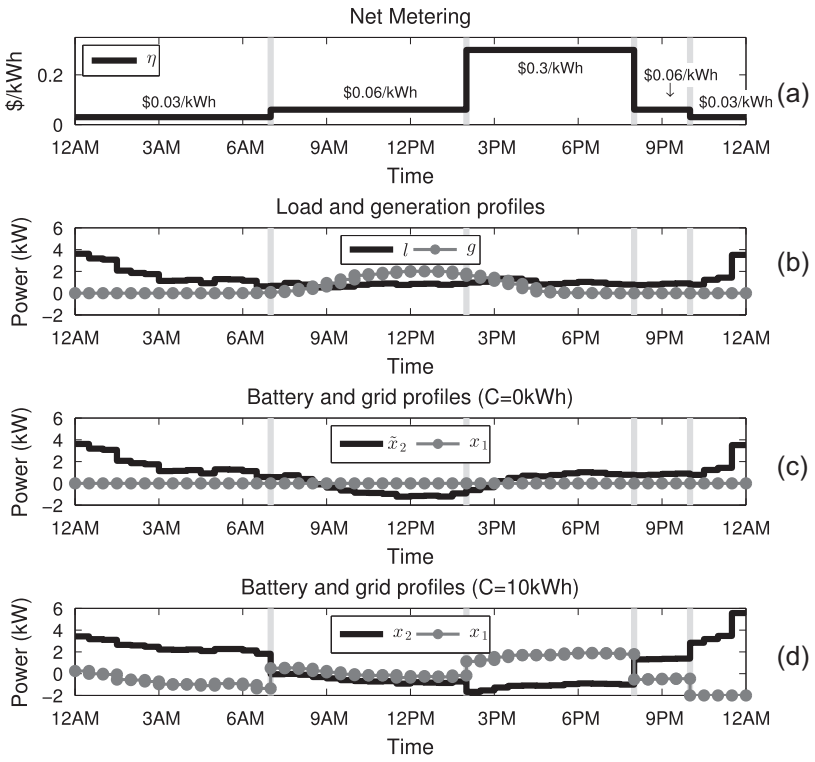

Fig. 2. The financial policy and profiles in Example 3.2. Financial policy (a), load and generation profiles (b), baseline grid and battery profiles (c), and grid and battery profiles for $C = 10$ kWh (d).

voltage sufficiently to enable reverse power flow in the distribution grid [4].

Therefore, reverse power flows potentially imposes costs on the electrical distributor, when the distributor is required to implement (often new) control and protection schemes that ensure a safe, reliable supply of high quality electricity to all customers [6, Section 8].

In what follows we consider penalizing reverse power flow at the PCC to reduce voltage rise when net metering. To balance penalties for reverse power flow with increases in operational savings when net metering, we consider a quadratic program (QP)-based scheduling algorithm that minimizes a weighted grid profile

$$\sum_{k=1}^{s} h(k)(x_2(k))^2, \tag{20}$$

where $h(k)$ is a selectable weighting such that $h(k) \geqslant 1$ for all $k \in \{1, \ldots, s\}$. In this paper the weights $h(k)$ in Eq. (20) are calculated via the greedy-search algorithm in [42].

In more detail, the energy management system selects the weights $h(k)$ via the greedy-search algorithm presented in [42, Section 5], given a financial policy, load and generation profiles l and g, and battery constraints $\chi(0), C, \overline{B}$, and $\underline{B}$. The greedy-search algorithm assigns weights $h(k)$ (where larger weights are often assigned to the peak pricing period) to balance penalties for reverse and positive power flows with increases in operational savings that accrue to a customer with rooftop solar generation, a battery, and residential load as shown in Fig. 1. Therefore, the QP algorithm does not significantly penalize reverse power flow at the PCC for each individual customer across the entire day (e.g., the shoulder pricing period from 7 am to 2 pm, when PV generation is potentially significant). However, we show in Section 4.3 that the QP-based algorithm is very effective at reducing reverse power flow across the entire day for the majority of PV customers. Moreover, the computational time to QP energy-shift (including the time to find the preferred $\mathbf{H}$) on each day for each residential customer is on average 0.44 s with a 1.7 GHz Intel Core i7 2013 processor. That is, the QP nature of this metric enables us to solve the optimization problem quickly, illustrating its suitability for Receding Horizon Control (RHC) extensions.

To minimize expression (20) we design a battery profile x_1, subject to constraints (11) and (12) and the power balance equation in (2). That is, we require the day-ahead load and generation profiles l and g that are unnecessary when LP energy-shifting, to ensure the power balance equation in (2) holds. We assume the day-ahead forecasts of residential load and PV generation are known and perfect.

For known and specified weights $h(k)$, the following Lemma expresses the constrained minimization in (20) as a quadratic program (QP).

Lemma 3 [42, Lemma 1]. *The minimization of expression* (20), *subject to battery constraints* (11) and (12) *and the power balance* Eq. (2), *can be written as the following quadratic program:*

$$\min_{x \in \mathbb{R}^{2s}} x^T H x \tag{21}$$

such that

$$\overline{A}_1 x \leqslant b_1, \tag{22}$$

$$A_2 x = b_2, \tag{23}$$

where $x \in \mathbb{R}^{2s}, H \in \mathbb{R}^{2s \times 2s}, \mathbf{H} \in \mathbb{R}^{s \times s}, \overline{A}_1 \in \mathbb{R}^{4s \times 2s}, A_2 \in \mathbb{R}^{(s+1) \times 2s}$, $b_2 \in \mathbb{R}^{s+1}$, *and*

$$x := \begin{bmatrix} x_1^T & x_2^T \end{bmatrix}^T, \quad H := \begin{bmatrix} \mathbf{0} & \mathbf{0} \\ \mathbf{0} & \mathbf{H} \end{bmatrix},$$

$$\mathbf{H} := \operatorname{diag}(h(1), \ldots, h(s)), \quad \overline{A}_1 := [A_1 \quad \mathbf{0}],$$

$$A_2 := \begin{bmatrix} \mathbb{1}^T & \mathbf{0}^T \\ \mathbf{I} & \mathbf{I} \end{bmatrix}, \quad b_2 := \begin{bmatrix} 0 \\ l - g \end{bmatrix}.$$

The grid profile obtained by solving (21) subject to constraints (22) and (23) is said to be *QP energy-shifted* and we will refer to the process of a customer implementing the daily battery and grid profiles obtained by solving (21) subject to constraints (22) and (23) as QP energy-shifting.

4. Assessing the benefits of net metering

In this section we consider publicly released residential PV generation and load data for 300 de-identified customers located in an Australian distribution network, operated by Ausgrid [51]. The Ausgrid distribution network covers 22,275 km^2 and includes load centers in Sydney and regional New South Wales. The dataset included separately reported measurements of load and PV generation recorded as energy over windows of 30 min duration, which we convert to average powers in kW over the half hour period. Further, the Ausgrid dataset spans a 1 year period from 1 July 2010 and includes information on the installed capacity for each of the 300 residential-scale rooftop solar PV units (in kWp), with the installed capacity ranging from 1 kWp to 9.99 kWp.

In our earlier work [42] we identified several means by which anomalous records (for example, due to inverter failure) are identified and excised from the Ausgrid dataset, leaving a subset of 145 customers. In this paper we consider the load and generation profiles of this subset. Consequently, the load and generation profiles of each customer are not identical to each other, but rather, are historical average loads and historical average PV generation profiles. The load and generation profiles l and g for each of the 145 customers are defined with $T = 24$ h, $\Delta = 0.5$ h, and $s = T/\Delta = 48$, for each day in the 365 days. To assess the benefits of net metering we consider the load and generation profiles for each of the $N = 145$ customers.

In what follows we show that annual savings when energy-shifting are dependent on a variety of factors for each customer, including the algorithm selected for scheduling a battery, and the financial policy implemented. By bench-marking the operational savings when QP energy-shifting against the operational savings when LP energy-shifting, we examine the impact of variations in load and generation profiles.

4.1. Simulation parameters

In the LP-based and QP-based simulations that follow we specify $T = 24$ h, $\Delta = 0.5$ h and $s = T/\Delta = 48$ throughout. We fix the battery capacity at 10 kWh. In all cases the remaining battery constraints in (11) and (12) are $\chi(0) = 5$ kWh, and $\overline{B} = -\underline{B} = 5$ kW. That is, the battery charge/discharge limit is $\overline{B} = -\underline{B} = 5$ kW, and the initial state of charge is $\chi(0) = 5$ kWh (cf. Section 2.2).

With the Optimization Toolbox in MATLAB R2014b the interior-point algorithm is used to solve the LP energy-shift problem, and the interior-point-convex algorithm is used to solve the QP energy-shift problem. Moreover, when QP energy-shifting we specify the weights in **H** via the greedy-search algorithm presented in [42].

We consider three different financial policies that are defined with reference to bi-directional meter M. We employ time-of-use electricity billing for all financial policies, while altering electricity compensation profiles. We fix the length-s billing profiles (in \$/kWh) for each financial policy as follows:

$$\eta^b = [\eta^b(1), \ldots, \eta^b(s)]^T, \tag{24}$$

where $\eta^b(k) = 0.03$ for $k \in \{1, 2, \ldots, 14, 45, \ldots, 48\}$, $\eta^b(k) = 0.06$ for $k \in \{15, 16, \ldots, 28, 41, \ldots, 44\}$, and $\eta^b(k) = 0.3$ for $k \in \{29, 30, \ldots, 40\}$.

We denote by FP1, the financial policy which meets the requirements of net metering in (1) by $\eta(k) = \eta^b(k)$ for all k. We denote by FP2 the financial policy that includes a feed-in tariff, where the length-s compensation profile is $\eta^c = [0.4, \ldots, 0.4]^T$. We denote by FP3 the financial policy that does not incentivize excess generation, where the length-s compensation profile is $\eta^c = [0, \ldots, 0]^T$. The billing and compensation profiles for the three financial policies are shown in Fig. 3. We describe electricity billing from 10 pm to

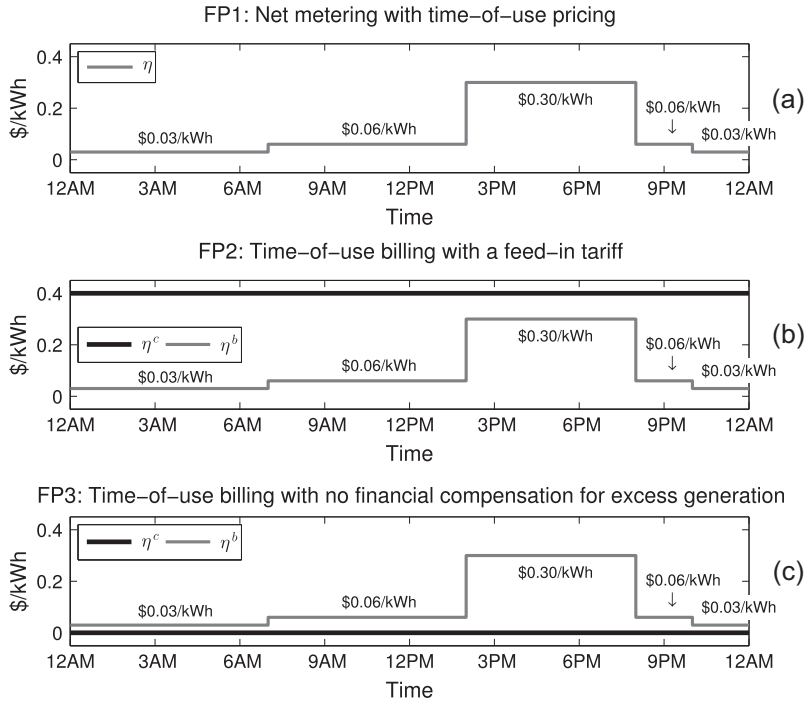

Fig. 3. We consider three financial policies. FP1: net metering with time-of-use pricing (a), FP2: time-of-use billing with a feed-in tariff (b), and FP3: time-of-use billing with no financial compensation for excess generation (c).

7 am at the rate of \$0.03/kWh as an *off-peak pricing period*, electricity billing from 7 am to 2 pm and again from 8 pm to 10 pm at the rate of \$0.06/kWh as a *shoulder pricing period* and electricity billing from 2 pm to 8 pm at the rate of \$0.30/kWh as a *peak pricing period*. Thus, the financial policy FP2 indeed compensates the consumer at the rate of \$0.40/kWh, which is higher than the peak pricing rate of \$0.30/kWh charged by the utility. This generous feed-in rate of \$0.40/kWh is representative of the feed-in tariffs that were offered to residential customers eligible for the NSW Solar Bonus Scheme in Australia that commenced in 2010 (and will end on 31 December 2016) together with the time-of-use rates for residential energy consumption (billing) during the same period [52]. In this paper, however, we consider the generous feed-in tariff in FP2 in the context of a customer with a single bi-directional meter as shown in Fig. 1, whereas the generous feed-in tariff offered under the NSW Solar Bonus Scheme required two meters at the residential premises to compensate PV generation separate to residential load.

In what follows we do not consider daily changes in electricity prices. That is, if FP1 is employed on the first day, on each consecutive day FP1 is also employed when LP or QP energy-shifting. Furthermore, we do not consider battery aging. That is, for any day-ahead battery profile x_1 we consider a 10 kWh battery is available, where $C = 10$ kWh on each consecutive day. Therefore, we do not consider uncertainty in the day-ahead battery capacity and the day-ahead electricity prices in the results that follows.

4.2. Assessing customer benefits

For the net metering policy described by FP1, we benchmark the annual savings for each customer when LP energy-shifting against the annual savings when QP energy-shifting. We recall LP energy-shifting maximizes the daily operational savings. In contrast, QP energy-shifting aims to increase, rather then maximize, the daily operational savings, while penalizing reverse power flow.

In Fig. 4 we observe the annual savings for each of the $N = 145$ customers subject to both LP and QP energy-shifting. Under LP energy-shifting, all customers accrue annual savings of \$986/yr, regardless of the variability in their respective load and generation profiles. In contrast, the annual savings when QP energy-shifting are less then the annual savings when LP energy-shifting, for all customers. In some instances, the annual savings when QP energy-shifting are negative.

Consequently, QP energy-shifting sacrifices a proportion of the maximum operational savings, and in some instances a customer is charged (negative savings) for scheduling battery storage. The residential costs or reduction in operational savings when QP energy-shifting is a result of the penalty applied to reverse power flow. We anticipate the comparison of LP-based versus QP-based annual savings will assist distributors in developing demand management strategies, where a subsidy for QP energy-shifting may encourage some customers to reduce reverse power flow that is otherwise incentivized by net metering.

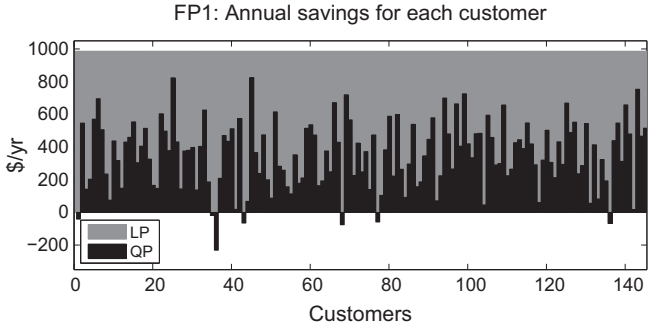

Fig. 4. Annual savings for each customer when net metering via FP1.

4.3. Assessing utility benefits

To quantify reverse power flow and peak load events for a utility, we define the *average load, generation, grid, and state of charge profiles* for the N customers as follows. The average load profile on a given day is defined by

$$\hat{l} := \frac{1}{N}\sum_{i=1}^{N} l^{(i)}$$

where $l^{(i)}$ denotes the load profile for the ith customer on the given day. The average generation, grid, and state of charge profiles $\hat{g}, \hat{x}_2$, and $\hat{\chi}$ are then defined analogously in terms of the corresponding customers' $g^{(i)}, x_2^{(i)}$, and $\chi^{(i)}$, respectively, on the given day.

For the net metering policy FP1, Fig. 5 illustrates the average load, generation, grid, and state of charge profiles on 9 January 2011, and 5 July 2010, when QP energy-shifting and LP energy-shifting. In Fig. 5(1a) we observe the average generation profile on 9 January 2011 exceeds the average load profile for part of the day (from 9.30 am to 4 pm). In Fig. 5(2a) we observe the average load profile exceeds the average generation profile for the entire day on 5 July 2010. Thus, when a utility connects each customer via a lossless feeder, from 9.30 am to 4 pm on 9 January 2011 excess generation $(N(\hat{g}(k) - \hat{l}(k))$ for all $k \in \{20, \ldots, 32\})$ is pushed upstream creating voltage rise in the absence of residential batteries to energy time-shift.

In Fig. 5(1b) and (2b) we observe the QP-based algorithm penalizes reverse power flow, while reducing the peak load that corresponds to peak pricing periods on both days, i.e., the QP energy-shifted average grid profile is approximately zeroed on both days during the peak-pricing period. In contrast, the LP-based algorithm permits reverse power flow during the peak pricing period, i.e., the LP energy-shifted average grid profile $\hat{x}_2$ is less than zero during the peak pricing period on both days. Therefore, when a utility connects each of the 145 customers via a lossless feeder, LP energy-shifting will push reverse power flow upstream $(N\hat{x}_2(k)$ for all $k \in \{29, \ldots, 40\})$, which will create voltage rise.

We envision load flow analysis will assist the distributor in predicting the severity of the voltage rise condition when each customer implements LP energy-shifting. The QP-based algorithm is an approach to mitigating non-compliant voltage rise identified by the distributor, which results from the financial incentive for reverse power-flow when net metering is used.

In Fig. 5(1b) and (2b) we also observe the LP energy-shifted *distance* between peak and minimum average power in $\hat{x}_2$ is reduced when QP energy-shifting. The distance is defined by the difference between the peak average power flow $\hat{x}_2(45)$ and the minimum average power flow $\hat{x}_2(29)$. On 9 January 2011 the distance is 4.9 kW when LP energy-shifting, which is reduced to 1.5 kW when QP energy-shifting. On 5 July 2010 the distance is 4.2 kW when LP energy-shifting, which is reduced to 2.9 kW when QP energy-shifting. Therefore, reducing the LP energy-shifted distance reduces the impact of large voltage swings related to reverse power flow and peak average power flow $\hat{x}_2(45)$.

In Fig. 5(1c) and (2c) we observe that when LP energy-shifting each customer has a battery that is fully discharged at 8 pm and 10 pm, and fully charged at 7 am and 2 pm, irrespective of the variations in each customer's load and generation profiles on either day. In contrast, the average state of charge profile when QP energy-shifting is significantly different to LP energy-shifting on 9 January 2011, since the QP-based algorithm strongly restricts reverse power flow during the peak pricing period.

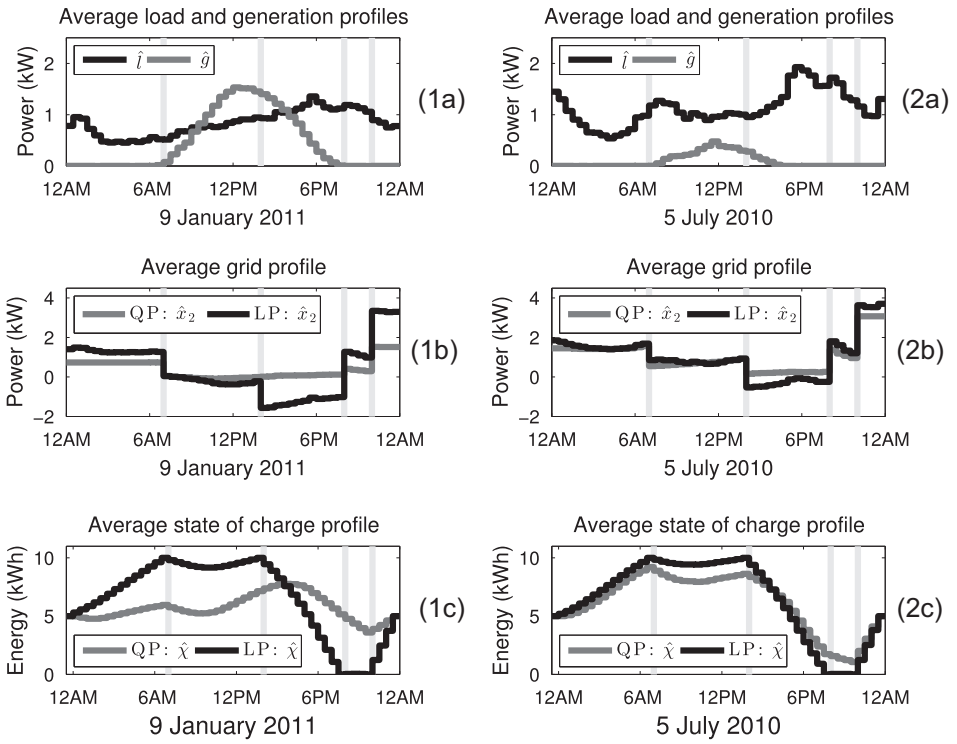

Fig. 5. Average profiles when every customer employs QP or LP energy-shifting with net metering (FP1). Average load and generation profiles given a day when generation often exceeds load, and vice versa (1a and 2a), grid profiles (1b and 2b), and average state of charge profiles (1c and 2c).

Fig. 6. Operational savings for two customers with financial policies: FP1 (1a-1b), FP2 (2a-2b), FP3 (3a-3b).

4.4. Assessing the financial policy

In this section we compare the operational savings for two particular customers when implementing QP energy-shifting for each financial policy defined in Section 4.1. We select customer A, a representative customer that often generates excess energy, and customer B, a representative customer that rarely generates excess energy. Recall, financial policy FP1 meets the requirements of net metering in (1) by $\eta(k) = \eta^b(k)$ for all k. Financial policy FP2 is representative of the generous feed-in tariffs that were offered to residential customers eligible for the NSW Solar Bonus Scheme in Australia. Financial policy FP3 provides no compensation for

reverse power flow at the PCC, yet includes time-of-use tariffs for electricity billing consistent with both financial policies FP1 and FP2.

In Fig. 6(1b), (2b), and (3b) we observe customer B financially benefits from QP energy-shifting, irrespective of the financial policy. By way of an explanation we consider the prevalence of positive power flows at the PCC of customer B, i.e., reverse power flows at the PCC are rare. In this context, the time-of-use billing profiles in FP1, FP2 and FP3 provide significant financial incentives to customer B to shift positive power flows at the PCC from the peak pricing periods to off-peak pricing periods. Moreover, when QP energy-shifting the greedy-search algorithm significantly penalizes positive power flows during the peak pricing period. Therefore, customer B financially benefits from QP energy-shifting since the significant penalties applied to positive power flows during the peak pricing period (via the greedy-search algorithm) additionally increase the operational savings.

In contrast, customer A in Fig. 6(1a) benefits from QP energy-shifting on some days when net metering (FP1), and on even fewer days in Fig. 6(2a) with a feed-in tariff (FP2). However, when the financial policy does not compensate reverse power flow (FP3), we observe in Fig. 6(3a) customer A benefits from QP energy-shifting on all days. By way of an explanation we consider the prevalence of reverse power flows at the PCC of customer A (that potentially occur during the shoulder and peak pricing periods). In this context, in Fig. 6(1a) and (2a) we observe negative operational savings occur while QP energy-shifting since financial policies FP1 and FP2 incentivize the reverse power flow that the QP-based algorithm penalizes. Therefore, not all customers benefit from QP energy-shifting when the financial policy includes incentives for reverse power flow.

5. Conclusions

In this paper we assessed the benefits of scheduling residential battery storage co-located with solar PV. For a typical net metering policy, we developed two optimization-based algorithms with different objective functions to schedule the residential batteries. The results of a case study including 145 residential customers located in an Australian distribution network confirmed that distributor objectives should to be taken into account when scheduling battery storage, to mitigate potential voltage rise associated with reverse power flow.

Our approach to scheduling battery storage to mitigate potential voltage rise associated with the financial incentive for reverse power flow when net metering, required no additional metering infrastructure. We envision this approach will assist distributors in developing demand management strategies, where a subsidy may encourage some customers to reduce reverse power flow, when required. Furthermore, understanding the monetary incentives that lead to potential voltage rise when scheduling battery storage will allow for more sophisticated energy pricing strategies.

Acknowledgments

Elizabeth L. Ratnam acknowledges the financial support of an Australian Postgraduate Award (APA) and a CSIRO – Energy Technology Postgraduate Research Scholarship (Ref: 2011094123).

References

[1] Ogimoto K, Kaizuka I, Ueda Y, Oozeki T. A good fit: Japan's solar power program and prospects for the new power system. IEEE Power Energy Mag 2013;11(2):65–74.
[2] Moosavian SM, Rahim NA, Selvaraj J, Solangi KH. Energy policy to promote photovoltaic generation. Renew Sustain Energy Rev 2013;25:44–58.
[3] von Appen J, Braun M, Stetz T, Diwold K, Geibel D. Time in the sun: the challenge of high PV penetration in the German electric grid. IEEE Power Energy Mag 2013;11(2):55–64.
[4] Walling RA, Saint R, Dugan RC, Burke J, Kojovic LA. Summary of distributed resources impact on power delivery systems. IEEE Trans Power Del 2008;23(3):1636–44.
[5] Coster EJ, Myrzik JMA, Kruimer B, Kling WL. Integration issues of distributed generation in distribution grids. Proc IEEE 2011;99(1):28–39.
[6] ARUP. Ausgrid smart grid smart city microgrid protection research (accessed 07.05.15). <https://ich.smartgridsmartcity.com.au/>.
[7] Masters CL. Voltage rise the big issue when connecting embedded generation to long 11 kV overhead lines. Power Eng J 2002;16(1):5–12.
[8] Katiraei F, Agüero JR. Solar PV integration challenges. IEEE Power Energy Mag 2011;9(3):62–71.
[9] Stetz T, Marten F, Braun M. Improved low voltage grid-integration of photovoltaic systems in Germany. IEEE Trans Sustain Energy 2013;4(2):534–42.
[10] Baran ME, Hooshyar H, Shen Zhan, Huang A. Accommodating high PV penetration on distribution feeders. IEEE Trans Smart Grid 2012;3(2):1039–46.
[11] Tzartzev R, Grady WM, Patel J. Impact of high-penetration PV on distribution feeders. In: Proc IEEE PES Conf on Innovative Smart Grid Technologies, Berlin, Germany; 2012. p. 1–6.
[12] Hill CA, Such MC, Chen Dongmei, Gonzalez J, Grady WM. Battery energy storage for enabling integration of distributed solar power generation. IEEE Trans Smart Grid 2012;3(2):850–7.
[13] Tonkoski R, Turcotte D, El-Fouly THM. Impact of high PV penetration on voltage profiles in residential neighborhoods. IEEE Trans Sustain Energy 2012;3(3):518–27.
[14] Wissner M. The smart grid – a saucerful of secrets? Appl Energy 2011;88(7):2509–18.
[15] Kabir MN, Mishra Y, Ledwich G, Xu Z, Bansal RC. Improving voltage profile of residential distribution systems using rooftop PVs and battery energy storage systems. Appl Energy 2014;134:290–300.
[16] Mulder G, Six D, Claessens B, Broes T, Omar N, Mierlo JV. The dimensioning of PV-battery systems depending on the incentive and selling price conditions. Appl Energy 2013;111:1126–35.
[17] Callaway DS, Hiskens IA. Achieving controllability of electric loads. Proc IEEE 2011;99(1):184–99.
[18] Corradi O, Ochsenfeld H, Madsen H, Pinson P. Controlling electricity consumption by forecasting its response to varying prices. IEEE Trans Power Syst 2013;28(1):421–9.
[19] Lin C-H, Hsieh W-L, Chen C-S, Hsu C-T, Ku T-T. Optimization of photovoltaic penetration in distribution systems considering annual duration curve of solar irradiation. IEEE Trans Power Syst 2012;27(2):1090–7.
[20] Hossain MJ, Saha TK, Mithulananthan N, Pota HR. Robust control strategy for PV system integration in distribution systems. Appl Energy 2012;99:355–62.
[21] Jahangiri P, Aliprantis DC. Distributed Volt/VAr control by PV inverters. IEEE Trans Power Syst 2013;28(3):3429–39.
[22] Kabir MN, Mishra Y, Ledwich G, Dong ZY, Wong KP. Coordinated control of grid-connected photovoltaic reactive power and battery energy storage systems to improve the voltage profile of a residential distribution feeder. IEEE Trans Ind Inform 2014;10(2):967–77.
[23] Moghaddam MP, Abdollahi A, Rashidinejad M. Flexible demand response programs modeling in competitive electricity markets. Appl Energy 2011;88(9):3257–69.
[24] Mohsenian-Rad A-H, Leon-Garcia A. Optimal residential load control with price prediction in real-time electricity pricing environments. IEEE Trans Smart Grid 2010;1(2):120–33.
[25] Valenzuela J, Thimmapuram PR, Kim J. Modeling and simulation of consumer response to dynamic pricing with enabled technologies. Appl Energy 2012;96:122–32.
[26] Nair NC, Nayagam R, Francis R. New Zealand utility experiences with demand side management. In: Proc 2008 IEEE Power & Energy Society General Meeting, Pittsburgh (PA); 2008. p. 1–5.
[27] Ueda Y, Kurokawa K, Tanabe T, Kitamura K, Sugihara H. Analysis results of output power loss due to the grid voltage rise in grid-connected photovoltaic power generation systems. IEEE Trans Ind Electron 2008;55(7):2744–51.
[28] Sweet B. California's energy-storage mandate. Tech rep, IEEE spectrum EnergyWise newsletter; 6th November 2013.
[29] Nottrott A, Kleissl J, Washom B. Energy dispatch schedule optimization and cost benefit analysis for grid-connected, photovoltaic-battery storage systems. Renew Energy 2013;55:230–40.
[30] Ru Y, Kleissl J, Martínez S. Storage size determination for grid-connected photovoltaic systems. IEEE Trans Sustain Energy 2013;4(1):68–81.
[31] Ru Y, Kleissl J, Martínez S. Exact sizing of battery capacity for photovoltaic systems. Eur J Contr 2014;20(1):24–37.
[32] Hill J, Nwankpa C. System constraints effects on optimal dispatch schedule for battery storage systems. In: Proc IEEE PES Conf on Innovative Smart Grid Technologies, Washington (DC); 2012. p. 1–8.
[33] Riffonneau Y, Bacha S, Barruel F, Ploix S. Optimal power flow management for grid connected PV systems with batteries. IEEE Trans Sustain Energy 2011;2(3):309–20.
[34] Hubert T, Grijalva S. Modeling for residential electricity optimization in dynamic pricing environments. IEEE Trans Smart Grid 2012;3(4):2224–31.

[35] Alam MJE, Muttaqi KM, Sutanto D. Mitigation of rooftop solar PV impacts and evening peak support by managing available capacity of distributed energy storage systems. IEEE Trans Power Syst 2013;28(4):3874–84.
[36] Matallanas E, Castillo-Cagigal M, Gutiérrez A, Monasterio-Huelin F, Caamaño-Martín E, Masa D, Jiménez-Leube J. Neural network controller for active demand-side management with PV energy in the residential sector. Appl Energy 2012;91(1):90–7.
[37] Yang H-T, Huang C-M, Huang Y-C, Pai Y-S. A weather-based hybrid method for 1-day ahead hourly forecasting of PV power output. IEEE Trans Sustain Energy 2014;5(3):917–26.
[38] Wang T, Kamath H, Willard S. Control and optimization of grid-tied photovoltaic storage systems using model predictive control. IEEE Trans Smart Grid 2014;5(2):1010–7.
[39] Wang X, Palazoglu A, El-Farra NH. Operational optimization and demand response of hybrid renewable energy systems. Appl Energy 2015;143:324–35.
[40] Darghouth NR, Barbose G, Wiser RH. Customer-economics of residential photovoltaic systems (Part 1): The impact of high renewable energy penetrations on electricity bill savings with net metering. Energy Policy 2014;67:290–300.
[41] Black AJ. Financial payback on California residential solar electric systems. Sol Energy 2004;77(4):381–8.
[42] Ratnam EL, Weller SR, Kellett CM. An optimization-based approach to scheduling residential battery storage with solar PV: assessing customer benefit. Renew Energy 2015;75:123–34.
[43] Ratnam EL, Weller SR, Kellett CM. An optimization-based approach for assessing the benefits of residential battery storage in conjunction with solar PV. In: Proc IX IEEE Int Symp Bulk Power System Dynamics and Control (IREP'13), Rethymnon, Greece; 2013. p. 1–8.
[44] Candelise C, Winskel M, Gross RJK. The dynamics of solar PV costs and prices as a challenge for technology forecasting. Renew Sustain Energy Rev 2013;26:96–107.
[45] Nair N-KC, Garimella N. Battery energy storage systems: assessment for small-scale renewable energy integration. Energy Build 2010;42(11):2124–30.
[46] Brown S, Pyke D, Steenhof P. Electric vehicles: the role and importance of standards in an emerging market. Energy Policy 2010;38(7):3797–806.
[47] Hredzak B, Agelidis VG, Jang M. A model predictive control system for a hybrid battery-ultracapacitor power source. IEEE Trans Power Electron 2014;29(3):1469–79.
[48] Lu B, Shahidehpour M. Short-term scheduling of battery in a grid-connected PV/battery system. IEEE Trans Power Syst 2005;20(2):1053–61.
[49] Barsali S, Ceraolo M. Dynamical models of lead-acid batteries: implementation issues. IEEE Trans Energy Convers 2002;17(1):16–23.
[50] Tesla. Powerwall tesla home battery (accessed 11.05.15). <http://www.teslamotors.com/powerwall>.
[51] Ausgrid. Solar home electricity data (accessed 28.01.15). <http://www.ausgrid.com.au/Common/About-us/Corporate-information/Data-to-share/Data-to-share/Solar-household-data.aspx>.
[52] NSW Government. Solar bonus scheme (accessed 11.05.15). <http://www.resourcesandenergy.nsw.gov.au/energy-consumers/solar/solar-bonus-scheme>.

Part 3

Battery scheduling: Coordinated residential systems

5

Power management in a distribution network

Part 3 of this thesis is comprised of Chapter 5 and Chapter 6, that incorporate the residential system presented in Part 2 into a larger distribution network. In Part 3 we more directly consider the management of bi-directional power flows in a distribution network, placing an indirect focus on modest requirements for sensing and communication infrastructure. In all cases, residential battery storage is coordinated in the context of the financial policy of net metering, as defined in Part 2.

Chapter 5 consists of the paper titled *Central versus localized optimization-based approaches to power management in distribution networks with residential battery storage*,[1] that addresses the problem of managing reverse power flow and peak loads within a distribution network. This paper extends and combines the problem formulations from Chapter 4, by incorporating design parameters in the form of scalar weights. These design parameters facilitate the balance in benefits associated with managing bi-directional power flows, with further increase operational savings that accrue to residential customers. Guidance on selecting the design parameters is provided.

Chapter 6 addresses problems that may occur infrequently in Australian distribution networks, but could potentially lead to costly remediation for distribution operators. These problems include significant reverse power flows along a medium voltage feeder (designed for uni-directional power flow), peak electricity demand non-coincident with PV generation, and supply voltages in a low voltage network that are above or below allowable thresholds. We present problem formulations that include one or more of the objective functions presented in Chapter 5, thereby extending previous work.

[1] The title of the accepted paper has been changed to be more descriptive of the approach. Previously this paper was titled "Optimization-based approach to power management in distribution networks with residential battery storage."

Central versus localized optimization-based approaches to power management in distribution networks with residential battery storage

Elizabeth L. Ratnam[a,*], Steven R. Weller[a], Christopher M. Kellett[a]

[a]*School of Electrical Engineering and Computer Science, University of Newcastle, University Drive, Callaghan NSW 2308, Australia*

Abstract

In this paper we propose two optimization-based algorithms for coordinating residential battery storage when solar photovoltaic (PV) generation in excess of load is compensated via net metering. Our objective is to balance increases in daily operational savings that accrue to customers with the management of reverse power flows and/or peak loads approaching a network capacity. To achieve this objective we present a central quadratic program (QP)-based algorithm, where residential customers implement a distributor-specified day-ahead battery schedule. We also present a local QP-based algorithm, where each residential customer implements a day-ahead battery schedule subject to three distributor-specified weights. To complete our assessment of the distributor benefit, both QP-based scheduling algorithms are applied to measured load and generation data from 145 residential customers located in an Australian distribution network. The results of this case study confirm both QP-based scheduling algorithms manage reverse power flow and peak loads within a distribution network. In the context of net metering, all customers exhibit the same operational savings when implementing the central QP-based algorithm, while the local QP-based algorithm disproportionately penalizes some customers.

Keywords: Demand-response, battery scheduling, peak-load reduction, photovoltaics, reverse power flow.

1. Introduction

Recently, there has been a rapid uptake of grid-connected solar photovoltaics (PV) in many countries [1]. Drivers include the ever-decreasing cost of PV panels [2, 3], concerns regarding climate change, and government incentives such as feed-in tariffs and net metering offered directly to residents investing in on-site renewable generation [4–6].

Consequently, many electrical distributors are now faced with managing bi-directional power flows in distribution networks previously designed for one-way power flow [7, 8]. Of particular concern to distributors are power flows approaching a network capacity and reverse power flows inducing voltage rise, especially when either situation leads to substantial network investment [9–12].

Demand-side approaches to managing distribution power flows potentially defer (or possibly avoid) significant costs associated with distribution reinforcement [13–28]. The demand-side approach in [13] curbs PV production when such production induces significant voltage rise, creating a need for grid reinforcement [14]. To further improve distribution supply voltages the demand-side approach in [15] considers a sophisticated controller in the PV inverter

*Corresponding author: Elizabeth L Ratnam, Tel.: +61 2 492 16026, Fax: +61 2 492 16993.

Email addresses: elizabeth.ratnam@ieee.org (Elizabeth L. Ratnam), Steven.Weller@newcastle.edu.au (Steven R. Weller), Chris.Kellett@newcastle.edu.au (Christopher M. Kellett)

that adjusts the real and reactive power supplied to, or absorbed by, the distribution grid. For the purpose of improving supply voltages in a distribution network the approach in [16] is to charge residential battery storage co-located with solar PV when a predetermined threshold for PV generation is exceeded. Other demand-side approaches that potentially manage distribution supply voltages and/or peak demand include direct load control [17–22], and price-responsive load control [23–25]. For example, distributor-specified time-of-use electricity prices are included in the category of price-responsive load control [25]. A customer implementing a distributor's request to switch a thermal load on or off is an example of direct load control [22].

However, without careful coordination, the potential benefits of demand-side approaches to managing bi-directional power flows in a distribution network might not be realized [19, 26, 29–32]. For example, a second load peak in the distribution grid may arise when autonomous, time-based electric vehicle charging schedules are implemented [19], potentially leading to a need for costly distribution reinforcement. Furthermore, increases in reverse power flows (or peak loads) potentially arise when a battery connected to a distribution grid is discharged (or charged) in response to time-varying electricity prices [31, 33], which may also necessitate network investment. Moreover, PV storage systems designed to increase self consumption may not explicitly assist distributors in avoiding PV-related voltage rise [26, 32].

Several authors have investigated coordinated approaches to scheduling demand-side battery storage with the objective of alleviating the need for grid reinforcement by managing bi-directional power flows in a distribution network [14, 26, 31, 34, 35]. For example, a linear program (LP) is employed in [31] to reduce peak power flows (potentially in the reverse direction) through a distribution substation. Furthermore, [31] proposes direct control of a customer's battery schedule by the distributor when the LP-based power flow reductions are required. To support PV self-consumption in addition to minimizing significant voltage rise in a distribution grid, different control strategies are proposed in [26], which are benchmarked and evaluated in terms of economic viability. The optimization problem in [34] includes penalties for large power fluctuations to and from an interconnection point that connects a smart grid to an upstream electricity network. To reduce power fluctuations within a distribution grid, [34] proposes direct control of demand-side battery schedules by a distributor. In contrast, a central energy management system (EMS) in [35] coordinates supply and demand within a microgrid in a number of ways. For example, a central EMS in [35] either dispatches power flow references to customers connected to a microgrid, or directly controls battery charge and discharge schedules of each microgrid customer. That is, each microgrid customer in [35] has a local EMS that manages residential battery schedules subject to central EMS references or directives.

In the recent literature most approaches to scheduling residential battery storage focus on the (potentially infrequent) need for managing bi-directional power flows in a distribution grid [14, 26, 34, 35] or look to reduce electricity bills for the customer [36, 37]. In contrast, our recent work looks to balance these two objectives, namely increasing the operational savings that accrue to residential customers with PV storage systems against the management of distribution power flows to alleviating voltage and or load conditions that necessitate grid reinforcement [33, 38]. In this paper we propose two approaches that more directly balance these two objectives, thereby extending our previous work in [33, 38]. Further, we apply the forecasting methodology proposed in [39] to assess the effectiveness of each algorithm when there exists uncertainty in day-ahead load and generation forecasts.

More specifically, in this paper we present two coordinated demand-side approaches to managing bi-directional power flows within a distribution grid, when excess generation is compensated via net metering. The first approach is referred to as central quadratic program (QP) energy-shifting, where selected customers implement a distributor-specified day-ahead battery schedule. The second approach is referred to as local QP energy-shifting, where three distributor-specified weights are incorporated into the QP-based algorithm of selected customers to obtain a day-

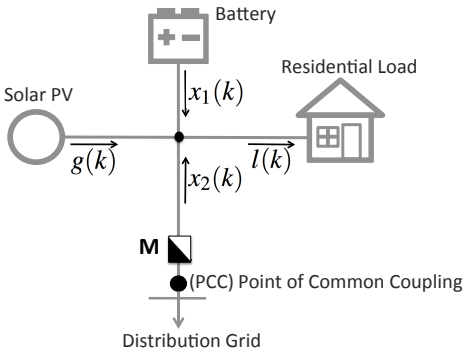

Figure 1: Residential system illustrating the direction of positive power flows and the bi-directional meter **M**. Arrows associated with $g(k)$, $l(k)$, $x_1(k)$ and $x_2(k)$ illustrate the assumed direction of positive power flow. Meter **M** measures and records (in kW) power flow $x_2(k)$, where k is a time index.

ahead battery charge and discharge schedule. In both QP-based approaches our objective is to balance an increase in operational savings that accrue to customers scheduling battery storage, with reductions in reverse power flows and/or load peaks within a distribution grid. We apply each QP-based approach to measured load and generation data from 145 Australian residential customers and investigate customer and distributor benefits of coordinated residential battery scheduling.

To implement central QP energy-shifting a distributor does the following: (1) identifies a region in the distribution grid to implement a coordinated approach to residential battery scheduling; (2) forecasts the day-ahead power flows along an interconnection point to the distribution region; (3) runs optimization-based algorithms daily; and (4) broadcasts a day-ahead battery charge and discharge schedule to each regional customer. Furthermore, each regional customer requires an energy management system that: (1) coordinates with Advanced Metering Infrastructure (AMI) to advise the distributor of existing battery parameters including the current state of charge; (2) coordinates with the AMI to receive a day-ahead battery charge and discharge schedule from the distributor; and (3) schedules battery storage in the day-ahead.

To implement local QP energy-shifting a distributor does the following: (1) identifies a region in the distribution grid to implement a coordinated approach to residential battery scheduling; and (2) broadcasts three day-ahead weights to each regional customer. Furthermore, each regional customer requires an energy management system that: (1) coordinates with AMI to receive day-ahead prices for energy delivered to and from the grid; (2) coordinates with AMI to receive the three distributor-specified weights to be applied in the day-ahead; (3) forecasts the day-ahead residential load and PV generation; (4) runs optimization-based algorithms daily; and (5) schedules battery storage in the day-ahead.

This paper is organized as follows. In Section 2 we introduce a distribution region with graph notation and define a residential system. In Section 3 we represent a distribution network with a directed graph, and introduce a methodology for distributor-based and customer-based forecasts. In Section 4 we present two QP-based algorithms to coordinate residential battery charge and discharge schedules within a distribution region. In Section 5 the two QP-based algorithms are implemented and evaluated given real-world data from an Australian electricity distributor.

Notation

Let $\mathbb{R}^s$ denote s-dimensional vectors of real numbers and $\mathbb{R}^s_{\geq 0}$ s-dimensional vectors with all non-negative components where, as usual, $\mathbb{R}^1 = \mathbb{R}$. $\mathbf{I}$ denotes the s-by-s identity matrix and $\mathbb{1} \in \mathbb{R}^s_{\geq 0}$ denotes the all-1s column vector of length s.

0 denotes an all-zero matrix, or an all-zero column vector, where the context will make clear the dimension intended, and $\mathbf{T} = [t_{ij}]$ denotes the s-by-s matrix satisfying $t_{ij} = 1$ for $i \geq j$ and $t_{ij} = 0$ elsewhere.

2. Preliminaries

In what follows each residential customer connected to a distribution network may deliver power to, or receive power from, a distributor. Fig. 1 represents the residential system of each customer connected to a distribution network. To manage bi-directional power flows in a distribution network we consider coordinated approaches to charging and discharging residential battery storage.

In more detail, we consider a *region* in the distribution network. We identify residential customers in the specified region, and consider ways to coordinate their day-ahead battery schedules. We envision our coordinated approach to scheduling residential battery storage will assist distributors seeking to reduce peak demand and/or manage reverse power flows approaching a regional capacity. To define a region in the distribution grid we employ a graph notation similar to that in [40].

2.1. Directed graphs

A directed graph $\mathcal{G}$ consists of a set of M vertices $\mathcal{V} = \{1, \ldots, M\}$ and a set of directed edges $\mathcal{E} \subseteq \mathcal{V} \times \mathcal{V}$. Each directed edge from vertex i to vertex j is represented by $(i, j) \in \mathcal{E}$. The *transitive closure* of $\mathcal{G} = (\mathcal{V}, \mathcal{E})$ that defines the set of all directed paths is denoted by the matrix $\mathcal{M}^{\mathcal{G}}$. The entries of $\mathcal{M}^{\mathcal{G}}$, where vertices $i, j \in \mathcal{V}$, are $\mathcal{M}^{\mathcal{G}}_{ji} = 1$ if there exists a directed path from vertex i to vertex j, or $i = j$, otherwise $\mathcal{M}^{\mathcal{G}}_{ji} = 0$.

In this paper all graphs $\mathcal{G}$ are assumed to be *simple*, i.e., there are no repeated edges or self loops $(i, i) \notin \mathcal{E}$, for any vertex $i \in \mathcal{V}$. Furthermore, we assume a graph $\mathcal{G}$ is also a *rooted tree*, where the root vertex is labeled M. Thus, for every other vertex $k \in \mathcal{V}$, $k \in \{1, \ldots, M-1\}$, there is a unique directed path from M to k.

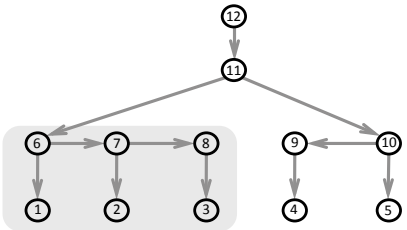

Figure 2: An example directed graph $\mathcal{G}$, where the M^{th} vertex 12 denotes the root, and vertices 1-5 represent leaves in the rooted tree. The shaded region highlights the subgraph $\mathcal{G}_6$.

For each vertex $i \in \mathcal{V}$, we define the set of its *downstream vertices* $\mathcal{V}_i$ by

$$\mathcal{V}_i = \{j \in \{1, \ldots, M\} \mid \mathcal{M}^{\mathcal{G}}_{ji} = 1\}. \tag{1}$$

That is, $j \in \mathcal{V}_i$ if and only if a directed path exists from vertex i to vertex j, or $i = j$. Edges that connect the set of downstream vertices $\mathcal{V}_i$ are referred to as *downstream edges*. That is, edge $(j, k) \in \mathcal{E}$ is a downstream edge if and only if vertices $j, k \in \mathcal{V}_i$. Consequently, for each vertex $i \in \mathcal{V}$ we denote a set of downstream edges by $\mathcal{E}_i \subset \mathcal{E}$, where a set of downstream edges $\mathcal{E}_i$ connect a set of downstream vertices $\mathcal{V}_i$.

With the above as background we define a subgraph by $\mathcal{G}_i := (\mathcal{V}_i, \mathcal{E}_i)$. That is, subgraph $\mathcal{G}_i$ consists of the set of downstream vertices $\mathcal{V}_i \subset \mathcal{V}$, and the set of downstream edges $\mathcal{E}_i \subset \mathcal{E}$. Consequently, subgraph $\mathcal{G}_i$ is itself a rooted tree, where $i \in \mathcal{V}$ denotes the root. In what follows we define a distribution region by a subgraph $\mathcal{G}_i = (\mathcal{V}_i, \mathcal{E}_i)$.

2.2. Residential systems

Fig. 1 illustrates the assumed topology of each residential system under consideration. Meter **M** measures and records bi-directional power flows, where $x_2(k)$ denotes the measured power flow (in kW) over the k^{th} interval of length Δ. By convention measured power flows from (to) the grid to (from) the residential system over the period $((k-1)\Delta, k\Delta)$ are represented by $x_2(k) > 0$ ($x_2(k) < 0$) for all $k \in \{1, \ldots, s\}$. To represent all measured power flows over a time window $[0, T]$, where s is the number of time intervals of length Δ, and $T = s\Delta$ (in hours) is the time window of interest, we define the *grid profile* by $x_2 := [x_2(1), \ldots, x_2(s)]^T \in \mathbb{R}^s$. By combining measured power flows with prices for buying and selling electricity, we can determine if a resident incurs an energy bill, or rather, is compensated for excess generation.

In this paper we consider the financial policy of *net metering* widely adopted in the United States [5, 6, 41, 42], the defining characteristic of which is that each resident is billed at the same rate as they are compensated for excess generation [6, 33]. To represent daily variations in electricity prices we define a *net metering profile* of length s, where s is the number of time intervals of length Δ, and $T = s\Delta$ (in hours) is the time window of interest. We denote the electricity price (in \$/kWh) over the period $((k-1)\Delta, k\Delta)$ corresponding to the measured power flow $x_2(k)$ at meter **M** by $\eta(k)$ for all $k \in \{1, \ldots, s\}$, and we define the *net metering profile* over $[0, T]$ by $\eta := [\eta(1), \ldots, \eta(s)]^T \in \mathbb{R}^s_{\geq 0}$. In this paper we generally consider $T = 24$ hours and $\Delta = 1/2$ hour (30 minutes), which implies $s = 48$. Other choices are straightforward, subject only to commensurability of T, Δ, and s.

The remaining power flows represented in Fig. 1 are defined as follows. We represent the average power delivered to the residential load (in kW) over the period $((k-1)\Delta, k\Delta)$ by $l(k)$ for all $k \in \{1, \ldots, s\}$, and define the *load profile* over $[0, T]$ as $l := [l(1), \ldots, l(s)]^T \in \mathbb{R}^s_{\geq 0}$. Likewise we represent the average PV generation (kW) over the period $((k-1)\Delta, k\Delta)$ by $g(k)$ for all $k \in \{1, \ldots, s\}$, and define the *generation profile* over $[0, T]$ as $g := [g(1), \ldots, g(s)]^T \in \mathbb{R}^s_{\geq 0}$.

We represent the average power (kW) delivered from (or to) the battery over the period $((k-1)\Delta, k\Delta)$ by $x_1(k) > 0$ (or $x_1(k) < 0$) for all $k \in \{1, \ldots, s\}$, and define the *battery profile* over $[0, T]$ as $x_1 := [x_1(1), \ldots, x_1(s)]^T \in \mathbb{R}^s$. By convention we represent charging (discharging) of the battery by $x_1(k) < 0$ ($x_1(k) > 0$).

From the configuration of the residential energy system in Fig. 1, we observe that the power balance equation

$$x_2(k) = l(k) - g(k) - x_1(k) \tag{2}$$

must hold for all $k \in \{1, \ldots, s\}$.

With the above as background, we define the energy bill associated with the financial policy of net metering by $\Sigma := \Delta \eta^T x_2$. In the absence of a battery, this reduces to the *baseline energy bill* defined by $\tilde{\Sigma} := \Delta \eta^T (l - g)$, since the battery profile satisfies $x_1(k) = 0$ for all $k \in \{1, \ldots, s\}$.

The *operational savings* (in \$/day) allow us to quantify the effectiveness of scheduling a battery. We define the operational savings, ψ, as the difference between the energy bills obtained with and without a battery as follows:

$$\psi := \tilde{\Sigma} - \Sigma. \tag{3}$$

The operational savings in (3) may also be expressed in terms of the battery profile x_1 as shown in the following Lemma.

Lemma 1 ([33, Lemma 1])**.** *Consider a residential energy network employing a financial policy of net metering, where $\eta \in \mathbb{R}^s_{\geq 0}$ is assumed fixed and known. Let $x_1 \in \mathbb{R}^s$ represent the battery profile over $[0,T]$ where $T = s\Delta$. Then the operational savings are given by*

$$\psi = \Delta \eta^T x_1. \tag{4}$$

Remark 1. *If there exists $a \in \mathbb{R}_{>0}$ so that $\eta = a\mathbb{1}$, then the operational savings in equation* (4) *are \$0 [38, Lemma 2].*

In this paper we assume each residential system under consideration is sufficiently rated, as in our previous work [33, 38]. That is, excluding the battery constraints, we assume there are no additional residential constraints for any proposed battery schedule. For example, we assume a conductor extending from a point of common coupling to a residential PV inverter imposes no thermal limit.

2.3. Battery constraints

To capture the limited "charging/discharging power" of the battery, we include the battery profile constraint $\underline{B}\mathbb{1} \leq x_1 \leq \overline{B}\mathbb{1}$, where $\underline{B} \in \mathbb{R}_{\leq 0}$ and $\overline{B} \in \mathbb{R}_{\geq 0}$. Given the battery profile x_1, the *state of charge* of the battery (in kWh) at time $k\Delta$ is denoted by $\chi(k)$, where

$$\chi(k) := \chi(0) - \sum_{j=1}^{k} x_1(j)\Delta \qquad \text{for all } k \in \{1,\ldots,s\},$$

and $\chi(0)$ denotes the initial state of charge of the battery. We represent the battery capacity (in kWh) by $C \in \mathbb{R}_{\geq 0}$, the *state of charge profile* by $\chi := [\chi(0),\ldots,\chi(s)]^T \in \mathbb{R}^{s+1}$, and we represent the state of charge profile constraint by

$$\mathbf{0} \leq \chi \leq C \begin{bmatrix} 1 \\ \mathbb{1} \end{bmatrix}.$$

That is, we employ a deliberately simplified battery model to assess the distributor and/or customer benefits of coordinating residential battery schedules when net metering, which may be extended for more specific battery technologies. This simplified battery model was previously used in [33, 37, 38]. The complexity of additional battery constraints is covered in more detail in [43].

In order to avoid an energy-shifting bias in our results, we include the constraint $\chi(s) = \chi(0)$, where $\chi(s)$ is the final state of charge at time $s\Delta$ [38]. To simplify the notation in what follows we define $\underline{\mathbf{C}} := (\chi(0)/\Delta)\mathbb{1}$, and $\overline{\mathbf{C}} := (1/\Delta)(C-\chi(0))\mathbb{1}$, where the initial state of charge satisfies $0 \leq \chi(0) \leq C$. Further, let $A_1 := \begin{bmatrix} \mathbf{I} & -\mathbf{I} & \mathbf{T} & -\mathbf{T} \end{bmatrix}^T \in \mathbb{R}^{4s\times s}$, and $b_1 := \begin{bmatrix} \overline{B}\mathbb{1}^T & \underline{B}\mathbb{1}^T & \underline{\mathbf{C}}^T & \overline{\mathbf{C}}^T \end{bmatrix}^T \in \mathbb{R}^{4s}$. Thus, we succinctly write the battery constraints as

$$A_1 x_1 \leq b_1, \tag{5}$$

$$\mathbb{1}^T x_1 = 0. \tag{6}$$

3. Problem formulation

In this section we present an approach to quantify, and forecast, bi-directional power-flows in a lossless distribution network.

3.1. Distribution network

We consider a single line diagram of a lossless, radial power distribution network. The point of supply from the transmission network to the distribution network is referred to as the Bulk Supply Point (BSP). Each customer connected to the specified distribution network is represented by a residential system of the form shown in Fig. 1. A Point of Common Coupling (PCC) depicted in Fig. 1 is simply a point where a single residential system connects to the distribution network. We refer to the distribution network as the supply-side, and customers connected to the distribution network as the demand-side.

In what follows our primary interest is bi-directional power flows that approach the capacity of infrastructure in the specified distribution network. However, this condition is not essential to applying our methodology. For example, we may consider power flows that induce a voltage rise for which remediation with voltage regulation infrastructure is limited. Similarly, we may consider peak power flows that approach the thermal capacity of distribution infrastructure. In contrast, we may simply consider bi-directional power flows in the distribution network, where the distribution capacity, or infrastructure limits, are unknown.

With the above as background, we represent a single line diagram of a radial distribution network with a directed graph $\mathcal{G}$, as defined in Section 2.1. In what follows a graph $\mathcal{G}$ is also a rooted tree, where the root vertex M is the BSP, and each leaf in the rooted tree corresponds to a PCC. The set of directed paths from the root vertex M, to every other vertex $k \in \mathcal{V}$, $k \in \{1,\ldots,M-1\}$, corresponds to the directions of positive power flows. Power flows against the positive direction are negative, and are referred to as reverse power flows.

In this paper we are primarily interested in power flows that are approaching the supply-side capacity as identified by the distributor with the assistance of load flow analysis. A directed edge $(j,i) \in \mathcal{E}$ associated with a power flow approaching the supply-side capacity is called an *edge of interest* and is labeled E_i. We represent the capacity of the edge E_i by an *upper limit* in kW denoted by $\overline{P} \in \mathbb{R}_{\geq 0}$, and a *lower limit* in kW denoted by $\underline{P} \in \mathbb{R}$. To ensure customers receive a reliable supply of electricity, power flows along the edge E_i must not exceed the upper limit $\overline{P}$, or fall below the lower limit $\underline{P}$.

To manage power flows along edge E_i, a directed edge from vertex $j \in \mathcal{V}$ to vertex $i \in \mathcal{V}$, we consider a subgraph $\mathcal{G}_i$. Recall, a subgraph $\mathcal{G}_i$ is defined in Section 2.1. We call the root vertex of subgraph $\mathcal{G}_i$ the *Supply Point* (SP). The leaves of subgraph $\mathcal{G}_i$ represent Points of Common Coupling (PCC). The N customers with a PCC included in the subgraph $\mathcal{G}_i$ are represented by $n = \{1,\ldots,N\}$. We refer to the N demand-side customers as *subgraph members*. Fig. 3 highlights an example subgraph $\mathcal{G}_6$, with $N = 3$ demand-side customers, an SP vertex $i = 6$, and an edge of interest denoted by E_6.

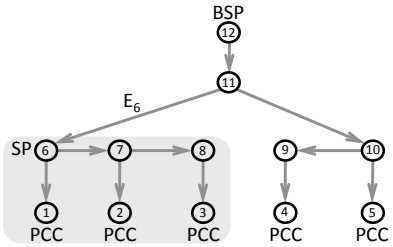

Figure 3: A directed graph $\mathcal{G}$, where E_6 represents the edge of interest. The shaded region highlights the subgraph $\mathcal{G}_6$, where vertex 6 denotes the SP.

To define the power flows along edge E_i, we formulate the definitions of *subgraph load, subgraph generation, subgraph battery, and subgraph grid profiles* over $[0,T]$ by

$$L := \sum_{n=1}^{N} l^{(n)}, \qquad G := \sum_{n=1}^{N} g^{(n)}, \qquad X_1 := \sum_{n=1}^{N} x_1^{(n)}, \qquad X_2 := \sum_{n=1}^{N} x_2^{(n)}, \tag{7}$$

where $l^{(n)}$, $g^{(n)}$, $x_1^{(n)}$, $x_2^{(n)}$ denote the load, generation, battery and grid profiles, respectively, for subgraph member n over $[0,T]$. Note that L, G, X_1, and $X_2 \in \mathbb{R}^s$. Neglecting power losses, power flows (in kW) along edge E_i over $[0,T]$ are represented by the subgraph grid profile X_2. Furthermore, the subgraph grid profile can be written as $X_2 = L - G - X_1$, which is a direct result of the power balance equation in (2).

Example: In this example the distribution network $\mathcal{G}$ is presented in Fig. 3, where vertex 12 denotes the BSP. Assume the distribution operator identifies the edge of interest $E_6 = (11,6)$ within $\mathcal{G}$, with limits $\overline{P} = 25$kW and $\underline{P} = -10$kW. The inputs required to identify a subgraph of $\mathcal{G}$ are shown in Table 1.

Table 1: Inputs required to identify subgraph $\mathcal{G}_i$

Inputs	Example
Directed graph: $\mathcal{G}$	directed graph Fig. 3
BSP: vertex M	vertex 12 in Fig. 3
Edge of interest: $E_i = (j,i)$	E_6 in Fig. 3

The inputs in Table 1 yield the subgraph $\mathcal{G}_6$. In more detail, vertex 6 associated with the edge of interest $E_6 = (11,6)$ denotes the subgraph root, and is labeled the SP. The vertex set of subgraph $\mathcal{G}_6$ is defined by the set of downstream vertices, that is, the downstream vertices of the SP are $\mathcal{V}_6 = \{1,2,3,6,7,8\}$. Each subgraph leaf represents the PCC of a subgraph member, where the set of subgraph leaves are $\{1,2,3\} \subset \mathcal{V}_6$. Consequently, the subgraph $\mathcal{G}_6$ contains the PCC of $N = 3$ subgraph members. Each directed path from vertex 6 (the SP) to a PCC is included in the subgraph $\mathcal{G}_6$.

As a concrete example, one possible scenario describing the edge of interest E_6 upper in lower limits is as follows: the upper limit $\overline{P} = 25$kW on the edge of interest E_6 reflects a thermal rating of an electrical conductor, while the lower limit $\underline{P} = -10$kW on the edge of interest reflects a voltage rise constraint, i.e., voltage rise at the PCC of each subgraph member is within allowable limits when reverse power flow is limited to -10kW along edge E_6. Other scenarios that describe the edge of interest upper and lower limits are certainly possible.

3.2. Forecasts

In this paper we consider two demand-side approaches to managing power flows along an edge of interest. Both approaches coordinate demand-side battery schedules of customers with a PCC downstream of the SP. The first approach (central QP energy-shifting) requires the distributor to forecast the day-ahead subgraph load and subgraph generation profiles, (cf., equation (7)). The second approach (local QP energy-shifting) requires each subgraph member to forecast their day-ahead load and generation profiles.

In this section we do not suggest specific approaches the distributor, or customer, may take to perform such forecasts, but rather, describe methods to emulate forecast data appropriate for simulation from known and available data. To emulate load and generation forecasts for each subgraph member we consider known and available load and generation profiles, respectively. Further, to emulate distributor-based forecasts we consider the emulated forecasts of load and generation pertaining to each subgraph member, respectively.

To emulate generation forecasts for each subgraph member we use the methodology proposed in [39]. That is, we emulate the generation forecast for subgraph member n by apply a moving average window to a known and fixed generation profile $g^{(n)}$ as follows:

$$\hat{g}^{(n)}(k) = \frac{1}{3}(g^{(n)}(k-1) + g^{(n)}(k) + g^{(n)}(k+1)), \tag{8}$$

for all $k \in \{2,3,\ldots,s-1\}$, and we let $\hat{g}^{(n)}(k) = g^{(n)}(k)$ for $k \in \{1,s\}$. We define the *generation forecast* over $[0,T]$ by $\hat{g}^{(n)} := [\hat{g}^{(n)}(1),\ldots,\hat{g}^{(n)}(s)]^T \in \mathbb{R}^s_{\geq 0}$. Further, we emulate the *subgraph generation forecast* over $[0,T]$ as follows:

$$\widehat{G} := \sum_{n=1}^{N} \hat{g}^{(n)}, \tag{9}$$

where $\hat{g}^{(n)}$ is an emulated forecast of a generation profile for subgraph member n on a given day.

Likewise, we emulate the day-ahead load forecast for each subgraph member using the methodology proposed in [39]. To emulate the *load forecast* for subgraph member n, denoted by $\hat{l}^{(n)} \in \mathbb{R}^s_{\geq 0}$, we use a known and fixed load profile $l^{(n)}$ and include uncertainty in the forecast as follows

$$\hat{l}^{(n)}(k) := l^{(n)}(k) + \delta(k)$$

for all $k \in \{1,\ldots,s\}$, where $\delta(k)$ is a random number generated from a normal distribution of mean zero with a standard deviation of 20% of $l^{(n)}(k)$. We define the load forecast over $[0,T]$ by $\hat{l}^{(n)} := [\hat{l}^{(n)}(1),\ldots,\hat{l}^{(n)}(s)]^T \in \mathbb{R}^s_{\geq 0}$. Further, we emulate the *subgraph load forecast* over $[0,T]$ as follows:

$$\widehat{L} := \sum_{n=1}^{N} \hat{l}^{(n)}, \tag{10}$$

where $\hat{l}^{(n)}$ is an emulated forecast of a load profile for subgraph member n on a given day.

Furthermore, we denote a *grid forecast* for subgraph member n by $\hat{x}_2^{(n)}$, where day-ahead power balance equation for the residential energy system in Fig. 1 is

$$\hat{x}_2^{(n)}(k) = \hat{l}^{(n)}(k) - \hat{g}^{(n)}(k) - x_1^{(n)}(k), \tag{11}$$

which must hold for all $k \in \{1,\ldots,s\}$. We define the grid forecast over $[0,T]$ by $\hat{x}_2^{(n)} := [\hat{x}_2^{(n)}(1),\ldots,\hat{x}_2^{(n)}(s)]^T \in \mathbb{R}^s$.

Neglecting power losses, potential day-ahead power flows along an edge of interest E_i are determined via a forecast, that is, the *subgraph forecast*. We denote the subgraph forecast by $\widehat{X}_2$, where the day-ahead power balance equation

$$\widehat{X}_2(k) = \widehat{L}(k) - \widehat{G}(k) - X_1(k) \tag{12}$$

holds for all $k \in \{1,\ldots,s\}$. We define the subgraph forecast over $[0,T]$ by $\widehat{X}_2 := [\widehat{X}_2(1),\ldots,\widehat{X}_2(s)]^T \in \mathbb{R}^s$.

Example: Consider $N = 145$ customers connected to a subgraph $\mathcal{G}_i$, where $\mathcal{G}_i$ represents a region in the distribution network. The subgraph $\mathcal{G}_i$ therefore contains 145 leaves, where each leaf represents the PCC of a subgraph members. In what follows we consider the $N = 145$ subgraph members to quantify uncertainty in emulated load and generation forecasts.

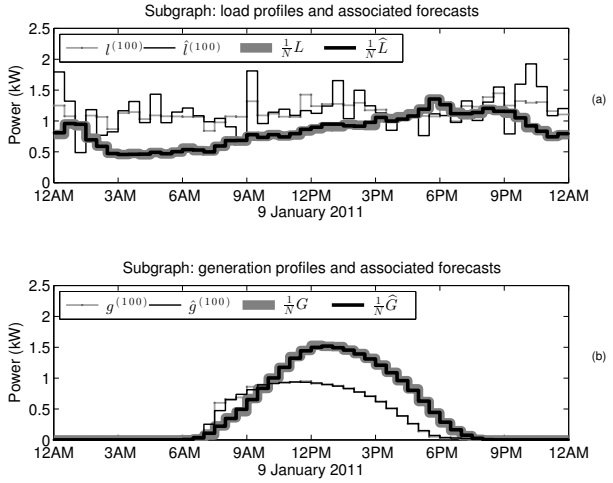

Figure 4: Subgraph member 100: (a) load profile and load forecasts, and (b) generation profile and generation forecasts. Scaled by a factor of $1/N$: (a) subgraph load profile and subgraph load forecast, and (b) subgraph generation profile and subgraph generation forecast.

Fig. 4 compares emulated load and generation forecasts for a subgraph member (for use in local QP energy-shifting) with emulated forecasts for a distributor considering the entire subgraph (scaled by $1/N$ and for use in central QP energy-shifting). We observe the subgraph load L and subgraph generation G profiles scaled by a factor of $1/N$ are distinctly different from the load $l^{(100)}$ and generation $g^{(100)}$ profiles of subgraph member 100, respectively. This observation reflects the diversity in the load profile of each subgraph member, and the diversity in the PV panel orientation of each subgraph member, respectively.

In Fig. 4(a) we observe the distributor-based forecast of load $\widehat{L}$ is closely aligned to the subgraph load profile L. In contrast, the load forecast of subgraph member 100, $\hat{l}^{(100)}$, is not closely aligned to the corresponding load profile $l^{(100)}$. In Fig. 4(b) we observe the distributor-based forecast of generation $\widehat{G}$ scaled by a factor of $1/N$ is closely aligned with the subgraph generation profile G scaled by a factor of $1/N$. In contrast, the generation forecast of subgraph member 100, $\hat{g}^{(100)}$, is not closely aligned to the corresponding generation profile $g^{(100)}$, with particular reference to the period between 7.30am-8am. These observations are consistent with our assumption that day-ahead distributor-based forecasts of power flows along an edge of interest are typically more accurate with respect to day-ahead forecasts of load and PV generation determined by subgraph member n.

4. Two algorithms for battery scheduling

In what follows the distributor selects and transmits the day-ahead net metering financial policy η to all grid-connected customers. Furthermore, the distribution operator conducts load flow analysis to identify the day-ahead edge of interest (if any) in the distribution grid $\mathcal{G}$, together with the limits $\overline{P}$ and $\underline{P}$ associated with the edge of interest. The distributor also identifies the SP vertex associated with the edge of interest, which denotes the root of the subgraph under consideration in the sequel.

For an identified supply point in the distribution grid $\mathcal{G}$, we consider two approaches to scheduling demand-side battery storage to manage power flows along an edge of interest. The first approach is referred to as *central QP energy-shifting*, where the distributor sends each subgraph member a battery profile for the day-ahead. The second approach is referred to as *local QP energy-shifting*, where each subgraph member determines their day-ahead battery profile subject to three distributor-specified weights. Both approaches aim to increase the operational savings of each subgraph member while respecting the constraints associated with the edge of interest.

4.1. Central QP energy-shifting

Central QP energy-shifting refers to the process of each subgraph member implementing a distributor-specified battery profile. That is, the distributor manages bi-directional power flows along the edge of interest by insisting that each subgraph member implements the distributor-specified day-ahead battery charge and discharge schedule.

The central QP energy-shifting objective function is to maximize

$$\sum_{k=1}^{s} w\Delta\eta(k)X_1(k) - \eta(k)(\widehat{X}_2(k))^2 \tag{13}$$

for all $k \in \{1,\ldots,s\}$, where w is a distributor weighting, $\eta(k)$ is the net metering electricity price in \$/kWh over the k^{th} interval of length Δ, $X_1(k)$ represents is the k^{th} entry in the subgraph battery profile (7), and $\widehat{X}_2(k)$ represent the subgraph forecast (in kW) (cf., equation (12)).

The central QP energy-shifting objective function (13) consists of two terms. The first term is weighted by w and maximizes the *operational savings of the subgraph*, denoted by Ψ and defined by

$$\Psi := \sum_{n=1}^{N} \psi^{(n)} = \Delta\eta^T X_1, \tag{14}$$

where N is the number of subgraph members, and $\psi^{(n)}$ represents the operational savings of subgraph member n as in (4), η is the net metering profile, and X_1 is the subgraph battery profile (7). The second term in (13) reduces reverse power flow along an edge of interest, that potentially arises during the peak pricing period when maximizing the subgraph operational savings Ψ [33]. More specifically, in [33] it was observed that scheduling battery storage to maximize the operational savings led to significant reverse power flow during the peak pricing period. To counteract this reverse power flow arising from increasing the operational savings, we weight the second term in (13) by η.

To further manage day-ahead power flows along an edge of interest, with limits $\underline{P}$, $\overline{P}$, we consider the following *subgraph forecast constraint*

$$\underline{\mathbf{P}}\mathbb{1} \leq \widehat{X}_2 \leq \overline{\mathbf{P}}\mathbb{1}. \tag{15}$$

Additionally, the battery constraints when central QP energy-shifting are scaled by the number of subgraph members N, as follows

$$A_1 X_1 \leq N b_1, \tag{16}$$

$$\mathbb{1}^T X_1 = 0. \tag{17}$$

That is, for the purpose of simplicity we assume in (16) that all subgraph members have battery parameters and identical constraints as in (5). Extensions to heterogeneous battery constraints are certainly possible. Such extensions will lead to different numerical results when central QP energy-shifting, however, we anticipate that the qualitative results would be similar.

For a known and specified weight w, financial policy η, subgraph forecast constraints $\underline{\mathbf{P}}$, $\overline{\mathbf{P}}$, and a subgraph load and generation forecast $\widehat{L}$, $\widehat{G}$, the following Lemma expresses the constrained objective function in (13) as a quadratic program (QP).

Lemma 2. *The maximization of expression* (13)*, subject to battery constraints* (16)–(17)*, the power balance equation* (12)*, subgraph forecast constraints* (15)*, can be written as the following quadratic program:*

$$\max_{x \in \mathbb{R}^{2s}} \quad x^T H x + c^T x \tag{18}$$

such that

$$\overline{A}_1 x \leq \overline{b}_1, \tag{19}$$

$$A_2 x = b_2, \tag{20}$$

where $x \in \mathbb{R}^{2s}$, $H \in \mathbb{R}^{2s \times 2s}$, $\mathbf{H} \in \mathbb{R}^{s \times s}$, $c \in \mathbb{R}^{2s}$, $w \in \mathbb{R}$, $\overline{A}_1 \in \mathbb{R}^{6s \times 2s}$, $A_2 \in \mathbb{R}^{(s+1) \times 2s}$, $\overline{b}_1 \in \mathbb{R}^{6s}$, $b_2 \in \mathbb{R}^{s+1}$, *and*

$$x := \begin{bmatrix} X_1{}^T & \widehat{X}_2{}^T \end{bmatrix}^T \tag{21}$$

$$H := \begin{bmatrix} \mathbf{0} & \mathbf{0} \\ \mathbf{0} & -\mathbf{H} \end{bmatrix} \tag{22}$$

$$\mathbf{H} := \operatorname{diag}(\eta(1), \ldots, \eta(s)) \tag{23}$$

$$c := w\Delta \begin{bmatrix} \eta \\ \mathbf{0} \end{bmatrix} \tag{24}$$

$$\overline{A}_1 := \begin{bmatrix} A_1 & \mathbf{0} \\ \mathbf{0} & \mathbf{I} \\ \mathbf{0} & -\mathbf{I} \end{bmatrix} \quad \overline{b}_1 := \begin{bmatrix} N b_1 \\ \overline{\mathbf{P}} \mathbb{1} \\ \underline{\mathbf{P}} \mathbb{1} \end{bmatrix} \tag{25}$$

$$A_2 := \begin{bmatrix} \mathbb{1}^T & \mathbf{0}^T \\ \mathbf{I} & \mathbf{I} \end{bmatrix} \quad b_2 := \begin{bmatrix} 0 \\ \widehat{L} - \widehat{G} \end{bmatrix}. \tag{26}$$

Proof. The result follows directly from Lemma 1 given the battery constraints (5)–(6) defined in Section 2.3, a financial policy of net metering, and the power balance equation (2). ■

We will refer to the process of a subgraph member implementing the daily battery profile $x_1^{(n)} = \frac{1}{N} X_1$, where X_1 is obtained by solving (18) subject to constraints (19)-(20) as *central QP energy-shifting*.

4.2. Local QP energy-shifting

Local QP energy-shifting refers to the process of each subgraph member implementing a daily battery profile, subject to three distributor-specified weights. That is, to manage bi-directional power flows along the edge of interest, the distribution operator transmits three weights to each subgraph member for the day-ahead. The three distributor-specified weights are incorporated into an objective function in an optimization problem, that each subgraph member solves in the day-ahead. In solving the optimization problem, each subgraph member determines a day-ahead battery profile that is implemented when local QP energy-shifting.

The local QP energy-shifting objective function is to maximize

$$\sum_{k=1}^{s} w_1 \Delta \eta(k) x_1^{(n)}(k) - w_2 \eta(k) (\hat{x}_2^{(n)}(k))^2 - w_3 (\hat{x}_2^{(n)}(k))^2, \tag{27}$$

for all $k \in \{1, \ldots, s\}$. The three distributor specified weights are denoted by w_1, w_2, and w_3, and are applied to each term in the QP objective function. Recall n denotes the subgraph member, $\eta(k)$ denotes the net metering electricity price in \$/kWh, $\Delta \eta(k) x_1^{(n)}(k)$ denotes the operational saving over the k^{th} interval of length Δ (see (4) in Lemma 1), and $\hat{x}_2^{(n)}(k)$ represents the forecast power flow (in kW) for subgraph member n as in (11).

The first term in (27) maximizes the operational savings that accrue to each subgraph member as done in [33], and is weighted by w_1. The second term reduces reverse power flow that potentially arises during the peak pricing period when each subgraph member maximizes their operational savings, and is weighted by w_2. The third term reduces peak power flows that potentially arise during the off-peak pricing period when each subgraph member maximizes their operational savings (similar to that in [19, 29]), and is weighted by w_3. In the simulations that follow we investigate the significance of each term, by adjusting the assigned weight.

For the distributor specified weights w_1, w_2, w_3, and financial policy η, the following Lemma expresses the constrained maximization in (27) as a quadratic program (QP).

Lemma 3. *The maximization of expression* (27)*, subject to battery constraints* (5)–(6)*, the power balance equation* (2)*, can be written as the following quadratic program:*

$$\max_{x \in \mathbb{R}^{2s}} \quad x^T H x + c^T x \tag{28}$$

such that

$$A_1 x \leq b_1, \tag{29}$$

$$A_2 x = b_2, \tag{30}$$

where A_1 and b_1 are as in (5) *and $x \in \mathbb{R}^{2s}$, $H \in \mathbb{R}^{2s \times 2s}$, $\mathbf{H} \in \mathbb{R}^{s \times s}$, $c \in \mathbb{R}^{2s}$, $w_1 \in \mathbb{R}$, $w_2 \in \mathbb{R}$, $w_3 \in \mathbb{R}$, $A_2 \in \mathbb{R}^{(s+1) \times 2s}$,*

$b_2 \in \mathbb{R}^{s+1}$, *and*

$$\begin{aligned} x &:= \begin{bmatrix} x_1^{(n)T} & \hat{x}_2^{(n)T} \end{bmatrix}^T \\ H &:= \begin{bmatrix} \mathbf{0} & \mathbf{0} \\ \mathbf{0} & -(w_2\mathbf{H} + w_3\mathbf{I}) \end{bmatrix} \\ \mathbf{H} &:= \text{diag}(\eta(1), \ldots, \eta(s)) \\ c &:= w_1 \Delta \begin{bmatrix} \eta \\ \mathbf{0} \end{bmatrix} \\ A_2 &:= \begin{bmatrix} \mathbb{1}^T & \mathbf{0}^T \\ \mathbf{I} & \mathbf{I} \end{bmatrix} \quad b_2 := \begin{bmatrix} 0 \\ \hat{l}^{(n)} - \hat{g}^{(n)} \end{bmatrix}. \end{aligned}$$

Proof. The result follows directly from Lemma 1 given the battery constraints (5)–(6) defined in Section 2.3, a financial policy of net metering, and the power balance equation (2). ■

We will refer to the process of a subgraph member implementing the daily battery profile $x_1^{(n)}$ obtained by solving (28) subject to constraints (29)-(30) as *local QP energy-shifting*. Extensions to heterogeneous battery constraints when local QP energy-shifting are accommodated by constraints (29)-(30) in Lemma 3.

5. Assessing the benefits

We analyzed measured load and generation profiles from 1 July 2010 to 30 June 2011, for each of 145 randomly selected low voltage customers located in an Australian distribution network operated by Ausgrid [41, 44]. The Ausgrid distribution network covers 22,275 km^2 and includes load centers in Sydney and regional New South Wales. The load and generation profiles $l^{(n)}$ and $g^{(n)}$ for each of the 145 customers are defined with $T = 24$ hours, $\Delta = 30$ minutes, and $s = T/\Delta = 48$, for each day over the course of 52 weeks. The 'Ausgrid data set' refers to the load and generation profiles for each of these 145 customers, on each day over the course of 52 weeks.

In the simulations that follow we consider a subgraph $\mathcal{G}_i$, where $\mathcal{G}_i$ represents a region in a distribution network that contains 145 subgraph members. The load and generation profiles of each subgraph member, on each day over the course of a year, are defined by the Ausgrid data set. To emulate forecast data for the subgraph, and each subgraph member, we employ the methodology described in Section 3.2. For each of the $N = 145$ customer connected to the subgraph $\mathcal{G}_i$ we fix $T = 24$ hours, $\Delta = 30$ minutes, and $s = T/\Delta = 48$. In all cases, the residential battery constraints in (5)–(6) are fixed, where

$$C = 10\,\text{kWh}, \quad \chi(0) = 5\,\text{kWh}, \quad \overline{B} = -\underline{B} = 5\,\text{kW}. \tag{31}$$

On each day over the course of 52 weeks the length-s net metering policy (in \$/kWh) is fixed as follows:

$$\eta = [\eta(1), \ldots, \eta(s)]^T, \tag{32}$$

where $\eta(k) = 0.03$ for $k \in \{1, \ldots, 14, 45, \ldots, 48\}$, $\eta(k) = 0.06$ for $k \in \{15, \ldots, 28, 41, \ldots, 44\}$ and $\eta(k) = 0.3$ for $k \in \{29, \ldots, 40\}$. When central QP energy-shifting we denote by $SL1$ the subgraph forecast constraints

$$SL1: \quad \overline{\mathbf{P}} = 300, \quad \underline{\mathbf{P}} = -\infty. \tag{33}$$

To compare operational savings when central QP energy-shifting, we denote by *SL2* the subgraph forecast constraints

$$SL2: \quad \overline{\mathbf{P}} = \infty, \quad \underline{\mathbf{P}} = -\infty. \tag{34}$$

We assume the subgraph grid profile X_2 (7) represents power flows (in kW) along the edge of interest E_i over $[0,T]$. That is, we neglect power losses in the subgraph $\mathcal{G}_i$. Furthermore, we assume the $N = 145$ subgraph members receive a reliable supply of electricity when bi-directional power flows that enter or leave the subgraph $\mathcal{G}_i$ via the edge of interest E_i do not exceed $\overline{P} = 300$kW, or fall bellow $\underline{P} = -150$kW. That is, upper and lower limits on the edge of interest are

$$\overline{P} = 300, \quad \underline{P} = -150. \tag{35}$$

The remainder of this section is organized as follows. In Section 5.1 we define a baseline profile to benchmark the distributor benefits of local and/or central QP energy-shifting presented in the sequel. In Section 5.2 we present two examples to motivate the importance of coordinating day-ahead residential battery schedules. In Section 5.3 we quantify the operational savings that accrue to subgraph members when local, or central QP energy-shifting, and we reflect on the qualitative benefits of each approach.

5.1. Baseline profile

To assess the benefits of residential battery scheduling we define an important special case; that is, battery charge/discharge powers of each subgraph member satisfy $x_1^{(n)}(k) = 0$ for all $k \in \{1,\dots,s\}$. Then, in this special case, the *subgraph grid profile* X_2 in (7) reduces to the *baseline profile* defined over $[0,T]$ by

$$\widetilde{X}_2 = \sum_{n=1}^{N} l^{(n)} - g^{(n)}. \tag{36}$$

We note the baseline profile $\widetilde{X}_2$ is also defined in the absence of residential battery storage in the residential system of each subgraph member. In what follows we consider 52 weeks of daily baseline profiles (i.e., we consider 365 baseline profiles), obtained directly from the Ausgrid data set.

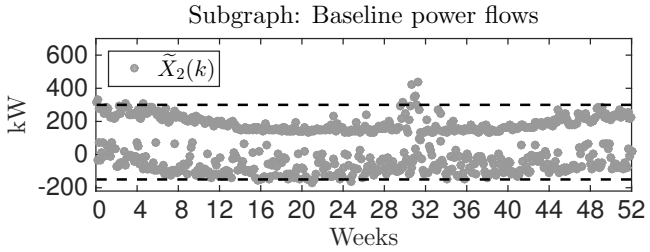

Figure 5: Daily peak and minimum power flows from each baseline profile $\widetilde{X}_2$. Dashed lines represent the upper and lower limits on the edge of interest.

In Fig. 5 we present the daily peak and minimum power flows of each daily baseline profile, with reference to a 52 week period. The dotted lines in Fig. 5 show the upper and lower limits on the edge of interest, as in (35).

In Fig. 5 we observe the baseline profile exceeds the upper limit for the edge of interest at $\overline{P} = 300$kW on 9 days in the year, and falls below the lower limit at $\underline{P} = -150$kW on 5 days in the year. Therefore, on most days, subgraph members receive a reliable supply of electricity when they do not have, or they do not use, a battery.

5.2. Distribution power flows

We now present two examples, where we investigate the design parameters associated with local and/or central QP energy-shifting. In particular, we consider specific weights associated with local or central QP energy-shifting, and determine resulting bi-directional power flows entering or leaving the subgraph via the edge of interest E_i. Recall, subgraph members receive a reliable supply of electricity when power flows along the edge of interest E_i do not exceed an upper limit, $\overline{P} = 300$kW, or fall below a lower limit, $\underline{P} = -150$kW, as in (35).

Table 2 presents the design parameters considered in the following two examples. In the first example we consider the design parameters associated with Case A, and in the second example we consider the design parameters associated with Case B and C. Note that the design parameters included in Table 2 have been carefully selected to highlight the importance of coordinating day-ahead residential battery schedules. That is, a careful comparison of weights and constraints was conducted, informing the choice of design parameters in Table 2.

Table 2: Design parameters for two examples in Section 5.2

	Reference	Central QP energy-shifting	Reference	Local QP energy-shifting
Case A. Increase operation savings	*CQPa*	$w = 10$, *SL*2 (34)	*LQPa*	$w_1 = 9, w_2 = 1, w_3 = 0$
Case B. Manage bi-directional power flows	*CQPb*	$w = 2$, *SL*1 (33)	*LQPb*	$w_1 = 9, w_2 = 1, w_3 = 1$
Case C. Manage bi-directional power flows	*CQPc*	$w = 0$, *SL*1 (33)	*LQPc*	$w_1 = 5, w_2 = 0, w_3 = 2$

In the two examples that follow the battery constraints are specified in (31) for all subgraph members. The day-ahead net metering financial policy is specified in (32). Additionally, subgraph grid profile X_2 corresponds to power flows along the edge of interest, since we disregard network losses.

Example 1: *Increase operational savings*

In this example we consider design parameters associated with Case A in Table 2 to motivate the importance of coordinating day-ahead residential battery schedules. When local QP energy-shifting, the design parameters *LQPa* are selected to preference increases in operational savings that accrue to customers, where a large value of w_1 is selected with respect to weights w_2 and w_3. When central QP energy-shifting the design parameters *CQPa* are selected to preference increases in operational savings, where a large weight $w = 10$ together with relaxed subgraph forecast constraint *SL*2 reflect this preference.

Fig. 6 presents the daily peak and minimum power flows from each subgraph grid profile X_2 obtained over the course of 52 weeks, when local or central QP energy-shifting. That is, in Fig. 6(a) we consider power flows along the edge of interest when local QP energy-shifting on each day in the 52 weeks. In Fig. 6(b) we consider power flows along the edge of interest when central QP energy-shifting on each day in the 52 weeks. The dotted lines in Fig. 6 show the upper and lower limits on the edge of interest, as in (35).

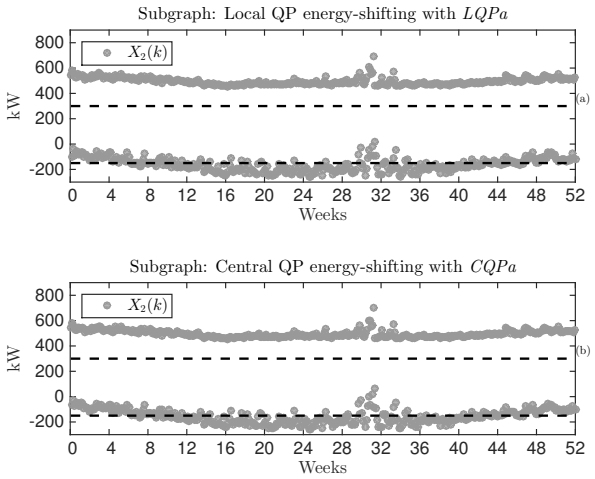

Figure 6: The daily peak and minimum power flows from the subgraph grid profile X_2. (a) Local QP energy-shifting with $w_1 = 9$, $w_2 = 1$, and $w_3 = 0$. (b) Central QP energy-shifting with $w = 10$ and $SL2$ given by (34).

The baseline profile $\widetilde{X_2}$ considered in Fig. 5 did not exceed the upper and lower limits, $\overline{P} = 300$kW, $\underline{P} = -150$kW, on the edge of interest E_i on most days. In contrast, we observe in Fig. 6(a), and in Fig. 6(b), peak power flows from a subgraph grid profile X_2 exceed 300kW on every day in the year. Further, in Fig. 6 we observe peak reverse power flows from each subgraph grid profile X_2 fall below the lower limit at -150kW on most days in the year. Moreover, the subgraph grid profile X_2 associated with local QP energy-shifting is visually similar to the subgraph grid profile X_2 associated with central QP energy-shifting. Thus, a consequence of the preference to increase operational savings is a subgraph grid profile X_2 when local, or central QP energy-shifting that approaches the uncoordinated case, where each residential customer employs a battery schedule designed to maximize their operational saving; see [33] for further details.

Therefore, a distributor must carefully select the design parameters when local, or central QP energy-shifting. Otherwise, residential battery schedules may approach the uncoordinated case. In the following example we consider approaches to improve coordination of residential battery schedules.

Example 2: *Manage bi-directional power flows*

In this example we consider the design parameters associated with Case B and Case C, as specified in Table 2. When local QP energy-shifting the design parameters *LQPb* or *LQPc* are selected, where decreases in w_1 and/or increases in w_3 offer considerable reductions in peak bi-directional power flows. When central QP energy-shifting the design parameters *CQPb* or *CQPc* are selected, where w is decreased to reduce reverse power flows and constraint $SL1$ selected to limit peak power flows. The dotted lines in Fig. 7 show the upper and lower limits on the edge of interest, as in (35).

Fig. 7 presents the daily peak and minimum power flows from each subgraph grid profile X_2 obtained over the course of 52 weeks, when local or central QP energy-shifting. That is, in Fig. 7(a) we consider power flows along the edge of interest when local QP energy-shifting on each day in the 52 weeks. In Fig. 7(b) we consider power flows along the edge of interest when central QP energy-shifting on each day in the 52 weeks.

We observe in Fig. 7(a) peak power flows from a subgraph grid profile X_2 exceed 300kW on two day in the year, with either set of design parameters, *LQPb*, *LQPc*. Furthermore, peak reverse power flows from a subgraph grid profile X_2 in Fig. 7(a) are above the lower limit of -150kW on every day in the year with either set of design parameters, *LQPb*, *LQPc*. Therefore, subgraph members do receive a reliable supply of electricity when local QP energy-shifting with

design parameters *LQPb* or *LQPc* on all but these two days in the given year.

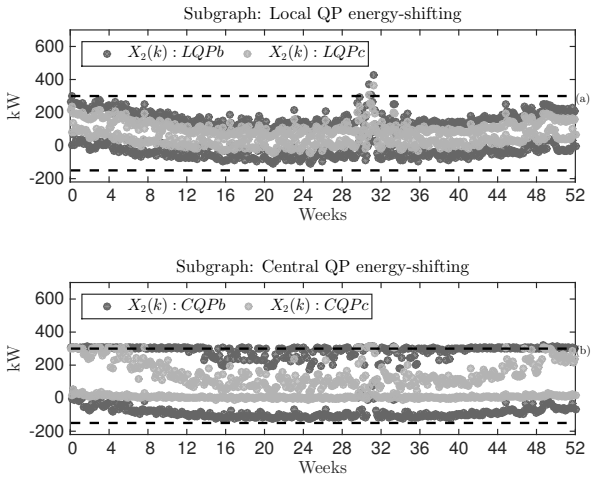

Figure 7: Daily peak and minimum power flows from the subgraph grid profile X_2. (a) Local QP energy-shifting with *LQPb* and *LQPc*, and (b) central QP energy-shifting with *CQPb* and *CQPc*.

Furthermore, on the two days in the year when peak power flows exceed the upper limit on the edge of interest in Fig. 7(a), we note these power flows are lower in magnitude than the respective peak power flows in the baseline considered in Fig. 5. Therefore, local QP energy-shifting manages power flows in a distribution grid via the coordination of residential battery schedules, where the design parameters determine the level of coordination.

In Fig. 7(b) we observe peak power flows from a subgraph grid profile X_2 slightly exceed 300kW on a number of day in the year when central QP energy-shifting with design parameters *CQPc*. Furthermore, peak power flows from a subgraph grid profile X_2 slightly exceed 300kW on each day in the year, when central QP energy-shifting with design parameters *CQPb*. These slight increases in peak power flow are the direct result of forecasting error, which may be corrected by lowering the constraint $\overline{\mathbf{P}} = 300$kW when central QP energy-shifting. In contrast, reverse power flows from a subgraph grid profile X_2 in Fig. 7(b) are above the lower limit at -150kW on every day in the year, with either set of design parameters, *CQPb*, *CQPc*.

Therefore, local, or central QP energy-shifting improves the coordination of residential battery schedules when the design parameters are carefully selected. Well-coordinated residential battery schedules potentially ensure power flows remain within the upper and/or lower limits on the edge of interest.

5.3. Operational savings

To further assess local and central QP energy-shifting we consider the daily operational saving that accrue to subgraph members. In what follows the operational savings that accrue to a single subgraph member when local, or central QP energy-shifting over a period of 52 weeks are denote by *annual savings* in \$/yr. Thus, when the annual savings of a subgraph member are positive, there exists an operational benefit to scheduling a battery. In contrast, when the annual savings are negative there is an operational cost to scheduling a battery.

Local QP energy-shifting: In Fig. 8 we present the annual savings of each subgraph member when local QP energy-shifting on each day of the year. In Fig. 8(a) the annual savings are obtained with design parameters *LQPb*. In Fig. 8(b) the annual savings are obtained with design parameters *LQPc*.

In Fig. 8(a) we observe two customers accrue a small negative annual saving when local QP energy-shifting, which is consistent with previous findings [33, 38]. Specifically, in [33, 38] residential-scale batteries were scheduled to significantly penalize bi-directional power flows during the peak pricing period, which resulted in some customers accruing negative operational savings when PV production exceeded residential demand. In Fig. 8(b) we observe a number of customers accrue negative annual savings when local QP energy-shifting, a consequence of lowering the weighting on the operational savings ($w_1 = 5$) while increasing penalties for peak power flows across the day ($w_3 = 2$). Therefore, local QP energy-shifting may disproportionately penalize some customers, with particular reference to the operational costs some customers incur when implementing a local QP-based battery schedule.

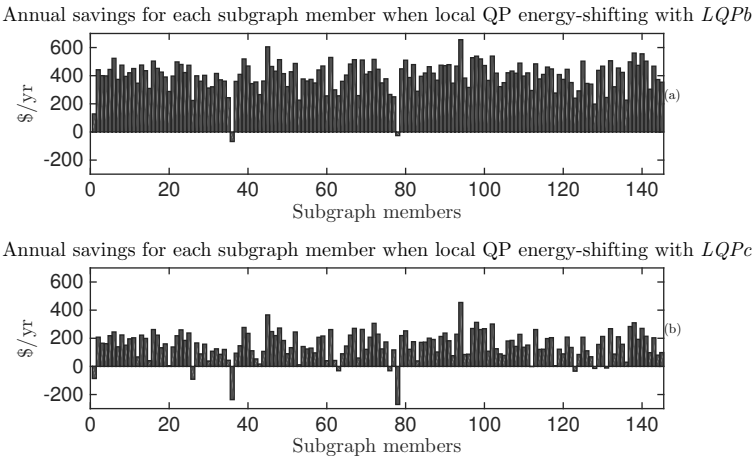

Figure 8: Annual savings for each subgraph member when local QP energy-shifting with design parameters from Table 2: (a) mean annual savings of \$398 with design parameters as specified by *LQPb*, (b) mean annual savings of \$149 with design parameters as specified by *LQPc*.

Central QP energy-shifting: Recall each subgraph member receives an identical day-ahead battery schedule when central QP energy-shifting, cf., Section 4.1. Therefore, each subgraph member accrues the same operational savings when central QP energy-shifting, a direct result of Lemma 1. Consequently, in the results that follow each subgraph member accrues the same annual savings when central QP energy-shifting.[1]

In Fig. 9 we consider the annual savings of each subgraph member when central QP energy-shifting with fixed design parameters on each day of the year. That is, we consider the annual savings obtained when central QP energy-shifting with a weight $w \in \{0, 1, \ldots, 10\}$ and constraints *SL*1 (33) or *SL*2 (34), applied across the entire year.

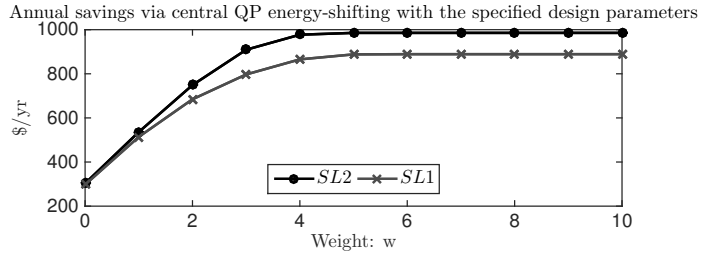

Figure 9: Annual savings for each subgraph member when central QP energy-shifting on each day in a year with weight $w \in \{0, 1, \ldots, 10\}$ and *SL*1 or *SL*2.

In Fig. 9 we observe small weights ($w < 4$) reduce the annual savings, but when the weights are large ($w \geq 4$)

[1] We anticipate, in cases where each subgraph member has heterogeneous battery constraints, the distributor-specified battery schedules will ensure a fair distribution of the available subgraph operational saving, as in (14). That is, no subgraph member will be disproportionately penalized with negative operational savings, while another member accrues significant positive operational savings, when central QP-energy-shifting.

constraints $SL1$ limits the annual saving. We also observe the annual savings with constraints $SL1$ are approximately \$100 less than the annual savings with constraints $SL2$, for larger weights $w \geq 5$. Moreover, annual savings with large weights together with constraint $SL2$ approach the maximum operational savings as defined in our previous work [33].

To approximate the annual savings a customer with a 10 kWh battery may anticipate when central QP energy-shifting, we consider the design parameters as specified in Table 2. With design parameters *CQPa*, a maximum annual savings of \$986/year is inferred from Fig. 9. With design parameters *CQPb*, a maximum annual saving of approximately \$620/year is inferred from Fig. 9. With design parameters *CQPc*, a maximum annual saving of approximately \$320/year is inferred from Fig. 9. Therefore, improving the coordination of battery schedules (i.e., managing bi-directional power flows as in Fig. 7(b)) potentially leads to a reduction in annual savings for a customer when central QP energy-shifting.[2]

In summary, this section presented a motivating example to illustrate the importance of coordinating residential battery schedules within a distribution region. We provided guidance on approaches to select the design parameters of both QP-based algorithms, which determine the level of demand-side coordination. We found the central QP-based approach was preferable in that all customers received the same annual savings. In contrast, the local QP-based algorithm lead to annual costs, rather than savings, for some customers.

6. Conclusions

In this paper we presented two approaches to coordinating residential battery schedules when customers are offered net metering PV incentives with time-based electricity prices. In assessing the benefits of both approaches we found the central QP-based approach was preferable in that no customer was disproportionately penalized for reducing peak load and/or reverse power flow in a distribution network. By means of a case study using measured load and generation data from 145 residential customers located in an Australian distribution network, we found that all customers accrued annual savings in the vicinity of \$620 when central QP energy-shifting with a 10 kWh battery.

The design parameters considered in this paper were carefully chosen to highlight the flexibility of the local and central QP-based algorithms. By carefully selecting the design parameters it was demonstrated that peak loads and/or reverse power flow problems in a distribution grid are potentially mitigated. However, this mitigation typically comes at a cost to the consumer in the context of reductions in operational savings.

Future work will also explore trade-offs between self-consumption and revenue streams for distribution operators. Additional case studies with real network topologies requiring demand management strategies to reduce peak loads or reverse power flows are possible, with a view to quantifying the impact on operational savings to customers offered feed-in tariffs rather than net metering.

7. Acknowledgments

Elizabeth L. Ratnam acknowledges the financial support of an Australian Postgraduate Award (APA) and a CSIRO - Energy Technology Postgraduate Research Scholarship (Ref: 2011094123).

[2] Factoring in the efficiency of the residential system, including the battery and associated inverters, will naturally reduce the annual savings.

References

[1] S. M. Moosavian, N. A. Rahim, J. Selvaraj, K. H. Solangi, Energy policy to promote photovoltaic generation, Renewable & Sustainable Energy Reviews 25 (2013) 44 – 58.

[2] M. Bazilian, I. Onyeji, M. Liebreich, I. MacGill, J. Chase, J. Shah, D. Gielen, D. Arent, D. Landfear, S. Zhengrong, Re-considering the economics of photovoltaic power, Renewable Energy 53 (2013) 329 – 338.

[3] T. Lang, E. Gloerfeld, B. Girod, Don't just follow the sun - A global assessment of economic performance for residential building photovoltaics, Renewable & Sustainable Energy Reviews 42 (2015) 932 – 951.

[4] A. Poullikkas, A comparative assessment of net metering and feed in tariff schemes for residential PV systems, Sustainable Energy Technologies and Assessments 3 (2013) 1 – 8.

[5] A. Campoccia, L. Dusonchet, E. Telaretti, G. Zizzo, Comparative analysis of different supporting measures for the production of electrical energy by solar PV and wind systems: Four representative European cases, Solar Energy 83 (3) (2009) 287 – 297.

[6] A. J. Black, Financial payback on California residential solar electric systems, Solar Energy 77 (4) (2004) 381 – 388.

[7] F. Katiraei, J. R. Agüero, Solar PV integration challenges, IEEE Power and Energy Mag. 9 (3) (2011) 62–71.

[8] R. Tonkoski, D. Turcotte, T. H. M. El-Fouly, Impact of high PV penetration on voltage profiles in residential neighborhoods, IEEE Trans. Sustain. Energy 3 (3) (2012) 518–527.

[9] J. von Appen, M. Braun, T. Stetz, K. Diwold, D. Geibel, Time in the sun: the challenge of high PV penetration in the German electric grid, IEEE Power and Energy Mag. 11 (2) (2013) 55–64.

[10] C. L. Masters, Voltage rise the big issue when connecting embedded generation to long 11 kV overhead lines, Power Engineering Journal 16 (1) (2002) 1–8.

[11] K. Büdenbender, M. Braun, T. Stetz, P. Strauss, Multifunctional PV systems offering additional functionalities and improving grid integration, International Journal of Distributed Energy Resources 7 (2) (2011) 109–128.

[12] J. von Appen, T. Stetz, B. Idlbi, M. Braun, Enabling high amounts of PV systems in low voltage grids using storage systems, in: Proc. 29th European Photovoltaic Solar Energy Conference and Exhibition, Amsterdam, 2014, pp. 1–7.

[13] R. Tonkoski, L. A. C. Lopes, T. H. M. El-Fouly, Coordinated active power curtailment of grid connected PV inverters for overvoltage prevention, IEEE Trans. Sustain. Energy 2 (2) (2011) 139–147.

[14] T. S. Brinsmead, P. Graham, J. Hayward, E. L. Ratnam, L. Reedman, Future Energy Storage Trends: An Assessment of the Economic Viability, Potential Uptake and Impacts of Electrical Energy Storage on the NEM 2015-2035, CSIRO, Australia. Report No. EP155039 (2015).

[15] P. Jahangiri, D. C. Aliprantis, Distributed Volt/VAr control by PV inverters, IEEE Trans. Power Syst. 28 (3) (2013) 3429–3439.

[16] F. Marra, G. Yang, C. Traeholt, J. Ostergaard, E. Larsen, A decentralized storage strategy for residential feeders with photovoltaics, IEEE Trans. Smart Grid 5 (2) (2014) 974–981.

[17] S. Shao, M. Pipattanasomporn, S. Rahman, Demand response as a load shaping tool in an intelligent grid with electric vehicles, IEEE Trans. Smart Grid 2 (4) (2011) 624–631.

[18] S. Bashash, H. K. Fathy, Modeling and control of aggregate air conditioning loads for robust renewable power management, IEEE Trans. Control Systems Technology 21 (4) (2013) 1318–1327.

[19] D. S. Callaway, I. A. Hiskens, Achieving controllability of electric loads, Proceedings of the IEEE 99 (1) (2011) 184–199.

[20] M. Pipattanasomporn, M. Kuzlu, S. Rahman, An algorithm for intelligent home energy management and demand response analysis, IEEE Trans. Smart Grid 3 (4) (2012) 2166–2173.

[21] N. Ruiz, I. Cobelo, J. Oyarzabal, A direct load control model for virtual power plant management, IEEE Trans. Power Syst. 24 (2) (2009) 959–966.

[22] M. Negnevitsky, K. Wong, Demand-side management evaluation tool, IEEE Trans. Power Syst. 30 (1) (2015) 212–222.

[23] O. Corradi, H. Ochsenfeld, H. Madsen, P. Pinson, Controlling electricity consumption by forecasting its response to varying prices, IEEE Trans. Power Syst. 28 (1) (2013) 421–429.

[24] A.-H. Mohsenian-Rad, A. Leon-Garcia, Optimal residential load control with price prediction in real-time electricity pricing environments, IEEE Trans. Smart Grid 1 (2) (2010) 120–133.

[25] M. P. Moghaddam, A. Abdollahi, M. Rashidinejad, Flexible demand response programs modeling in competitive electricity markets, Applied Energy 88 (9) (2011) 3257 – 3269.

[26] J. von Appen, T. Stetz, M. Braun, A. Schmiegel, Local voltage control strategies for PV storage systems in distribution grids, IEEE Trans. Smart Grid 5 (2) (2014) 1002–1009.

[27] F. Braam, R. Hollinger, M. Llerena Engesser, S. Muller, R. Kohrs, C. Wittwer, Peak shaving with photovoltaic-battery systems, in: Proc. IEEE PES Conf. on Innovative Smart Grid Technologies (ISGT-Europe), Istanbul, 2014, pp. 1–5.

[28] J. Bergner, J. Weniger, T. Tjaden, V. Quaschning, Feed-in power limitation of grid-connected PV battery systems with autonomous forecast-based operation strategies, in: Proc. 29th European Photovoltaic Solar Energy Conference and Exhibition, Amsterdam, 2014, pp. 1–8.

[29] Y. Li, B. L. Ng, M. Trayer, L. Liu, Automated residential demand response: Algorithmic implications of pricing models, IEEE Trans. Smart Grid 3 (4) (2012) 1712–1721.

[30] P. Palensky, D. Dietrich, Demand side management: Demand response, intelligent energy systems, and smart loads, IEEE Trans. Ind. Informatics 7 (3) (2011) 381–388.

[31] S. Nykamp, M. G. C. Bosman, A. Molderink, J. L. Hurink, G. J. M. Smit, Value of storage in distribution grids – competition or cooperation of stakeholders?, IEEE Trans. Smart Grid 4 (3) (2013) 1361–1370.

[32] J. Moshövel, K.-P. Kairies, D. Magnor, M. Leuthold, M. Bost, S. Gährs, E. Szczechowicz, M. Cramer, D. U. Sauer, Analysis of the maximal possible grid relief from PV-peak-power impacts by using storage systems for increased self-consumption, Applied Energy 137 (2015) 567–575.

[33] E. L. Ratnam, S. R. Weller, C. M. Kellett, Scheduling residential battery storage with solar PV: Assessing the benefits of net metering, Applied Energy 155 (2015) 881 – 891.

[34] K. Tanaka, K. Uchida, K. Ogimi, T. Goya, A. Yona, T. Senjyu, T. Funabashi, C.-H. Kim, Optimal operation by controllable loads based on smart grid topology considering insolation forecasted error, IEEE Trans. Smart Grid 2 (3) (2011) 438–444.

[35] H. Kanchev, D. Lu, F. Colas, V. Lazarov, B. Francois, Energy management and operational planning of a microgrid with a PV-based active generator for smart grid applications, IEEE Trans. Ind. Electron. 58 (10) (2011) 4583–4592.

[36] Y. Ru, J. Kleissl, S. Martínez, Storage size determination for grid-connected photovoltaic systems, IEEE Trans. Sustain. Energy 4 (1) (2013) 68 –81.

[37] Y. Ru, J. Kleissl, S. Martínez, Exact sizing of battery capacity for photovoltaic systems, European Journal of Control 20 (1) (2014) 24–37.

[38] E. L. Ratnam, S. R. Weller, C. M. Kellett, An optimization-based approach to scheduling residential battery storage with solar PV: Assessing customer benefit, Renewable Energy 75 (2015) 123 – 134.

[39] A. Nottrott, J. Kleissl, B. Washom, Energy dispatch schedule optimization and cost benefit analysis for grid-connected, photovoltaic-battery storage systems, Renewable Energy 55 (2013) 230 – 240.

[40] J. Swigart, S. Lall, Optimal controller synthesis for decentralized systems over graphs via spectral factorization, IEEE Trans. Autom. Control 59 (9) (2014) 2311–2323.

[41] E. L. Ratnam, S. R. Weller, C. M. Kellett, A. Murray, Residential load and rooftop PV generation: An Australian distribution network dataset, Int. J. Sustain. Energ. Now available online.

[42] N. R. Darghouth, G. Barbose, R. H. Wiser, Customer-economics of residential photovoltaic systems (Part 1): The impact of high renewable energy penetrations on electricity bill savings with net metering, Energy Policy 67 (2014) 290 – 300.

[43] K. Cavanagh, J. K. Ward, S. Behrens, A. I. Bhatt, E. L. Ratnam, E. Oliver, J. Hayward, Electrical Energy Storage: Technology Overview and Applications, CSIRO, Australia. Report No. EP154168 (2015).

[44] Ausgrid, Solar home electricity data [Online], Available: http://www.ausgrid.com.au/Common/About-us/Corporate-information/Data-to-share/Data-to-share/Solar-household-data.aspx (Accessed 28 January 2015).

6

A case study incorporating a GridLAB-D distribution model

In Part 3 our overarching objective is to improve the balance in managing bi-directional power flows in a distribution network with increases in operational savings that accrue to customers. Emphasis is given to approaches requiring only modest sensing and communication infrastructure. In all cases, operational savings that accrue to customers are considered in the context of the financial policy of net metering, as defined in Part 2.

In Chapter 5 the problem formulations were designed to balance the management of bi-directional power flows in a distribution grid with increases in operational savings that accrued to residential customers. We presented two approaches to coordinating residential battery storage, and showed a centralized approach provided improved performance, and offered a more equitable distribution in operational savings that accrued to customers.

In Chapter 6 we address the problem of managing bi-directional power flows in a distribution network, with a greater focus on influencing supply voltages in a low voltage network. We propose two receding horizon optimization-based algorithms for coordinating residential battery storage, the first of which is a Distributed-Receding Horizon Optimization (D-RHO) algorithm, and second an Adaptive-Receding Horizon Optimization (A-RHO) algorithm. Both algorithms incorporate one or more of the objective functions presented in Chapter 5, and are applied to a GridLAB-D model of an Australian distribution region located in the suburb of Elermore Vale, NSW.

Receding horizon optimization-based approaches to managing supply voltages and power flows in a distribution grid with battery storage co-located with solar PV

Elizabeth L. Ratnam* and Steven R. Weller

School of Electrical Engineering and Computer Science, University of Newcastle, University Drive, Callaghan NSW 2308, Australia

Abstract

In this paper we propose two optimization-based algorithms for coordinating residential battery storage to manage bi-directional power flows and supply voltages in a distribution grid. Our objectives are threefold: (1) to reduce reverse power flow creating significant voltage rise, (2) to reduce peak loads approaching a network capacity, and (3) to improve voltages delivered to residential customers with solar PV. To achieve our objectives we present a Distributed-Receding Horizon Optimization (D-RHO) algorithm, where charge and discharge rates of residential battery storage are coordinated to directly influence power flows along a distribution feeder. We also present an Adaptive-Receding Horizon Optimization (A-RHO) algorithm, where charge and discharge rates of residential battery storage are coordinated to more directly manage supply voltages. To assess the distributor benefit, both RHO-based algorithms are applied to a publicly available model of an Australian distribution region located in Elermore Vale. The results of this case study confirm that the A-RHO algorithm improves supply voltages in a low voltage network, and that the D-RHO algorithm offers a peak load reduction of 32% along the Elermore Vale medium voltage feeder.

Keywords: solar photovoltaics, residential battery, quadratic program, distribution grid, supply voltages.

1. Introduction

The recent rapid uptake of grid-connected solar photovoltaics (PV) in many countries has led to concerns regarding the management of bi-directional power flows in distribution networks previously designed for one-way power flow [1, 2]. Distributors are typically concerned with power flows approaching a network capacity and reverse power flows inducing voltage rise, especially when either situation leads to substantial network investment [3, 4].

*Corresponding author: Elizabeth L. Ratnam, Tel.: +61 2 492 16026, Fax: +61 2 492 16993.
Email address: elizabeth.ratnam@ieee.org and Steven.Weller@newcastle.edu.au (Elizabeth L. Ratnam* and Steven R. Weller)

Demand-side approaches to managing distribution power flows potentially defer (or possibly avoid) significant costs associated with distribution reinforcement [5–20]. The demand-side approach in [5] curbs PV generation in response to significant voltage rise in the distribution grid. The demand-side approaches in [6, 7] control a PV inverter that adjusts the real and reactive power supplied to, or absorbed by, the distribution grid. Other demand-side approaches include direct load control [8–13], and price-responsive load control (e.g., time-of-use pricing) [14–16]. Several authors have also investigated coordinated approaches to charge and discharge battery storage with the objective of managing bi-directional power flows in a distribution network [17–20].

In this paper we present two coordinated demand-side approaches to managing bi-directional power flows within a distribution region. In the first approach, referred to as Distributed-Receding Horizon Optimization (D-RHO), charge and discharge rates of residential battery storage are coordinated to reduce peak loads and reverse power flow in the upstream distribution grid. In the second approach, referred to as Adaptive-Receding Horizon Optimization (A-RHO), charge and discharge rates of residential battery storage are coordinated to more directly manage supply voltages while influencing (to a lesser extent) power flows in the upstream distribution grid. In each approach a customer solves an optimization problem subject to current and future constraints, with each problem formulated as a quadratic program (QP).

To implement D-RHO an electrical distributor is required to broadcast to Advanced Metering Infrastructure (AMI) forecasts of aggregate day-ahead power flows, day-ahead electricity prices, and a design parameter in the form of a scalar weight. Furthermore, each customer requires an energy management system with an AMI interface that is capable of executing optimization-based algorithms, applying battery charge/discharge rates, and updating the battery state of charge. The A-RHO approach extends the system architecture required for D-RHO, wherein the energy management system of each customer requires additional functionality. Specifically, to implement A-RHO the energy management system of each customer must also: (1) forecast day-ahead residential load and PV generation; (2) retrieve weights from a look-up table; and (3) select an optimization-based algorithm to run.

Other approaches to improve supply voltages in a distribution network are considered in [21–23], and include charging a residential battery co-located with solar PV when a predetermined threshold for PV generation is exceeded [21]. In [22, 23] a main control center coordinates battery charge/discharge rates, where the main control center in Lee et al. [22] collects supply voltages, supply frequencies, and the state of charge of each battery. With the exception of [23], each of these approaches does not incorporate increases in operational savings that accrue to customers with battery storage as defined in previous work [24]. In this paper we incorporate operational savings into the objective functions of each algorithm, thereby extending our previous work in [23, 24]. In particular, we extend previous work by employing Receding Horizon Optimization in both algorithms. Also, we apply the D-RHO and A-RHO algorithms to a GridLAB-D model of an Australian distribution region, and consider the case where approximately 50% of customers have solar PV systems.

This paper is organized as follows. In Section 2 we define a single residential system that we incorporate into a publicly available model of an Australian distribution region. In Section 3 we propose two optimization-based approaches to manage power and voltage profiles in a distribution network. In Section 4 we present simulation results that are based on a GridLAB-D model of an Australian distribution feeder located in Elermore Vale, NSW.

Notation

Let $\mathbb{R}^s$ denote s-dimensional vectors of real numbers and $\mathbb{R}^s_{\geq 0}$ s-dimensional vectors with all non-negative components where, as usual, $\mathbb{R}^1 = \mathbb{R}$. $\mathbf{I}$ denotes the s-by-s identity matrix and $\mathbb{1} \in \mathbb{R}^s_{\geq 0}$ denotes the all-1s column vector of length s. $\mathbf{0}$ denotes an all-zero matrix, or an all-zero column vector, where the context will make clear the dimension intended, and $\mathbf{T} = [t_{ij}]$ denotes the s-by-s matrix satisfying $t_{ij} = 1$ for $i \geq j$ and $t_{ij} = 0$ elsewhere.

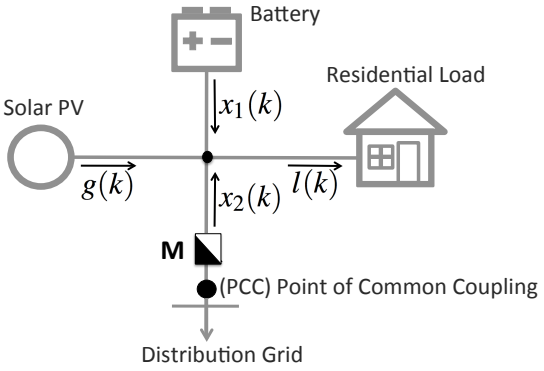

Figure 1: Residential system illustrating the direction of positive power flows and the bi-directional meter **M**. Arrows associated with $g(k)$, $l(k)$, $x_1(k)$ and $x_2(k)$ illustrate the direction of positive power flow. Meter **M** measures and records (in kW) power flow $x_2(k)$, where k is a time index.

2. Preliminaries

In Section 2.1 we define a single residential system with solar PV co-located with battery storage as depicted in Fig. 1. We incorporate this residential system into a larger distribution model which we introduce in Section 2.2. In particular, our residential system replaces the assumed topology behind the Point of Common Coupling (PCC) for approximately 50% of customers in the distribution model. Our forecasting methodology for residential load and PV generation is presented in Section 2.3.

2.1. Residential system

Before introducing a publicly available distribution model we start with defining a single residential system. Our simple definition of a residential system is consistent with previous work [24], and is included in this paper to im-

prove clarity of the forecasting methodology presented in Section 2.3, and the problem formulation presented in Section 3.

Fig. 1 illustrates the assumed topology of the residential system under consideration. We denote by $x_2(k)$ the measured power flow (in kW) over the k^{th} interval of length Δ. By convention measured power flows from (to) the grid to (from) the residential system over the period $((k-1)\Delta, k\Delta)$ are represented by $x_2(k) > 0$ $(x_2(k) < 0)$ for all $k \in \{1,\ldots,s\}$. To represent all measured power flows over a time window $[0,T]$, where s is the number of time intervals of length Δ, and $T = s\Delta$ (in hours) is the time window of interest, we define the *grid profile* by $x_2 := [x_2(1),\ldots,x_2(s)]^T \in \mathbb{R}^s$.

In this paper we consider a financial policy of *net metering*, where each resident is billed at the same rate as they are compensated for excess generation as defined in earlier work [24]. To represent daily variations in electricity prices we define a *net metering profile* by $\eta := [\eta(1),\ldots,\eta(s)]^T \in \mathbb{R}^s_{\geq 0}$, where $\eta(k)$ is the k^{th} entry in the net metering profile representing an electricity price (in \$/kWh) over the period $((k-1)\Delta, k\Delta)$. In this paper we generally consider $T = 24$ hours and $\Delta = 1/2$ hour, which implies $s = 48$. Other choices are straightforward, subject only to commensurability of T, Δ, and s.

The remaining power flows represented in Fig. 1 are defined as follows. We represent the average power delivered to the residential load (in kW) over the period $((k-1)\Delta, k\Delta)$ by $l(k)$ for all $k \in \{1,\ldots,s\}$, and define the *load profile* over $[0,T]$ as $l := [l(1),\ldots,l(s)]^T \in \mathbb{R}^s_{\geq 0}$. Likewise we represent the average PV generation (kW) over the period $((k-1)\Delta, k\Delta)$ by $g(k)$ for all $k \in \{1,\ldots,s\}$, and define the *generation profile* over $[0,T]$ as $g := [g(1),\ldots,g(s)]^T \in \mathbb{R}^s_{\geq 0}$.

We represent the average power (kW) delivered from (or to) the battery over the period $((k-1)\Delta, k\Delta)$ by $x_1(k) > 0$ (or $x_1(k) < 0$) for all $k \in \{1,\ldots,s\}$, and define the *battery profile* over $[0,T]$ as $x_1 := [x_1(1),\ldots,x_1(s)]^T \in \mathbb{R}^s$. By convention we represent charging (discharging) of the battery by $x_1(k) < 0$ $(x_1(k) > 0)$.

From the configuration of the residential energy system in Fig. 1, we observe that the power balance equation

$$x_2(k) = l(k) - g(k) - x_1(k) \tag{1}$$

must hold for all $k \in \{1,\ldots,s\}$.

The *operational savings* (in \$/day) allow us to quantify the effectiveness of scheduling a battery. We define the operational savings, ψ, as the difference between the energy bills obtained with and without a battery. In previous work [24] we show the operational savings may also be expressed in terms of the battery profile x_1 as shown in the following Lemma.

Lemma 1 ([24, Lemma 1])**.** *Consider a residential energy network employing a financial policy of net metering, where $\eta \in \mathbb{R}^s_{\geq 0}$ is assumed fixed and known. Let $x_1 \in \mathbb{R}^s$ represent the battery profile over $[0,T]$ where $T = s\Delta$. Then*

the operational savings are given by $\psi = \Delta\eta^T x_1$.

Remark 1. *If there exists* $a \in \mathbb{R}_{>0}$ *so that* $\eta = a\mathbb{1}$*, then the operational savings are* $\psi = \$0$ *[25, Lemma 2].*

In this paper we assume each residential system under consideration is sufficiently rated. That is, excluding the battery constraints, we assume there are no additional residential constraints for any proposed battery schedule. For example, we assume a conductor extending from a point of common coupling to a residential PV inverter imposes no thermal limit.

To capture the limited "charging/discharging power" of the battery, we include the battery profile constraint $\underline{B}\mathbb{1} \leq x_1 \leq \overline{B}\mathbb{1}$, where $\underline{B} \in \mathbb{R}_{\leq 0}$ and $\overline{B} \in \mathbb{R}_{\geq 0}$. Given the battery profile x_1, the *state of charge* of the battery (in kWh) at time $k\Delta$ is denoted by $\chi(k)$, where

$$\chi(k) := \chi(0) - \sum_{j=1}^{k} x_1(j)\Delta \qquad \text{for all } k \in \{1,\ldots,s\},$$

and $\chi(0)$ denotes the initial state of charge of the battery. We represent the battery capacity (in kWh) by $C \in \mathbb{R}_{\geq 0}$, the *state of charge profile* by $\chi := [\chi(0),\ldots,\chi(s)]^T \in \mathbb{R}^{s+1}$, and we represent the state of charge profile constraint by $\mathbf{0} \leq \chi \leq C\begin{bmatrix}1 & \mathbb{1}\end{bmatrix}^T$. That is, we employ a deliberately simplified battery model to assess the distributor benefits of coordinating residential battery schedules, which may be extended for more specific battery technologies as presented in [26, 27].

In order to avoid an energy-shifting bias in our results, we include the constraint $\chi(s) = \chi(0)$, where $\chi(s)$ is the final state of charge at time $s\Delta$ [25]. To simplify the notation in what follows we define $\underline{\mathbf{C}} := (\chi(0)/\Delta)\mathbb{1}$, and $\overline{\mathbf{C}} := (1/\Delta)(C-\chi(0))\mathbb{1}$, where the initial state of charge satisfies $0 \leq \chi(0) \leq C$. Further, let $A_1 := \begin{bmatrix}\mathbf{I} & -\mathbf{I} & \mathbf{T} & -\mathbf{T}\end{bmatrix}^T \in \mathbb{R}^{4s\times s}$, and let $b_1 := \begin{bmatrix}\overline{B}\mathbb{1}^T & \underline{B}\mathbb{1}^T & \underline{\mathbf{C}}^T & \overline{\mathbf{C}}^T\end{bmatrix}^T \in \mathbb{R}^{4s}$. Thus, we succinctly write the battery constraints as

$$A_1 x_1 \leq b_1, \tag{2}$$

$$\mathbb{1}^T x_1 = 0. \tag{3}$$

2.2. Distribution network

Fig. 2 illustrates key aspects of a GridLAB-D model of the Elermore Vale distribution region located in NSW, Australia [28]. The Elermore Vale GridLAB-D model is publicly available and was developed as part of the federally funded Australian Smart Grid Smart City (SGSC) program. The vast majority of customers in the Elermore Vale distribution model do not have a PV system, and no existing customers in the Elermore Vale model have a battery storage system. To investigate the impacts of significant reverse power flow in the Elermore Vale distribution region, we modify the existing GridLAB-D model. For approximately 50% of customers in the Elermore Vale model the existing topology

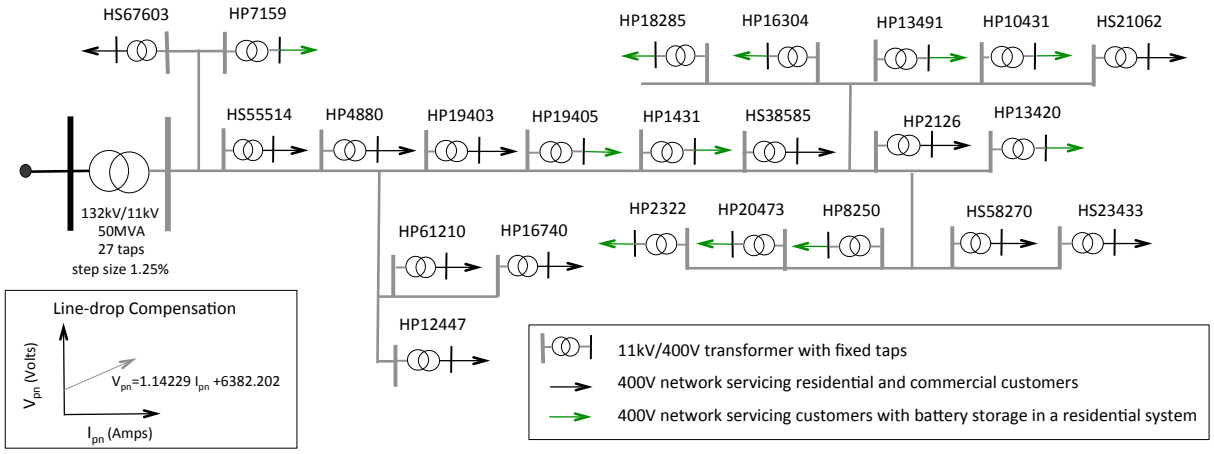

Figure 2: A visual representation of the GridLAB-D model for Elermore Vale developed during the Australian SGSC program. Each of 17 pole mounted 11kV/400V distribution transformers include the prefix *HP* in their associated ID, and each of the remaining 6 ground-type distribution transformers include the prefix *HS* in their associated ID. From 11 pole mounted distribution transformers the associated 400V network is highlighted to indicate (all) downstream customers have a residential system as defined in Section 2.1.

behind the PCC is replaced by the residential system defined in Section 2.1. Each customer represented by a residential system is connected to the 400V network highlighted in Fig. 2, where the majority of residential systems have a single phase connection. This modified GridLAB-D model forms the bases of our case study in Section 4.

Before describing the publicly available Elermore Vale distribution model we introduce typical operational requirements for Australian distribution operators. When power flows within a distribution network approach thermal limits of electrical infrastructure, or voltages fall outside set tolerances, a distribution operator typically incurs remediation costs. In the eastern states of Australia distribution voltages generally fall into one of two categories, Low Voltage (LV) defined by a nominal phase-to-neutral 230V with a tolerance of $+10\%/-6\%$, and Medium Voltage (MV) defined by a range of phase-to-phase values from a nominal 1kV to a nominal 22kV [29].

In this paper our primary interest is maintaining voltages within a $+10\%/-6\%$ tolerance in the LV distribution network while reducing peak loads approaching a thermal capacity in the upstream MV feeder. However, this voltage condition and/or a thermal capacity limit is not essential to applying our methodology. For example, we may simply consider bi-directional power flows in a distribution network, where the distribution capacity, or infrastructure limits, and voltage tolerances are unknown.

To illustrate an application for our methodology we modify a publicly available GridLAB-D model of an urban distribution region located in the suburb of Elermore Vale. The publicly available Elermore Vale GridLAB-D model includes

- an On-Line Tap Changing (OLTC) Delta—grounded Wye 50 MVA 132kV/11kV transformer with an impedance of $Z = 0.0075 + j0.358$ and 27 taps with step sizes of 1.25%,

- a line drop compensation scheme that lowers or raises the taps of the 132kV/11kV transformer to improve the voltage delivered to downstream customers,
- a (single) three phase radial MV feeder that spans 31.68 km and is operated at a nominal 11kV,
- 23 fixed-tap Delta—grounded Wye 11kV/400V distribution transformers where 17 are classified as pole mounted and the remainder are classified as a ground-type (or pad-mount),
- for each 11kV/400V transformer the associated downstream three phase 400V network,
- per unit length impedances for each conductor (physical data that includes conductor spacing and the geometric mean radius of each conductor is also provided),
- the PCC for each of 1785 customers, of which 1051 customers are identified as residential households, 36 customers are identified as business and the remaining 698 customers are left unclassified,[1]
- simulated *average load profiles* for each of the 1785 existing customers, and
- simulated PV generation for each of 164 existing customers.

In the publicly available Elermore Vale GridLAB-D model an average load profile for each existing customer is simulated. The primary objective for simulating average load profiles is to maintain privacy for each customer while improving the accuracy of simulated voltages and power flows along the MV feeder. A consequence of this primary objective is limited diversity in customer load profiles within the Elermore Vale model. Further details on the approach to determine average load profiles for each customer in the Elermore Vale model is available on the Australian Smart Grid Smart City website [28].

In this paper we consider the impacts of significant residential PV penetration by representing approximately 50% of LV customers supplied by the Elermore Vale feeder with a residential system depicted in Fig. 1. Specifically, the phase-to-phase 400V network that connects each of $N = 845$ customers to one of the 11 pole-mounted distribution transformers is highlighted in Fig. 2. Each customer supplied by one of the 11 pole-mounted transformers is denoted by $n \in \{1,\dots,N\}$, and is referred to as an *aggregate member*. The existing topology behind the PCC for each aggregate member is replaced with a residential system as defined in Section 2.1. In the Elermore Vale model the assumed topology behind the PCC of the remaining 940 (commercial and residential) customers connected to one of the other twelve 11kV/400V transformers remains unmodified. Consequently, the Elermore Vale distribution model considered in the sequel depicts the scenario where approximately 50% of residential customers have solar PV co-located with battery storage. Recall, the vast majority of existing customers in the Elermore Vale distribution model

[1]The suburb of Elermore Vale has over 2000 residential households and a relatively small number of businesses [30]. Thus, we assume the majority of unclassified customers are residential.

did not previously have a PV system, and no customer in the Elermore Vale model previously had a battery storage system.

For each aggregate member we formulate definitions of *aggregate demand* and *aggregate grid profiles* over $[0,T]$ by

$$D := \frac{1}{N}\sum_{n=1}^{N} l^{(n)} - g^{(n)}, \qquad X_2 := \frac{1}{N}\sum_{n=1}^{N} x_2^{(n)}, \tag{4}$$

where $l^{(n)}$, $g^{(n)}$, $x_2^{(n)}$ denote the load, generation and grid profiles over $[0,T]$, respectively, for aggregate member n. Note that $D, X_2 \in \mathbb{R}^s$.

To manage peak loads and associated voltage dips together with reverse power flow inducing significant voltage rise at the PCC of each aggregate member we consider distributed approaches to charge/discharge residential battery storage. For simplicity in assessing distributed approaches, we assume each inverter in a residential system is 100% efficient and operates in a manner that ensures unity power factor at a residential point of common coupling.

2.3. Forecasting methodology

Before introducing distributed approaches to charge/discharge residential battery storage we define our forecasting methodology for residential and aggregate demand. To emulate generation forecasts for each aggregate member we use the methodology proposed in [31]. That is, we emulate the generation forecast for aggregate member n by applying a moving average window to a known and fixed generation profile $g^{(n)}$ as follows:

$$\hat{g}^{(n)}(k) = \frac{1}{3}(g^{(n)}(k-1) + g^{(n)}(k) + g^{(n)}(k+1)),$$

for all $k \in \{2,3,\ldots,s-1\}$, and we let $\hat{g}^{(n)}(k) = g^{(n)}(k)$ for $k \in \{1,s\}$. We define the *generation forecast* over $[0,T]$ by $\hat{g}^{(n)} := [\hat{g}^{(n)}(1),\ldots,\hat{g}^{(n)}(s)]^T \in \mathbb{R}^s_{\geq 0}$.

Likewise, we emulate the day-ahead load forecast for each aggregate member using the methodology proposed in [31]. To emulate the *load forecast* for aggregate member n, denoted by $\hat{l}^{(n)} \in \mathbb{R}^s_{\geq 0}$, we use a known and fixed load profile $l^{(n)}$ and include uncertainty in the forecast as follows

$$\hat{l}^{(n)}(k) := l^{(n)}(k) + \delta(k)$$

for all $k \in \{1,\ldots,s\}$, where $\delta(k)$ is a random number generated from a normal distribution of mean zero with a standard deviation of 20% of $l^{(n)}(k)$. We define the load forecast over $[0,T]$ by $\hat{l}^{(n)} := [\hat{l}^{(n)}(1),\ldots,\hat{l}^{(n)}(s)]^T \in \mathbb{R}^s_{\geq 0}$.

We denote a *grid forecast* for aggregate member n by $\hat{x}_2^{(n)}$, where the day-ahead power balance equation for the residential energy system in Fig. 1 is

$$\hat{x}_2^{(n)}(k) = \hat{l}^{(n)}(k) - \hat{g}^{(n)}(k) - x_1^{(n)}(k), \tag{5}$$

which must hold for all $k \in \{1,\ldots,s\}$. We define the grid forecast over $[0,T]$ by $\hat{x}_2^{(n)} := [\hat{x}_2^{(n)}(1),\ldots,\hat{x}_2^{(n)}(s)]^T \in \mathbb{R}^s$.

Similar to the approach described in [23], we emulate a *demand forecast* over $[0,T]$ as follows:

$$\widehat{D} := \frac{1}{N}\sum_{n=1}^{N} \hat{l}^{(n)} - \hat{g}^{(n)}, \tag{6}$$

where $\hat{l}^{(n)}$ is an emulated forecast of a load profile and $\hat{g}^{(n)}$ is an emulated forecast of a generation profile for aggregate member n over a time window of interest $[0,T]$. We denote the *aggregate forecast* for member n by $\widehat{X}_2^{(n)}$, where the day-ahead power balance equation

$$\widehat{X}_2^{(n)}(k) = \widehat{D}(k) - x_1^{(n)}(k) \tag{7}$$

holds for all $k \in \{1,\ldots,s\}$. We define the aggregate forecast over $[0,T]$ by $\widehat{X}_2 := [\widehat{X}_2(1),\ldots,\widehat{X}_2(s)]^T \in \mathbb{R}^s$.

In the simulations that follow forecasts of load $\hat{l}^{(n)}$, PV generation $\hat{g}^{(n)}$, and demand $\widehat{D}$ for aggregate member n connected to a LV network in a distribution region are emulated. Indeed future work will replace emulated forecasts with actual forecasts that predict load and PV generation based on past/real-time measurements.

3. Problem formulation

In this section we present two approaches to coordinating battery charge/discharge rates of each aggregate member, where each member is represented by a residential system as depicted in Fig 1. In each approach we assume a demand forecast $\widehat{D}$ and a net metering profile η are made available by a distributor. To simulate a demand forecasts over a time window of interest $[0,T]$ we use the methodology presented in Section 2.3.

The first approach to coordinating battery charge/discharge rates of each aggregate member is presented in Section 3.1. In this first approach increases in operational savings that accrue to customers are balanced with managing power flows along a MV feeder. In the second approach presented in Section 3.2 voltages from the PCC of each aggregate member are additionally incorporated into the problem formulation. Our objectives in each approach are threefold: (1) to reduce reverse power flow creating significant voltage rise, (2) to reduce peak loads approaching a capacity constraint

along a MV feeder, and (3) improve voltages at the PCC of each aggregate member. In defining each approach we introduce notation similar to that in [32].

3.1. Distributed-Receding Horizon Optimization (D-RHO)

In the first approach, referred to as *D-RHO*, a distributor sends each aggregate member *exogenous inputs* [33] that include a day-ahead demand forecast $\widehat{D}$, a day-ahead net metering profile η, and a weight w. All exogenous inputs are updated by a distributor on time-step j of interval length Δ. To implement D-RHO at each time step j each aggregate member

1. solves an optimization problem over the time window $[j\Delta,(j+s)\Delta]$, which is subject to constraints,
2. yields a sequence of control actions $\{[x_1[1|j],\ldots,x_1[s|j]\}$, where the notation $[k|j]$ denotes prediction time-step k relative to actual time-step j as in [32],
3. applies a battery charge/discharge rate obtained from the first instant of the control sequence $x_1(j) := x_1[1|j]$,
4. estimates the battery state of charge $\chi^{(n)}[1|j] = \chi^{(n)}[0|j] + \Delta x_1^{(n)}[1|j]$,
5. updates the initial state of charge of the battery $\chi^{(n)}(0) = \chi^{(n)}[1|j]$ in preparation for the next time step,
6. fetches updates for exogenous inputs $\widehat{D}$, w, and η,
7. sets $j = j+1$ and repeats step 1. Note that the constraint of zero daily change in the state of charge (i.e., $\chi(s) = \chi(0)$) is not enforced over this process.

For the optimization problem considered at Step 1 the overarching objective function is to maximize

$$\sum_{k=1}^{s} w\Delta\eta[k|j]x_1^{(n)}[k|j] - \eta[k|j]\left(\widehat{X}_2^{(n)}[k|j]\right)^2 \tag{8}$$

for all $k \in \{1,\ldots,s\}$ relative to each time step j. On each time step j a weight w is specified by a distributor, $\eta[k|j]$ is the k^{th} entry in the day-ahead net metering profile η in \$/kWh, $x_1^{(n)}[k|j]$ is the k^{th} entry in the battery profile of aggregate member n, and $\widehat{X}_2^{(n)}[k|j]$ represent the k^{th} entry in the aggregate forecast (in kW) of aggregate member n (cf., equation (7)).

Similar to the objective function for central QP energy-shifting defined in [23] the D-RHO objective function in (8) consists of two terms. The first term is weighted by w and maximizes the *operational savings of aggregate member n*, denoted by ψ and defined in Lemma 1. The second term in (8) reduces aggregate reverse power flow that potentially arises during the peak pricing period when maximizing the operational savings ψ of each aggregate member [24].

For a known and specified weight w, financial policy η, and aggregate demand forecast $\widehat{D}$, the following Lemma expresses the constrained objective function in (8) as a quadratic program (QP). That is, the optimization problem to be solved during step 1 is formulated as a QP for which there are a number of market-ready solvers available.

Lemma 2. *The maximization of expression* (8)*, subject to battery constraints* (2)–(3) *and the power balance equation* (7)*, can be written as the following quadratic program:*

$$\max_{x\in\mathbb{R}^{2s}} \quad x^T Hx + c^T x \tag{9}$$

$$\textit{such that} \quad A_1 x \leq b_1, \quad A_2 x = b_2, \tag{10}$$

where A_1 and b_1 are as in (2) *and $x \in \mathbb{R}^{2s}$, $H \in \mathbb{R}^{2s\times 2s}$, $\mathbf{H} \in \mathbb{R}^{s\times s}$, $c \in \mathbb{R}^{2s}$, $w \in \mathbb{R}$, $A_2 \in \mathbb{R}^{(s+1)\times 2s}$, $b_2 \in \mathbb{R}^{s+1}$, and*

$$\begin{aligned} x &:= \begin{bmatrix} x_1^{(n)T} & \widehat{X}_2^{(n)T} \end{bmatrix}^T \\ H &:= \begin{bmatrix} \mathbf{0} & \mathbf{0} \\ \mathbf{0} & -\mathbf{H} \end{bmatrix} \qquad \mathbf{H} := \operatorname{diag}(\eta(1),\ldots,\eta(s)) \\ c &:= w\Delta \begin{bmatrix} \eta \\ \mathbf{0} \end{bmatrix} \quad A_2 := \begin{bmatrix} \mathbb{1}^T & \mathbf{0}^T \\ \mathbf{I} & \mathbf{I} \end{bmatrix} \quad b_2 := \begin{bmatrix} 0 \\ \widehat{D} \end{bmatrix}. \end{aligned}$$

Proof. The result follows directly from Lemma 1 given the battery constraints (2)–(3) defined in Section 2.1, a financial policy of net metering, and the power balance equation (1). ■

We will refer to the process of aggregate member n implementing a battery charge/discharge rate $x_1^{(n)}(1|j)$ at each time step j obtained by solving (9) subject to constraints (10) as *D-RHO energy-shifting*.

3.2. Adaptive- Receding Horizon Optimization (A-RHO)

The system architecture for the A-RHO algorithm for aggregate member n is depicted in Fig. 3. As illustrated in Fig. 3 exogenous inputs include a day-ahead demand forecast $\widehat{D}$, a day-ahead net metering profile η, and a weight w, which are provided by a distributor. Further, day-ahead load and generation forecasts $\hat{l}^{(n)}$, $\hat{g}^{(n)}$, and three weights w_1, w_2, w_3, are additional exogenous inputs that are specified by aggregate member n. Sensor outputs relative to time step j include the voltage at the PCC $V^{(n)}(j)$, and the battery charge/discharge power $x_1^{(n)}(j)$. The feedback loop that incorporates the voltage measurements at the PCC, a latch with two output states $L \in \{0,1\}$, and time-of-day as an input, determines the objective function to apply in the A-RHO problem. Specifically, we propose two objective functions for the A-RHO algorithm: one that is defined by (8), and another that more directly influences voltages at the PCC of each aggregate member.

To implement A-RHO the latch output $L = 1$ is held until midnight on a day when voltages at a PCC exceed a maximum or fall below a minimum threshold. The maximum and minimum voltage thresholds are denoted by $\overline{V}$ and

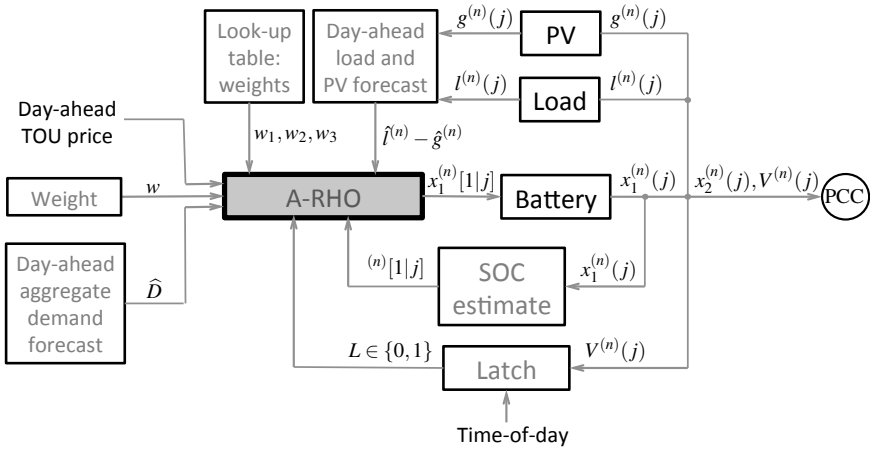

Figure 3: System architecture for A-RHO algorithm for aggregate member n. For the purpose of simplicity, in this paper real-time day-ahead load, generation and demand forecasts $\hat{l}^{(n)}$, $\hat{g}^{(n)}$, $\widehat{D}$, for aggregate member n are emulated as described in Section 2.3. For the grey box denoted A-RHO, one of two QP-based algorithms is solved at each time step j to yeild the battery charge/discharge rate $x_1^{(n)}[1|j]$.

$\underline{V}$, respectively. Latch output $L = 1$ is released at midnight, although we envision the latch could be released at any time when voltages are consistently within set tolerances. For example, the latch may instead be released at 2am the following day when reverse power flow creating voltage rise is not typically expected. At all other times the latch output is $L = 0$.

For a latch output of $L = 0$ the aggregate member solves an optimization problem where the objective function is defined by (8). Otherwise, for a latch output $L = 1$ the aggregate member solves an optimization problem where the overarching objective function is to maximize

$$\sum_{k=1}^{s} w_1 \Delta \eta[k|j] x_1^{(n)}[k|j] - w_2 \eta[k|j](\hat{x}_2^{(n)}[k|j])^2 - w_3(\hat{x}_2^{(n)}[k|j])^2, \tag{11}$$

for all $k \in \{1,\ldots,s\}$ relative to time step j. The three weights in (11) are denoted by w_1, w_2, and w_3, and are applied to each term in the objective function. Recall n denotes the aggregate member, $\eta[k|j]$ denotes the net metering electricity price in \$/kWh over the k^{th} interval of length Δ, $\Delta\eta[k|j]x_1^{(n)}[k|j])$ denotes the operational saving over the k^{th} interval of length Δ (cf. Lemma 1), and $\hat{x}_2^{(n)}[k|j]$ represents a forecast power flow (in kW) for aggregate member n as in (5).

Similar to the objective function for local QP energy-shifting defined in [23], the first term in (11) maximizes the operational savings that accrue to each aggregate member as done in [24], and is weighted by w_1. The second term reduces reverse power flow that potentially arises during the peak pricing period when each aggregate member maximizes their operational savings, and is weighted by w_2. The third term reduces peak power flows at all times, and is weighted by w_3. In [23] we investigated the significance of each term, by adjusting the assigned weight. In the simulations that follow supply voltages in the Elermore Vale model are influenced significantly when a preference for

reducing peak power flows at all times is incorporated through weight selection.

To implement A-RHO as depicted in Fig. 3, at each time step j each aggregate member

1. solves an optimization problem for the time window $[j\Delta,(j+s)\Delta]$, which is subject to current and future constraints, and the output state of latch L,
2. yields a sequence of optimal open-loop control actions $\{[x_1[1|j],\ldots,x_1[s|j]\}$, where the prediction time-step k is relative to actual time-step j as in [32],
3. applies a battery charge/discharge rate obtained from the first instant of the control sequence $x_1(j) := x_1[1|j]$,
4. estimates the battery state of charge $\chi^{(n)}[1|j] = \chi^{(n)}[0|j] + \Delta x_1^{(n)}[1|j]$,
5. updates the initial state of charge of the battery $\chi^{(n)}(0) = \chi^{(n)}[1|j]$ in preparation for the next time step,
6. fetches updates for exogenous inputs that include $\widehat{D}$, η, $\hat{l}^{(n)}$, $\hat{g}^{(n)}$, w, w_1, w_2, w_3,
7. sets $j = j+1$ and repeats step 1.

Given weights w_1, w_2, w_3, a financial policy η, and day-ahead load and generation forecasts $\hat{l}^{(n)}$, $\hat{g}^{(n)}$, for aggregate member n, the following Lemma expresses the constrained maximization in (11) as a quadratic program (QP). That is, the optimization problem to be solved during step 1, when latch output $L = 1$, is formulated as a QP.

Lemma 3. *The maximization of expression* (11)*, subject to battery constraints* (2)–(3)*, the power balance equation* (1)*, can be written as the following quadratic program:*

$$\max_{x\in\mathbb{R}^{2s}} \quad x^T H x + c^T x \tag{12}$$

$$\textit{such that} \quad A_1 x \le b_1, \quad A_2 x = b_2, \tag{13}$$

where A_1 and b_1 are as in (2) *and $x \in \mathbb{R}^{2s}$, $H \in \mathbb{R}^{2s\times 2s}$, $\mathbf{H} \in \mathbb{R}^{s\times s}$, $c \in \mathbb{R}^{2s}$, $w_1 \in \mathbb{R}$, $w_2 \in \mathbb{R}$, $w_3 \in \mathbb{R}$, $A_2 \in \mathbb{R}^{(s+1)\times 2s}$, $b_2 \in \mathbb{R}^{s+1}$, and*

$$\begin{aligned} x &:= \begin{bmatrix} x_1^{(n)T} & \hat{x}_2^{(n)T} \end{bmatrix}^T \\ H &:= \begin{bmatrix} \mathbf{0} & \mathbf{0} \\ \mathbf{0} & -(w_2\mathbf{H} + w_3\mathbf{I}) \end{bmatrix} \quad \mathbf{H} := \operatorname{diag}(\eta(1),\ldots,\eta(s)) \\ c &:= w_1\Delta \begin{bmatrix} \eta \\ \mathbf{0} \end{bmatrix} \quad A_2 := \begin{bmatrix} \mathbb{1}^T & \mathbf{0}^T \\ \mathbf{I} & \mathbf{I} \end{bmatrix} \quad b_2 := \begin{bmatrix} 0 \\ \hat{l}^{(n)} - \hat{g}^{(n)} \end{bmatrix}. \end{aligned}$$

Proof. The result follows directly from Lemma 1 given the battery constraints (2)–(3) defined in Section 2.1, a financial policy of net metering, and the power balance equation (1). ■

We use the term *A-RHO energy-shifting* to denote the process of aggregate member n implementing a battery charge/discharge rate $x_1^{(n)}[1|j]$ at each time step j obtained when latch output $L=0$ by solving (9) subject to constraints (10), or when latch output $L=1$ by solving (12) subject to constraints (13).

4. Assessing the benefits

In this section we present simulation results for the A-RHO and D-RHO algorithms, where our objectives are to (1) reduce reverse power flow creating significant voltage rise, (2) reduce peak loads along an 11kV feeder, and (3) improve voltages delivered to aggregate members. In all simulations we consider the Elermore Vale GridLAB-D model, where the model includes solar generation from approximately 50% of residential customers as described in Section 2.2. To assess the performance of the D-RHO algorithm we present power flows (in kW) directly from the 11kV bus depicted in Fig. 2. To compare the performance of each RHO-based algorithm we present supply voltage profiles for each of 37 aggregate members connected to pole mounted transformer HP1431. These 37 customers are carefully selected to benchmark improvements in supply voltages when each aggregate member implement a RHO-based algorithm. In all simulations the GridLAB-D model incorporates a line-drop compensation scheme that lowers and raises taps on the 132kV/11kV transformer to improve voltages delivered to downstream customers as depicted in Fig. 2.

Power flows representing load and PV generation for each of $N=845$ aggregate members, on each 30 minute interval for a five day period 7 January 2013 — 11 January 2013 are defined by real historical data as described in [34]. Specifically, to represent all $N=845$ customers with real historical data we duplicate a clean Ausgrid dataset no more then three times, where 291 customers make it into the clean Ausgrid dataset defined in [34]. With this real historical data we emulate forecast data for each aggregate member at each time step j via the methodology described in Section 2.3.

For each aggregate member connected to the Elermore Vale distribution region we fix $T=24$ hours, $\Delta=0.5$ hours, and $s=T/\Delta=48$. On 7 January 2013 the length-s net metering profile (in \$/kWh) is fixed as follows $\eta=[\eta(k),\ldots,\eta(s)]^T$, where $\eta(k)=0.03$ for $k\in\{1,\ldots,14,45,\ldots,48\}$, $\eta(k)=0.06$ for $k\in\{15,\ldots,28,41,\ldots,44\}$ and $\eta(k)=0.3$ for $k\in\{29,\ldots,40\}$. On each subsequent day the length-s net metering profile (in \$/kWh) remains as per 7 January 2013.

Initially, each aggregate member has a battery with state of charge $\chi(0)=5\,\text{kWh}$. At each time step j the initial state of charge for the battery of aggregate member n is updated. For the purpose of simplicity, all remaining residential battery constraints in (2)–(3) are fixed, where $C=10\,\text{kWh}$ and $\overline{B}=-\underline{B}=5\,\text{kW}$ for each aggregate member.

Given approximately 50% of residential customers have solar PV in the Elermore Vale model under consideration,

reverse power flow inducing voltage rise above 253V (i.e., 10% above nominal 230V) potentially arises. Recall from Section 2.2 a strict tolerance of $+10\%/-6\%$ from a nominal phase-to-neutral 230V must be maintained at the PCC of each customer at all times. In the simulations that follow we aim to reduce reverse power flow inducing voltage rise above 253V by selecting $w = 0$ when D-RHO energy-shifting, and $w = 0$, $w_1 = 0.1$, $w_2 = 1$, $w_3 = 25$ when A-RHO energy-shifting, where [23] provides further details on weight selection. To reduce voltage rise when A-RHO energy-shifting the design of voltage threshold $\overline{V}$ that triggers latch output $L = 1$ also requires careful consideration. In our simulations we consider a maximum voltage threshold below the 10% tolerance i.e., $\overline{V} = 1.08 \times 230V$, and a minimum threshold consistent with the -6% tolerance, i.e., $\underline{V} = 0.94 \times 230V$. Table 1 provides further details on the design parameters considered in this paper when D-RHO or A-RHO energy-shifting.

Table 1: Design parameters considered in Section 4

D-RHO algorithm	A-RHO algorithm
$w = 0$	$w = 0, w_1 = 0.1, w_2 = 1, w_3 = 25$ $\overline{V} = 248.4V, \quad \underline{V} = 216.2V$

To assess the distributor benefits of coordinating residential battery charge/discharge rates we define an important special case; that is, battery charge/discharge powers of each aggregate member satisfies $x_1^{(n)}(j) = 0$ for all $j \in \{1,2,\ldots,240\}$. Then, in this special case, the *aggregate grid profile* X_2 in (4) reduces to the *aggregate demand profile* D on each day. In the examples that follows we benchmark D-RHO and A-RHO against this special case where $X_2 = D$ on each day. In what follows we will refer this case as the *special baseline case*.

4.1. Power flows along the MV feeder

In this example we benchmark D-RHO energy-shifting against the special baseline case. To benchmark D-RHO energy-shifting we consider power flows along the Elermore Vale feeder directly from the 11kV bus (cf. Fig. 2). Further, we consider the number of tap operations arising from the line-drop compensation scheme incorporated into the GridLAB-D model depicted in Fig. 2.

In Fig. 4(a) we present power flows (in MW) directly from the 11kV bus arising from the special baseline case. In Fig. 4(b) we present power flows (in MW) directly from the 11kV bus arising when each aggregate member D-RHO energy-shifts. In Fig. 4(a) we observe a peak load of 6MW on 8 January 2013, which coincided with the fifth highest temperature on record at Observatory Hill in Sydney (located approximately 200km south of Elermore Vale) [35]. We also observe a minimum load of 0.308MW on 7 January 2013, a direct result of significant reverse power flow along the 11kV feeder. In Fig. 4(b) we observe a peak load of 4.07MW, which is 32% less then the peak load arising from the special baseline case. Also, bi-directional power flows along the 11kV feeder on 7 Jan 2013 result in a minimum

load of 0.846MW directly from the 11kV bus, an increase from the special baseline case. From Fig. 4 we infer peak loads and reverse power flows along the 11kV feeder are successfully reduced when D-RHO energy-shifting.

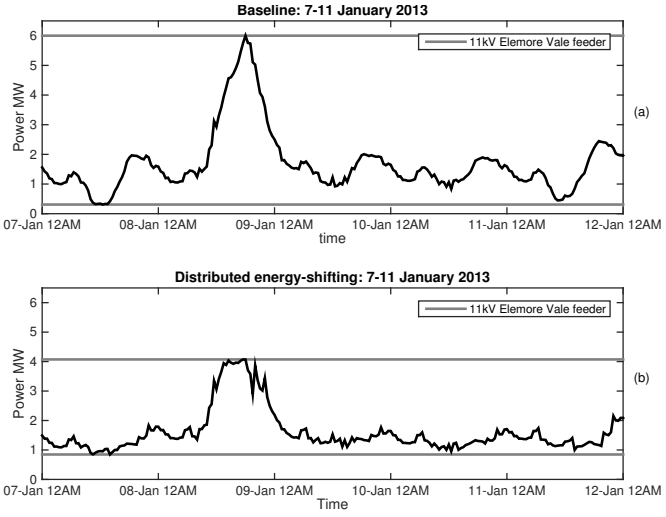

Figure 4: Power flows from the 11kV bus to the Elermore Vale feeder for (a) the special baseline case (b) when D-RHO energy-shifting.

The GridLAB-D model incorporates a line-drop compensation scheme that lowers and raises taps on the 132kV/11kV transformer to improve voltages delivered to downstream customers. Over the 5 day period considered in Fig. 4(a), 36 tap operations were recorded for the special baseline case. In contrast, when each aggregate member D-RHO energy-shifts over the 5 day period considered in Fig. 4(b), only 26 tap change operations were recorded. This reduction in tap operations when D-RHO energy-shifting potentially leads to lower maintenance costs for distribution operators. That is, maintenance costs for tap changers on 132kV/11kV transformers are typically commensurate with the number of tap operations.

4.2. Supply voltages in a LV network

In this example we consider three scenarios, and for each scenario voltage profiles at the PCC for a small subset of 37 aggregate members connected to pole transformer HP1431 are presented. Each aggregate member in this small subset is denoted by $n_{37} \in \{1,\ldots,37\}$, and is carefully selected to illustrate voltages outside set tolerances in a LV network are potentially remediated with a coordinated approach to charge and discharge residential battery storage. That is, the voltage profiles of the remaining 43 customers connected to pole transformer HP1431 are not considered, as voltage violations did not occur at the PCC of these customers during the simulations. Voltage rise that exceeds the upper tolerances of $+10\%$, and voltage dips that falls below the lower tolerances of -6%, are considered for remediation in what follows.

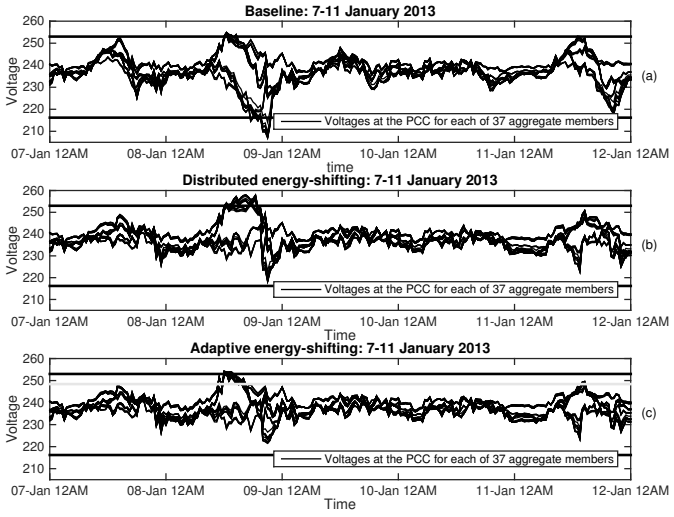

Figure 5: Voltage profiles at the PCC for each of 37 aggregate members downstream of pole mounted distribution transformer HP1431 for (a) the special baseline case, (b) when D-RHO energy-shifting, and (c) when A-RHO energy-shifting.

In the first scenario we consider the special baseline case for each aggregate member, with Fig. 5(a) depicting the resulting voltage profiles for each aggregate member in n_{37}. In the second scenario each aggregate member implements D-RHO energy-shifting, with Fig. 5(b) depicting the resulting voltage profiles for each aggregate member in n_{37}. In the third scenario, a subset of 80 of the $N = 845$ customers, comprised of those aggregate members connected to pole transformer HP1431, implement A-RHO while the remaining 765 aggregate members implement D-RHO energy-shifting. Fig. 5(c) depicts the resulting voltage profiles for each aggregate member in n_{37}. In Fig. 5(c) upper and lower tolerances of $+10\%/-6\%$ from the nominal 230V together with a maximum voltage threshold $\overline{V} = 248.4V$ as in Table 1 are also depicted.

In Fig. 5(a) we observe voltage profiles for each aggregate member in n_{37} exceed the upper and/or lower tolerances of $+10\%/-6\%$ from the nominal 230V in the context of the special baseline case. In Fig. 5(b) we observe the voltage profiles for each of 23 aggregate members in n_{37} exceed the upper tolerance of $+10\%$ from the nominal 230 V. In contrast, the voltage profiles of the remaining 14 aggregate members in n_{37} are within the upper and lower tolerances of $+10\%/-6\%$ from the nominal 230V when D-RHO energy-shifting. Further, in Fig. 5(b) voltages are closer to the nominal 230 V for all aggregate members in n_{37} on 7 January and 11 January, when compared to the baseline. In Fig. 5(c) we observe the voltage profiles for each of 17 aggregate members in n_{37} slightly exceed the upper tolerance of $+10\%$ from the nominal 230V. In contrast, the voltage profiles of the remaining 20 aggregate members in n_{37} are within the upper and lower tolerances of $+10\%/-6\%$ from the nominal 230V when A-RHO energy-shifting. A reduction in the maximum voltage threshold (e.g., $\overline{V} = 1.03 \times 230V$) will indeed improve supply voltages to all aggregate member when A-RHO energy-shifting.

The results of this case study confirm that both RHO-based algorithms improved supply voltages in a low voltage network. In particular, the D-RHO-based algorithm improved voltage dips and instances of voltage rise on some days, and the A-RHO-based algorithm reduced both peaks and dips in supply voltage profiles on all days. Moreover, the results highlight that when substantial and sustained voltage violations occur, customer-specific forecasts of load and PV generation as opposed to aggregate demand forecasts allow for considerable improvements in voltage regulation, as demonstrated with the A-RHO-based algorithm.

With the centralized QP-based algorithm presented in [23] considered as background, we infer that the D-RHO approach is preferable in that all customers received an equal distribution in annual savings commensurate with their respective battery constraints. In contrast, the A-RHO approach is potentially preferred by an aggregate member when voltages at a PCC would otherwise exceed or fall below strict tolerances resulting in the disconnection of a PV inverter [7]. Future work will quantify the financial benefits of the A-RHO approach under conditions where significant voltage rise triggers the disconnection of a PV inverter.

5. Conclusions

In this paper we presented two receding horizon optimization-based approaches to coordinating residential battery charge and discharge rates when customers are offered net metering PV incentives with time-based electricity prices. In assessing the benefits of both approaches we found the A-RHO approach was preferable when voltages at a residential PCC exceeded or fell below set tolerances. By means of a case study using a publicly available GridLAB-D model of an Australian distribution region, we achieved a peak load reduction of 32% when approximately 50% of residential customers implemented the D-RHO algorithm. Future work will consider control algorithms for a residential PV inverter to adjust the real and reactive power supplied to, or absorbed by, a distribution grid. We envision such controls will potentially offer further improvements in supply voltages for residential PV customers.

Acknowledgments

The authors acknowledge the assistance of Ausgrid employees Neil Stephens and Dr. Alan Murray in facilitating use of the Elermore Vale GridLAB-D model developed as part of the federally funded Australian Smart Grid Smart City program.

[1] F. Katiraei, J. R. Agüero, Solar PV integration challenges, IEEE Power Energy Mag. 9 (3) (2011) 62–71.

[2] R. Tonkoski, D. Turcotte, T. H. M. El-Fouly, Impact of high PV penetration on voltage profiles in residential neighborhoods, IEEE Trans. Sustain. Energy 3 (3) (2012) 518–527.

[3] J. von Appen, M. Braun, T. Stetz, K. Diwold, D. Geibel, Time in the sun: the challenge of high PV penetration in the German electric grid, IEEE Power Energy Mag. 11 (2) (2013) 55–64.

[4] C. L. Masters, Voltage rise the big issue when connecting embedded generation to long 11 kV overhead lines, Power Eng. J. 16 (1) (2002) 1–8.

[5] R. Tonkoski, L. A. C. Lopes, T. H. M. El-Fouly, Coordinated active power curtailment of grid connected PV inverters for overvoltage prevention, IEEE Trans. Sustain. Energy 2 (2) (2011) 139–147.

[6] P. Jahangiri, D. C. Aliprantis, Distributed Volt/VAr control by PV inverters, IEEE Trans. Power Syst. 28 (3) (2013) 3429–3439.

[7] L. Collins, J. K. Ward, Real and reactive power control of distributed PV inverters for overvoltage prevention and increased renewable generation hosting capacity, Renew. Energ. 81 (2015) 464–471.

[8] S. Shao, M. Pipattanasomporn, S. Rahman, Demand response as a load shaping tool in an intelligent grid with electric vehicles, IEEE Trans. Smart Grid 2 (4) (2011) 624–631.

[9] S. Bashash, H. K. Fathy, Modeling and control of aggregate air conditioning loads for robust renewable power management, IEEE Trans. Control Syst. Technol. 21 (4) (2013) 1318–1327.

[10] D. S. Callaway, I. A. Hiskens, Achieving controllability of electric loads, Proc. IEEE 99 (1) (2011) 184–199.

[11] M. Pipattanasomporn, M. Kuzlu, S. Rahman, An algorithm for intelligent home energy management and demand response analysis, IEEE Trans. Smart Grid 3 (4) (2012) 2166–2173.

[12] N. Ruiz, I. Cobelo, J. Oyarzabal, A direct load control model for virtual power plant management, IEEE Trans. Power Syst. 24 (2) (2009) 959–966.

[13] M. Negnevitsky, K. Wong, Demand-side management evaluation tool, IEEE Trans. Power Syst. 30 (1) (2015) 212–222.

[14] O. Corradi, H. Ochsenfeld, H. Madsen, P. Pinson, Controlling electricity consumption by forecasting its response to varying prices, IEEE Trans. Power Syst. 28 (1) (2013) 421–429.

[15] A.-H. Mohsenian-Rad, A. Leon-Garcia, Optimal residential load control with price prediction in real-time electricity pricing environments, IEEE Trans. Smart Grid 1 (2) (2010) 120–133.

[16] M. P. Moghaddam, A. Abdollahi, M. Rashidinejad, Flexible demand response programs modeling in competitive electricity markets, Appl. Energ. 88 (9) (2011) 3257 – 3269.

[17] S. Nykamp, M. G. C. Bosman, A. Molderink, J. L. Hurink, G. J. M. Smit, Value of storage in distribution grids – competition or cooperation of stakeholders?, IEEE Trans. Smart Grid 4 (3) (2013) 1361–1370.

[18] K. Tanaka, K. Uchida, K. Ogimi, T. Goya, A. Yona, T. Senjyu, T. Funabashi, C.-H. Kim, Optimal operation by controllable loads based on smart grid topology considering insolation forecasted error, IEEE Trans. Smart Grid 2 (3) (2011) 438–444.

[19] H. Kanchev, D. Lu, F. Colas, V. Lazarov, B. Francois, Energy management and operational planning of a microgrid with a PV-based active generator for smart grid applications, IEEE Trans. Ind. Electron. 58 (10) (2011) 4583–4592.

[20] X. Wang, A. Palazoglu, N. H. El-Farra, Operational optimization and demand response of hybrid renewable energy systems, Appl. Energ. 143 (2015) 324–335.

[21] F. Marra, G. Yang, C. Traeholt, J. Ostergaard, E. Larsen, A decentralized storage strategy for residential feeders with photovoltaics, IEEE Trans. Smart Grid 5 (2) (2014) 974–981.

[22] S. J. Lee, J. H. Kim, C. H. Kim, S. K. Kim, E. S. Kim, D. U. Kim, K. K. Mehmood, S. U. Khan, Coordinated control algorithm for distributed battery energy storage systems for mitigating voltage and frequency deviations, IEEE Trans. Smart Grid PP.

[23] E. L. Ratnam, S. R. Weller, C. M. Kellett, Central versus localized optimization-based approaches to power management in distribution networks with residential battery storage, Int. J. Elec. Power, accepted for publication 27 Jan., 2016.

[24] E. L. Ratnam, S. R. Weller, C. M. Kellett, Scheduling residential battery storage with solar PV: Assessing the benefits of net metering, Appl. Energ. 155 (2015) 881–891.

[25] E. L. Ratnam, S. R. Weller, C. M. Kellett, An optimization-based approach to scheduling residential battery storage with solar PV: Assessing customer benefit, Renew. Energ. 75 (2015) 123–134.

[26] K. Cavanagh, J. K. Ward, S. Behrens, A. I. Bhatt, E. L. Ratnam, E. Oliver, J. Hayward, Electrical energy storage: technology overview and applications, CSIRO, Australia. Report No. EP154168 (2015).

[27] X. Luo, J. Wang, M. Dooner, J. Clarke, Overview of current development in electrical energy storage technologies and the application potential in power system operation, Appl. Energ. 137 (2015) 511–536.

[28] K. Proctor, A. Bruce, J. Dangar, M. Chatters, A. Murray, N. Stephens, J. Courtney, D. Dawson, M. Kavousian, GA1675 —Smart Grid PS+EDGE Modelling Platform (2004), Available: https://ich.smartgridsmartcity.com.au, Accessed 27 Sep. 2015.

[29] T. S. Brinsmead, P. Graham, J. Hayward, E. L. Ratnam, L. Reedman, Future Energy Storage Trends: An Assessment of the Economic Viability, Potential Uptake and Impacts of Electrical Energy Storage on the NEM 2015-2035, CSIRO, Australia. Report No. EP155039 (2015).

[30] The City of Newcastle, Elermore Vale 2011 Census results (2015), Available: http://www.newcastle.nsw.gov.au/Explore/Parks/Recreation-Planning/Western-Corridor-Planning-Project, Accessed 24 Sep. 2015.

[31] A. Nottrott, J. Kleissl, B. Washom, Energy dispatch schedule optimization and cost benefit analysis for grid-connected, photovoltaic-battery storage systems, Renew. Energ. 55 (2013) 230–240.

[32] M. R. Almassalkhi, I. A. Hiskens, Model-predictive cascade mitigation in electric power systems with storage and renewables — Part I: Theory and implementation, IEEE Trans. Power Syst. 30 (1) (2015) 67–77.

[33] J. C. Doyle, A. F. Bruce, A. R. Tannenbaum, Feedback Control Theory, Maxwell Macmillan International, 1992.

[34] E. L. Ratnam, S. R. Weller, C. M. Kellett, A. T. Murray, Residential load and rooftop PV generation: An Australian distribution network dataset, Int. J. Sustain. Energ., accepted for publication 11 Sep. 2015 (11 Sep. 2015) 1–20.

[35] Commonwealth of Australia, Bureau of Meteorology, Sydney in January 2013: An extreme month for Sydney, Available: http://www.bom.gov.au/climate/current/month/nsw/archive/201301.sydney.shtml, Accessed 27 Sep. 2015.

Conclusions and future work

Overview

This thesis addressed key challenges for distribution operators looking to accommodate significant rooftop PV generation. In the thesis we have studied two issues that potentially arise in distribution networks with significant residential PV generation, namely, (i) reverse power flow that leads to significant voltage rise; and (ii) peak loads that occur infrequently, but potentially lead to costly network augmentation when PV generation is unavailable.

In the first part of the thesis, we have seen that grid-connected battery storage offers significant opportunities to power system operators looking to reduce peak demand approaching capacity constraints. We also reported a publicly available dataset of measured load and PV generation from 300 residential customers located in an Australian distribution network. This dataset formed the basis of all case studies presented in the thesis.

In the second part of the thesis, we considered the customer benefits of co-locating battery storage with solar PV, in the context of feed-in tariffs and financial policies of net metering. Moreover, our proposed QP-based framework allowed for a variety of financial incentives and their required metering topologies. We formulated the QP-based algorithm for day-ahead scheduling of residential battery storage, and showed a balance in reductions of load during during peak pricing periods with penalties for reverse power flow during the same period.

For a net metering policy with time-based electricity prices, we also proposed a linear program (LP)-based algorithm to schedule battery storage co-located with residential solar photovoltaics (PV). By means of a case study, we have shown that the objective of maximizing the operational savings that accrue to customers with battery storage potentially leads to undesirable consequences for a utility. In contrast, the QP-based approach to scheduling battery storage in the day ahead balanced the operational savings that accrue to a customer with the utility benefit of reducing peak load and reverse power flow coincident with the peak pricing period.

In the third part of the thesis, coordinated approaches to scheduling residential battery storage were presented. We proposed two day-ahead optimization-based algorithms for coordinating residential battery storage co-located with solar photovoltaic (PV) when customers are offered net metering

PV incentives with time-based electricity prices. In assessing the benefits of both approaches, we found the central QP-based approach was preferable in that no customer was disproportionately penalized for reducing peak load and/or reverse power flow in a distribution network.

We also presented two receding horizon optimization-based approaches to coordinating residential battery charge and discharge rates, both of which incorporated updates in forecast information at each time step. By means of a case study using a publicly available GridLAB-D model of an Australian distribution region, we achieved a peak load reduction of 32% when approximately 50% of residential customers implemented the D-RHO algorithm.

Summary of contributions by chapter

Part 1 Overview and context

- **Chapter 1** investigated the economic viability of large-scale battery storage. We proposed two case studies to investigate factors influencing the economic viability of energy storage for (1) power system operators and (2) large industrial-sized customers, respectively. We found grid-connected battery storage offered significant opportunities to power system operators in managing peak demand. We also found battery storage offers opportunities to reduce the cost of connection for large industrial-sized customers.
- **Chapter 2** reported a publicly available dataset that was considered throughout the thesis. We identified several means by which anomalous records (e.g. due to inverter failure) were identified and excised from the dataset.

Part 2 Battery scheduling: A single residential system

- **Chapter 3** proposed an optimization-based algorithm for the scheduling of residential battery storage co-located with solar PV, in the context of PV incentives such as feed-in tariffs. We presented a quadratic program (QP)-based algorithm that was applied to measured load and generation data from 145 residential customers located in an Australian distribution network. The results of the case study confirmed the QP-based scheduling algorithm significantly penalized reverse power flow and peak loads corresponding to peak time-of-use billing.
- **Chapter 4** presented a linear programming (LP)-based approach to designing day-ahead battery charge and discharge schedules with the objective of maximizing the operational savings that accrue to customers offered the financial policy of net metering. To benchmark the LP-based approach, we considered the QP-based algorithm from Chapter 3 in the context of net metering. We found an undesirable consequence to the

utility is reverse power flow during the peak pricing period when residential customers implement the LP-based scheduling algorithm. In contrast, we found that the QP-based approach balanced the objective of the utility in limiting reverse power flow, with the customer objective of increasing operational savings, in the context of net metering.

Part 3 Battery scheduling: Coordinated residential systems

- **Chapter 5** addressed the problem of managing reverse power flow and peak loads within a distribution network. We proposed two optimization-based algorithms for coordinating residential battery storage when solar photovoltaic (PV) generation in excess of load is compensated via net metering. Our approach extended the framework presented in Chapter 4, whereby increases in operational savings were balanced with penalties for reverse power flow during the peak pricing period. By means of a case study, using measured load and generation data from 145 residential customers located in an Australian distribution network, we found the customer payback period for a 10 kWh battery was in the vicinity of 6 years.
- **Chapter 6** addressed the problem of managing bi-directional power flows in a distribution grid, with a focus on improving supply voltages in a low voltage network. We proposed two receding horizon optimization-based algorithms for coordinating residential battery storage. These two algorithms extended the framework presented in Chapter 5, where the respective objective functions and design parameters were introduced. In assessing the benefits of both approaches we found the A-RHO approach was preferable when voltages at a residential PCC exceeded or fell below set tolerances.

Future Research

The results of the thesis have the potential to be extended in several directions. Opportunities for extensions are presented below.

Battery Model

Recently, the capital costs associated with purchasing residential-scale batteries has dropped significantly, and it is expected that this trend will continue into the next decade [14, 86]. In this context, the Australian Energy Market Commission (AEMC) integration of storage study identified five key battery technologies for grid-side and/or customer-side applications [86]. Future work could extend the simple battery model in this thesis in a direction to incorporate each of these five battery technologies.

More specifically, reference [86] presents details on the complexity of incorporating additional battery constraints for five key battery technologies suitable for grid applications. For example, the efficiency of the Zinc-Bromine flow battery is around 75%, compared to the round-trip efficiency of a $LiNiMnCoO_2$ of around 95%. Further, the Zinc-Bromine flow battery is designed to be fully discharged each day. In contrast, advanced lead-acid batteries are designed for a the depth of discharge of 40-50%, otherwise the lifetime of the battery is significantly reduced.

Pricing

In this thesis we have considered the potential operational savings that accrue to residential customer with battery storage co-located with solar PV, in the context of existing financial incentives such as feed-in tariffs and net metering with time-of-use electricity prices. Straightforward extensions to dynamic day-ahead pricing schedules [53–56], are certainly possible within the thesis framework. Extensions that assess the market benefits of dispatchable renewable energy could also be considered within the thesis framework.

Communication

In this thesis we have assumed two-way communication infrastructure between a distributor and customer is available and lossless. Emphasis was given to approaches requiring only modest sensing and communication infrastructure. Potential extensions to our framework might consider more realistic scenarios where the availability of communication-based services are less reliable. In particular, further work to incorporate communication network delays or bandwidth constraints are possible. Moreover, the scalability, security, and distances involved with more realistic communication-based services could also be explored [87].

Forecasting

Future work will replace emulated load and generation forecasts with actual forecasts. Extentions to forecast solar PV production as in [88–91], are possible.

Real-time dynamic ratings

In Chapter 1 we introduced distribution equipment ratings that depend on a number of factors including preceding load variations, ambient temperatures, and cooling systems. Future research to dynamically model distribution equipment ratings for the purpose of identifying capacity con-

straints requiring remediation in a distribution grid [92] would assist distributors in selecting the design parameters introduced in Part 3 of the thesis.

Control

Control algorithms for a residential PV inverter to adjust the real and reactive power supplied to, or absorbed by, a distribution grid, as considered in [58,64], could be incorporated in the GridLAB-D model presented in Chapter 6 in future publications. We envision such controls will potentially offer further improvements in supply voltages for residential PV customers with battery storage systems.

The adaptive receding horizon optimization-based approach in Chapter 6 lends itself to formalization in the form of a Model Predictive Control (MPC) problem. One advantage of such an approach is the opportunity to formally establish conditions for stability. The time-based switching of the latch would likely complicate this approach, however, so that the assumptions needed to guarantee stability might be difficult to satisfy in practice. Likewise the ubiquity of model uncertainty would further complicate the analysis [93]. We therefore leave the task of formally establishing robust stability of an MPC formalization to future research.

Other distribution network topologies

This thesis considered Australian distribution networks and their associated topologies. Emphasis was placed on radial network topologies where voltage regulation is likely to be problematic. Extensions to other distribution network topologies, where a smaller number of urban customers are connected to distribution transformers [94], for example, are left to future research.

A

APPENDIX

ENERGY
www.csiro.au

10 Murray Dwyer Circuit, Mayfield West NSW 2304
PO Box 330, Newcastle NSW 2300, Australia
T (02) 4960 6000 • **ABN** 41 687 119 230

1st October 2015

Our Ref: Elizabeth L. Ratnam PhD Thesis

Associate Professor Michael Stockenhuber
Assistant Dean (Research Training)
The University of Newcastle
ATC building, University Drive Callaghan, NSW 2308 Australia
E: michael.stockenhuber@newcastle.edu.au

Dear A/Prof Michael Stockenhuber,

The CSIRO report titled "*An Assessment of the Economic Viability, Potential Uptake and Impacts of Electrical Energy Storage on the NEM 2015-2035*" with Report No. EP155039 was subject to a detailed technical review by Australian Energy Market Commission (AEMC) employees Mr Stuart Slack, Miss Claire Richards, and Mrs Chantelle Bramley on three (3) occasions, with each review leading to revisions and a response by the CSIRO project team including Mrs Elizabeth L. Ratnam. Moreover, the report was twice (2) reviewed internally for CSIRO by Dr John Ward, a Senior Scientist of the Grid and Energy Efficient Systems program.

The AEMC now own the copyright of this document, and have approved it for public release (see link for more information http://www.aemc.gov.au/Major-Pages/Integration-of-storage), with a release date to be determined in the near future. AEMC have also provided written approval for Mrs Ratnam to reproduce Sections 5.1 and 5.2.2 of the report in her PhD thesis.

If you have any questions relating to Mrs Elizabeth L. Ratnam contributions to the report, please feel free to contact me directly.

Kind regards,

Dr Sam Behrens
Group Leader
E: Sam.Behrens@csiro@csiro.au
T: +61 2 4960 6133

Bibliography

[1] S. Chu and A. Majumdar, "Opportunities and challenges for a sustainable energy future," *Nature*, vol. 488, pp. 294–303, Aug. 2012.

[2] S. M. Moosavian, N. A. Rahim, J. Selvaraj, and K. H. Solangi, "Energy policy to promote photovoltaic generation," *Renew. Sust. Energ. Rev.*, vol. 25, pp. 44–58, Sep. 2013.

[3] Y. Hou and J. Zhong, "Challenges ahead: Currents status and future prospects for Chinese energy," *IEEE Power Energy Mag.*, vol. 10, no. 3, pp. 38–47, May 2012.

[4] E. L. Ratnam, S. R. Weller, and C. M. Kellett, "An optimization-based approach to scheduling residential battery storage with solar PV: Assessing customer benefit," *Renew. Energ.*, vol. 75, pp. 123–134, Mar. 2015.

[5] T. Del Carpio-Huayllas, D. S. Ramos, and R. Vasquez-Arnez, "Feed-in and net metering tariffs: An assessment for their application on microgrid systems," in *Proc. 6th IEEE/PES Latin America Conf. and Exposition on Transmission and Distribution (T&D-LA'12)*, Montevideo, Uruguay, 3–5 Oct. 2012, pp. 1–6.

[6] A. Campoccia, L. Dusonchet, E. Telaretti, and G. Zizzo, "Feed-in tariffs for grid-connected PV systems: The situation in the European community," in *Proc. IEEE Conf. on Power Tech*, Lausanne, Switzerland, 1–5 Jul. 2007, pp. 1981–1986.

[7] L. Hirth and F. Ueckerdt, "Redistribution effects of energy and climate policy: The electricity market," *Energ. Policy*, vol. 62, pp. 934–947, Nov. 2013.

[8] N. R. Darghouth, G. Barbose, and R. H. Wiser, "Customer-economics of residential photovoltaic systems (Part 1): The impact of high renewable energy penetrations on electricity bill savings with net metering," *Energ. Policy*, vol. 67, pp. 290–300, Apr. 2014.

[9] A. Campoccia, L. Dusonchet, E. Telaretti, and G. Zizzo, "Comparative analysis of different supporting measures for the production of electrical energy by solar PV and wind systems: Four representative European cases," *Solar Energy*, vol. 83, no. 3, pp. 287–297, Mar. 2009.

[10] A. J. Black, "Financial payback on California residential solar electric systems," *Sol. Energy*, vol. 77, no. 4, pp. 381–388, Oct. 2004.

[11] E. L. Ratnam, S. R. Weller, and C. M. Kellett, "Scheduling residential battery storage with solar PV: Assessing the benefits of net metering," *Appl. Energ.*, vol. 155, pp. 881–891, Jul. 2015.

[12] J. P. Chaves-Avila, K. Wurzburg, T. Gomez, and P. Linares, "The green impact: How renewable sources are changing EU electricity prices," *IEEE Power Energy Mag.*, vol. 13, no. 4, pp. 29–40, Jul. 2015.

[13] V. Fthenakis, "Considering the total cost of electricity from sunlight and the alternatives [Point of View]," *Proc. IEEE*, vol. 103, no. 3, pp. 283–286, Mar. 2015.

[14] T. S. Brinsmead, P. Graham, J. Hayward, E. L. Ratnam, and L. Reedman, *Future Energy Storage Trends: An Assessment of the Economic Viability, Potential Uptake and Impacts of Electrical Energy Storage on the NEM 2015-2035*, 2015, CSIRO, Australia. Report No. EP155039.

[15] K. Ogimoto, I. Kaizuka, Y. Ueda, and T. Oozeki, "A good fit: Japan's solar power program and prospects for the new power system," *IEEE Power Energy Mag.*, vol. 11, no. 2, pp. 65–74, Mar. 2013.

[16] J. Schoene, V. Zheglov, D. Houseman, J. C. Smith, and A. Ellis, "Photovoltaics in distribution systems — Integration issues and simulation challenges," in *Proc. 2013 IEEE Power & Energy Society General Meeting*, Vancouver, BC, Jul. 2013, pp. 1–5.

[17] A. Radchik, I. Skryabin, J. Maisano, A. Novikov, and T. Gazarian, "Ensuring long term investment for large scale solar power stations: Hedging instruments for green power," *Sol. Energy*, vol. 98, Part B, pp. 167–179, Dec. 2013.

[18] CSIRO, "Solar intermittency: Australia's clean energy challenge," CSIRO, Tech. Rep., June 2012.

[19] N. S. Pearre and L. G. Swan, "Renewable electricity and energy storage to permit retirement of coal-fired generators in Nova Scotia," *Sust. Energ. Technol. Asses.*, vol. 1, pp. 44–53, Mar. 2013.

[20] T. W. Haring, D. S. Kirschen, and G. Andersson, "Incentive compatible imbalance settlement," *IEEE Trans. Power Syst.*, vol. 30, no. 6, pp. 3338–3346, Nov. 2015.

[21] D. J. Hill, T. Liu, and G. Verbic, "Smart grids as distributed learning control," in *Proc. 2012 IEEE Power & Energy Society General Meeting*, San Diego, CA, Jul. 2012, pp. 1–8.

[22] S. M. Moosavian, N. A. Rahim, J. Selvaraj, and K. H. Solangi, "Energy policy to promote photovoltaic generation," *Renew. Sust. Energ. Rev.*, vol. 25, pp. 44–58, Sep. 2013.

[23] B. K. Sahu, "A study on global solar PV energy developments and policies with special focus on the top ten solar PV power producing countries," *Renew. Sust. Energ. Rev.*, vol. 43, pp. 621–634, 2015.

[24] AEMO, *Fact Sheet: The Evolving Supply Mix Within the National Electricity market 2015 [Online]*, Accessed 2 Feb. 2016, Available: http://www.aemo.com.au.

[25] B. Kroposki and B. Mather, "Rise of distributed power: Integrating solar energy into the grid," *IEEE Power Energy Mag.*, vol. 13, no. 2, Mar. 2015.

[26] B. Kroposki, R. Margolis, and K. Lynn, "Power to the people," *IEEE Power Energy Mag.*, vol. 9, no. 3, pp. 16–22, May 2011.

[27] J. von Appen, M. Braun, T. Stetz, K. Diwold, and D. Geibel, "Time in the sun: the challenge of high PV penetration in the German electric grid," *IEEE Power Energy Mag.*, vol. 11, no. 2, pp. 55–64, Mar. 2013.

[28] E. Demirok, D. Sera, R. Teodorescu, P. Rodriguez, and U. Borup, "Clustered PV inverters in LV networks: An overview of impacts and comparison of voltage control strategies," in *Proc. 2009 IEEE Conf. on Electrical Power Energy (EPEC)*, Montreal, QC, Oct. 2009, pp. 1–6.

[29] C. L. Masters, "Voltage rise the big issue when connecting embedded generation to long 11 kV overhead lines," *Power Eng. J.*, vol. 16, no. 1, pp. 1–8, Feb. 2002.

[30] P. M. S. Carvalho, P. F. Correia, and L. A. F. Ferreira, "Distributed reactive power generation control for voltage rise mitigation in distribution networks," *IEEE Trans. Power Syst.*, vol. 23, no. 2, pp. 766–772, May 2008.

[31] P. Zhang, W. Li, S. Li, Y. Wang, and W. Xiao, "Reliability assessment of photovoltaic power systems: Review of current status and future perspectives," *Appl. Energ.*, vol. 104, pp. 822–833, Apr. 2013.

[32] L. Collins and J. K. Ward, "Real and reactive power control of distributed PV inverters for overvoltage prevention and increased renewable generation hosting capacity," *Renew. Energ.*, vol. 81, pp. 464–471, Sep. 2015.

[33] M. J. N. van Werven and M. J. J. Scheepers, "The changing role of distribution system operators in liberalised and decentralising electricity markets," in *Proc. IEEE Int. Conf. on Future Power Systems*, Amsterdam, Netherlands, 18 Nov. 2005, pp. 1–6.

[34] T. Stetz, F. Marten, and M. Braun, "Improved low voltage grid-integration of photovoltaic systems in Germany," *IEEE Trans. Sustain. Energy*, vol. 4, no. 2, pp. 534–542, Apr. 2013.

[35] R. Tzartzev, W. M. Grady, and J. Patel, "Impact of high-penetration PV on distribution feeders," in *Proc. 3rd IEEE PES Int. Conf. and Exhibition on Innovative Smart Grid Technologies (ISGT Europe)*, Berlin, Germany, 14–17 Oct. 2012, pp. 1–6.

[36] M. E. Baran, H. Hooshyar, Z. Shen, and A. Huang, "Accommodating high PV penetration on distribution feeders," *IEEE Trans. Smart Grid*, vol. 3, no. 2, pp. 1039–1046, Jun. 2012.

[37] R. Tonkoski, D. Turcotte, and T. H. M. El-Fouly, "Impact of high PV penetration on voltage profiles in residential neighborhoods," *IEEE Trans. Sustain. Energy*, vol. 3, no. 3, pp. 518–527, Jul. 2012.

[38] F. Katiraei and J. R. Agüero, "Solar PV integration challenges," *IEEE Power Energy Mag.*, vol. 9, no. 3, pp. 62–71, May/June 2011.

[39] R. A. Walling, R. Saint, R. C. Dugan, J. Burke, and L. A. Kojovic, "Summary of distributed resources impact on power delivery systems," *IEEE Trans. Power Del.*, vol. 23, no. 3, pp. 1636–1644, Jul. 2008.

[40] C. A. Hill, M. C. Such, D. Chen, J. Gonzalez, and W. M. Grady, "Battery energy storage for enabling integration of distributed solar power generation," *IEEE Trans. Smart Grid*, vol. 3, no. 2, pp. 850–857, Jun. 2012.

[41] S. Nykamp, A. Molderink, J. Hurink, and G. Smit, "Storage operation for peak shaving of distributed PV and wind generation," in *Proc. 2013 IEEE PES Conf. on Innovative Smart Grid Technologies (ISGT'13)*, Washington, DC, 24–27 Feb. 2013, pp. 1–6.

[42] Y. Ueda, K. Kurokawa, T. Tanabe, K. Kitamura, and H. Sugihara, "Analysis results of output power loss due to the grid voltage rise in grid-connected photovoltaic power generation systems," *IEEE Trans. Ind. Electron.*, vol. 55, no. 7, pp. 2744–2751, Jul. 2008.

[43] X. Liu, A. Aichhorn, L. Liu, and H. Li, "Coordinated control of distributed energy storage system with tap changer transformers for voltage rise mitigation under high photovoltaic penetration," *IEEE Trans. Smart Grid*, vol. 3, no. 2, pp. 897–906, Jun. 2012.

[44] E. J. Coster, J. M. A. Myrzik, B. Kruimer, and W. L. Kling, "Integration issues of distributed generation in distribution grids," *Proc. IEEE*, vol. 99, no. 1, pp. 28–39, Jan. 2011.

[45] T. Stetz, K. Diwold, M. Kraiczy, D. Geibel, S. Schmidt, and M. Braun, "Techno-economic assessment of voltage control strategies in low voltage grids," *IEEE Trans. Smart Grid*, vol. 5, no. 4, pp. 2125–2132, Jul. 2014.

[46] R. Tonkoski, L. A. C. Lopes, and T. H. M. El-Fouly, "Coordinated active power curtailment of grid connected PV inverters for overvoltage prevention," *IEEE Trans. Sustain. Energy*, vol. 2, no. 2, pp. 139–147, Apr. 2011.

[47] Y. V. Makarov, P. Du, M. C. W. Kintner-Meyer, C. Jin, and H. F. Illian, "Sizing energy storage to accommodate high penetration of variable energy resources," *IEEE Trans. Sustain. Energy*, vol. 3, no. 1, pp. 34–40, Jan. 2012.

[48] H. Sugihara, K. Yokoyama, O. Saeki, K. Tsuji, and T. Funaki, "Economic and efficient voltage management using customer-owned energy storage systems in a distribution network with high penetration of photovoltaic systems," *IEEE Trans. Power Syst.*, vol. 28, no. 1, pp. 102–111, Feb. 2013.

[49] S. Hashemi, J. Ostergaard, and G. Yang, "A scenario-based approach for energy storage capacity determination in LV grids with high PV penetration," *IEEE Trans. Smart Grid*, vol. 5, no. 3, pp. 1514–1522, May 2014.

[50] G. Mokhtari, G. Nourbakhsh, and A. Ghosh, "Smart coordination of energy storage units (ESUs) for voltage and loading management in distribution networks," *IEEE Trans. Power Syst.*, vol. 28, no. 4, pp. 4812–4820, Nov. 2013.

[51] D. S. Callaway and I. A. Hiskens, "Achieving controllability of electric loads," *Proc. IEEE*, vol. 99, no. 1, pp. 184–199, Jan. 2011.

[52] J. L. Mathieu, S. Koch, and D. S. Callaway, "State estimation and control of electric loads to manage real-time energy imbalance," *IEEE Trans. Power Syst.*, vol. 28, no. 1, pp. 430–440, Jul. 2012.

[53] E. Vrettos, K. Lai, F. Oldewurtel, and G. Andersson, "Predictive control of buildings for demand response with dynamic day-ahead and real-time prices," in *Proc. 2013 IEEE European Control Conference*, Zürich, Switzerland, 17–19 Jul. 2013, pp. 2527–2534.

[54] A. Safdarian, M. Fotuhi-Firuzabad, and M. Lehtonen, "Integration of price-based demand response in DisCos' short-term decision model," *IEEE Trans. Smart Grid*, vol. 5, no. 5, pp. 2235–2245, Sep. 2014.

[55] O. Corradi, H. Ochsenfeld, H. Madsen, and P. Pinson, "Controlling electricity consumption by forecasting its response to varying prices," *IEEE Trans. Power Syst.*, vol. 28, no. 1, pp. 421–429, Feb. 2013.

[56] R. Khalilpour and A. Vassallo, "Planning and operation scheduling of PV-battery systems: A novel methodology," *Renew. Sust. Energ. Rev.*, vol. 53, pp. 194–208, Jan. 2016.

[57] C.-H. Lin, W.-L. Hsieh, C.-S. Chen, C.-T. Hsu, and T.-T. Ku, "Optimization of photovoltaic penetration in distribution systems considering annual duration curve of solar irradiation," *IEEE Trans. Power Syst.*, vol. 27, no. 2, pp. 1090–1097, May 2012.

[58] P. Jahangiri and D. C. Aliprantis, "Distributed Volt/VAr control by PV inverters," *IEEE Trans. Power Syst.*, vol. 28, no. 3, pp. 3429–3439, Aug. 2013.

[59] M. J. E. Alam, K. M. Muttaqi, and D. Sutanto, "A multi-mode control strategy for VAr support by solar PV inverters in distribution networks," *IEEE Trans. Power Syst.*, vol. 30, no. 3, pp. 1316–1326, May 2015.

[60] A.-H. Mohsenian-Rad and A. Leon-Garcia, "Optimal residential load control with price prediction in real-time electricity pricing environments," *IEEE Trans. Smart Grid*, vol. 1, no. 2, pp. 120–133, Sep. 2010.

[61] N. Nair, R. Nayagam, and R. Francis, "New Zealand utility experiences with demand side management," in *Proc. 2008 IEEE Power & Energy Society General Meeting*, Pittsburgh, PA, 20–24 Jul. 2008, pp. 1–5.

[62] B. Sweet, "California's energy-storage mandate," IEEE Spectrum EnergyWise Newsletter, Tech. Rep., 6th Nov. 2013.

[63] O. Mégel, J. L. Mathieu, and G. Andersson, "Scheduling distributed energy storage units to provide multiple services under forecast error," *Int. J. Elec. Power*, vol. 72, pp. 48–57, Nov. 2015, the Special Issue for 18th Power Systems Computation Conference.

[64] M. N. Kabir, Y. Mishra, G. Ledwich, Z. Y. Dong, and K. P. Wong, "Coordinated control of grid-connected photovoltaic reactive power and battery energy storage systems to improve the voltage profile of a residential distribution feeder," *IEEE Trans. Ind. Informat.*, vol. 10, no. 2, pp. 967–977, May 2014.

[65] M. N. Kabir, Y. Mishra, G. Ledwich, Z. Xu, and R. C. Bansal, "Improving voltage profile of residential distribution systems using rooftop PVs and battery energy storage systems," *Appl. Energ.*, vol. 134, pp. 290–300, Dec. 2014.

[66] J.-Y. Kim, J.-H. Jeon, S.-K. Kim, C. Cho, J. H. Park, H.-M. Kim, and K.-Y. Nam, "Cooperative control strategy of energy storage system and microsources for stabilizing the microgrid during islanded operation," *IEEE Trans. Power Electron.*, vol. 25, no. 12, pp. 3037–3048, Dec. 2010.

[67] M. Datta and T. Senjyu, "Fuzzy control of distributed PV inverters/energy storage systems/electric vehicles for frequency regulation in a large power system," *IEEE Trans. Smart Grid*, vol. 4, no. 1, pp. 479–488, Mar. 2013.

[68] D. Wu, F. Tang, T. Dragicevic, J. C. Vasquez, and J. M. Guerrero, "Autonomous active power control for islanded AC microgrids with photovoltaic generation and energy storage system," *IEEE Trans. Energy Convers.*, vol. 29, no. 4, pp. 882–892, Dec. 2014.

[69] Y. Li, B. L. Ng, M. Trayer, and L. Liu, "Automated residential demand response: Algorithmic implications of pricing models," *IEEE Trans. Smart Grid*, vol. 3, no. 4, pp. 1712–1721, Dec. 2012.

[70] P. Palensky and D. Dietrich, "Demand side management: Demand response, intelligent energy systems, and smart loads," *IEEE Trans. Ind. Informat.*, vol. 7, no. 3, pp. 381–388, Aug. 2011.

[71] S. Nykamp, M. G. C. Bosman, A. Molderink, J. L. Hurink, and G. J. M. Smit, "Value of storage in distribution grids – competition or cooperation of stakeholders?" *IEEE Trans. Smart Grid*, vol. 4, no. 3, pp. 1361–1370, Sep. 2013.

[72] A. Nottrott, J. Kleissl, and B. Washom, "Energy dispatch schedule optimization and cost benefit analysis for grid-connected, photovoltaic-battery storage systems," *Renew. Energ.*, vol. 55, pp. 230–240, Jul. 2013.

[73] Y. Ru, J. Kleissl, and S. Martínez, "Storage size determination for grid-connected photovoltaic systems," *IEEE Trans. Sustain. Energy*, vol. 4, no. 1, pp. 68–81, Jan. 2013.

[74] Y. Ru, J. Kleissl, and S. Martínez, "Exact sizing of battery capacity for photovoltaic systems," *Eur. J. Control*, vol. 20, no. 1, pp. 24–37, Jan. 2014.

[75] Y. Riffonneau, S. Bacha, F. Barruel, and S. Ploix, "Optimal power flow management for grid connected PV systems with batteries," *IEEE Trans. Sustain. Energy*, vol. 2, no. 3, pp. 309–320, Jul. 2011.

[76] T. Hubert and S. Grijalva, "Modeling for residential electricity optimization in dynamic pricing environments," *IEEE Trans. Smart Grid*, vol. 3, no. 4, pp. 2224–2231, Dec. 2012.

[77] M. J. E. Alam, K. M. Muttaqi, and D. Sutanto, "Mitigation of rooftop solar PV impacts and evening peak support by managing available capacity of distributed energy storage systems," *IEEE Trans. Power Syst.*, vol. 28, no. 4, pp. 3874–3884, Nov. 2013.

[78] E. Matallanas, M. Castillo-Cagigal, A. Gutiérrez, F. Monasterio-Huelin, E. Caamaño-Martín, D. Masa, and J. Jiménez-Leube, "Neural network controller for active demand-side management with PV energy in the residential sector," *Appl. Energ.*, vol. 91, no. 1, pp. 90–97, Mar. 2012.

[79] J. Hill and C. Nwankpa, "System constraints effects on optimal dispatch schedule for battery storage systems," in *Proc. 2012 IEEE PES Int. Conf. on Innovative Smart Grid Technologies (ISGT)*, Washington, DC, Jan. 2012, pp. 1–8.

[80] K. Tanaka, K. Uchida, K. Ogimi, T. Goya, A. Yona, T. Senjyu, T. Funabashi, and C.-H. Kim, "Optimal operation by controllable loads based on smart grid topology considering insolation forecasted error," *IEEE Trans. Smart Grid*, vol. 2, no. 3, pp. 438–444, Sep. 2011.

[81] H. Kanchev, D. Lu, F. Colas, V. Lazarov, and B. Francois, "Energy management and operational planning of a microgrid with a PV-based active generator for smart grid applications," *IEEE Trans. Ind. Electron.*, vol. 58, no. 10, pp. 4583–4592, Oct. 2011.

[82] F. Marra, G. Yang, C. Traeholt, J. Ostergaard, and E. Larsen, "A decentralized storage strategy for residential feeders with photovoltaics," *IEEE Trans. Smart Grid*, vol. 5, no. 2, pp. 974–981, Mar. 2014.

[83] S. J. Lee, J. H. Kim, C. H. Kim, S. K. Kim, E. S. Kim, D. U. Kim, K. K. Mehmood, and S. U. Khan, "Coordinated control algorithm for distributed battery energy storage systems for mitigating voltage and frequency deviations," *IEEE Trans. Smart Grid*, vol. PrePrint, 2015.

[84] E. L. Ratnam, S. R. Weller, and C. M. Kellett, "Central versus localized optimization-based approaches to power management in distribution networks with residential battery storage," *Int. J. Elec. Power*, vol. , Accepted for publication, 27 Jan., 2016.

[85] E. L. Ratnam and S. R. Weller, "Receding horizon optimization-based approaches to managing supply voltages and power flows in a distribution grid with battery storage co-located with solar PV," *Submitted for publication*, Oct. 2015.

[86] K. Cavanagh, J. K. Ward, S. Behrens, A. I. Bhatt, E. L. Ratnam, E. Oliver, and J. Hayward, *Electrical Energy Storage: Technology Overview and Applications*, 2015, CSIRO, Australia. Report No. EP154168.

[87] R. H. Khan, *Machine-to-machine communications over an IEEE 802.16-based WiMAX network in the smart grid*. University of Newcastle PhD Thesis, 2014.

[88] H.-T. Yang, C.-M. Huang, Y.-C. Huang, and Y.-S. Pai, "A weather-based hybrid method for 1-day ahead hourly forecasting of PV power output," *IEEE Trans. Sustain. Energy*, vol. 5, no. 3, pp. 917–926, Jul. 2014.

[89] M. Delfanti, D. Falabretti, and M. Merlo, "Energy storage for PV power plant dispatching," *Renew. Energ.*, vol. 80, pp. 61–72, Aug. 2015.

[90] L. A. Fernandez-Jimenez, A. Muñoz-Jimenez, A. Falces, M. Mendoza-Villena, E. Garcia-Garrido, P. M. Lara-Santillan, E. Zorzano-Alba, and P. J. Zorzano-Santamaria, "Short-term power forecasting system for photovoltaic plants," *Renew. Energ.*, vol. 44, pp. 311–317, Aug. 2012.

[91] A. Mellit and S. A. Kalogirou, "ANFIS-based modelling for photovoltaic power supply system: A case study," *Renew. Energ.*, vol. 36, no. 1, pp. 250–258, Jan. 2011.

[92] J. Yang, X. Bai, D. Strickland, L. Jenkins, and A. M. Cross, "Dynamic network rating for low carbon distribution network operation — a U.K. application," *IEEE Trans. Smart Grid*, vol. 6, no. 2, pp. 988–998, Mar. 2015.

[93] L. Grüne and J. Pannek, *Nonlinear Model Predictive Control: Theory and Algorithms*. Springer Verlag, 2011.

[94] J. D. McDonald, B. Wojszczyk, B. Flynn, and I. Voloh, "Distribution systems, substations, and integration of distributed generation," in *Electrical Transmission Systems and Smart Grids*, M. M. Begovic, Ed. Springer New York, 2013, pp. 7–68.